University of Strathclyde
Department of Civil and Environmental Engineering

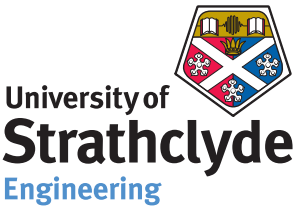

A Computational Study Of The Behaiour Of Hot-Rolled Steel Portal Frames In Fire

Dissertation submitted to the University of Strathclyde
for the degree of Doctor of Philosophy

by

Mahbubur Rahman

May 2012

Acknowledgements

I like to express my deep gratitude to my supervisors, Dr. Yixiang Xu of University of Strathclyde and Dr. James Lim of Queen's University, Belfast, for their continuous support and advice. They have provided assistance in numerous ways, including encouragement and heuristic discussion during the whole process of this research, and the sound advice and patience in reviewing this thesis. The financial support provided by The University of Strathclyde is also greatly acknowledged.

I would like to express my deep and sincere gratitude to my family, especially my parents and wife, and friends; their love gave me strength to accomplish this work.

Declaration

The author declares that, except for commonly understood and accepted ideas, or where specific reference is made to the work of other authors, the contents of this thesis are his own work and include nothing that is the outcome of work done in collaboration. This dissertation has not been previously submitted, in part or in whole, to any university or institution for any degree, diploma or other qualification. This dissertation is presented in 175 pages, excluding bibliography.

_____

Author signature

List of publications

Journal papers

- M. Rahman, J. Lim, Y. Xu, R. Hamilton, T. Comlekci and D. Pritchard (2012). "Effect of column base strength on steel portal frames in fire". Paper published in the Proceedings of the ICE - Structures and Buildings. **165** (SB1). DOI: 10.1680/stbu.11.00040
- M. Rahman, Y. Xu, J. Lim, C. Switzer, R. Hamilton, T. Comlekci and D. Pritchard (2012). "Comparison of Implicit and explicit finite element methods: Behaviour of steel portal frames in fire". Paper accepted for publication in the International Journal of Structural Stability and Dynamics.

Conference papers

- M. Rahman, J. Lim, R. Hamilton, T. Comlekci, D. Pritchard and Y. Xu (2009). "An investigation of overturning moment of portal frame at elevated temperature". Proceedings of the International Conference on Applications of Structural Fire Engineering, 19-20 February 2009, Prague, Czech Republic, pp. annex 2-6.
- M. Rahman, J. Lim, R. Hamilton, T. Comlekci, D. Pritchard and Y. Xu (2009). "Investigation of behaviour of portal frame at elevated temperature using explicit dynamic analysis". Simulia Customer Conference for ABAQUS user group 18-21 April, 2009, London, UK.
- Rahman M., Lim J., Hamilton R., Comlekci T., Pritchard D., Xu Y. (2009). "Effects of semi-rigid and partial strength column base on portal frame at elevated temperatures". Stability of Structures, XII-th symposium, Zakopane, Poland.
- Rahman M., Lim J., Hamilton R., Comlekci T., Pritchard D., Xu Y. (2009). "Effect of rotational stiffness at column base of portal frame at elevated temperature". 6th International Conference on Advances in Steel Structures, 16-18 December 2009, Hong Kong, China.

Abstract

Practicing engineers can confidently design hot-rolled steel portal frame structure if it is kept at ambient temperature. However, as they are not aware of the potential collapse behaviour of such frames in fire, they tend to use heavy foundations with expensive fire protection materials applied to all the columns, rafters and column bases to ensure the structural integrity, and prevent premature collapse.

The research presented in this thesis aims to provide computational techniques and solutions for studying the possible behaviour of different hot-rolled steel portal frames in fire considering the partial strength of column bases with partial insulations applied to the columns.

Before tackling the effect of partial strength of column bases, a comparative study between two different dynamic methods for solving such problems, the implicit dynamic method and the explicit dynamic method, has been undertaken considering fire, large deformations, complex geometry, boundary conditions and degradation of material stiffness. For such analyses, the cost of computation is important as well as the accuracy, robustness and stability of the analysis. It is found that obtaining similar results are possible by using both of the dynamic methods, however, the analyses time differ significantly. It has been established that if the applied artificial inertia forces in terms of residual forces can be magnified and if the automatic time incrementation scheme is activated in the implicit dynamic method then this method shows significant superiority over the explicit dynamic method both in terms of cost of computation and accuracy of results for analysing such structure. Once the proper dynamic method has been selected, all of the analyses of portal frame structure in fire have been conducted by using this particular dynamic method.

The developed model using the implicit dynamic method has been used for studying the effect of partial strength of column bases. A non-linear elasto-plastic implicit dynamic finite element model of a single-span pitched roof steel portal frame building in fire is set-up and used to assess the adequacy of the design method provided by the Steel Construction Institute (the SCI design method). Both 2-D and 3-D models are used to analyze a building similar to the Exemplar frame described in the SCI design guide. Using the 2-D model, a series of parametric study on different frames is conducted. It is shown that the value

of the overturning moment,M_{OTM}, calculated in accordance with the SCI design method, is not sufficient to prevent collapse of the frame before 890°C. It is established that if M_{OTM} is increased the eaves rotations are reduced significantly and reach close to 1° of the original shape, the limit specified by the SCI design method.

The developed model has been extended for analyzing three other portalised frames, such as, multi-span portal frames, portalised truss frames and asymmetric portal frames. It is found that, apart from the multi-span frame, the model can be readily applied to the portalised truss frames and asymmetric portal frames without any computational overhead and loss of accuracy. However, for the multi-span frame, the cost of computation is increased significantly. The computational cost is reduced by relaxing some tight tolerance parameters without losing any accuracy. For all of the frames, it has been observed that all the frames collapses when the column bases are perfectly pinned. However, when a partial strength is introduced at the column bases, the behaviour of the frames changed considerably. It is found that though the snap-through-buckling temperatures remain almost same, the collapse temperatures vary and the eaves rotations differ significantly. Similar to the single-span pitched roof portal frame it has been found that when M_{OTM} is increased the eaves rotations are reduced significantly and reached close to 1° of the original shape.

Based on the studies on different frames it is suggested that the M_{OTM} given by the SCI method should be increased and considered within the region of $1.5M_{SCI}$ to $2.0M_{SCI}$.

Key words: steel portal frames, stability, snap-through-buckling, quasi-static and dynamic analysis, partial strength, semi-rigidity

Contents

List of Symbols

Roman Symbols

A	Area or Portal frame parameter
B	Portal frame parameter
C	Portal frame parameter
C_d	Dilatational wave speed across material
D	Depth of an I-section or a Box-section
F	Applied force vector
i	iteration number
I	Internal force vector
I_{maj}	Section moment of inertia about major axis
I_x	Moment of inertia about local x-axis
I_y	Moment of inertia about local y-axis
G	Clear distance between end of haunches
H_R	Horizontal reaction at column bases
K	Modification factor or Stiffness matrix of structural system
L	Span of frame between column centres or Characteristic element dimension
M	Diagonal lumped mass matrix
M_{pl}	Plastic moment of resistance
$M_{pl,c}$	Plastic moment of resistance of column
$M_{pl,r}$	Plastic moment of resistance of rafter
M_{SCI}	Overturning moment at column bases based on the SCI method
N	Node number
r	Load ratio
r_e	External corner radii of a Box-section

r_i	Internal corner radii of a Box-section
S	Distance between frame centers
t	Stable time or Cross-section thickness
t_1	Solution time with a single processor
t_f	Thickness of flange of an I-section
t_w	Thickness of web of an I-section
t_x	Solution time with multiple processors
u	Displacement
$\dot{u}$	Velocity
$\ddot{u}$	Acceleration
V_R	Vertical reaction at column bases
W	Width of an I-section
W_D	Dead weight of wall
W_f	Load at the time of collapse
W_{pl}	Section plastic modulus
Y	Height from column bases up to end of haunches
x	Number of processors

Greek Symbols

α	Numerical damping parameter
β	Numerical damping parameter
γ	Numerical damping parameter
Γ	Efficiency parameter
η	Efficiency of a processor
σ_y	Yield Strength of steel
θ	Final pitch of rafter
θ_0	Initial or original pitch of rafter

Abbreviations

BS	British Standards
CPU	Central Processing Unit
EC3	Eurocode 3
IE	Internal Energy
ISO	International Standardization Organisation
KE	Kinetic Energy
ms	mass scaling factor
SCI	The Steel Construction Institute
SAPF	Standard Asymmetrical Portal Frame
SMSPF	Standard Multi-Span Portal Frame
SPTF	Standard Portalised Truss Frame
UB	Universal Beam section

List of Figures

List of Tables

Chapter 1

Introduction

1.1 Background

Single-storey steel buildings account for over 50% of the constructional steelwork in the UK each year due to its ease of fabrication and cost-efficiency. The most common form of these buildings is portal frame structure. A portal frame structure is a rigid plane frame with assumed full continuity at the intersections of the column and rafter members, and it is usually designed plastically (Wong, 2001). One of the major disadvantages of constructional steel is its sensitivity to fire, as it rapidly loses its strength and stiffness (Buchanan, 2001; Purkiss, 1996; Wang, 2002 and Wong, 2001). So, for steel portal frame buildings designed in fire, heavy foundation with expensive fire protection materials are applied to all columns, rafters and column bases in order to ensure structural integrity and prevent premature collapse. The use of such heavy foundation and fire protection materials is usually considered as prescriptive-based approach because it does not take into account the properties of steel at elevated-temperatures. The use of heavy foundation with with fire protection materials means that the different strength of column bases, i.e., partial strengths of column bases are not considered.

Alternatively, in performance-based approaches, the properties of steel at different elevated temperatures can be taken into account and partial strength of column bases can be considered in the design of such buildings. These usually lead to safe design of structure with less use of fire protection materials.

1.2 Statement of the problem

Steel portal frames are usually constructed from hot-rolled steel and the column bases are either completely pinned or completely rigidly connected to the foun-

dation which is based on traditional or prescriptive-based approaches at ambient temperature. This prescriptive-based approaches usually neglects the partial strength of column bases and are completely based on the fire resistance of steel and neglects the elevated-temperature properties of such material, and it requires that the steel elements of construction should stay much below a critical temperature, typically 550°C, for the fire resistance period of structure irrespective of any form of construction and thus requires high insulation cost to the whole structure (Lamont, 2001). The Steel Construction Institute (Simms and Newman, 2002) attempted to provide an alternative design guideline for such frame at elevated temperature. However, this guideline was based on arbitrary assumptions, and prescribes over-conservative design of portal frame in terms of material consumption and under-conservative design in terms of column base strength. Moreover, this design guideline assumed that all portal frames would collapse at a certain temperature, such as 890°C, irrespective of geometry, loadings and boundary conditions which is not always true. The behaviour of portal frames with reduced or increased strength of column bases and with partial insulations, such as columns are protected from fire and rafters are unprotected, is still a grey area for performance-based design at elevated temperatures.

1.3 Aim and scope of this research

The aim of this research is to provide computational techniques and solutions for studying the possible behaviour of different hot-rolled steel portal frames at elevated temperatures considering the partial strength of column bases with partial insulation to the frames. The aim of this research is achieved through the following specific objectives:

- To develop nonlinear elasto-plastic finite element analysis (FEA) models and validate them with published results,
- To identify possible instability and collapse mechanisms of different portal frames in fire,
- To investigate the effect of partial strength of column bases on portal frames at elevated temperatures,
- To apply the validated models on other types of portalised frames

1.4 Layout of thesis

This dissertation consists of six chapters and one appendix. Following this introduction chapter, Chapter 2 presents a review of previous relevant background

material and existing analysis methods for the study of the behaviour of steel frames at ambient and at elevated temperatures.

Chapter 3 presents the development and setting up of a finite element model of a portal frame at elevated temperatures. The elements, materials, loads, boundary conditions and temperatures used to model the steel portal frame are explained in detail. In this chapter, implementation details of different types of geometrically and materially non-linear finite element analyses, e.g. implicit dynamic and explicit dynamic analyses are provided and the sequence of analysis steps is laid out.

Chapter 4 presents the study of the effect of partial strength of column bases on symmetric pitched-roof portal frames at elevated temperature.

Chapter 5 extends the use of the method developed in Chapter 3 to investigate the behaviour of multi-span portal frames, portalised truss frames, asymmetrical portal frames at elevated temperatures.

The final Chapter 6 presents a general discussion and review of the work in the previous chapters and it draws conclusions from the work. Areas for further investigation are discussed.

Chapter 2

Literature review

2.1 Introductory remarks

In this chapter a brief discussion on different researches on the behaviour of portal frames at elevated temperatures and currently available design methods of portal frames at elevated temperatures have been presented. It has been found that there has been no research carried out on the effect of partial strength of column base on portal frames at elevated temperatures till to-date.

2.2 Industrial steel portal frame structure design

The primary aim of an industrial steel portal frame is to transfer load from the supported roofs or floors down to the foundations through the rafters and columns. Though different methods vary considerably, however, the primary aim behind all the design codes remains the same. For detailed information on such subject, design guides such as Allison (1991), Horne and Morris (1982), King (1995), Salter *et al.* (2004), and Woolcock *et al.* (1993) can be consulted. However, a short summary of the types of design and construction techniques for industrial frames both at ambient and elevated temperatures is presented in this chapter.

2.2.1 An overview of design of steel portal frame structure at ambient temperature

Industrial portal frames for single-storey buildings has become the most common construction form (King, 1995 and Trahair, 2008). A typical industrial frame

with portal assembly can have a span up to 40.0 m and with portalised truss assembly up to 60.0 m and eave height up to 12.0 m and roof pitch from 3° to 15° (Woolcock *et al.*, 1993).

The design of industrial portal frame varies depending on the forms of such frames. Though structures are usually three-dimensional in their context, sometimes they are essentially two-dimensional or even one-dimensional. So, three dimensional steel structures are often arranged so that they can act as if composed of independent two-dimensional frames or one-dimensional members (Figure 2.1). Many different shapes are available for single-storey industrial frames, as can be seen in Figure 2.2 for portal assembly and Figure 2.3 for truss assembly. Figure 2.4 shows various components of the frame. A dado masonry wall up to a height of 2.5 m is usually built along the edges of industrial warehouse. It is necessary that a portal frame is to be designed to comply with the deflection criteria which are specified for masonry construction. In order to provide stability, both during erection and in the completed building under full service loading, the resistance of the frames to wind load in the longitudinal direction is needed. An adequate anchorage is required for this purpose for the purlins and sheeting rails to ensure their function of restraining the rafters and columns. Bracing is, therefore, required both in-plane of rafters and vertically in the side walls. Purlins and side rails are designed to be continuous over the rafters to support the roof and side wall sheeting and also provide restraint to the rafters or columns (Salter *et al.*, 2004). Most of the times, the industrial frames are the basic pitched-roof variety shown in Figure 2.2 (b) and (c) (Wong, 2001). Nominally pinned bases are more popular with structural designer as high cost of construction of moment resisting bases can be avoided, as well as, the complexity and difficulty of forming a rigid connection. These nominally pinned bases are normally designed to provide resistance to the vertical loading on the roof and to horizontal loading caused by the wind. It is formed by a base plate, holding down bolts and a concrete foundation block as shown in Figure 2.5. If a moment-resisting base is required, a bigger lever arm for bolts, a stiffer base plate and additional gusset plates should be designed, as well as a much larger concrete foundation (Song, 2008).

Either elastic or plastic methods can be employed for designing industrial frames. In both cases, bending resistance at the eaves and apex connections between column and rafter determines the capacity of the frames; and connections should be rigid between each column and rafters, i.e., the connections between columns and rafters must be capable of transmitting moments between the members. Usually, haunches are added at the eaves and apex to reduce the section depth of rafters. In an elastic analysis, different computer softwares are normally used for solving a series of analyses with different load cases. Different factor of safety, in terms of loads and stresses, are applied. Once isolated member forces have been calculated, where both column and rafters are normally subjected to a combination of moment and forces, they are designed as normal beam-columns according to British Standards (BS5950, 1990. Special attentions are given to

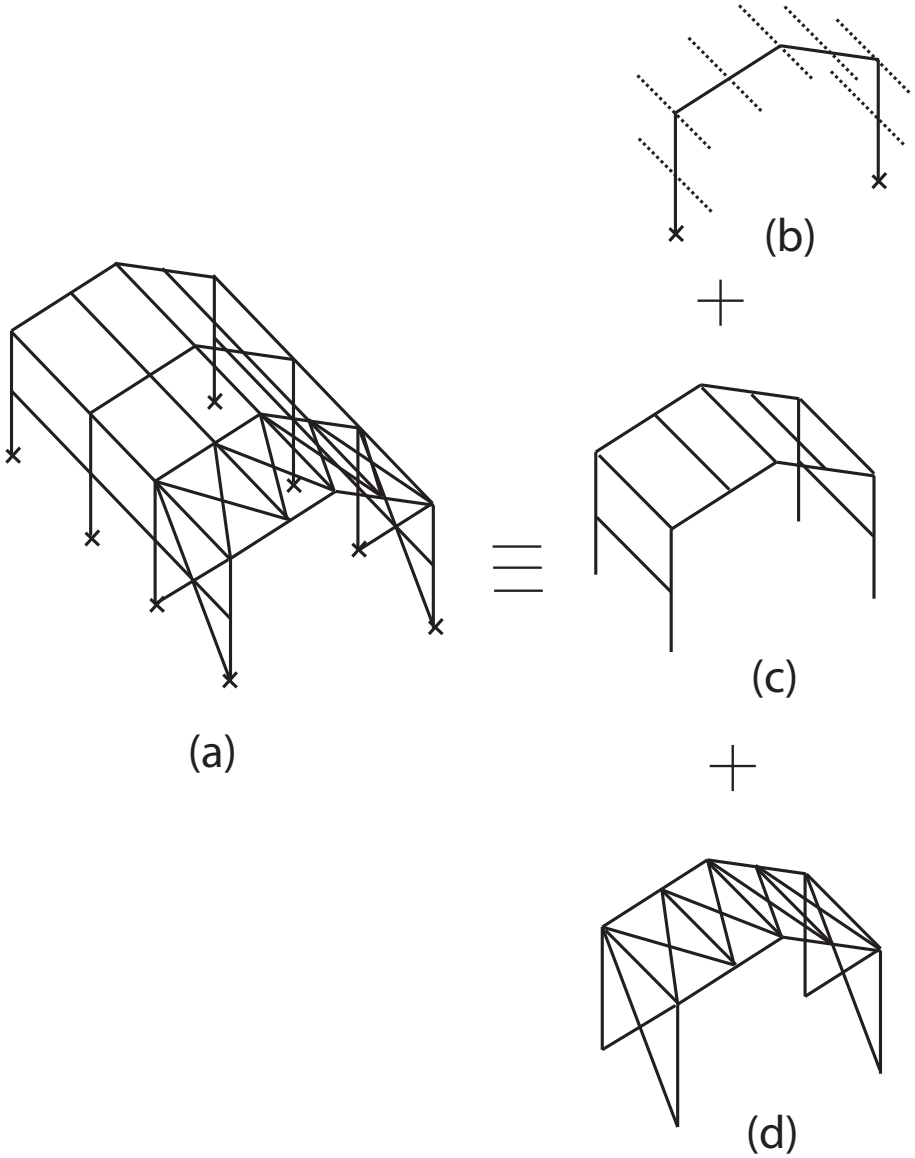

Figure 2.1: Reduction of a 3D frame into simpler forms: (a) 3D frame, (b) 2D rigid frame, (c) 1D beams (purlins and girts), (d) 2D bracing trusses (Trahair, 2008).

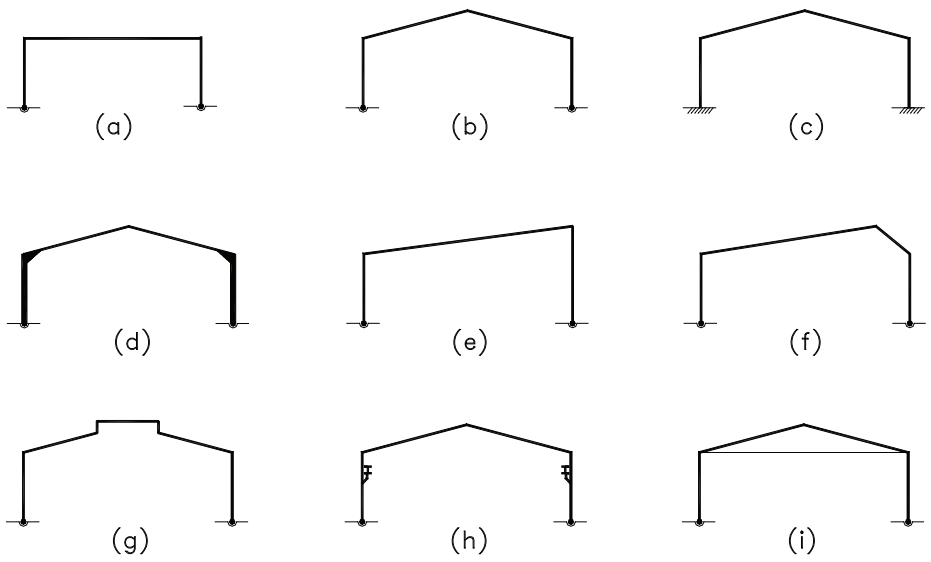

Figure 2.2: Different types of portal assembly: (a) flat roof; (b) pinned base; (c) fixed base; (d) different sections with haunches; (e) lean-to frame; (f)north light; (g) monitor roof; (h) portal with crane; (i) tied portal (Horne and Morris, 1982 as cited by Wong, 2001).

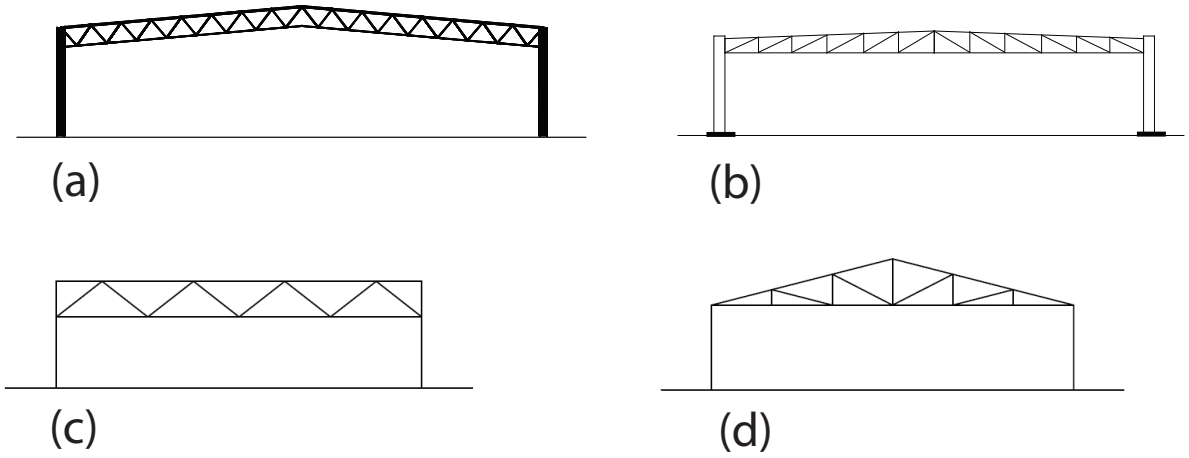

Figure 2.3: Different types of truss frames: (a) portalised truss roof, (b) typical truss roof, (c) warren truss roof and (d) pitched truss roof (Woolcock *et al.* 1993, and Simms and Newman 2002).

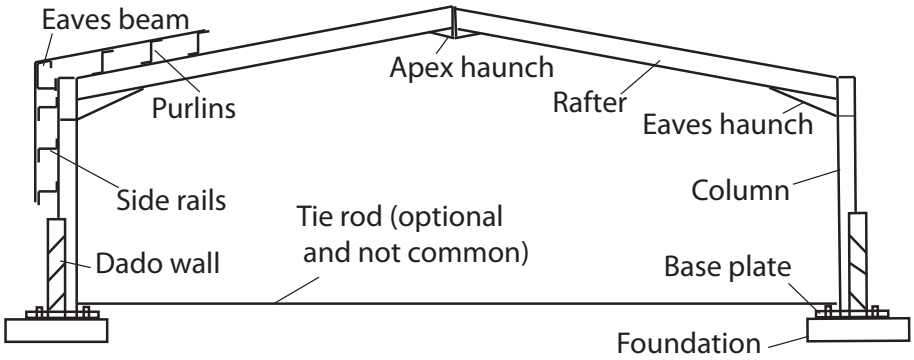

Figure 2.4: Components of a portal frame (Salter *et al.*, 2004).

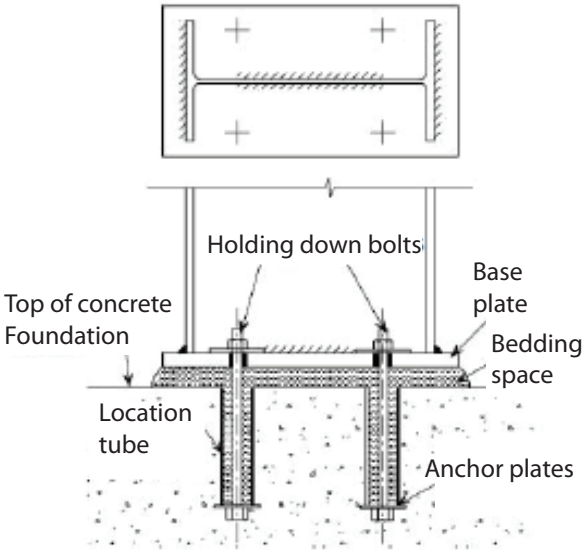

Figure 2.5: A typical nominally pinned base foundation (Salter *et al.*, 2004).

lateral-torsional buckling, where allowance is made for the restraining effects of purlins, sheeting rails and cladding attached to the outer flanges of the main frame members (Wong, 2001). However, after the development of plastic theory and its inclusion in British Standard in 1948, design of industrial frame in the U.K. has been widely based on the 'principles of plastic design' (Allison, 1991).

Plastic design method is based on the limit state design. In traditional 'safe stress' or elastic methods of design where various design requirements have tended to be hidden within the quotation of safe stresses. In contrast, various limit states against which a structure should be designed lead to the possibility of much more open statement of requirements of structural behaviour. Here plastic design enters as a central theme simply because safety in terms of strength tends to be the most important single criterion for the design of any structure. By understanding the factors which lead to plastic collapse, the designer acquires most readily the initial concepts in which his design ought to be based on. Central to the use of plastic design theory is the economic production of satisfactory rigid joints. Another great advantage of the use of plastic design theory is that it is much more directly usable as a design tool than an elastic analysis, as the latter is on the assumptions regarding stiffness ratios. Though one can find that in linear elastic method the stresses induced by various loads can be superimposed to find the effect of load combinations, which, in case of plastic design method, is not applicable. However this apparent disadvantage of plastic design method disappears when it is recognized that the derivation of a complete collapse state for load combinations is frequently not required. Identifying all possible collapse mechanisms of the industrial frames and considering the lowest collapse load is the basis of this method when suitable sections are required to be chosen. Further checks are performed to ensure that no other form of failure prevents the attainment of this collapse mechanism. Different publications which deal with the detail design of portal frames by plastic method can be found in Allison, 1991; Baker and Heyman, 1980; Trahair, 2008; and Davies, Brown and Steel Construction, 1996.

2.2.2 An overview of design of steel portal frame structure at elevated temperature

Most of the current regulations are prescriptive Building Standards. At present, building regulations (FPA, 2008) must be complied in the UK in order to show evidence that the requirements of building regulations have been met. The major aim of these regulations is of fire safety in terms of fire resistance of structure. These requirements state that the stability of a structure should be maintained for a 'reasonable period' and external walls should offer 'adequate' resistance to the spread of fire. To meet these requirements, the distance from the external wall of a single-storey building to the site boundary must be at least 15.0m, or fire protection of this external wall is necessary in order to limit radiation mechanism

of fire spreading. In addition, every structural member that is connected to support the external wall must have the same fire resistance as the boundary wall itself. For the purpose of designing of portal frame, it is considered as a 'single' structural element, as the connection between the rafter and columns are considered as rigid. This leads to the fact that in order to guarantee the longitudinal stability of the boundary wall when the frame is in fire the whole frame has to be protected with expensive insulation against fire.

Considering this fact, The Steel Construction Institute (Simms and Newman, 2002), herein termed as 'the SCI method', developed a simple design method that avoids the fire protection in rafter and allows it to collapse at elevated temperature. This design guideline suggests that fire protection is only required for columns but not necessarily for rafters, so long as the column bases are designed to resist an overturning moment, M_{SCI}, calculated in accordance with this design method. Since this is the only guideline available for designing portal frame at elevated temperature, it is widely used in the UK. The main purpose of this design guideline is to satisfy the requirement of building regulations that the spread of fire to another adjacent building is regulated. A number of assumptions have been made in this design guideline in order to develop simplified equations. It is assumed that the frame is symmetrical and the columns remain at ambient temperature (since fire protection is applied) and the rafter is heated uniformly to a maximum temperature of 890°C, which is the temperature at which 6.5% of the ambient strength of steel is assumed to remain. For a single-span building, it assumes that the rafters undergo symmetrical inward snap-through-buckling, after which the frame stabilizes with the rafters being suspended below the columns in catenary action.

In the UK, if a frame is designed in accordance with the SCI method and the column bases are designed to be able to resist M_{SCI}, the designer may assume that the columns will also remain 1° from the vertical, thus preventing inwards collapse of the walls. A maximum of 2% rafter elongation would be occurred after snap-through-buckling collapse. The haunch length is one-tenth of the span.

With reference to Figure 2.6, the equations of the SCI design guidelines are given as follows:

$$V_R = 0.5 W_f S L + W_D \tag{2.1}$$

$$H_R = K \left(w_f S G A - \frac{C M_{pl,c}}{G} \right) \tag{2.2}$$

$$M_{SCI} = K \left(w_f S G Y \left(A + \frac{B}{Y} \right) - M_{pl,c} \left(\frac{CY}{G} - 0.0065 \right) \right) \tag{2.3}$$

where,

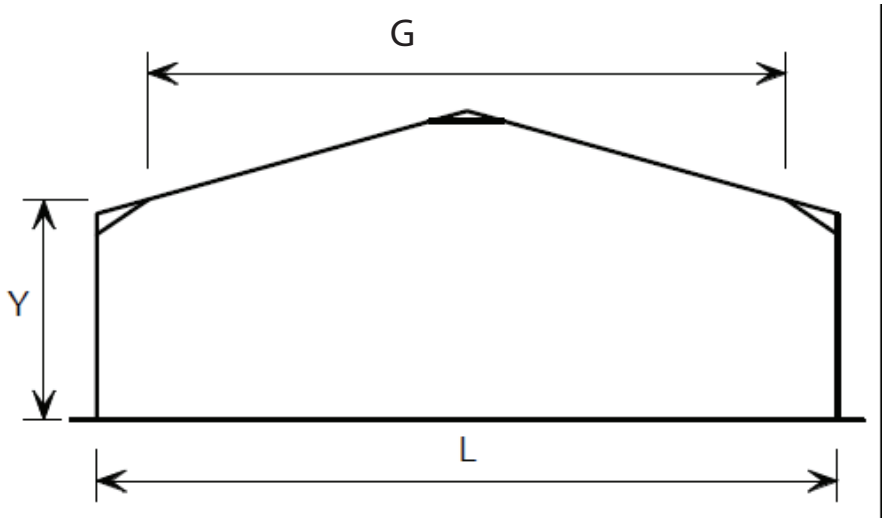

Figure 2.6: Frame dimensions used in calculation of overturning moment, MSCI, using the SCI design guideline(Simms and Newman, 2002).

A	Portal frame parameter
B	Portal frame parameter
C	Portal frame parameter
G	Clear distance between end of haunches
H_R	Horizontal reaction at column bases
K	Modification factor
L	Span of frame between column centres
M_{SCI}	Overturning moment at column bases based on the SCI method
$M_{pl,c}$	Plastic moment of resistance of column
S	Distance between frame centers
V_R	Vertical reaction at column bases
W_D	Dead weight of wall
W_f	Load at the time of collapse
Y	Height from column bases up to end of haunches
θ	Final pitch of rafter
θ_0	Initial or original pitch of rafter

When calculating overturning moment, M_{SCI}, if the values calculated from the equation is less than 10% of the plastic moment of resistance of column, $M_{pl,c}$, or negative then it is suggested that the minimum positive moment should be 10% of the plastic moment of resistance of column.

When the roof is inverted as it collapses due to snap-through-buckling collapse mechanism, the rafter takes the shape of a flexible catenary and tensile force at the ends of this rafter catenary pulls the top of columns inward which causes M_{SCI} at the column bases.

2.3 Research on behaviour of steel portal frame at elevated temperature

Though many researches and studies were carried out for thermal and structural performance of buildings, however, only a very limited number of physical or numerical tests have been carried out on portal frames in fire in the last couple of years. Although fire safety regulations differ in different countries, with different design goals, the underlying philosophy of those regulations remains the same. Columns may remain vertical at a relatively low temperature, but the effect of their base strength and flexibility can be significant on the global behaviour when the rafters are very hot and the catenary forces on the column tops are significant.

Some of the previous researches related to portal frames under fire are outlined in the next section.

2.3.1 O'Meagher (1992)

O'Meagher *et al.* (1992) has conducted research into single-storey industrial buildings in fire for the Australian Institute of Steel Construction as a supplement to the Building Code of Australia. They defined acceptable and unacceptable modes of failure based on the requirements of the Building Code of Australia. These modes of failure covered a number of different heating situations, for example, when only one column and one rafter are exposed to fire. The acceptable mode of failure is asymmetric with one column remaining near to vertical and the other column collapsing inwards. The unacceptable mode of failure is also asymmetric but one of the columns collapses outward, which is dangerous since it not only allows the fire to be spread to adjacent buildings but also represents a danger to fire fighters and occupants escaping from the building due to the collapsing walls. They concluded that the application of fire-protection to the columns of the steel portal frames would have no influence on the deformation mode or their fire resistance. There is also no need to fire-protect the roofs of the supporting steelwork when designed according to that code. They found that most of the frames failed with an acceptable failure mode.

2.3.2 Franssen (2004) and Vassart (2007)

Franssen (Franssen and Gens, 2004) described a double-span portal frame, which Vassart (Vassart *et al.*, 2007) adopted for their studies. Using the finite element program SAFIR (Franssen, Kodur and Mason, 2002), Vassart conducted a 2-D non-linear elasto-plastic implicit dynamic finite element analysis to predict the behaviour of the double-span frame to collapse.

2.3.3 Ali (2004)

Ali (Ali, Senseny and Alpert, 2004) also conducted a 2-D nonlinear elasto-plastic finite element analysis of a double-bay frame using the finite element program ABAQUS (Simulia, 2010) in order to determine the safe clearance required between the frame and firewall allowing the frame to expand laterally. They observed that lateral displacement of frames increases with an increase of spatial extent of fire. They also observed that the greater the roof height the sooner the failure of the frame occurs.

2.3.4 Wong (2001)

Wong (Wong, 2001) studied the responses of industrial pitched portal frame structures in fire both experimentally and numerically while he was in the process of extending the capabilities of specialized finite element software VULCAN. He conducted a series of indicative fire tests for ensuring the extended capabilities of the software. He then conducted three major fire tests on scaled portal frames in order to observe the behavior. One of his major findings is that the rafter may encounter large deflections and large elemental strains while it undergoes snap-through-buckling failure mechanism, in which fire hinges were identified. He developed a simplified method for estimating the critical temperatures of steel portal frames in fire. His method is limited to determining the snap-through-buckling of portal frame, without giving any consideration to the post snap-through-buckling behavior i.e. his model is not capable of studying the re-stabilization behavior of portal frame. He pointed out the necessity of performance-based design of portal frame, however, he did not suggest any specialized design methodology.

2.3.5 Song (2008) and and Song *et al.* (2009)

Song (2008) and Song *et al.* (2009) continued the work of Wong on single-span frames and used VULCAN to conduct a 2-D non-linear elasto-plastic implicit dynamic analysis of the portal frame. Their model was able to predict the post snap-through-buckling behaviour of the frame and they observed asymmetric failure mechanism. For models in which the column bases were modelled assuming linear rotational stiffness, they showed that a portal frame in fire can collapse in two consecutive phases, the first phase being snap-through-buckling collapse and subsequent stabilization of the rafter, and the second phase being opening of the plastic hinge near the eaves joint after which the frame loses stability and collapses.

2.3.6 Bong (2005) and Moss *et al.* (2009)

Bong (2005), as described by Moss *et al.* (2009), conducted a 3-D non-linear elasto-plastic implicit dynamic finite element analysis of a portal frame building in fire using the finite element program SAFIR. The building was designed in accordance with New Zealand practice (NZS4203, 1992 and NZS3404, 1997) with the lower half of each column encased in concrete and the top half exposed to fire. They found that the structure may collapse in any of the three different ways: (a) inwards mode: the frame collapses inside the compartment, (b) sway mode: the frame collapses outside the compartment, and (c) upright mode: the walls and column remain straight and standing, and rafter collapses inside the compartment. In this 3-D model, the purlins were also modelled. No consideration was given to the column base, which was again assumed to behave perfectly-pinned. They did not observe the snap-through-buckling behaviour or post snap-through-buckling stabilization of portal frame. Similar to Song *et al.*, it was shown that the failure mode of the portal frame was asymmetric, however, no sway mode of failure was observed as contrasted with the findings of Wong's study (Wong, 2001).

2.4 Concluding remarks

In this chapter, it has clearly been shown that there has been no research carried out on the effect of partial strength of column bases on different types of portal frames. In practice, a portal frame can be a single-span or a multi-span frame; and the rafter can either be a continuous element or a group of truss elements that is a combination of top, bottom and web diagonal elements. Column bases may be fully fixed or fully pinned in theory, though in practice, the column base is neither fully fixed nor fully pinned and achieving complete capacity of the column bases is never possible. The SCI method provides a means on how to calculate the overturning moment, M_{SCI}, for a symmetrical pitched frame assuming that the column base is fully fixed. In this research, a validated finite element analysis (FEA) model has been used to investigate the effect of partial strength of column bases of symmetrical single-span pitched roof steel portal frame assuming that a column base cannot achieve full strength while it is in fire. Later, similar study has been extended to three other portalised frames, such as, multi-span portal frames, portalised truss frames and asymmetrical portal frames. In the later two cases, only single-span frame has been considered.

Chapter 3

Comparison of implicit and explicit dynamic finite element analysis

3.1 Introduction

Steel portal frames (see in Fig. 3.1) are a popular form of construction for industrial single storey buildings due to their ease of construction and cost efficiency. One of the disadvantages of steel, however, is that in fire it rapidly loses its

Figure 3.1: Typical portal frame building

strength and stiffness and thus engineers need to consider the collapse behaviour of such buildings at elevated temperature.

The use of the finite element method for determining the behaviour of such frames in fire can be a viable alternative to full-scale testing (OMeagher *et al.* 1992, Wong 2001 and Song *et al.* 2008).

It is evident from Figure 3.2 that each iteration of a solution step, usually by Newton-Raphson numerical method, is governed by load increment, and the changes in the displacement become larger when approaching the desired solution and becoming less convergent. If the stiffness is further reduced and changes from positive to negative, the solution to the nearest tangent stiffness (the limit point) becomes divergent and is considered as the failure point for the structural system. At this point, the whole structural system experiences a snap-through buckling and the displacement is sudden and dramatically increased because of this sudden changes/loss of stiffness. After the snap-through buckling, the structure regains its stability and continues to deflect as if it were a stable structure. As the solution is divergent at the limit point, static analysis cannot be used for determining the full collapse behaviour of such frames in fire because the analysis gets terminated at this point. To continue the analysis after the snap-through buckling,

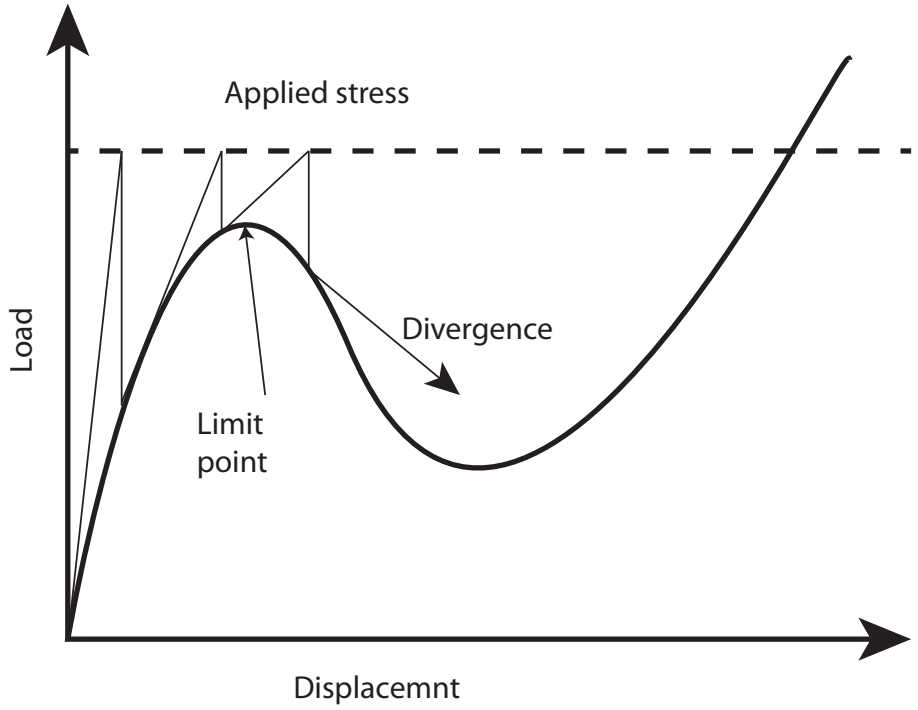

Figure 3.2: Snap-through behaviour

alternative methods of analysis, such as dynamic methods must be sought (Sun *et al.* 2000, Wong 2001, Song 2008 and Sun *et al.* 2012). Two dynamic methods of analysis are most commonly used: the implicit dynamic method and the explicit dynamic method. It is important to understand the nature, advantages and disadvantages of these methods while choosing the right method of analysis for investigating the collapse behaviour of steel portal frames in fire.

A number of studies are available comparing the results of implicit and explicit dynamic methods (Soltani *et al.* 1994, Sun *et al.* 2000, Kim 2002 and Harewood and McHugh 2007). While the focus of those studies is on metal forming and

crystal plasticity, they provide a useful indication of applicability of these two methods to other problems. The unconditionally stable implicit method usually encounters difficulties when the frame undergoes structural instability. This instantly occurs because the cost of computation of formation of the tangent matrix is significantly increased and may even be divergent as the time-incrementation is reduced. This instability can be avoided by artificially increasing the inertia forces in terms of residual forces of the structure. In contrast, the explicit method is conditionally stable, and it does not need to form the tangent matrix, and consequently no convergence problem occurs. However, in order for both the implicit and explicit dynamic methods to be applicable for a quasi-static problem, as is the case in the present study, the inertia force should be small enough that its effect can be neglected. Sun *et al.* (2012) developed a static-dynamic procedure for the VULCAN software for analysing progressive collapse of steel structures under fire conditions where the static and explicit dynamic methods are coupled and the analyses can be automatically switched between depending on the occurrence of instability. They have chosen the explicit method because the explicit method does not involve singularities as there is no matrix inversion involved in contrast to the implicit and static methods.

In this paper, the general purpose commercial finite element program ABAQUS (Simulia 2009) is used for both types of dynamic method and a comparison of results in terms of cost of computation and accuracy is presented. Different parameters are required in each method of analysis. In the case of the implicit dynamic method, a *half-increment residual force*, for inducing artificial inertia, is commonly employed for avoiding convergence problems and reducing the cost of computation. In addition, *numerical damping* is applied for avoiding numerical errors caused by non-dissipation of energy. For the case of the explicit dynamic method, *time scaling* and *mass scaling* are used for reducing the cost of computation while still maintaining the desired accuracy. The results provide suitable and efficient guidelines for researchers for investigating the collapse behaviour of portal frames in fire.

3.2 Solution method

For linear dynamic analysis, eigen-modes or modal or subspace projection methods, as a set of global Ritz functions, can provide an indication for the structural behavior that is not otherwise available (Simulia 2009). However, when the system is geometrically and materially nonlinear, dynamic or quasi-static, direct time integration operators are needed for solving a set of equations. These integration operators are broadly classified as the implicit dynamic method and the explicit dynamic method.

The implicit dynamic method uses an automatic increment strategy based on the success rate of the full Newton iterative solution method (Sun *et al.* 2000) as

given by

$$\Delta u_{i+1} = \Delta u_i + K^{-1}(F_i - I_i) \tag{3.1}$$

where K is the stiffness matrix of the structural system, F is the applied force vector and I is the internal force vector. The corresponding nodal acceleration $\ddot{u}$, velocity $\dot{u}$ and displacements u are updated according to the Hilber-Hughes-Taylor operator (Hilber and Hughes 1978, Hughes 1987 as cited by Simulia 2009) which is a generalization of the Newmark operator with controllable numerical damping, as follows:

$$M\ddot{u}^N_{i+1} = (1+\alpha)F_{i+1} - \alpha F_i \tag{3.2}$$

$$\dot{u}^N_{i+1} = \dot{u}^N_i + \triangle t\,((1-\gamma)\,\ddot{u}^N_i + \gamma\,\ddot{u}^N_{i+1}) \tag{3.3}$$

$$u^N_{i+1} = u^N_i + \triangle t\,\dot{u}^N_i + \frac{(\triangle t)^2}{2}[(1-2\beta)\,\ddot{u}^N_i + 2\,\beta\,\ddot{u}^N_{i+1}] \tag{3.4}$$

with

$$-\frac{1}{3} \leq \alpha \leq 0,\ \ \gamma = \frac{1-2\,\alpha}{2}\ \ and\ \ \beta = \left[\frac{1-\alpha}{2}\right]^2 \tag{3.5}$$

where superscript N denotes node, subscript i indicates the iteration number and α represents the numerical damping parameter.

The explicit method is based upon the implementation of an explicit integration rule and the use of diagonal or lumped element mass matrices. The method uses the central difference integration technique and the method of implementation of this integration rule as given by

$$\ddot{u}_i = M^{-1}(F_i - I_i) \tag{3.6}$$

$$\dot{u}^N_{i+\frac{1}{2}} = \dot{u}^N_{i-\frac{1}{2}} + \frac{\triangle t_{i+1} + \triangle t_i}{2}\,\ddot{u}^N_i \tag{3.7}$$

$$u^N_{i+1} = u^N_i + \triangle t_{i+1}\,u^N_{i+\frac{1}{2}} \tag{3.8}$$

where M is the diagonal lumped mass matrix. i, $(i+\frac{1}{2})$ and $(i+1)$ are the initial, middle and final increments of time.

The explicit method suffers from conditional stability. To achieve a *stable time increment* it must satisfy the condition

$$\triangle t = \frac{L}{C_d} \tag{3.9}$$

where L is the characteristic element dimension and C_d is dilatational wave speed across the material.

3.3 FE model

3.3.1 Building description

Frame description, loading and FE idealization

The steel portal frame used in this study is based on the benchmark frame given by Song *et al.* (2009) as shown in Fig. 3.3. It can be seen that the frame is of

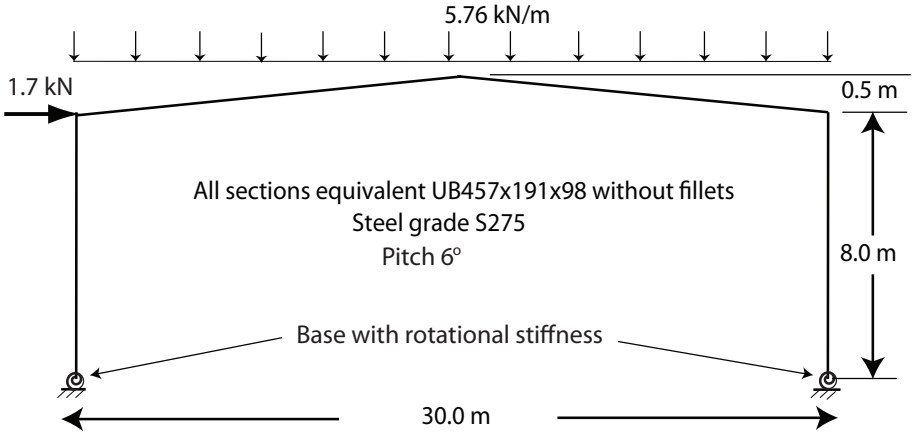

Figure 3.3: Details of single span portal frame after Song *et al.* (2009)

span of 30.0m, height to eaves of 8.0m and height to apex of 8.5m with an initial uniformly distributed vertical load of 5.76kN/m on the rafter and a horizontal force of 1.7 kN at the left eaves. The load ratio, a ratio of the applied load in fire to the ultimate load capacity at ambient temperature of the frame, is 0.53, which means that the frame is heavily loaded with low fire resistance i.e. the frame collapses much faster in fire compared to frames with a lower load ratio. Table 4.1 summarizes the section properties used for the columns and rafter. It should

Table 3.1: Properties of equivalent steel sections. (Note: fillets are not considered).

Section	A	σ_y	I_{maj}	W_{pl}	$M_{c,pl}$
	cm^2	$\frac{N}{mm^2}$	cm^4	cm^3	kNm
Column/Rafters	124.4	275	45700	1957	538

be noted that the section properties have been calculated without fillets because the finite element program ABAQUS does not provide fillets for cross-sections for beam elements, and inclusion of fillets through use of arbitrary cross sections increases the cost of computation significantly.

3.3.2 Finite element modelling

Details of the hot-rolled steel properties at elevated temperature and corresponding fire models are given in Sections 4.2.3 and 4.3 in Chapter 4. Figure 4.10 shows a typical finite element mesh.

3.3.3 Analysis steps

In this finite element analyses, the transient method is adopted where two analysis steps are required:

- Step 1: Dead load applied over rafter.
- Step 2: Elevated temperature applied.

Implicit dynamic method

Step 1: Dead load applied over rafter

The portal frame is analysed at ambient temperature using a non-linear static method. The results provide the initial stresses for the frame at the start of Step 2.

Step 2: Elevated temperature applied.

The portal frame is analysed using the implicit dynamic method. An initial time increment is specified with total duration of elevated temperature. Once the initial time increment is specified, an iterative procedure with an automatic incrementation scheme is used in which the solver determines the effective time increment for subsequent iterations. When certain tolerance criteria are met, the analysis can be stopped.

A half-increment residual forces parameter, *haftol*, is used to ensure an accurate dynamic solution while automatic time incrementation is activated. This parameter has dimensions of force and is usually chosen by comparison with typical actual force values, such as applied forces or expected reaction forces. For problems where considerable plasticity or other dissipation is expected to damp out the high frequency response, this parameter is chosen as 10.0 to 100.0 times the typical actual force values to obtain results with moderate accuracy and low cost of computation, and as 1.0 to 10.0 times the typical actual force values to obtain results with higher accuracy and increased cost of computation. Usually,

a haftol of 1.0 times the typical actual force values gives highest accuracy of results but with the most increased cost of computation. Proper choice of haftol can speed up the analysis while retaining satisfactory accuracy of results. Determination of a suitable value for this parameter is discussed later in Section 3.7.

It should be noted that the values $\alpha = -\frac{1}{3}$ and $\alpha = 0$ represent two opposite and extreme cases: $\alpha = 0$ provides no numerical damping and equivalent to the trapezoidal rule or Newmark-β method and usually gives the highest accuracy with increased cost of computation; $\alpha = -\frac{1}{3}$ gives the maximum numerical damping with lowest accuracy but with the cheapest cost of computation. Meanwhile α=-0.15 represents an average value and α=-0.05 is the default value set by the program to introduce just enough artificial damping in the system to allow the automatic time-stepping procedure to work smoothly without any loss of accuracy of results.

Explicit dynamic method

Step 1: Dead load applied over rafter

The portal frame is analysed at ambient temperature using the explicit dynamic method. The duration of load is chosen to be at least five times the period of vibration of the structure to avoid impact effects. The load is applied in a *smoothing-up* manner so that the initial and final acceleration and velocity of the frame become zero. Once the duration of load is specified, an explicit algorithm is used to calculate the acceleration, velocity and displacement at different point of time. Similar to the implicit method, the results provide the initial stresses for the frame at the start of Step 2.

Step 2: Elevated temperature applied.

Analysis of the frame with explicit dynamic method is continued from the previous step. Unlike the implicit dynamic method, specification of initial time is not necessary. However, the total duration of elevated temperature must be specified within this step. As before, once the duration of elevated temperature is specified, an explicit algorithm is used to calculate the acceleration, velocity and displacement at different points of time. Default viscosity parameters are applied. When certain criteria, i.e. rafter touches the ground or the temperature goes beyond 1100°C, are met, the analysis can be stopped, similar to the implicit method.

Solving a quasi-static problem using explicit dynamic method using a natural time can be impractical as the cost of computation would be excessively prohibitive. To improve the cost of computation, two types of scaling are applied: *time scaling* and *mass scaling*. A time scaling factor of 1.0 means the true time

or natural time is used; and a mass scaling factor of 1.0 means the analysis has no artificial inertia force induced; analysing frames with this set of parameter values gives the highest accuracy of results but at the expense of highest cost of computation. Higher values of these parameters usually speed up the computation but the accuracy of results is reduced.

3.4 Different phases of collapse

The behaviour of the frames with fixed initial load and increased temperature can be divided into certain phases, as can be seen in Fig. 3.4. In phase (a)

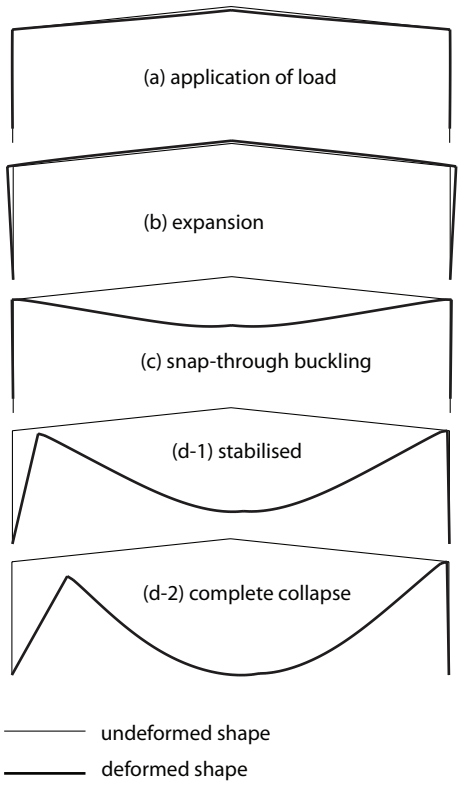

Figure 3.4: Different phases of collapse.

the response is linear as the stresses remain elastic. Phase (b) is the result of compressive forces developed due to the thermal expansion of steel within the rafter, that pushes the whole structure upwards and outwards. At this stage the thermal expansion dominates over steel stiffness. Once the temperature increases further, phase (c) starts in which the steel stiffness degrades as temperature increases. The compressive force in the rafter decreases eventually the forces become tensile. The apex of the rafter snaps through downward and becomes fully inverted. While the rafter is fully inverted, phase (d) starts, and depending

on the column base condition, the frame may be either stabilized, or collapses completely.

3.5 Validation

The model described in Section 3.3.1 has been used for the purposes of validation; the results of both the implicit dynamic method and the explicit dynamic method are compared with the results by Song *et al.* (2009).

The temperature of the rafter is increased in accordance with the ISO834 fire curve (ISO 1975) until the frame collapses. As the columns are protected in fire, they are assumed to remain at ambient temperature throughout the duration of analysis. Nominally pinned column bases with a non-dimensional rotational stiffness of 0.4 are used, as specified by Song *et al* (2009)., and recommendations by Salter *et al.* (2004).

For the implicit dynamic method, a factor of 1.0 times the applied load for haftol and a factor of -0.05 for numerical damping, α, and for the explicit dynamic method, a factor of 1.0 for mass scaling and time scaling is used to obtain the most accurate results. In both implicit and explicit dynamic methods, a mesh of 16 elements for each column and 64 elements for the whole rafter has been chosen based on the study of the effect of the mesh described in Section 3.6.1.

3.5.1 Validation of results

Fig. 3.5, Fig 3.6 and Fig 3.7, respectively, compare the variation of deflections of apex, left eaves and right eaves at different temperatures, calculated by the implicit and explicit dynamic methods, against those obtained by Song *et al* (2009). As can be seen, there is a good agreement between the results obtained using implicit and explicit methods and those obtained by Song *et al* (2009).

Fig. 3.9 and Fig. 3.10 compare the deformed shapes at different temperatures, calculated by the implicit and explicit dynamic methods for the case of nominally pinned column base against those obtained by Song *et al.* (2009) in Fig. 3.8. As can be seen, the mode of collapse is asymmetrical and the deformed shapes are similar. However, from Table 3.2, it can be seen that the cost of computation differs significantly for the implicit and explicit dynamic methods.

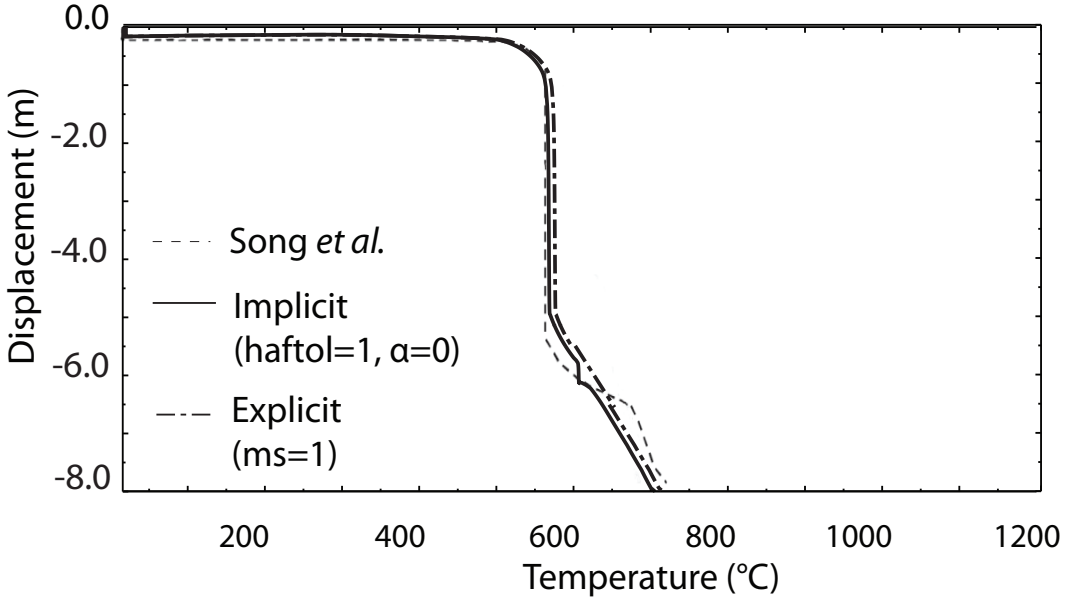

Figure 3.5: Variation of apex deflection against temperature for single span portal frame when column base is nominally pinned after Song *et al.* (2009)

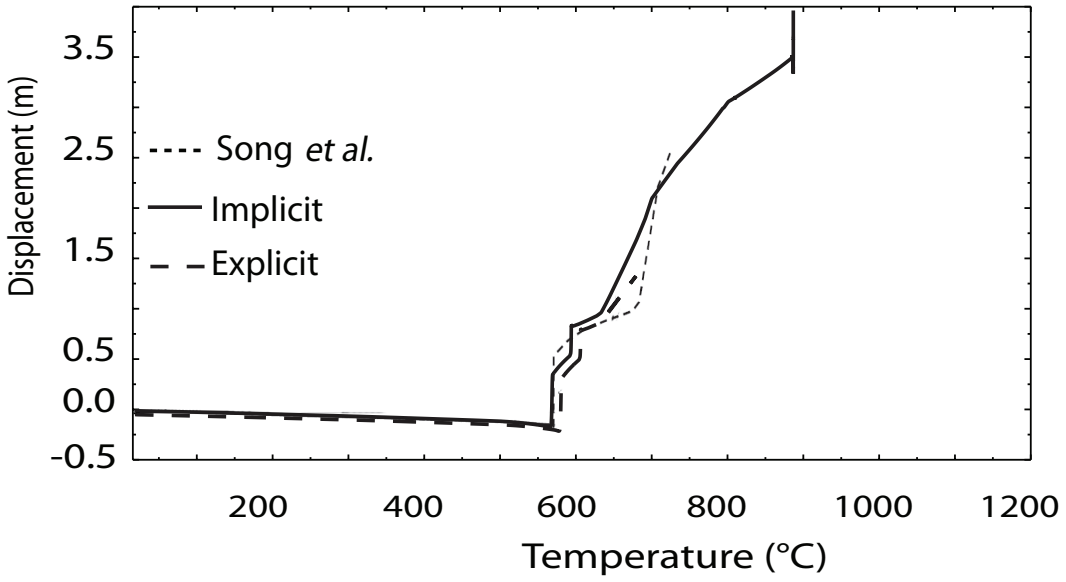

Figure 3.6: Variation of left eaves deflection against temperature for single span portal frame when column base is nominally pinned after Song *et al.* (2009)

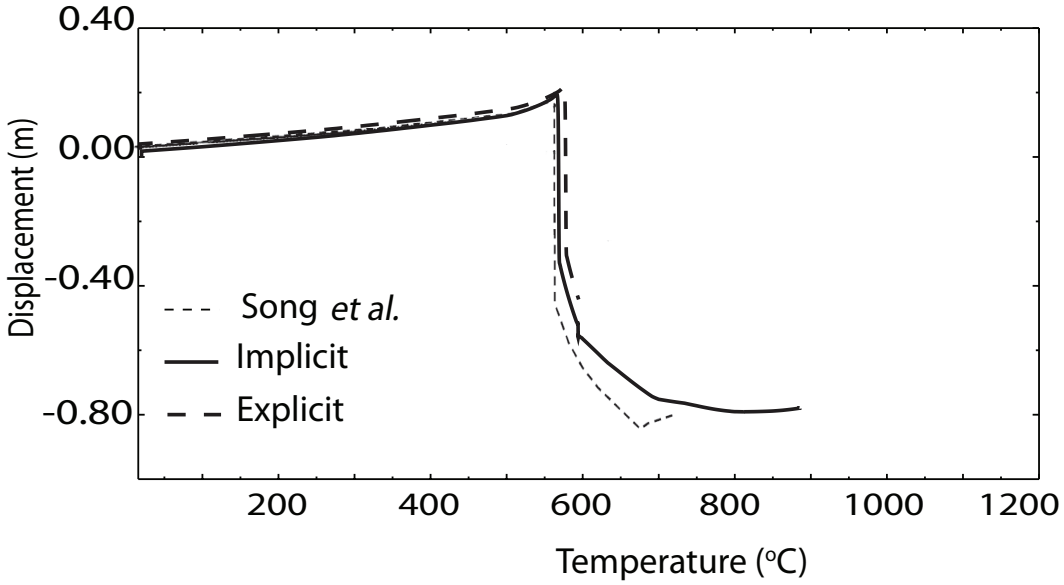

Figure 3.7: Variation of right eaves deflection against temperature for single span portal frame when column base is nominally pinned after Song *et al.* (2009)

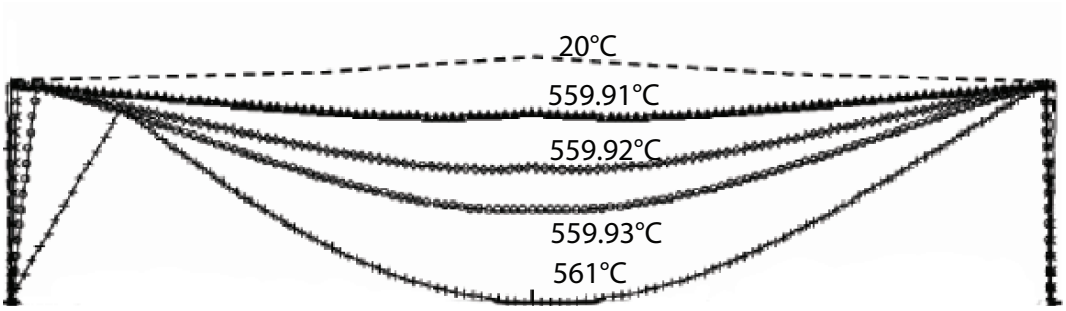

Figure 3.8: Deformed shape obtained by Song *et al.* (2009)

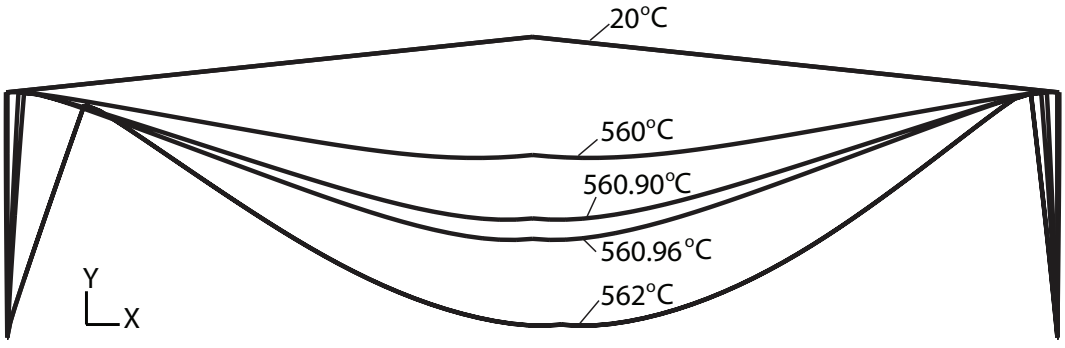

Figure 3.9: Deformed shape obtained by implicit dynamic method (ABAQUS)

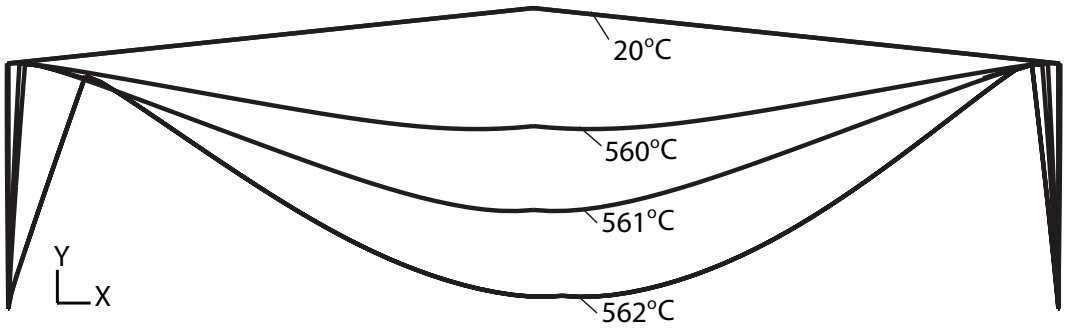

Figure 3.10: Deformed shape obtained by explicit dynamic method (ABAQUS)

Table 3.2: Computation time by implicit and explicit methods while validation of Song *et al.*'s (2009) frame with default parameters.

Implicit (haftol=1, $\alpha = -0.05$)	Explicit (time factor=1, ms=1)
40m 2s	15h 2m

3.6 Comparative study for two dimensional model

All the simulations have been performed using an Intel Core i7 1.60 GHz multi-processor, where as many as eight parallel processors can be used. It is possible to produce similar results by using the implicit and explicit methods as can be seen in Fig. 3.5 for apex displacement against temperature. However, the efficiency of the methods depends on certain parameters. In order to be able to make sensible comparisons of cost of computation and accuracy, there should be a common point where the analysis should either be completed or be terminated. For this purpose, the analysis is allowed to be continued until the apex reaches the column base level after the snap-through-buckling has occurred. Once the apex reaches the column base level, the analysis is terminated. In cases where the rafter is suspended after the snap-through-buckling has occurred and the apex does not reach the column base level, the analysis is continued for the whole temperature domain up to 1100°C.

3.6.1 Common comparative study

Effect of mesh size on the calculation time and structural response

Though mesh size significantly affects the calculation time and accuracy of both implicit and explicit dynamic methods, it is found that the explicit dynamic method is more sensitive to the element size because a finer mesh not only increases the number of degrees of freedom but also decreases the element size, which increases the dilatational wave speed, which essentially reduces the time increment size, and in turn increases the cost of computation.

In order to observe the effect of number of meshes, six different mesh cases, as shown in Table 3.3, have been studied. Comparison of the apex deflections

Table 3.3: Number of elements for different mesh cases.

Mesh cases	No. of elements in each column	No. of elements in each half of rafter
A	2	2
B	4	8
C	8	16
D	16	32
E	32	32
F	32	64

and elemental stress at apex against different temperatures for each mesh case for both implicit and explicit methods are shown in Figs. 3.11, 3.12, 3.13 and 3.14.

Based on the results of the study described in Section 3.7, haftol factors of 1.0 and 100.0 and fixed mass scaling factors of 1.0 and 4.0 are considered. For the explicit dynamic method, the true time scale is used and no time factor is taken into account. The time taken to solve the models is reported in Table 3.4 and compared in Figure 3.15.

As can be seen from Figures 3.11, 3.12, 3.13 and 3.14, mesh A gives inaccurate results, while meshes B to F gives very similar results for apex deflections in both the implicit and explicit dynamic methods. However, when elemental axial stresses are involved, it can be seen that meshes A, B and C give higher axial stresses than meshes D, E and F (as can be seen in the inset Figures. 3.13 and 3.14), which are almost identical. In terms of cost of computation, as can be seen in Table 3.4, Mesh A takes the lowest time to solve while Mesh F takes the highest time in both implicit and explicit dynamic methods. However, the cost of computation is significantly higher for the explicit dynamic method than for the implicit dynamic method. Considering the minimum number of elements required

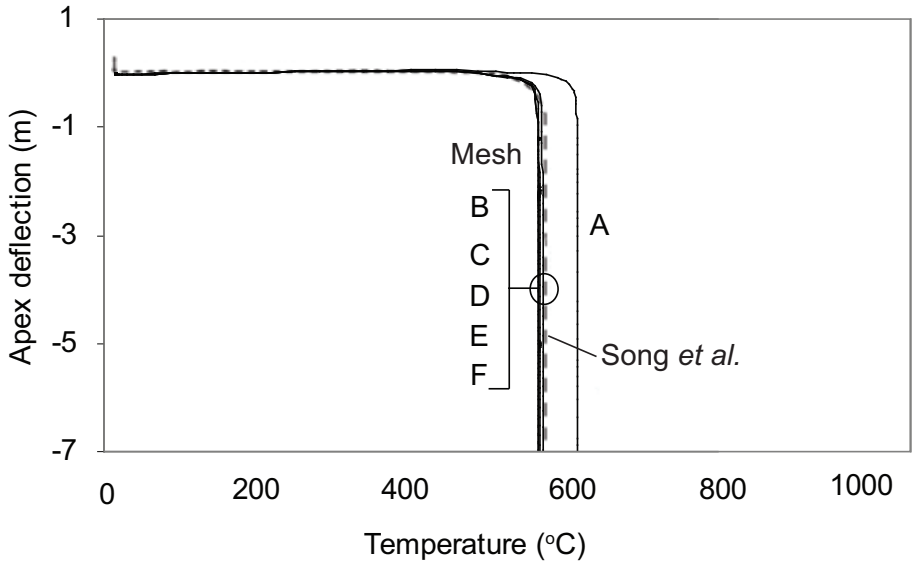

Figure 3.11: Apex deflection against temperatures for different mesh sizes with implicit method.

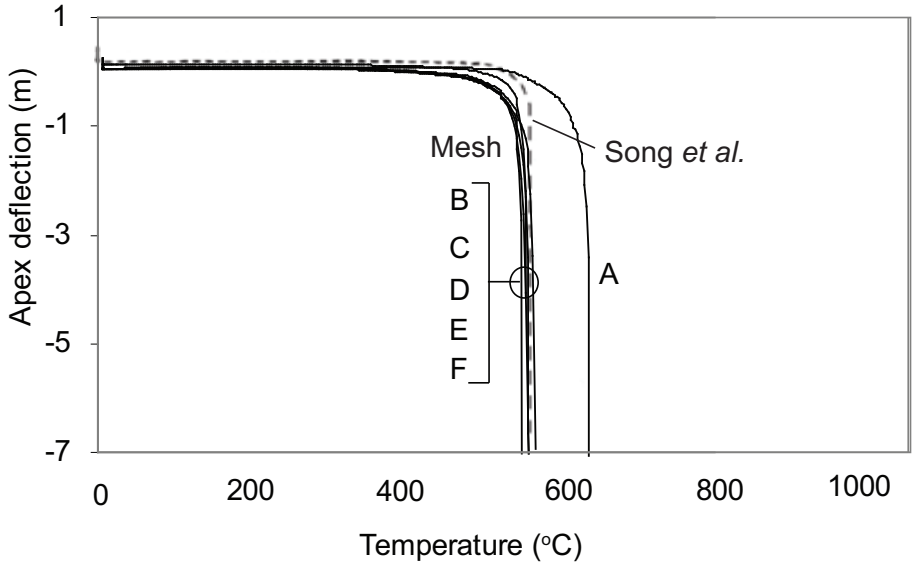

Figure 3.12: Apex deflection against temperatures for different mesh sizes with explicit method.

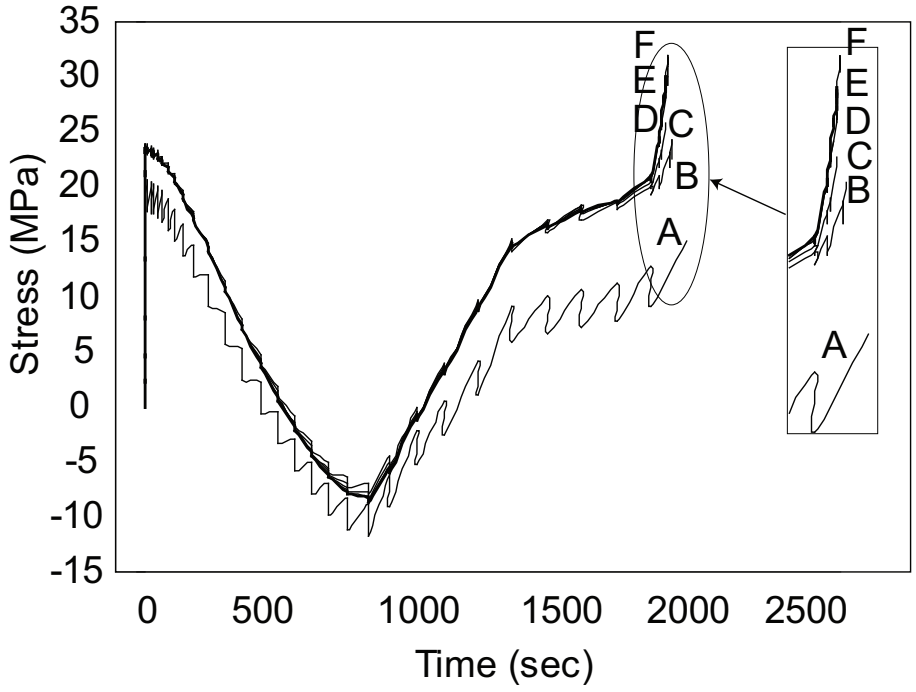

Figure 3.13: Axial stress at apex against time for different meshes with implicit method.

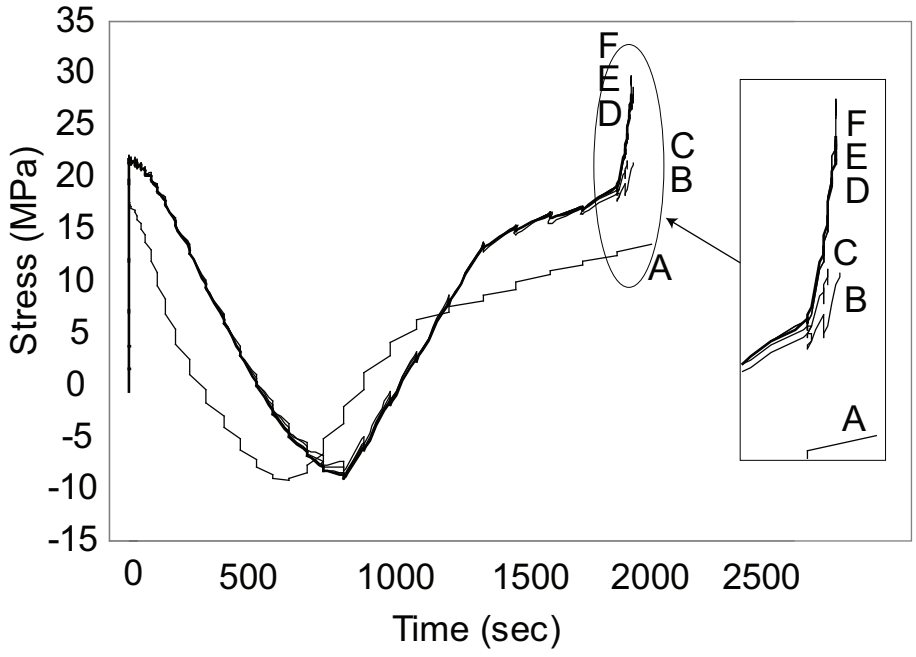

Figure 3.14: Axial stress at apex against time for different meshes with explicit method.

Table 3.4: Computation time for different mesh cases for implicit and explicit method.

Mesh cases	Implicit ($\alpha = -0.05$)		Explicit(time factor=1)	
	(haftol = 1)	(haftol = 100)	(ms = 1)	(ms = 4)
A	8m 1s	16s	1h 2m	32m
B	12m 36s	16s	1h 57m	1h 12m
C	28m 24s	17s	2h 28m	2h 30m
D	40m 2s	19s	15h 2m	3h 41m
E	52m 54s	21s	19h 49m	5h 3m
F	59m 6s	30s	5d 12h 56m	9h 16m

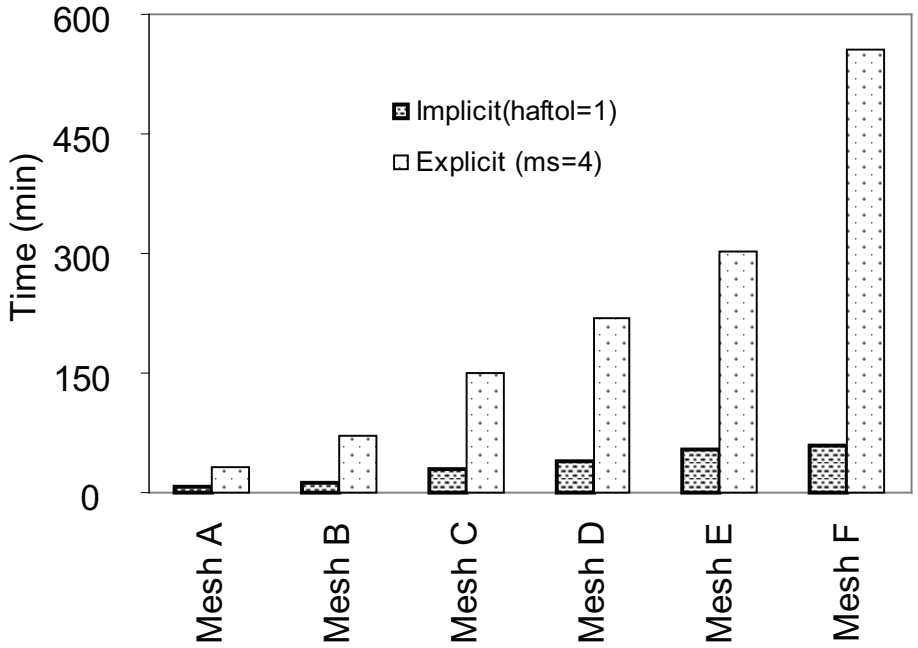

Figure 3.15: Comparison of computation time for different mesh cases for implicit and explicit method.

for obtaining accurate results and the time required to finish the analysis, it can be said that Mesh D is the optimum choice.

3.7 Separate comparative study

The parameters chosen for comparison in Section 3.6 were applicable to both the implicit and explicit dynamic methods. However, there are parameters that are applicable to either the implicit dynamic method or the explicit dynamic method, but not both. In the following subsections, the effect of these parameters has been

investigated.

3.7.1 Implicit dynamic method

A combination of factors of 1.0 for haftol and 0.00 for α gives the highest accuracy of results though the cost of computation is the highest with a computational time of 1830m (1d 8h 30m). An increase of the haftol factor and a slight increase of α significantly reduces the cost of computation as investigated below.

Effect of half-increment residual forces on structural response

A set of half residual force (haftol) factors, as given in Table 3.5, is selected

Table 3.5: Influence of half-increment residual forces as base reaction or, *haftol*, on solution time using implicit method ($\alpha = -0.05$).

haftol	CPU time
1	40m 2s
10	27m 0s
100	19s

for study with Mesh D and α=-0.05. As can be seen, if a smaller haftol is selected the cost of computation becomes very high as the time incrementation size gets increasingly smaller. A large haftol, on the other hand, reduces the cost of computation. Though, theoretically, smaller haftol gives more accurate results, as can be seen in Fig.3.16, it is seen that alteration of haftol has virtually no effect on the accuracy of results. There is only 1% loss of accuracy in the predicted snap-through-buckling temperature. It can be seen from Table 3.5 that it takes 40m 2s of CPU time for the implicit method (haftol of 1.0) as compared to 902m (15h 2m) (see Table 3.7) of CPU time taken by the explicit method (mass scaling factor of 1.0). When the value of haftol is increased to 100 times the reaction force, the CPU time reduces to 19s with a 1% loss in accuracy of the snap-through-buckling temperature.

Effect of artificial numerical damping on structural response

Four different numerical damping parameters, α, have been considered in this study: -0.333, -0.15, -0.05, and 0 with Mesh D and haftol of 1.0 times the reaction forces. Table 3.6 and Fig. 3.17 present the results of the study. As can be seen, if a smaller α is selected the cost of computation becomes significant while a larger α reduces the cost of computation significantly. Though, theoretically, a smaller

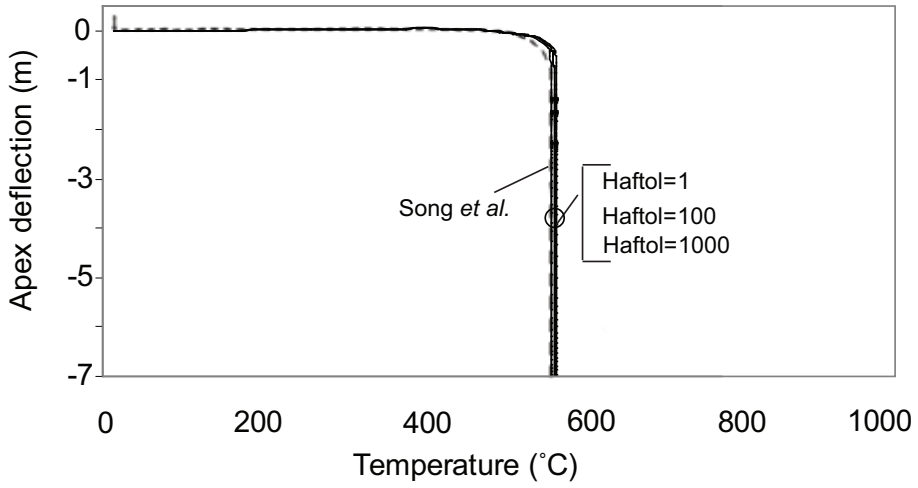

Figure 3.16: Influence of different half-increment residual forces on apex deflection using implicit method.

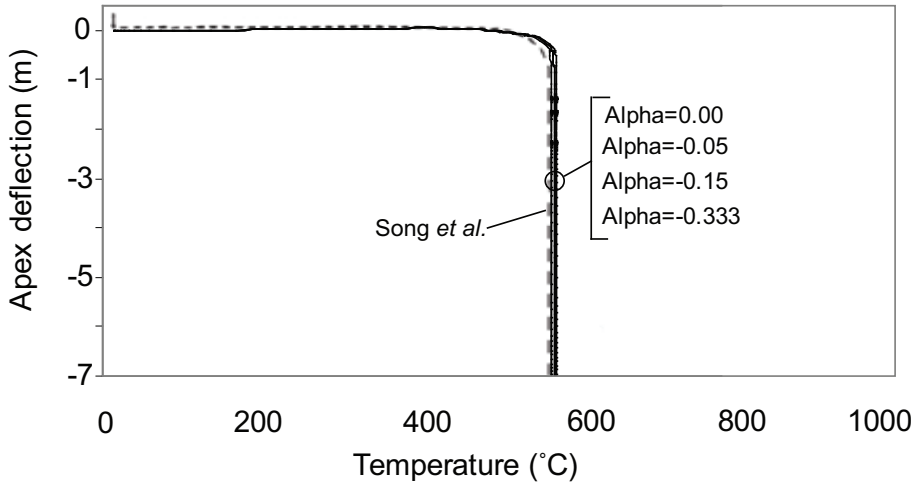

Figure 3.17: Influence of artificial numerical damping parameter on apex deflection using implicit method.

α gives accurate results and larger α gives inaccurate results, in the present study, as can be seen in Fig. 3.17, it is found that alteration of α has virtually no effect on the accuracy of results. It can be seen from Table 3.6 that it takes 1830m (1d

Table 3.6: Influence of artificial numerical damping, α, on solution time using implicit method (haftol=1.0).

Alpha	CPU time
-0.333	20m
-0.15	35m
-0.05	40m 2s
0	1830m

8h 30m) of CPU time for the implicit dynamic method with α=0 (haftol=1.0) as compared to 902m (15h 2m) (see Table 3.7) of CPU time taken by the explicit

Table 3.7: Effect of natural or true time scale using explicit dynamic method (Mesh D).

Implicit (haftol=1.0)	Explicit (true time scale and mass scale factor=1.0)
40m 2s	15h 2m

method (mass scaling factor of 1.0). When α is reduced to -0.333, the CPU time reduces to 20m. With an increased factor of haftol of 100, the cost of computation cost is even more reduced. As can be seen from Table 3.8, it takes 2h 30m 56s with α=0.0 and only 19s with α=-0.333.

Table 3.8: Influence of artificial numerical damping, α, on solution time using implicit method (haftol=100.0)

α	CPU time
-0.333	19s
-0.15	57s
-0.05	10m 57s
0	2h 30m 56s

3.7.2 Explicit dynamic method

In the explicit dynamic method, the parameters that influence the efficiency and accuracy are loading speed (or time scaling) and mass scaling. A combination of time scaling and mass scaling with factors of 1.0 each usually gives the highest accuracy of results.

Effect of loading speed on structural response

For a quasi-static method, the cost of computation becomes higher if the natural or true time scale of loading is used. To obtain an economical solution, this natural time of loading on structure needs to be scaled to a shorter time period and yet to keep the response of the structure almost static and give accurate results. If the natural time of load acting on the structure is larger than the natural period of vibration of the structure, then the model can be considered as almost static (Clough and Penzien, 1993). When the temperature increases, the model becomes highly nonlinear because of continuous stress redistribution. Compressive stresses can change direction and be transformed into tensile forces. To observe the effect of loading duration the structure is kept at ambient temperature and load is applied at specific rates. To assess the viability of loading rate, different loading durations have been considered according to Table 3.9. The results are compared against the results of the static and implicit dynamic

Table 3.9: Different loading durations.

Parameter	Values of parameter
Loading duration/ time scaling	1, 10, 100 and 500 sec

methods. The resultant reaction forces at the left column base are plotted against applied displacement as shown in Fig. 3.18 and 3.19. (Negative values indicate inwards reactions.)

For the static method, displacement-controlled analysis - an analysis, where, instead of loading, a displacement at a certain point is specified in the model, and reaction forces are calculated - is employed to make it easier to converge. As can be seen, for both implicit and explicit dynamic methods, loading times of 1.0 sec do not match with the static results as the dynamic effects are very much pronounced here. However, for loading times of 10.0 sec and higher, the results become smoother and get closer to the static method up to apex displacements of 5.0m, beyond which noise in the results is observed. This noise is caused by the dynamic effects as the materials are softened due to plasticity. Though the reactions are getting smoother and closer to the static results, it is still unclear if the dynamic effects are still pronounced there. To investigate this, kinetic energy,

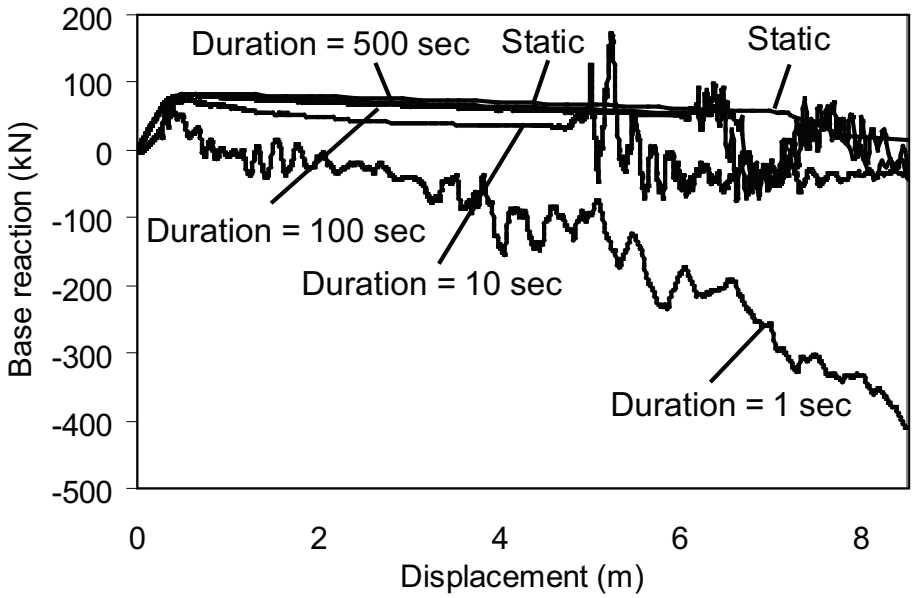

Figure 3.18: Comparison of column base reactions of static method and *implicit* dynamic method for different duration of loads.

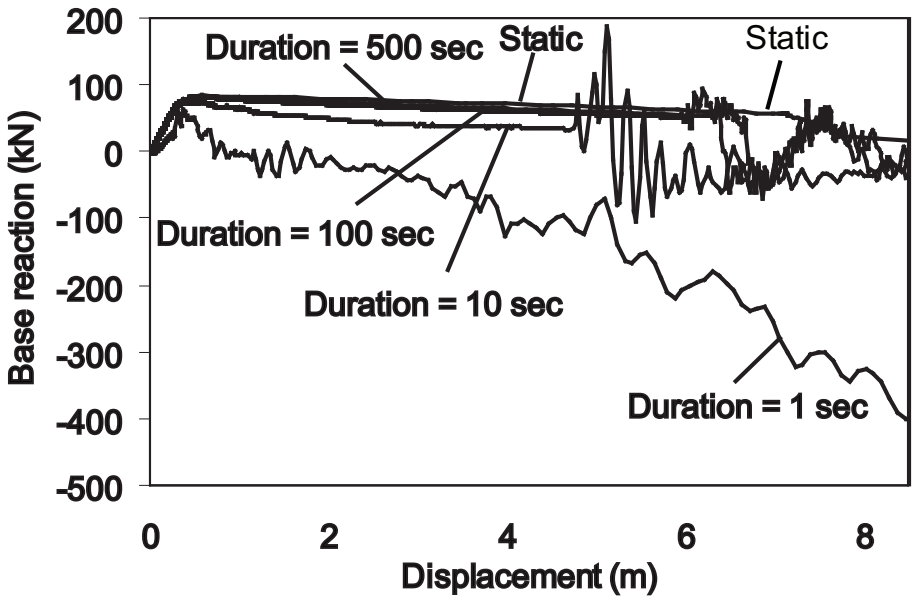

Figure 3.19: Comparison of column base reactions of static method and *explicit* dynamic method for different duration of loads.

KE, and internal energy, IE, and their ratio against time are plotted in Fig. 3.20 and Fig. 3.21 for the implicit and explicit dynamic methods respectively.

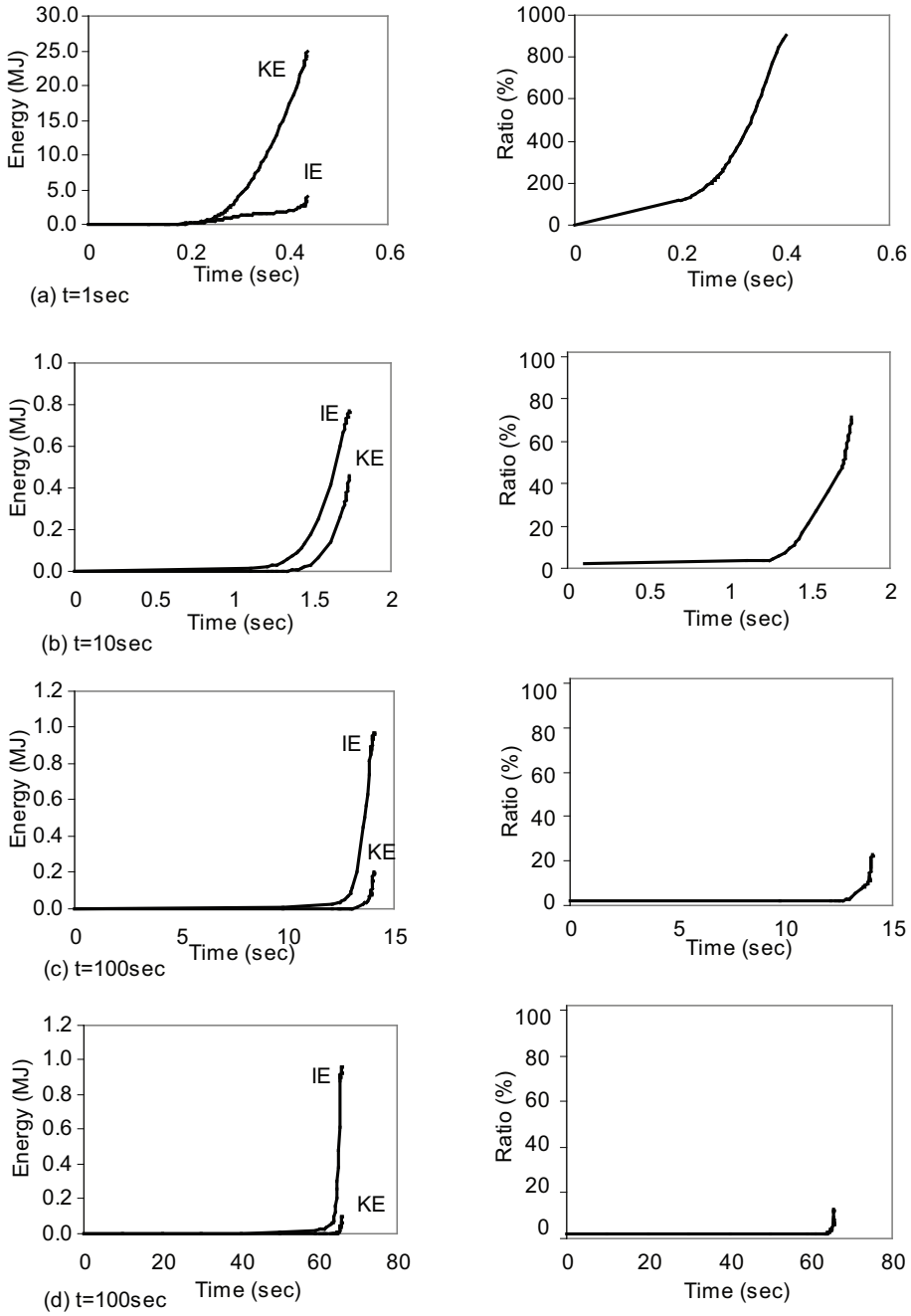

Figure 3.20: Kinetic Energy, KE, and Internal Energy, IE, history of different duration of loads using *implicit* method.

It can be seen that for smaller loading duration, say for 1.0 sec, the kinetic energy is much higher than the internal energy, and it indicates the behavior is fully dynamic i.e. no quasi-static behavior at all. As the duration of loading

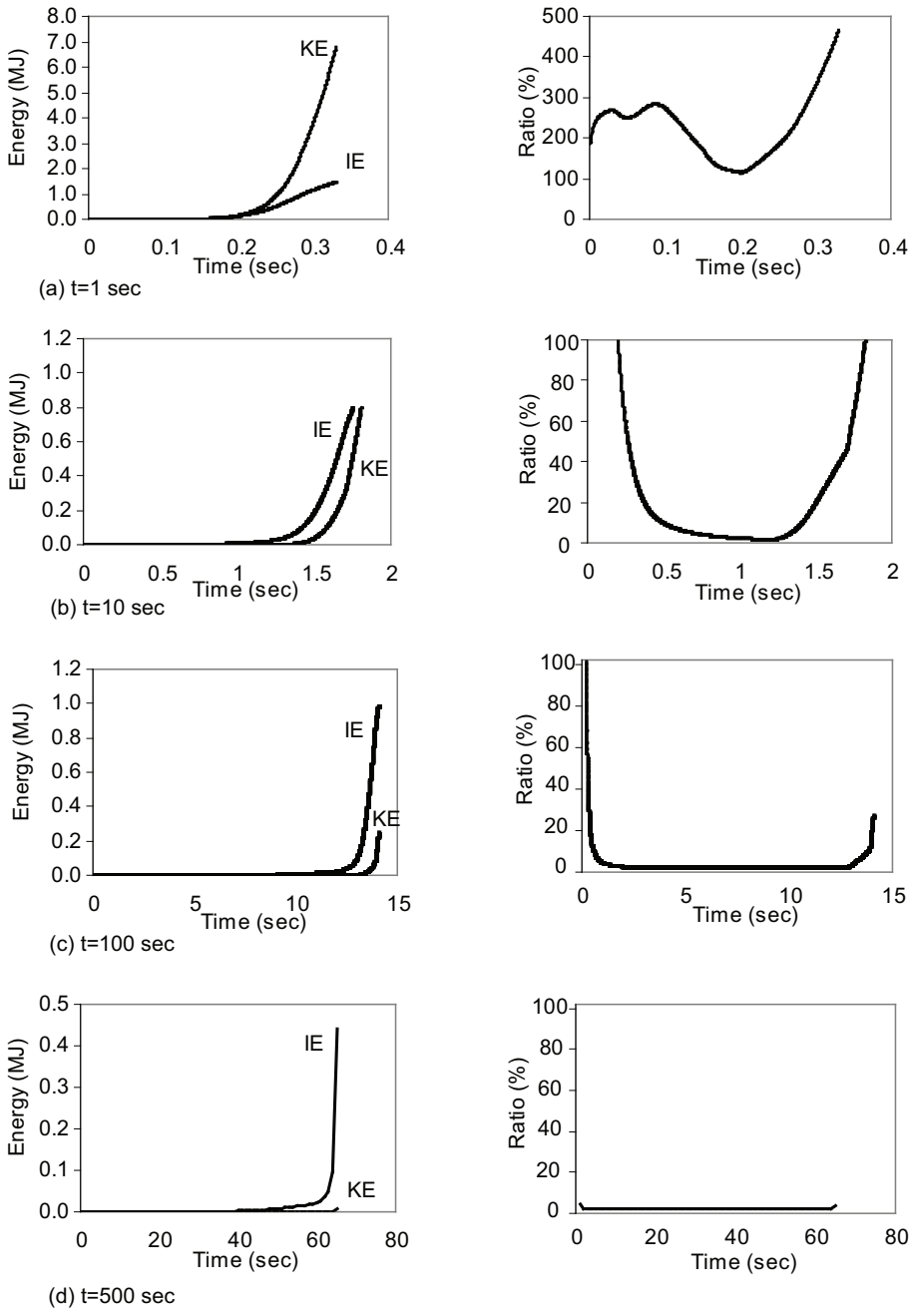

Figure 3.21: Kinetic Energy, KE, and Internal Energy, IE, history of different duration of loads using *explicit* method.

is increased the kinetic energy starts to decrease but still the dynamic behavior is pronounced as the ratio is still over 10% for loading duration up to 100 sec. When loading duration is over 500 sec the ratio of kinetic energy is lower than 5%, which ensures quasi-static behavior. It can be seen that when loading duration is higher than 500.0 sec, the analysis becomes unnecessarily time-consuming. Based on the analysis, it can be inferred that both implicit and explicit dynamic methods can be used to model quasi-static behavior, though there are certain limitations. Ramped loads make the structure dynamically responsive instead of statically or quasi-statically responsive.

Effect of mass scaling on structural response

Speeding up of load is not effective when a rate-dependent material, i.e. material whose properties varies upon time or other parameters such as temperature, is used. In such cases, increasing the density of material artificially, called mass scaling, speeds up the solution process. Mass scaling, in essence, increases the global stability limit of elements and fewer increments are needed to perform an analysis. In this study, a fixed mass scaling procedure is used. To assess the viability of mass scaling, six different factors according to Table 3.10 are used.

Table 3.10: Different mass scaling.

Parameter	Values of parameter
Mass scaling factor	1, 4, 9, 16, 25 and 100

The damping parameters remain the same in all the cases. The results for apex deflection and axial stress are plotted in Fig.3.22 and Fig. 3.23, and in terms of solution time in Table 3.11 and Fig. 3.24. As can be seen from Table 3.11 and Fig.

Table 3.11: Influence of mass scaling factors on solution time using explicit dynamic method (Mesh D).

Mass scaling factor	CPU time
1	15h 2m
2	11h 56m
4	3h 41m
9	2h 29m
16	1h 45m
25	1h 1m
100	56m

3.24, the increase of mass scaling reduces the cost of computation significantly

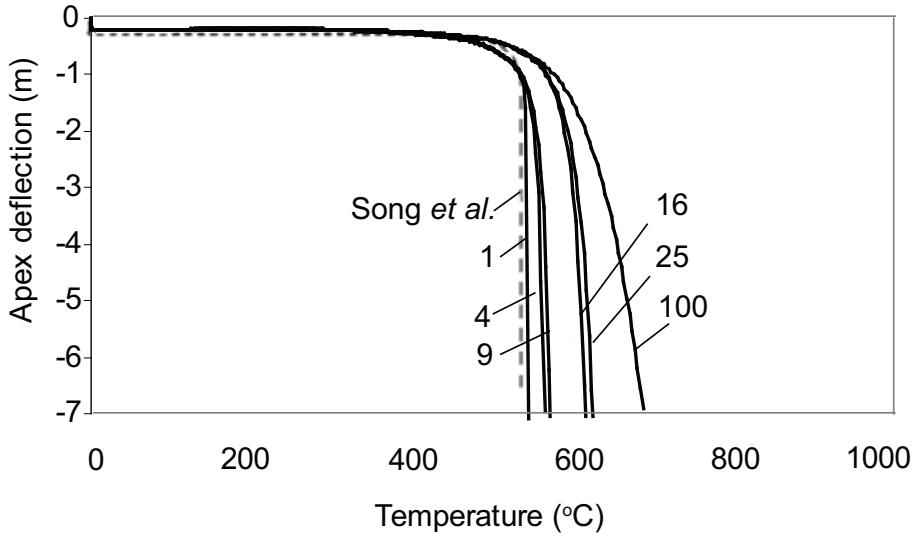

Figure 3.22: Influence of different mass scaling factor on apex deflection using the explicit method.

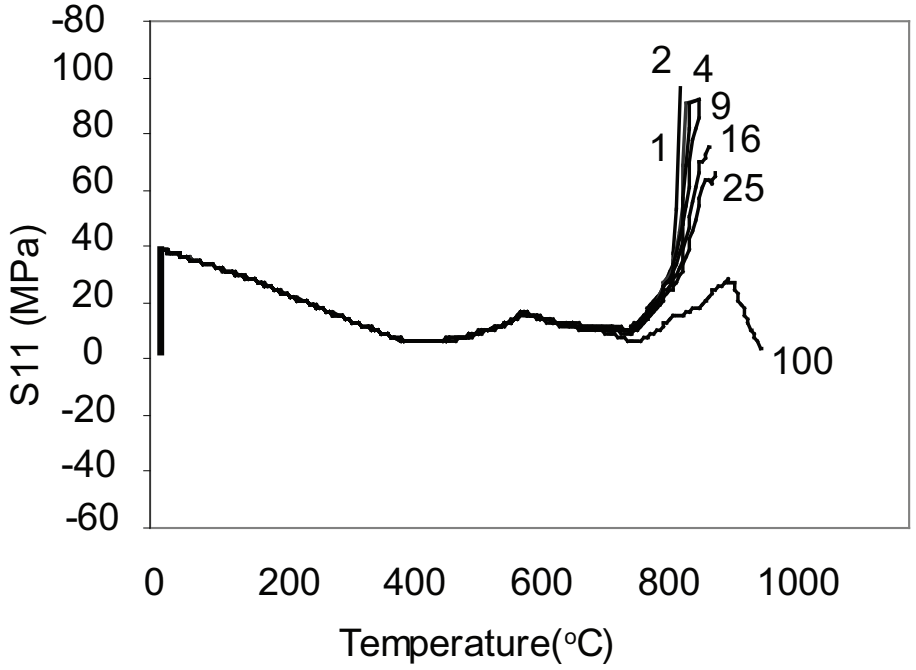

Figure 3.23: Influence of different mass scaling factor on axial stress using the explicit method.

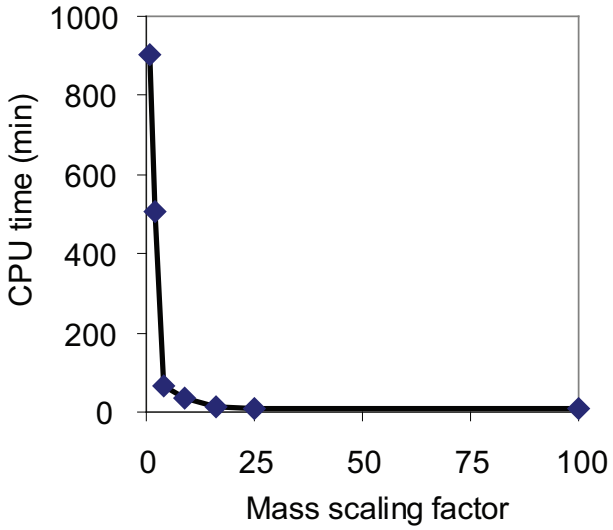

Figure 3.24: Mass scaling factor against solution time using explicit method.

though the accuracy of results is also reduced. As can be seen from Fig.3.22, the results are significantly different from the accurate results (i.e. when implicit and explicit dynamic analysis give the same results and mass scaling factor = 1.0). For example, there is a 10% loss in accuracy in results of apex deflections when the mass scaling factor is increased from 1.0 to 4.0, and the inaccuracy is more than 100% while the mass scaling factor is increased to 100.0. This indicates that if time scaling and mass scaling factors are not chosen carefully it is difficult to obtain reasonably accurate results with a reduced cost of computation by means of the explicit method. However, it can be seen from Figs. 3.22 and 3.23 that the response of the structure remains almost the same before the instability occurs.

3.8 Comparative study for three dimensional models

In the previous sections, comparisons have been made for two-dimensional models. However, as there are possibilities that out-of-frame deflection can have an effect on the overall behavior of the structure, analysis of three-dimensional frames should be investigated and compared. In an earlier paper by the authors (Rahman *et al.* 2012), it has been established that the increased number of frames in the out-of-plane direction can increase the overall stability of the structure during local fires.

The model used in the three-dimensional analyses is geometrically similar to the two-dimensional model except there are a number of frames (five frames) extruded along the out-of-plane directions connected by purlins and rails as can

be seen in Fig. 3.25. Since the two-dimensional model is stiffer, i.e. the snap-

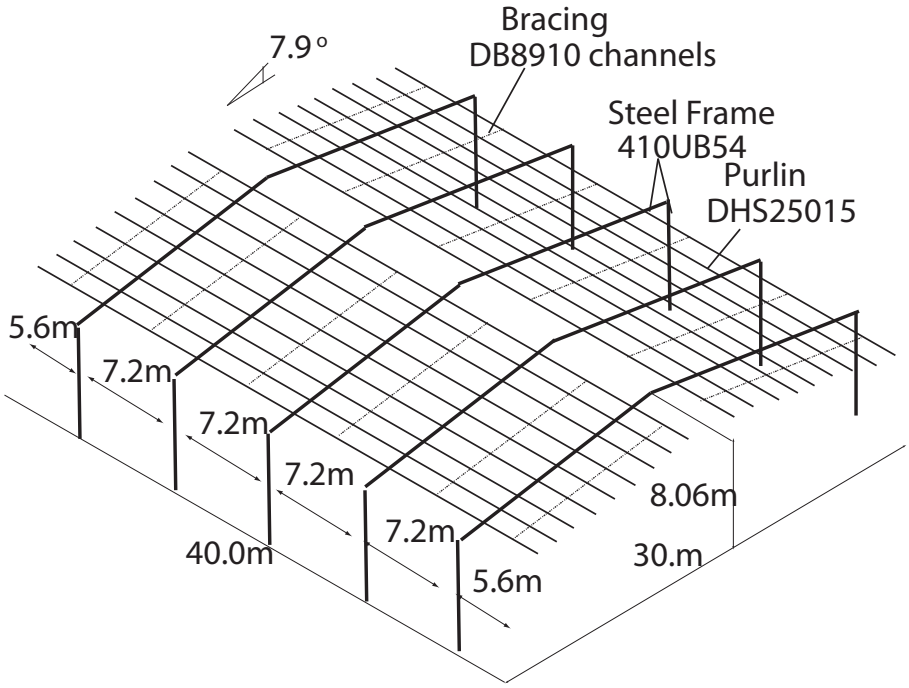

Figure 3.25: Three dimensional model for study.

through-buckling collapse occurs at a higher temperature and it does not undergo any instability in the out-of-plane direction, the cost of computation for the three-dimensional version is higher. Moss *et al. 2009)* has been selected for the three dimensional study to reduce the cost of computation. The whole frames have been meshed with three-dimensional Euler-Bernoulli beam elements (B31).

The values for haftol and α are taken to be the same as for the two dimensional implicit dynamic method. The mass scaling factors of 2.0 and 4.0 have been used for the explicit dynamic method. As before, with a mass scaling factor of 1.0, which gives closer results to the implicit dynamic analysis, the explicit dynamic method has virtually been impossible to carry forward as the cost of computation has been high. The comparison of results between the implicit and explicit dynamic methods for three dimensional study is shown in Fig.3.26. It can be seen that with a lower mass scaling factor the implicit and explicit dynamic methods results closely match, as expected. However, the difference in results is more pronounced in three dimensional analysis than in two dimensional analysis when higher mass scaling factors are used.

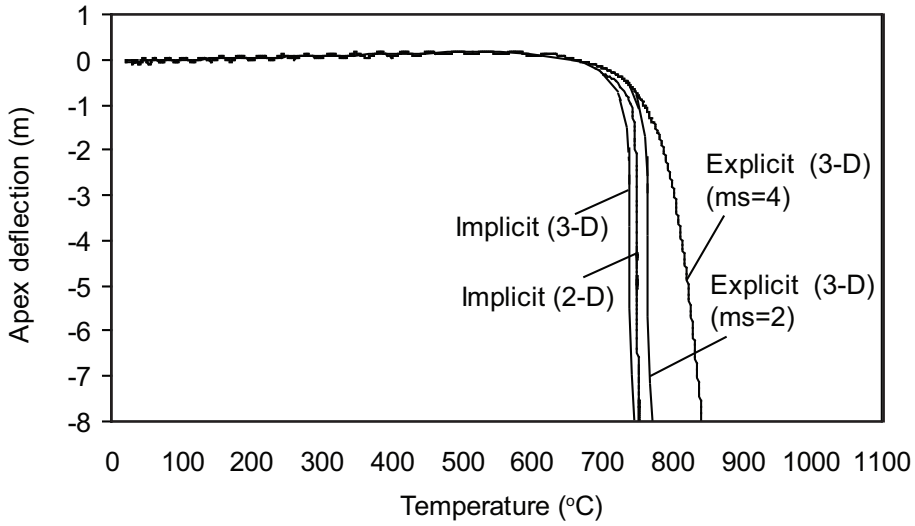

Figure 3.26: Comparison of apex deflection for three dimensional frame

3.9 Speed up of solution process by computer processor parallelization

As mentioned before, there are as many as eight parallel processors that have been used for analysis. Use of multiple processors may not necessarily enhance the efficiency of computation. The efficiency, η, of multiple processors usually follows Eqn. 3.10 (Harewood and McHugh 2007).

$$\eta = 100 \times sgn(\Gamma) \times \sqrt{\Gamma}, \tag{3.10}$$

where

$$\Gamma = \left[\frac{t_1}{t_x x} - \frac{1}{x}\right] \div \left[1 - \frac{1}{x},\right] \tag{3.11}$$

$sgn(\Gamma)$ is the sign of Γ, a positive sign indicates time saving in solution and a negative sign indicates increase of solution time when multiple processors are used. t_1 is the solution time with a single processor and t_x is the solution time when x processors are involved in the calculation.

Clearly, from Table 3.12, it can be seen that for the implicit dynamic method, increasing the number of processors does not speed up the solution process; instead efficiency is lost as the number of processors are increased. This loss of efficiency occurs because extra computation time is required for assembling the system equations together from each processor. This phenomenon suggests that, for an implicit dynamic method a single faster processor should improve the solution process. On the other hand, increasing the number of processors speeds up the solution process when explicit dynamic method is used, though increase of processors does not linearly speed up the solution time, rather the linearity

Table 3.12: Comparison of efficiency of implicit and explicit method when different number of computer processors are used (Mesh D).

Method of analysis	Number of computer processors	CPU time	Efficiency %
Implicit	1	8m 1s	-
	2	8m 59s	-33
	4	9m 11s	-21
	8	10m 21s	-18
Explicit	1	15h 2m	-
	2	13h 13m	37
	4	12h 1m	29
	8	11h 51m	20

is diminishing. The solution process involving the explicit dynamic method is faster here because no overhead is involved for assembling system equations from different processors.

3.10 Strategies for optimal solution

In order to achieve optimal solution, solution parameters must be carefully chosen, otherwise, unnecessary overhead cost would reduce the overall efficiency of the solvers. For the implicit dynamic method, a haftol factor of 100 and α of -0.15 would be the best combination. In terms of mesh size, a coarse mesh reduces the accuracy of the results and so a convergence study should be undertaken. For the explicit dynamic method, the mass scaling factor should be within the range 2.0 to 4.0, as below 2.0 the cost of computation would be prohibitively high and above 4 the quality of results severely degrades. This will retain the quasi-static behavior of the model without losing accuracy of results. For the implicit dynamic method, a single faster processor would be the best option whereas for the explicit dynamic method a higher number of parallel processors solves the model faster. This indicates that implicit method can suitably used in most desktop computers that employ a single faster processor. For the present study, where a choice between the implicit and explicit dynamic methods must be made, it is found that the implicit method is better in terms of cost of computation if true time scale is used.

3.11 Conclusions

In this paper, implicit and explicit dynamic methods have been used to simulate the collapse of steel portal frames in fire. For the benchmark frame, it has been shown that both methods of analysis produce similar results when the solution options within ABAQUS are selected to achieve the most accurate results, with the implicit dynamic method solving in 40 minutes compared with 15 hours for the explicit dynamic method. However, the computational cost for the implicit dynamic method can be reduced further to 19 seconds with only 1% loss in accuracy of the snap-through-buckling temperature by setting haftol of 100 and numerical damping of -0.15. On the other hand, reducing the cost of computation for the explicit method to under 4 hours was achieved within 10% loss in accuracy by setting a mass scaling factor of 4.0. In most cases, a desktop computer with a single faster processor is suitable for the implicit dynamic method. The implicit dynamic method is both more accurate and significantly more computationally efficient and viable than the explicit dynamic method for the simulating the collapse of steel portal frames in fire.

Chapter 4

Effect of column base strength on steel portal frame building in fire

4.1 Introductory remarks

In the UK, single-storey steel portal frame buildings account for over 50% of the constructional steelwork used each year. In fire, however, steel rapidly loses its strength and stiffness, and so for steel portal frame buildings designed in fire boundary conditions, expensive fire protection is often required in order to ensure structural integrity and prevent premature collapse.

The UK Building Regulations (FPA, 2008) make reference to the SCI design method (Simms and Newman, 2002), which suggests that expensive fire protection is only required for columns but not necessary for rafters, so long as the column bases are designed to resist an overturning moment M_{OTM} calculated in accordance with the SCI design method. The SCI design method makes the assumption that the columns remain at ambient temperature (since fire protection is applied) and that both rafters are heated uniformly to a maximum temperature of 890°C, which is the temperature at which 6.5% of the ambient strength of steel is assumed to remain. For a single-span building, it assumes that the rafters undergo symmetrical inward snap-through-buckling, after which the frame stabilizes with the rafters being suspended below the columns in catenary action (see Figure 4.1 and Figure 4.2). The SCI design method also assumes that the inverted position of the rafter after snap-through buckling is the ultimate limit state of the frame. In the UK, if a frame is designed in accordance with the SCI design method and the column bases are designed to be able to resist M_{OTM}, the designer may assume that the columns will also remain 1° from the vertical, thus preventing inwards collapse of the walls. In contrast to the assumption of the SCI design method, the frame may undergo asymmetrical snap-through-buckling and they may sway either acceptable inwards mode or outwards unacceptable mode,

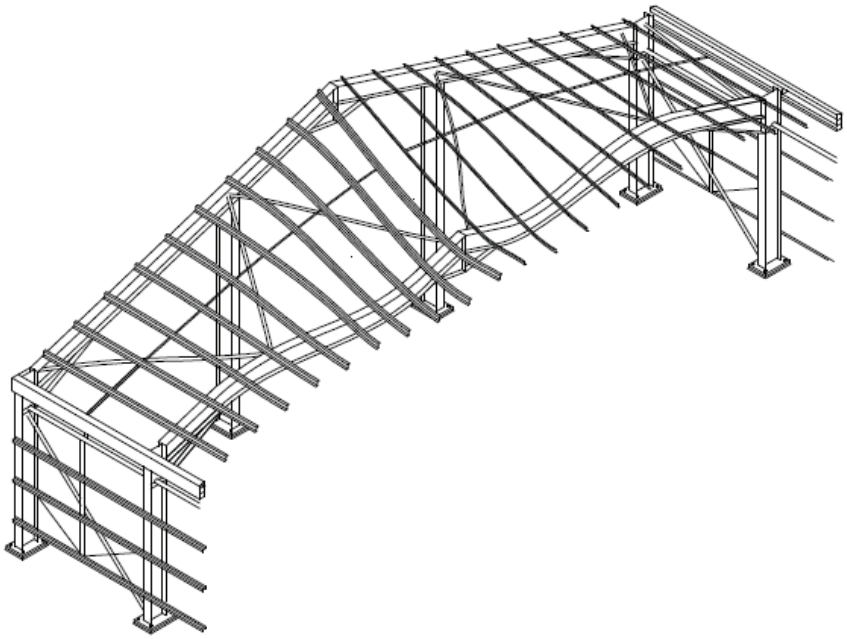

Figure 4.1: Symmetrical inwards snap-through buckling collapse mechanism as assumed in SCI design guide (3-D) (Simms and Newman 2002)

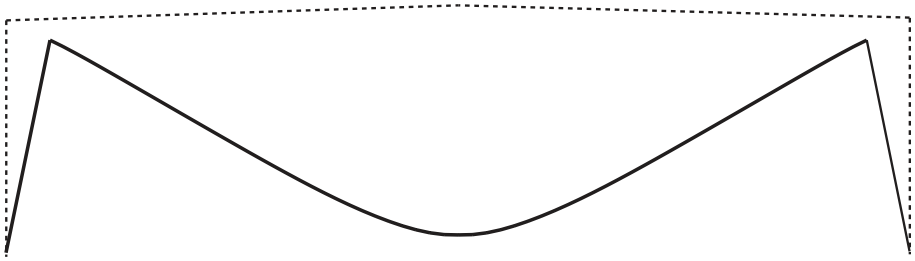

Figure 4.2: Symmetrical inwards snap-through buckling collapse mechanism (2-D)

as can be seen in Figure 4.3 (O'Meagher *et al.*, 1992).

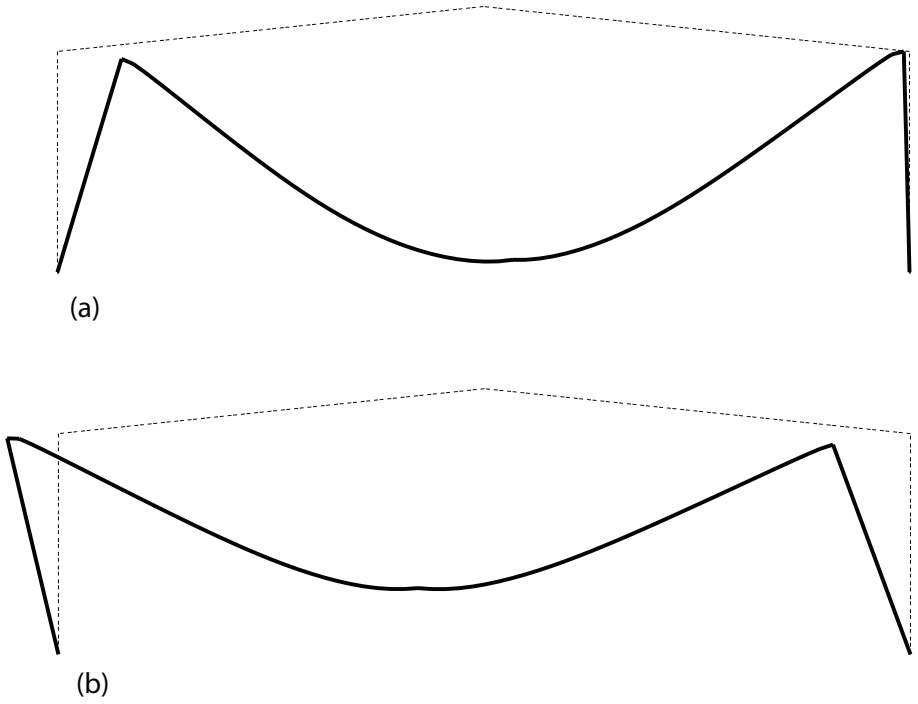

Figure 4.3: Asymmetrical (a) acceptable and (b) unacceptable collapse mechanisms after O'Meagher *et al.* (1992)

The objective of this chapter is to evaluate the existing SCI design method. In this paper, the column base overturning moment M_{OTM}, calculated in accordance with the SCI design method, is assessed using both 2-D and 3-D non-linear elastic-plastic implicit dynamic finite element analyses. The 2-D and 3-D finite element models are each verified against the results of Song *et al.* and Moss *et al.*, respectively. A frame similar to the exemplar frame given in the SCI design guide is then modelled, taking into account the limiting strength of the column base, M_{OTM}.

4.2 Standard building

4.2.1 Building dimensions

In the study described in Section 4.6, both 2-D and 3-D finite element models of a single-span building in fire will be considered. This building will be referred to as the Standard Building. The overall frame dimensions of the Standard Building are the same as those used for the Exemplar frame described in the SCI design guide (Simms and Newman, 2002), shown in Figure 4.3. As can be seen, the span

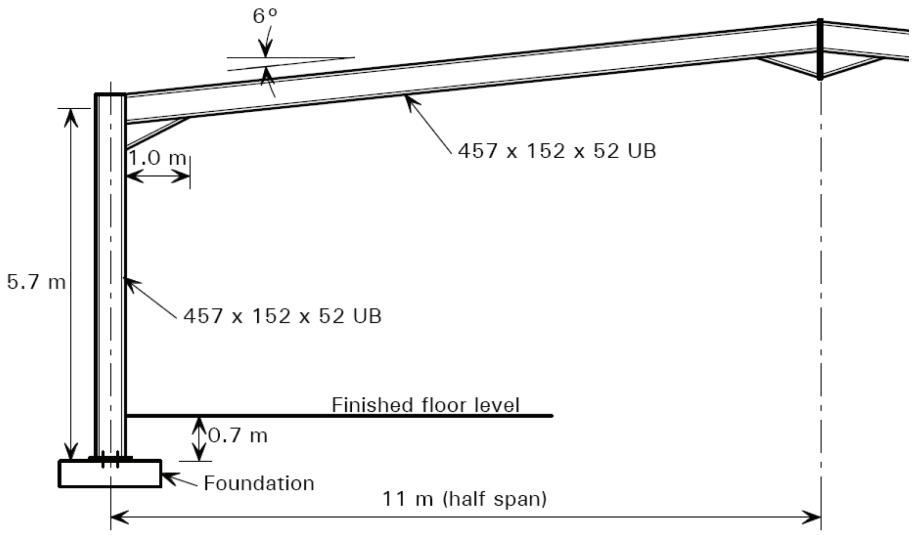

Figure 4.4: Frame used in SCI worked example (Simms and Newman 2002)

of each frame is 22.0m with a pitch of 6°, and height to the eaves of 5.7m. The distance between the adjacent frames is 6m. In the SCI design guide, the columns and rafters are UB 457x152x52 S275. Since the SCI design guide only considers a 2-D representation, the cold-formed steel sections and spacing used for the purlins and the side rails are not specified. In this paper, it is assumed that the purlins and side rails are Steadman 17015 zed sections (Steadmans, 2010) with a yield stress of 390N/mm^2, spaced at 1500mm centers for both columns and rafters.

Figure 4.5 shows a 2-D representation of one of the frames in the Standard Building considered in this paper. To simplify the model, the haunch is not modelled. It should also be noted that the cross-section properties used for the members are slightly different than those given in standard section property tables. This is because the finite element program ABAQUS used for the analysis is unable to provide default cross-sections with fillets and modelling cross-sections with fillets will significantly increase the computational time. The section properties without fillets are given in Table 4.1.

Table 4.1: Properties of equivalent steel sections (without filets) used for the Standard Building.

Section	A	σ_y	I_{maj}	W_{pl}	$M_{pl,c}$
	cm^2	$\frac{N}{mm^2}$	cm^4	cm^3	kNm
Columns / Rafters	65.8	275	20969	1077	296.2
Purlins	4.52	390	197	19.4	5.3

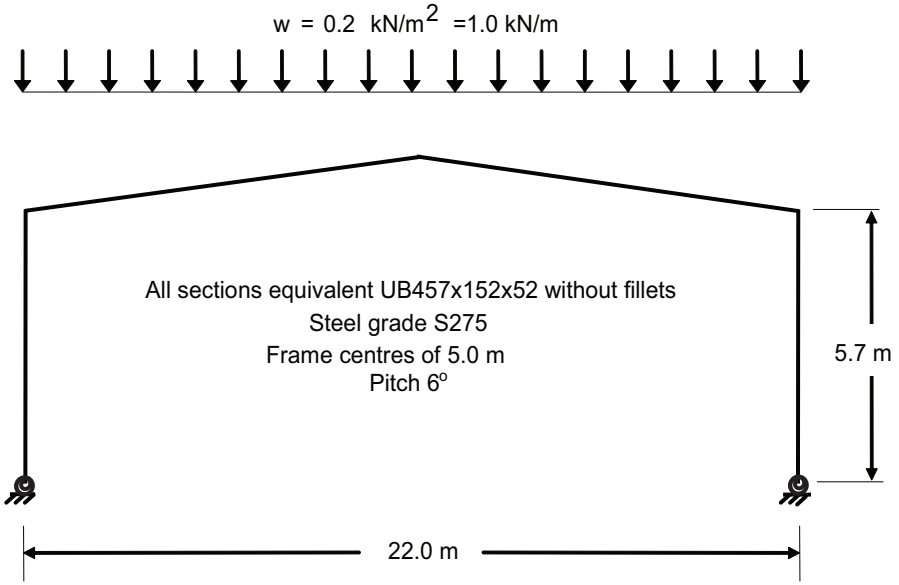

Figure 4.5: Details of standard frame with rotational spring at column base

As can also be seen from Figure 4.5, a vertical dead load of 1.0 kN/m is applied to the frame as a uniformly distributed load. This vertical dead load is consistent with the SCI design guide in which 1.0 kN/m is also applied including the self-weight of the purlins. In order to be consistent with the SCI design guide, for the case of the 2-D model, the purlins are not physically modelled. On the other hand, in the 3-D model the purlins are modelled and have self-weight. For the case of the 3-D model, therefore, the vertical dead load applied to each frame is reduced to 0.75 kN/m. Both 2-D and 3-D frames therefore have the same total vertical dead load.

4.2.2 Overturning moment

For the Standard Building, according to SCI design method, the value of M_{OTM} that needs to be resisted is 61.2 kNm. (It should be noted that if this calculation is repeated including the fillets and haunches, then the value of M_{OTM} required reduces to 54.2 kNm). A value of M_{OTM} of 61.2 kNm represents approximately 20% of the plastic moment capacity of the section, $M_{pl,c}$, of 296.2 kNm. The SCI method assumes that both the columns and the column bases are fully protected from fire. In reality, when column is protected from fire with concrete covering, the temperature usually does not rise more than 350°C, and almost all of the strength of the material is retained. The Authors have run simulations in the past and this has had little effect on the results. It should be noted that, the SCI method does not state the rotational stiffness of the column base.

4.2.3 Material properties at elevated temperature

Figure 4.6 shows engineering stress-strain curves for steel at elevated temperatures

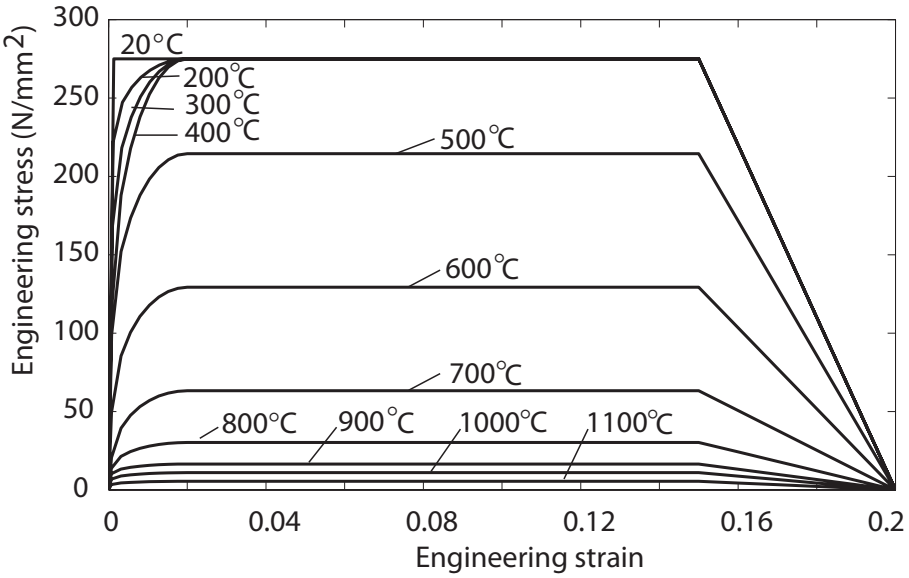

Figure 4.6: Engineering stress-strain curves for steel grade S275 at different temperatures after Eurocode 3 (CEN 2005)

ranging from 22°C to 1100°C. In this paper, the temperature of the portal frame will be increased until collapse of the frame. These engineering stress-strain curves are obtained from Eurocode 3 (CEN 2005). It should be noted that strain-hardening and creep are inherently considered in the stress-strain curves as given by the code.

Figure 4.7 shows the variation of yield strength and Young's elastic modulus of steel against temperature. The values shown are normalized against their corresponding values at ambient temperature. As can be seen, there is no loss in yield strength for temperatures up to 400°C; the elastic modulus starts to decrease from 100°C.

The remaining thermal properties required to predict the changed behaviour of the steel structure is the coefficient of thermal expansion. Figure 4.8 shows this coefficient according to Eurocode 3. The steel is considered as an isotropic material with a density of 7850.0 kg/m^3 as required by dynamic and quasi-static analysis. In this study, the Poisson's ratio is taken as 0.3 under fire conditions. Generally, the Poisson's ratio is assumed to be independent of temperature (Kaitila, 2002; Zha, 2003).

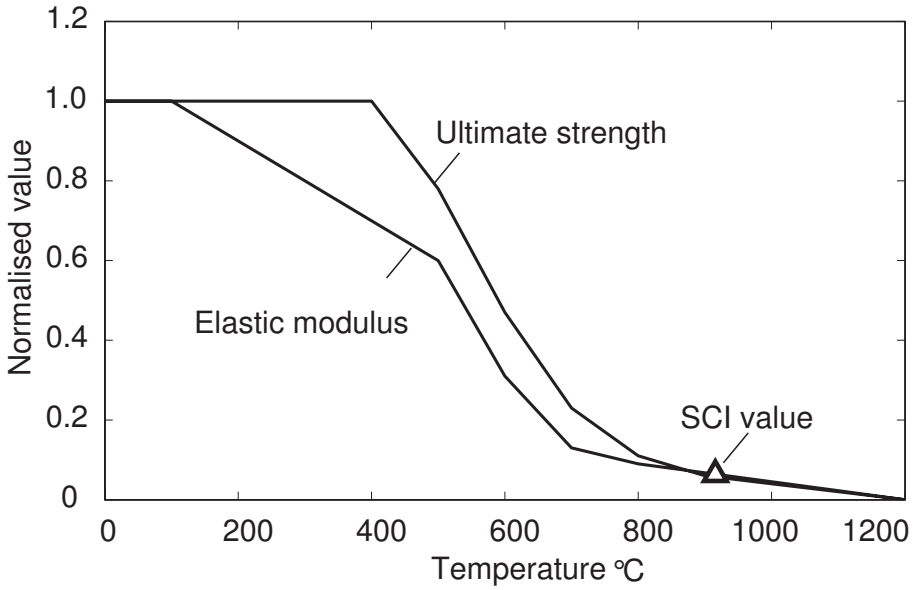

Figure 4.7: Variation of normalised yield strength and young's elastic modulus at different temperatures after Eurocode (CEN 2005)

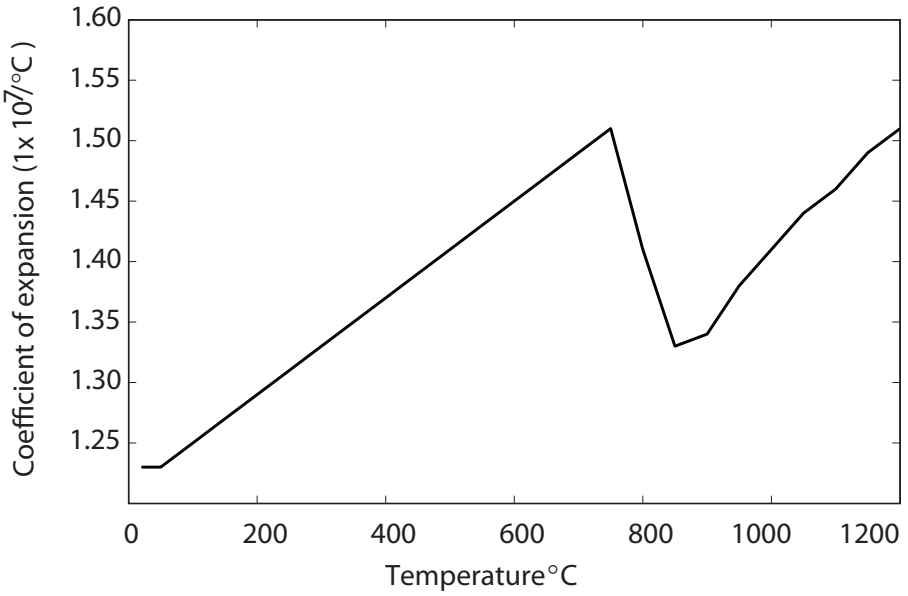

Figure 4.8: Coefficient of thermal expansion of steel grade S275 at different temperatures after Eurocode 3 (CEN 2005)

4.3 Fire model

The ISO834 standard time-temperature curve (Figure 4.9) is assumed for the

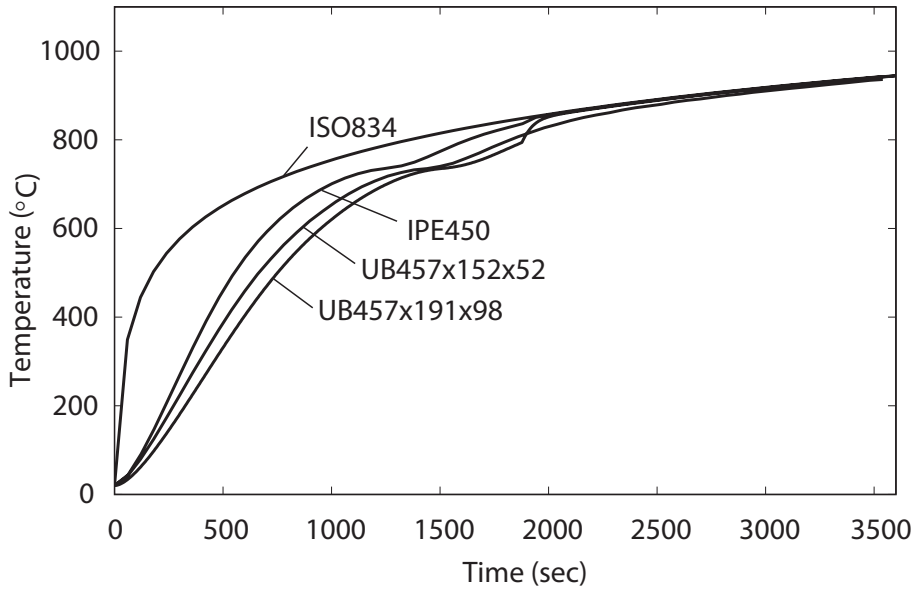

Figure 4.9: ISO834 standard time-temperature curve (fire curve) and computed Eurocode 3 curve for various sections (ISO 1975 and CEN2005)

combustion of gases that surround the steel frames exposed to fire. Although it is well-known that this curve does not represent a practical fire, it is widely used in fire engineering; the ISO834 curve is also used in the SCI design guide. In this paper, the developed temperature is calculated according to Eurocode 3, based on this standard time-temperature curve, and is applied to the steel section; each steel section has a different associated time-temperature curve.

4.4 Finite element modelling

4.4.1 Finite element model

The general purpose finite element program ABAQUS (Simulia 2009) is used for the numerical investigations. Figure (Figure 4.10) shows details of the typical finite element model. The effect of different number of elements for the column and rafter was investigated in order to provide both accurate results and reduced computation time. It was found that 96 elements were sufficient for the analysis with 16 elements for each column and 32 elements for each half of the rafter for the 2-D plane frame model.

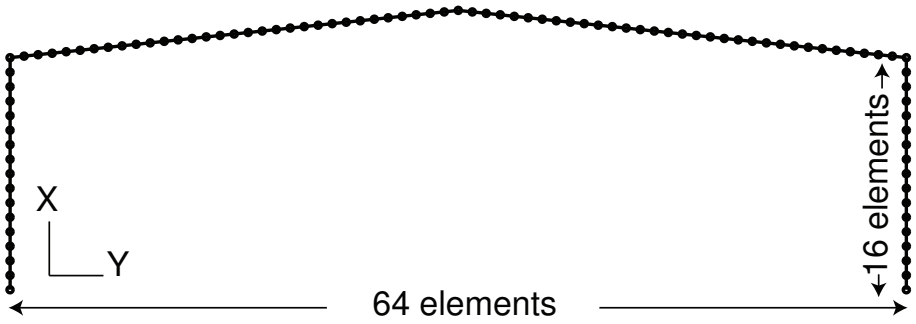

Figure 4.10: Details of finite element mesh for 2-D frame

The columns and rafters are modelled using beam elements B21 (2-D) and B31 (3-D). Note that other possible second order elements, e.g. B22, B32 are avoided due to the so-called 'volumetric locking' problem which is induced by the large elemental strain in the deformed configuration. In the numerical models, non-linear stress-strain material curves are modelled. Since the analysis involves large inelastic strains, the engineering stress-strain curve is converted to a true stress and logarithmic plastic strain curve for different temperatures. These true stress and plastic strain data against different temperatures are specified in ABAQUS.

Rotational spring elements SPRING2 are used to model the rotational stiffness of the column bases.

Figure 4.11 shows the two different types of moment-rotation curves that are

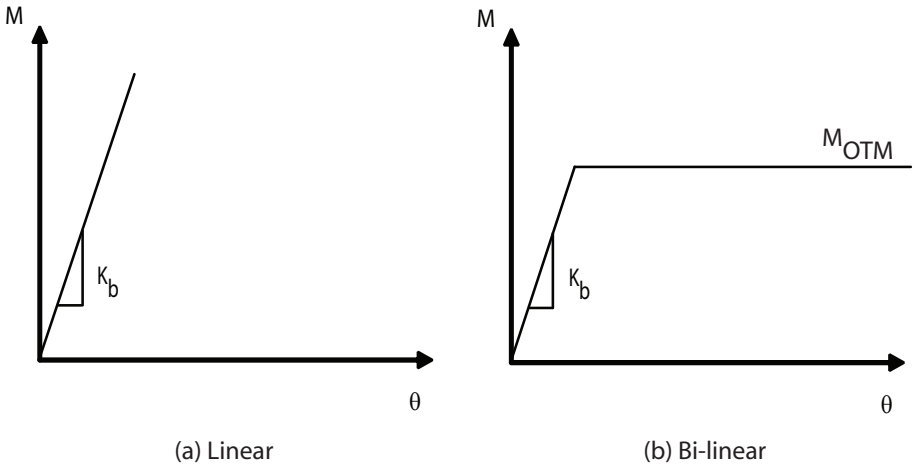

Figure 4.11: Moment-rotation curve used for column base

considered for the column base in this paper: linear and bi-linear with a maximum moment of M_{OTM}.

Song adopted values for the nominal initial stiffness of the column base, kb,

based on the definition of non-dimensional stiffness in Eurocode 3 as given in Eqn. 4.1.

$$K_b = \frac{k_b}{\frac{EI_{maj}}{h}} \tag{4.1}$$

where k_b is the rotational stiffness of the column base, EI_{maj} the bending stiffness of the column and h the height of the column.

Theoretically, a value of K_b of zero is a pinned column base, whilst a value of infinity corresponds to a fully rigid column base. It should be noted that Song considered only the case of column bases having linear stiffness and did not cover the case of bi-linear column bases where the strength is limited. In this study, the behaviour of portal frames with bi-linear column bases will be studied.

4.5 Analysis procedure

The simulation follows the transient method of analysis to study the behaviour of the portal frame. In this method two simulation steps are considered:

- Step 1: Set up the finite element model and apply a dead load over the rafter whilst keeping the rafter at ambient temperature, i.e. 20°C.
- Step 2: Keep the initial loading on the rafter and apply the time-varying elevated temperature to investigate the response of the structure.

Step 1 is a geometrically non-linear static analysis. This step would provide initial stresses for the whole frame before carrying out the analysis at elevated temperature. Though this step will not involve material non-linearity, as the stresses in the structure is within the elastic limit, the stress-strain curve and temperature curve need to be defined at this step so that they will be automatically activated in the subsequent dynamic step. It was also observed that this step can be carried out without applying any numerical damping.

Step 2 uses implicit dynamic analysis. The reason for choosing dynamic analysis over static analysis is that a static analysis cannot handle the structural instability while the structure starts to snap-through, and stops calculation because of convergence problem. Material nonlinearity, geometric nonlinearity, inertia forces, structural damping, and material stiffness degradation are taken into account in the dynamic analysis as large displacements and plastic deformations are likely to occur. This step uses an iterative procedure with an automatic incrementation scheme so that the solver determines effective time increments for different iterations, because a fixed time incrementation scheme is slow and can even terminate the calculation while the material property is highly non-linear. A half-step residual control, *haftol*, is used to ensure an accurate dynamic solution.

After careful observation, it is found that a combination of α = -0.15, haftol = 1×10^2, and smallest time increment set to 1.0×10^{-15} sec can achieve reasonably fast convergence whilst not affecting overall accuracy. It is also observed that by setting Extrapolation=No and Unsymm=No also rapidly accelerates the rate of convergence. Rayleigh mass proportional damping is used in this analysis in order to introduce some mechanism to dissipate kinetic energy to get quantitatively accurate results in an unstable structure. It can be noted that a value of 5% Rayleigh mass proportional damping is sufficient.

4.6 Validation

Before carrying out detailed analyses on the standard building, results of both a 2-D frame and a 3-D model are validated by ABAQUS against results reported in the literature. Some additional studies are also carried out in order to draw preliminary conclusions.

4.6.1 2-D model validation

Frame description and FE idealization

In this Section, the results of a 2-D ABAQUS model are compared against that of a model described by Song (2008 and 2009). Figure 4.12 shows details of the

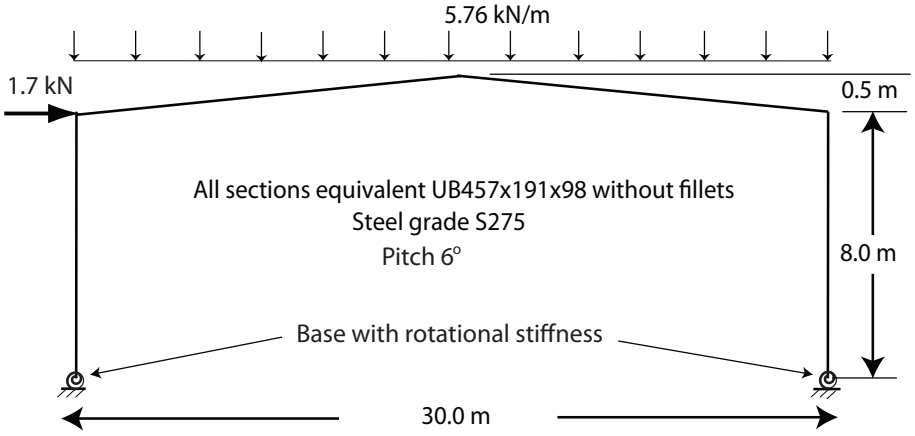

Figure 4.12: Details of single span portal frame after Song *et al.* (2009)

single-span portal frame investigated by Song using VULCAN. As can be seen, the frame is of span 30m, height to eaves of 8 m and height to apex of 8.5m. The frame is initially loaded through a uniformly distributed vertical load of 5.76kN/m on the rafter and a horizontal force of 1.7kN at the left eaves. The

load ratio, a ratio of the applied load in fire to the ultimate load capacity at ambient temperature of the frame, is 0.53, i.e. heavily loaded and lower fire resistance. Lower fire resistance means that the frame will collapse much faster. Table 4.2 shows the details of equivalent steel section properties.

Table 4.2: Properties of equivalent steel sections used by Song *et al.* (2009).

Section	A	σ_y	I_{maj}	W_{pl}	$M_{pl,c}$
	cm^2	$\frac{N}{mm^2}$	cm^4	cm^3	kNm
Columns / Rafters	124.4	275	45700	1957	538

The temperature of the rafters is increased, according the ISO834 fire curve (ISO 1975), until the frame collapses. As the columns are protected in fire, they are assumed to remain at ambient temperature throughout the analysis.

For the column base, Song used values of K_b of 0.4, 2.2 and 4.4 corresponding to cases of nominally pinned, nominally semi-rigid and nominally rigid, respectively, as recommended by Salter (Salter, 2004).

Results

Figure 4.13, Figure 4.14 and Figure 4.15 compare the variation of deflection against temperature with those obtained by Song for the cases of the column base being nominally pinned, semi-rigid and rigid. As can be seen, there is a good agreement between the results obtained using ABAQUS and those obtained by Song.

Figure 4.16 compares the deformed shape at different temperatures for the case of the pinned column base against those obtained by Song. As can be seen, the mode of collapse is asymmetrical and the deformed shapes are similar.

4.6.2 3-D model validation

Frame description and FE idealization

In this Section, two models are validated: first, the results of a 3-D ABAQUS model are compared against the results of a model labeled as 'Case 1' by Moss (2009) and Bong (2005), and second the results are compared against physical experiment on a small-scale portal frame in fire conducted at the University of Edinburgh.

- Validation against 'Case 1' by Moss (2009) and Bong(2005)

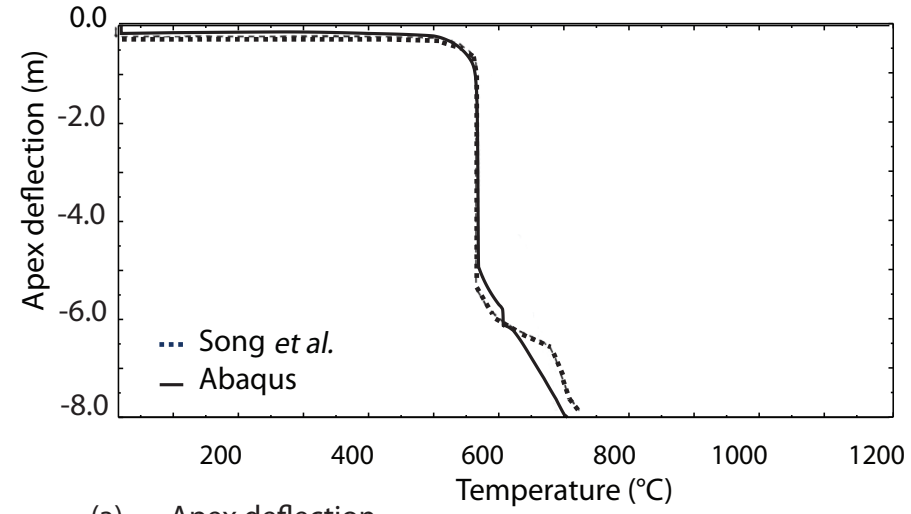

(a) Apex deflection

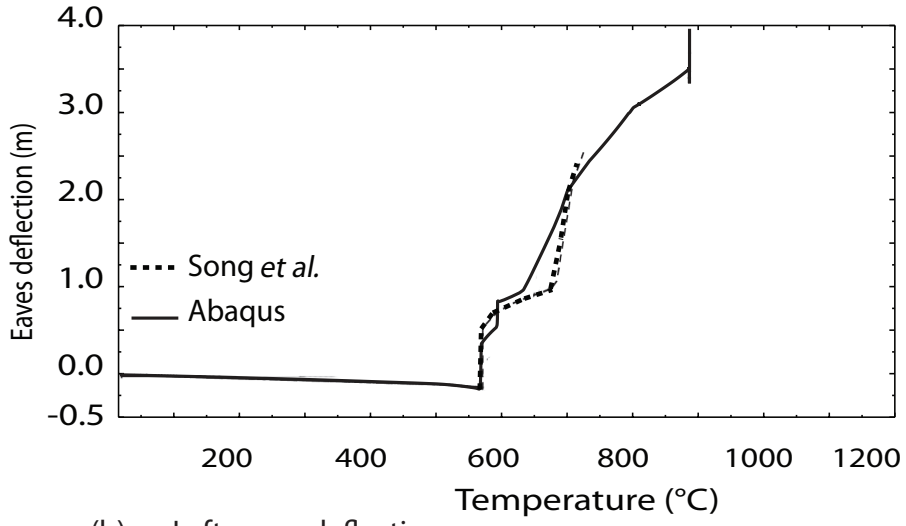

(b) Left eaves deflection

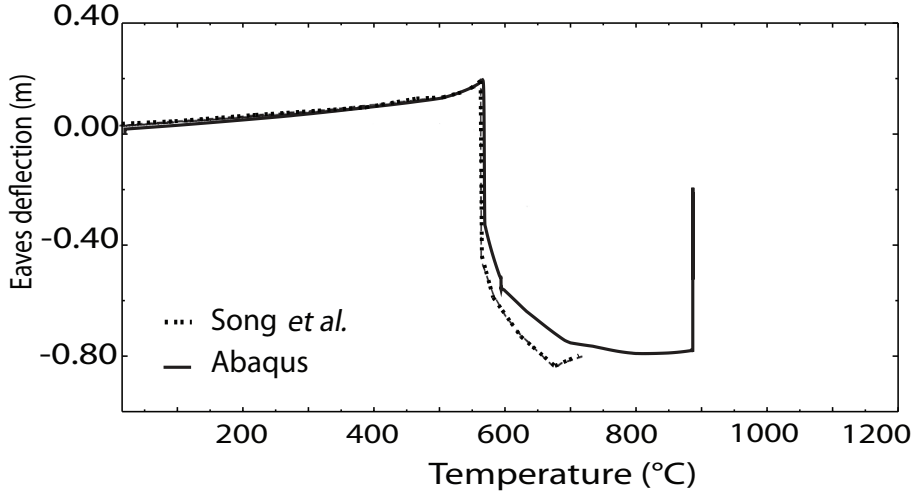

(c) Right eaves deflection

Figure 4.13: Variation of deflection against temperature for single span portal frame when column base is nominally pinned (K_b=0.4) after Song *et al.* (2009): (a) apex (b) left eaves and (c) right eaves

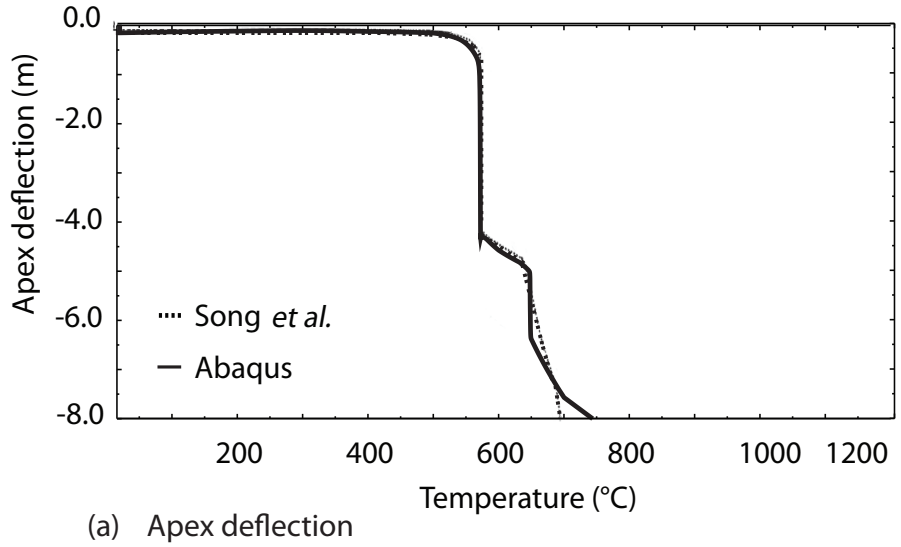

(a) Apex deflection

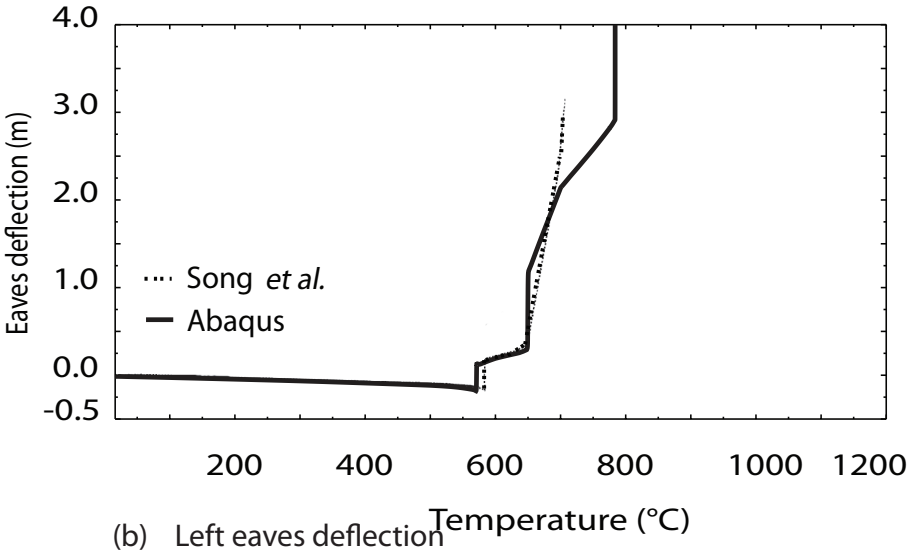

(b) Left eaves deflection

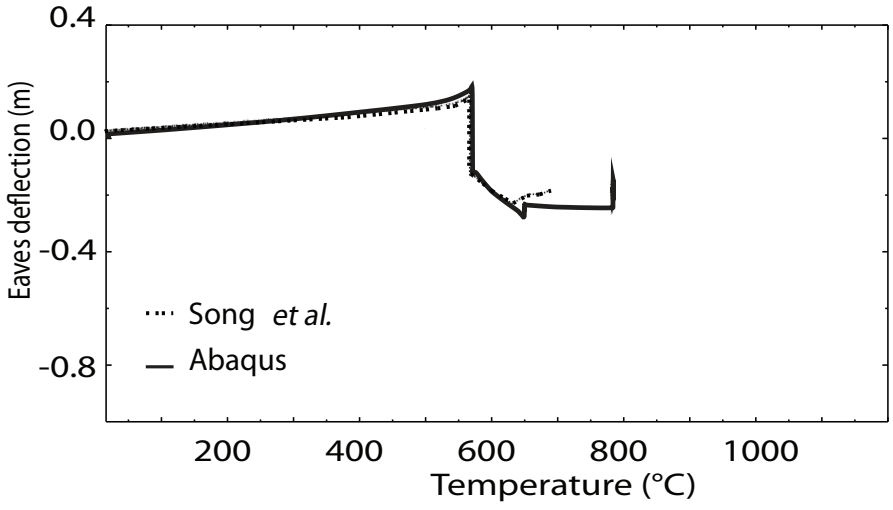

(c) Right eaves deflection

Figure 4.14: Variation of deflection against temperature for single span portal frame when column base is nominally semi rigid (K_b=2.2) after Song *et al.* (2009): (a) apex (b) left eaves and (c) right eaves

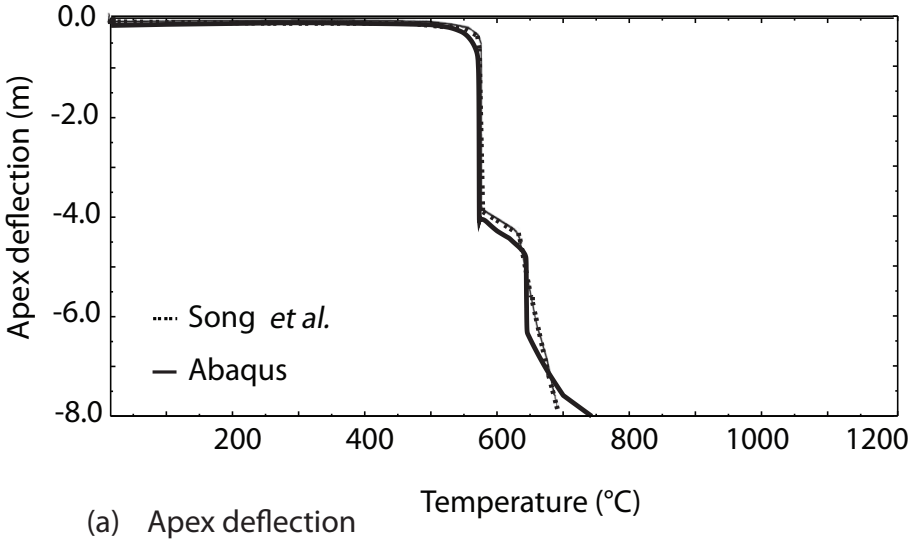

(a) Apex deflection

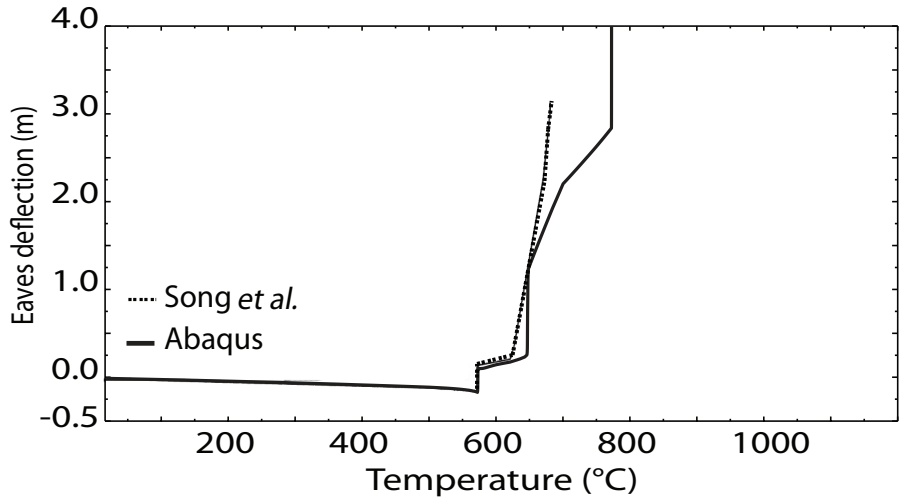

(b) Left eaves deflection

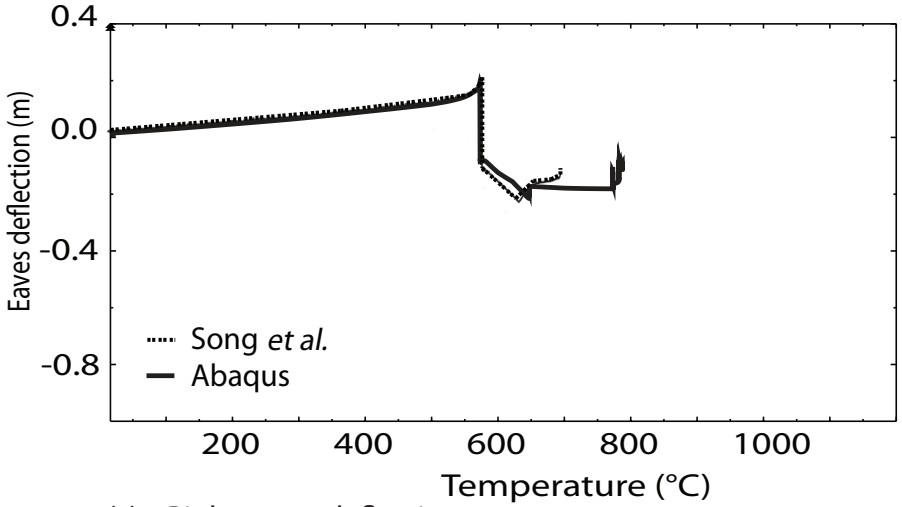

(c) Right eaves deflection

Figure 4.15: Variation of deflection against temperature for single span portal frame when column base is nominally rigid (K_b=4.4) after Song *et al.* (2009): (a) apex (b) left eaves and (c) right eaves

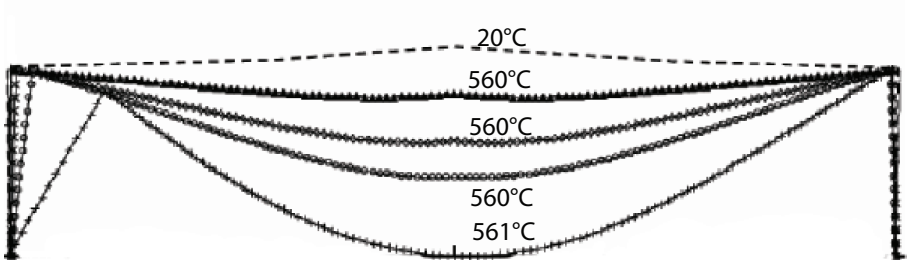

(a) Song *et al.*

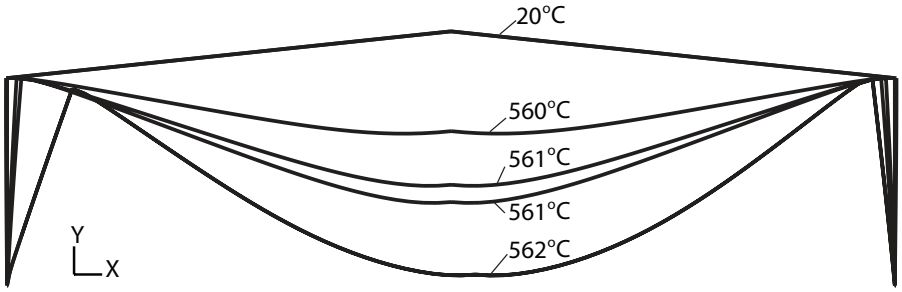

(b) ABAQUS

Figure 4.16: Comparison of deformed shape for a standard frame having pinned column base after Song et al. (2008): (a)Song et al., (b) ABAQUS

Figure 4.17 shows details of the building considered by Moss. As can be seen, the

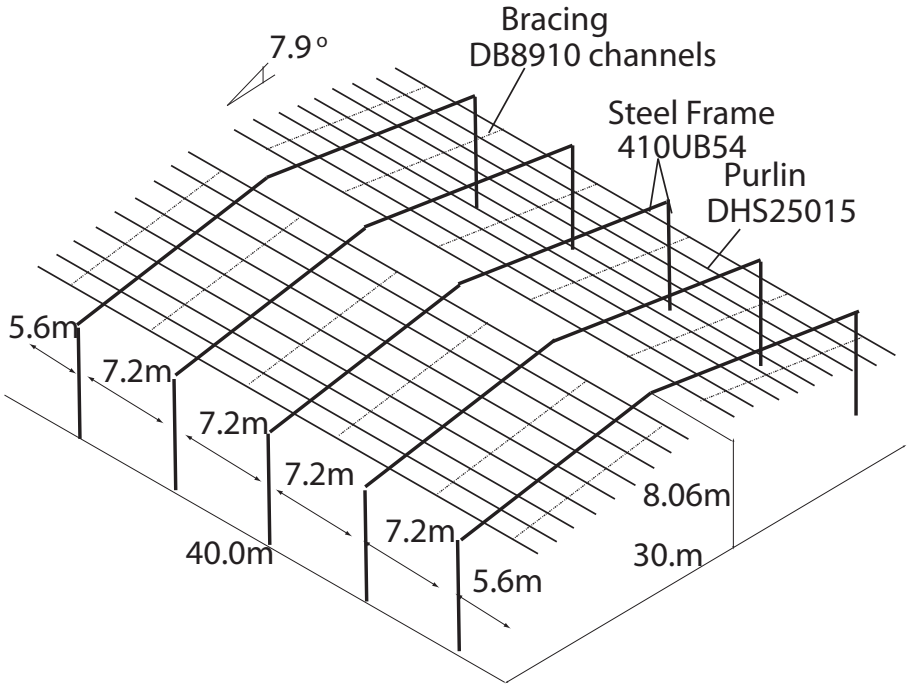

Figure 4.17: Details of the building considered by Moss et al. (2009) and Bong (2005)

building comprises five frames with purlins running over the rafters of the frame. The building has a span of 30.0m, height to eaves of 6.0m and a pitch of 7.9°; the distance between adjacent bays is 7.2m and the purlins are spaced at 1.5m. As purlins are susceptible to buckling laterally, bracing channels are provided to all purlins at mid-span. All sections are modelled without fillets, and Table 4.3 summarizes the equivalent section properties.

Table 4.3: Properties of equivalent steel sections used by Moss *et al.* (2009).

Section	A	σ_y	I_{maj}	W_{pl}	$M_{pl,c}$
	cm^2	$\frac{N}{mm^2}$	cm^4	cm^3	kNm
Columns / Rafters	67.8	275	1672	249	68.4
Purlins	6.2	275	583	69	19
Bracing	4	275	22	5.8	1.6

Unlike the frame described by Song., no additional mass was applied to the frame by Moss et al.; instead the frame was modelled to collapse only under its self-weight and the self-weight of the purlins. The equivalent uniformly distributed load is 1.3kN/m. This corresponds to a load ratio of 0.21 and 0.18 for

pinned and fixed column bases, respectively; such a load ratio is more reasonable for a building. A lower load ratio gives higher fire resistance.

Figure 4.18 shows details of the building idealization. All sections are modelled

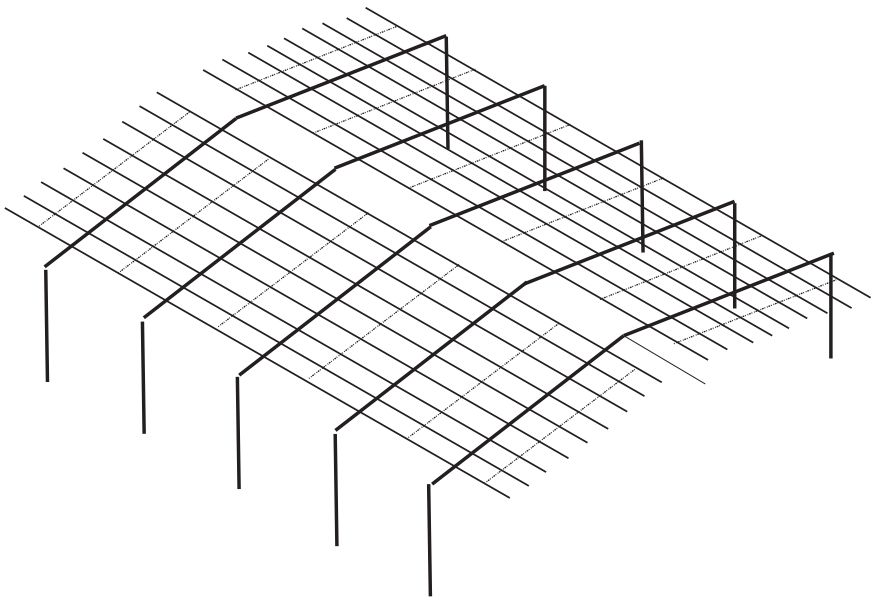

Figure 4.18: Details of the frame idealization with restraints of the portal frame by Moss et al. (2009) and Bong (2005)

in ABAQUS using B31 beam elements. As can be seen, the ends of the purlins are restrained in the global X and Y directions, transverse to the direction of the purlins running along the length of the building. The purlins are not restrained in their axial direction. Each frame is restrained laterally in the out-of-plane direction at three positions: mid-height of columns, top of columns, and apex.

Figure 4.19 shows details of the connection between the purlins and rafters. The connection is pinned in all directions other than the on-plan plane of roof where the connection was continuous. In ABAQUS, this connection constraint is achieved by using MPC PIN parameters. It should be noted that for the frame and loading conditions considered in this paper, little difference has been noted in the graphs of deflection against temperature whether the connections had been pinned in all directions or rigid in all directions.

- Small-scale physical experiment

Figure 4.20 shows the experimental set up on a small scale portal frame in fire. The experiment has been conducted at the BRE facility of the University of Edinburgh.

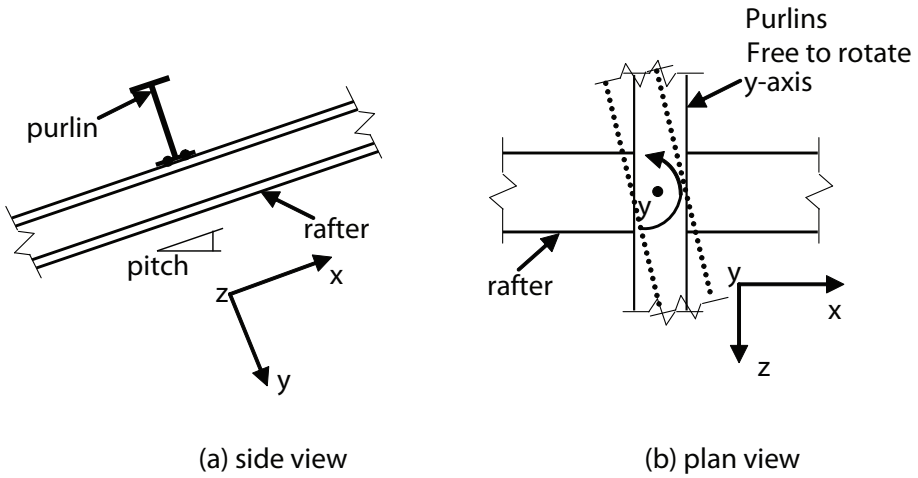

Figure 4.19: Details of connection between purlins and rafters as used by Moss et al. (2009) and Bong (2005)

Fire location

Moss considered various fire scenarios. For the purpose of validation, only the scenario where a fully developed fire is applied to the middle frame of the structure is considered.

Results

Figure 4.21 shows the variation of apex deflection against temperature for the cases considered by Moss when fire is imposed in the whole structure. Figure 4.22 compares the collapsed shape of the buildings. As can be seen, there is a good agreement between the results obtained using ABAQUS and that reported by Moss.

For the physical experiment on a small-scale portal frame in fire, the result for the apex deflection is given in Figure 4.23. As can be seen, there is a good agreement between the experimental result and the result by ABAQUS.

4.7 Study on standard building

In the previous Sections, both 2-D and 3-D ABAQUS models were validated against different models described in the literature. For a building in fire boundary conditions, the behaviour of a 2-D plane frame model, in which no restraint is provided by the purlins (or side rails), can be considered as being a lower bound solution. On the other hand, a 3-D model having an infinite number of frames, in

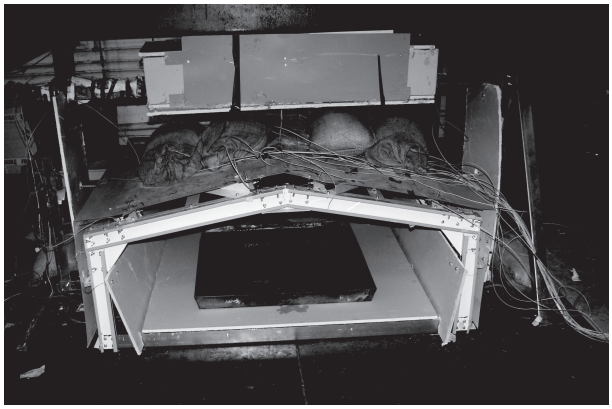

Before fire

In fire

After fire

Figure 4.20: Small-scale experiment

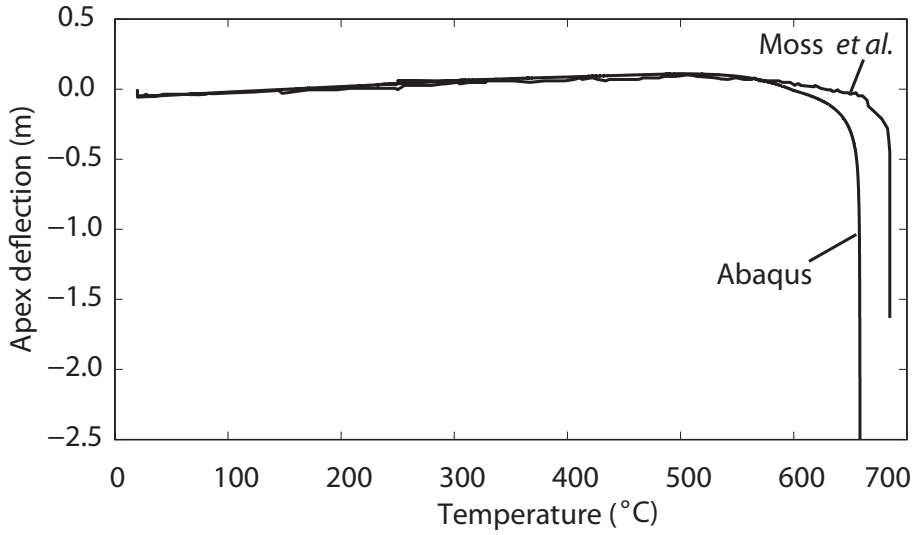

Figure 4.21: Validation of model after Moss et al. (2009) and Bong (2005)

which only the centre frame and purlins connected to central frame are modelled in fire, can be considered as being an upper bound solution.

In this Section, four different Fire Scenarios will be considered for the Standard Building, denoted by Fire Scenarios A, B, C and D, representing one, three, five and all frames in fire, respectively.

Figure 4.24 shows details of the frames and purlins in fire for Fire Scenarios A, B and C. As can be seen, the purlins adjacent to the frames in fire are also modelled at elevated temperature. For the case of Fire Scenario A (see Figure 4.24a), the model adopted is similar to that described in the Section 4.5.2, with five frames modelled of which the middle frame is modelled at elevated temperatures; there are therefore two frames on either side of the central frame in fire with purlins providing restraint. Although an infinite number of frames on either side would be the true upper bound solution, in the interest of computational efficiency and after carrying out a series of preliminary simulations, it has been found that that two are sufficient.

For the case of Fire Scenario B (see Figure 4.24b), in order to keep the amount of restraint provided by the purlins to be the same as that of Fire Scenario A, with two frames at both ends providing restraint, seven frames are modelled of which the middle three are in fire. Similarly, for the case of Fire Scenario C (see Figure 4.24c), nine frames are modelled. Fire Scenario D, considering all frames in fire with no restraint provided by the purlins, is idealized using the 2-D plane frame model (see Figure 4.24d).

In this Section, the effect of different column bases moment rotation curves is investigated for each of the Fire Scenarios described above.

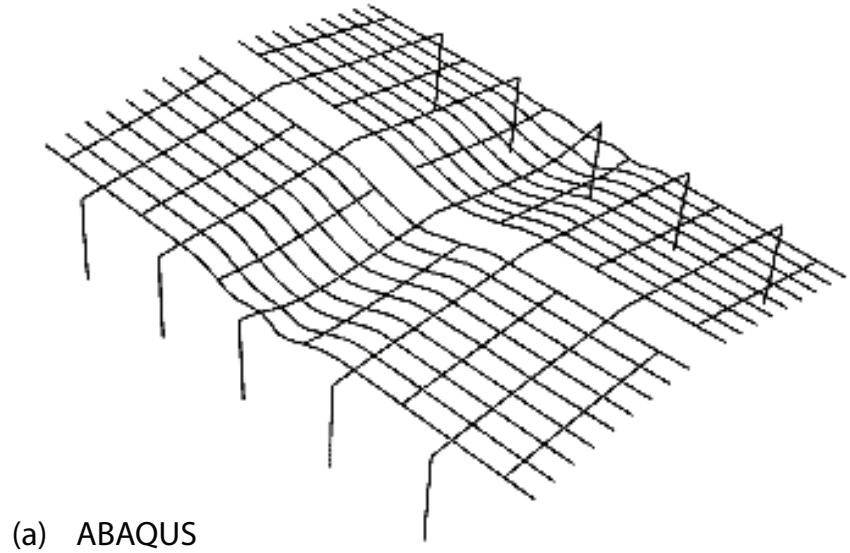

(a) ABAQUS

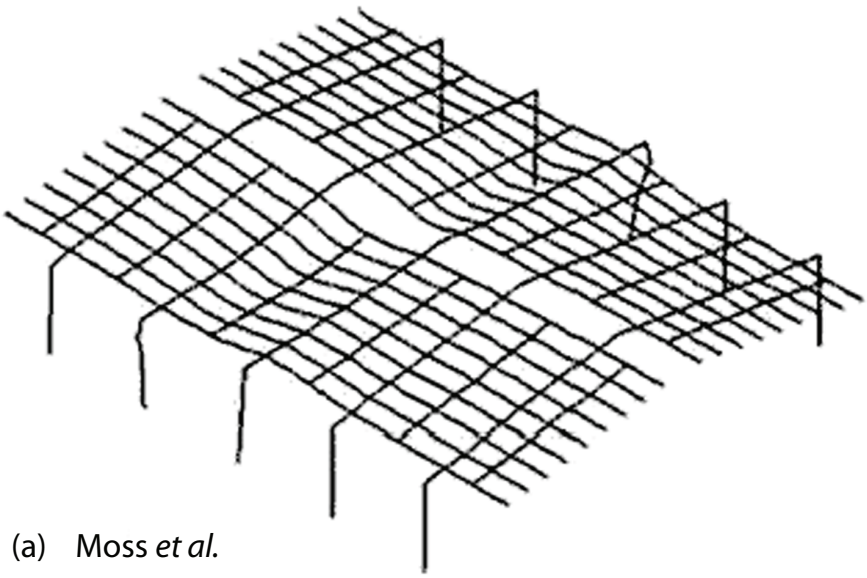

(a) Moss *et al.*

Figure 4.22: Comparison of collapsed building shape : (a) collapsed shape from Abaqus, (b) collapsed shape after Moss et al. (2009)

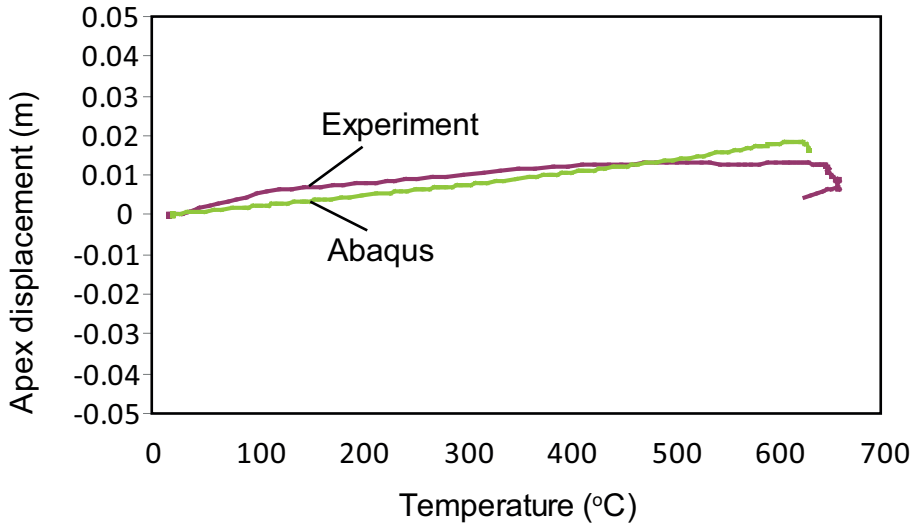

Figure 4.23: Validation of model with the results of physical experiment on small-scale portal frame in fire

4.7.1 Behaviour of building of perfectly-pinned column bases

Figure 4.25 shows the variation of deflection against temperature for the Standard Building for each of the four fire scenarios. In all cases, the column bases are perfectly pinned. The deformed shape for Fire Scenarios A and D are shown in Figure 4.26, and the results are summarized in Table 4.4.

Table 4.4: Summary of behaviour of Standard Building with pinned column base.

Fire Scenario	Snap-through-buckling temperature°C	Collapse temperature°C	Maximum outward column rotation by 890°C
A	>1100	>1100	0.56°
B	822	1039	9.1°
C	810	926	12.0°
D	809	811	Collapsed

As can be seen, for Fire Scenario A, the rafters remain suspended below the columns throughout the duration of fire due to catenary action of purlin; the building has therefore not collapsed up to a temperature of 1100°C.

From Table 4.4 it can be seen that the snap-through-buckling temperature decreases only slightly from 822°C for Fire Scenario B to a temperature of 809°C

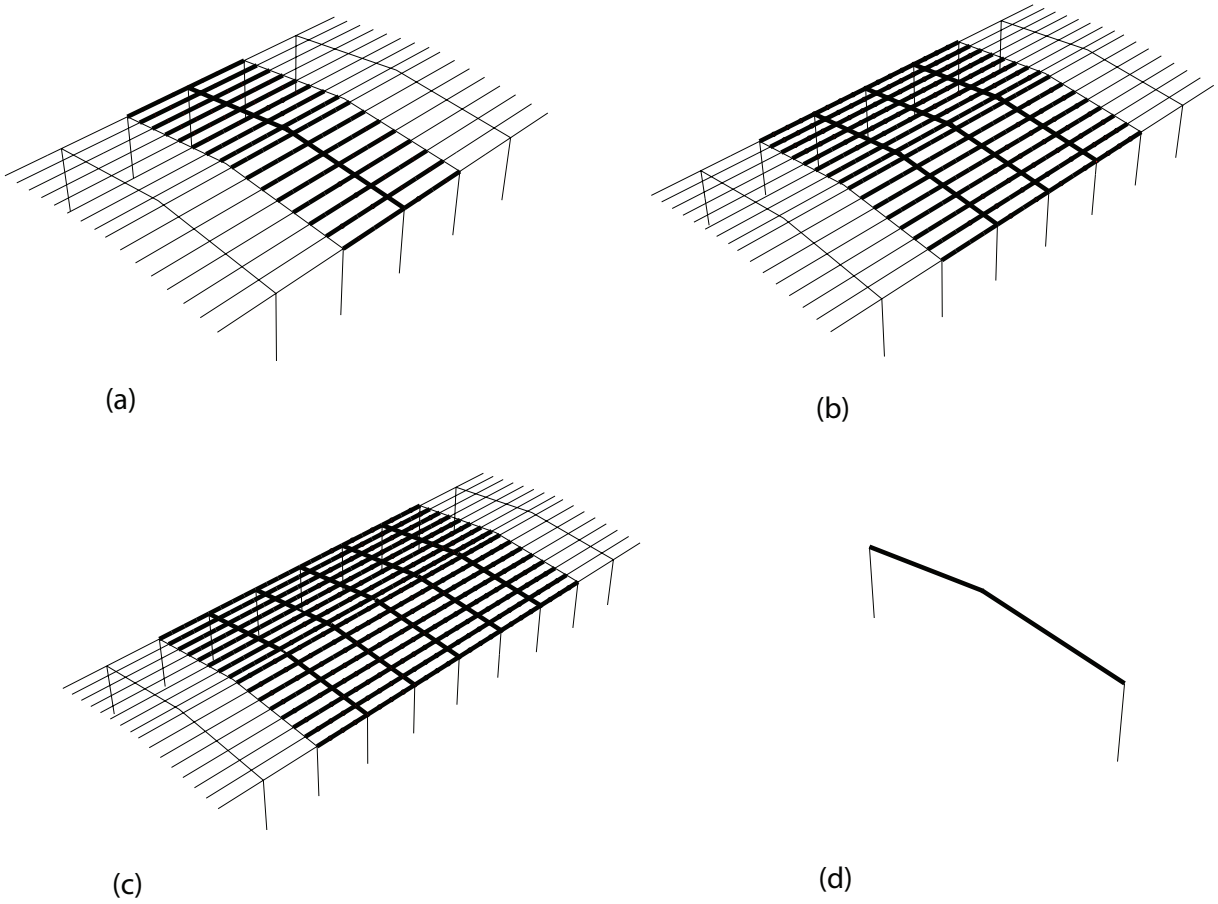

Figure 4.24: Different Fire Scenarios (Note: Bold line indicates members in fire and thin line indicates member at ambient temperature) : (a) Fire Scenario A, (b)Fire Scenario B, (c) Fire Scenario C and (d) Fire Scenario D (Thick line indicates member in fire and thin line indicates member at ambient temperature)

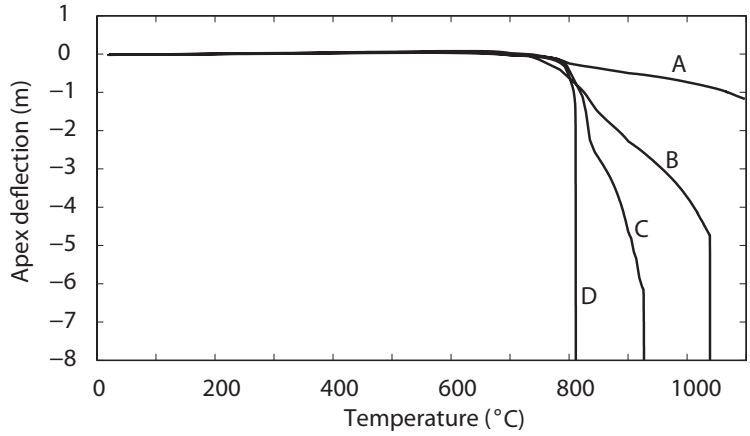

(a) Apex deflection

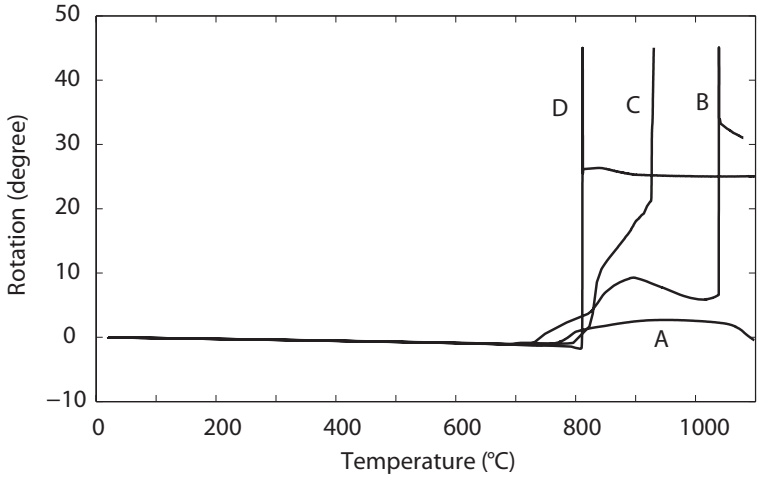

(b) Left eaves rotation

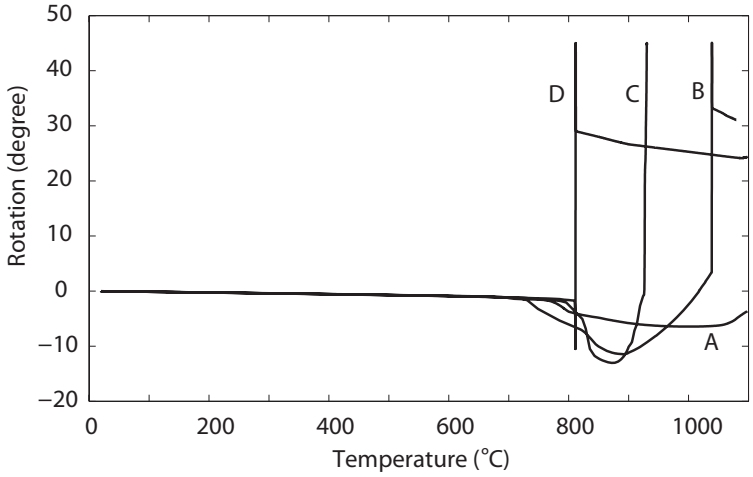

(c) Right eaves rotation

Figure 4.25: Variation of deflection against temperature for Standard Building with perfectly pinned column bases : (a) apex deflection, (b) left eaves rotation and (c) right eaves rotation

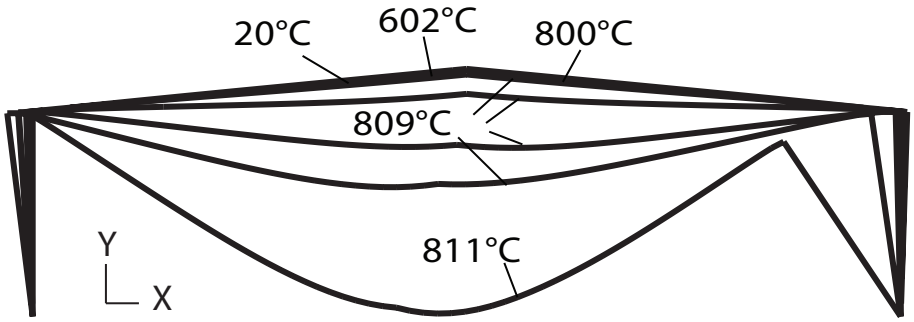

(a) Fire scenario A

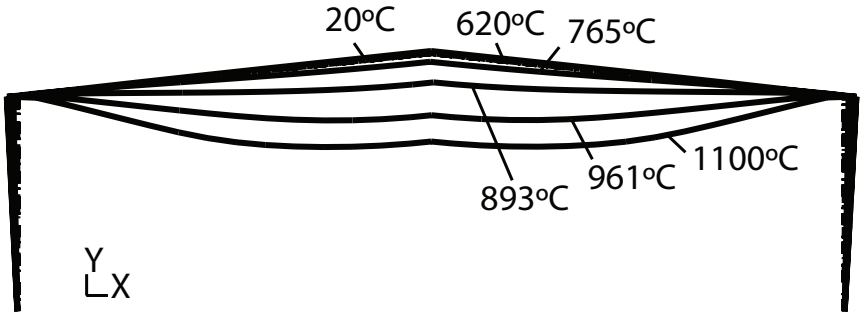

(b) Fire scenario B

Figure 4.26: Deformed shape for Standard Building with pinned column bases for two fire scenarios : (a) Fire Scenario A and (b) Fire Scenario D

for Fire Scenario D. It should be noted, however, that the change in collapse temperature is larger, decreasing from 1039°C to 811°C. Whilst these temperatures are similar to that of the maximum temperature of 890°C assumed by the SCI design method, for all Fire Scenarios the outward rotations of the columns are much higher than the 1° specified by the SCI design method.

Using Wong's (2001) method for calculating the snap-through buckling temperature, it was shown that the snap-through buckling temperature was 709°C.

4.7.2 Effect on building of linear stiffness of column bases

As discussed in Section 4.4.2 the SCI design method does not provide values for the rotational stiffness K_b of the column base. Song (2008) used values of K_b of 0.4, 2.2 and 4.4 corresponding to cases of nominally pinned, nominally semi-rigid and nominally rigid, respectively.

For the lower bound Fire Scenario D, Figure 4.27, shows the variation of deflection against temperature for different column base rotational stiffness. The results for the perfectly-pinned and perfectly-rigid column bases are also shown in Table 4.5.

Table 4.5: Summary of behaviour of Standard Building under Fire Scenario D with column base having linear stiffness

Column base stiffness	Snap-through-buckling temperature °C	Collapse temperature °C	Maximum outward column rotation by 890 °C	Maximum inward column rotation by 890 °C
Pinned	809	811	14.1°	Collapsed
Nominally pinned	822	1082	1.7°	2.3°
Nominally semi-rigid	875	1082	1.4°	0.8°
Nominally rigid	914	1082	1.4°	0.7°
Rigid	936	1069	1.0°	0.3°

As can be seen from Figure 4.27 and Table 4.5, the snap-through buckling temperature increases from 809°C for the perfectly pinned column base to 936°C for the perfectly rigid column base. Unlike the case of the perfectly pinned column base, the two phase collapse mechanism discussed by Song can clearly be seen.

From Table 4.5, for the nominally pinned column base, the outward and inward eaves rotation at the top of the columns is 1.7° and 2.3°. These values are only slightly larger than the 1° specified by the SCI design method.

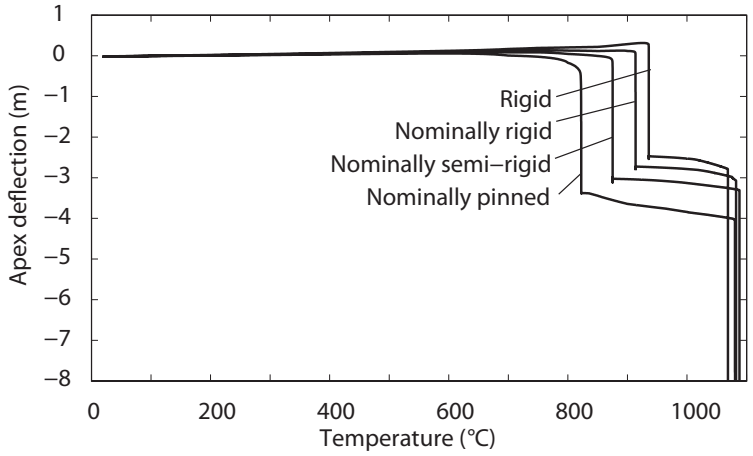

(a) Apex deflection

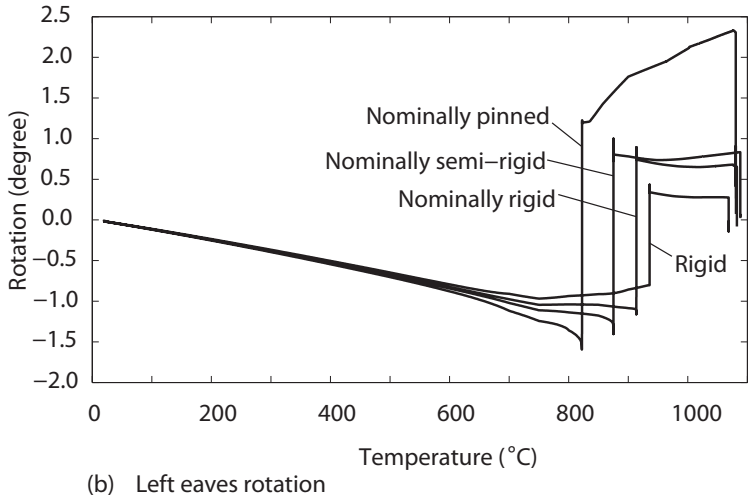

(b) Left eaves rotation

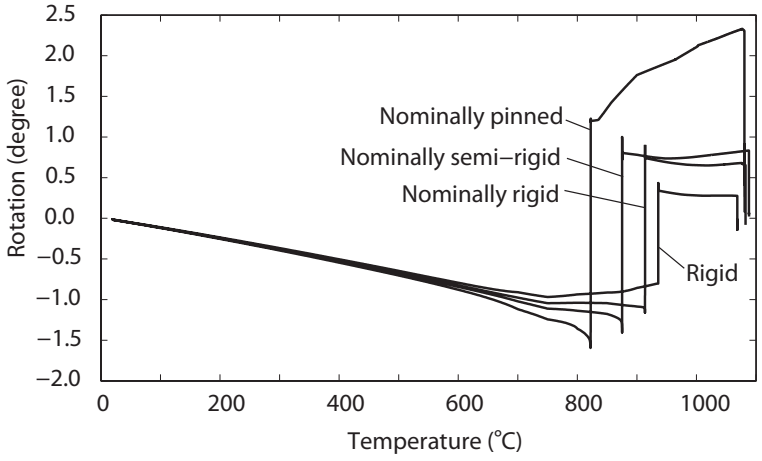

(c) Right eaves rotation

Figure 4.27: Variation of deflection and eaves rotation against temperature for standard Building analyzed as a 2-D plane frame with linear column base : (a) apex deflection, (b) left eaves rotation, and (c) right eaves rotation

4.7.3 Effect on building of partial strength column bases

M_{OTM} of 1.0M_{SCI}

In Section 4.2.1 it was stated that in accordance with the SCI design method, the column base needs only be designed to sustain an overturning moment, M_{OTM}, of 61.2kNm. Such an overturning moment represents approximately 20% of the plastic moment capacity of the section.

Figure 4.28, shows the variation of deflection against temperature for Fire Scenario D for three different column base rotational stiffness having a partial strength M_{OTM} of 61.2kNm. The results are summarized in Table 4.6.

Table 4.6: Summary of behaviour of Standard Building under Fire Scenario D having a value of M_{OTM} of 61.2 kNm with column base having linear stiffness

Column base stiffness	Snap-through-buckling temperature °C	Collapse temperature °C	Maximum outward column rotation by 890 °C	Maximum inward column rotation by 890 °C	Maximum inward column rotation by 1000 °C
Nominally pinned	818	869	1.7°	Collapsed	Collapsed
Nominally semi-rigid	818	879	1.7°	Collapsed	Collapsed
Nominally rigid	818	1010	1.7°	14.0°	16.5°

As can be seen, for all three different column base rotational stiffness, the snap-through buckling temperature is 818°C, only slightly higher than 809°C for the pinned support. The effect of the partial strength column base means that the frame behaves similarly to that of a frame with a perfectly pinned column base. Increasing the column base rotational stiffness from nominally pinned to either nominally semi-rigid or nominally rigid has very little effect. The maximum outward column rotation is 1.7°.

Figure 4.29, shows the same results for Fire Scenarios A, B and C; the results are summarized in Table 4.7. As can be seen, for Fire Scenario A, the building remains stable and suspended throughout the duration of the fire. For Fire Scenarios B and C, the frame undergoes snap-through-buckling at temperatures of 828°C and 818°C, respectively. These temperatures are only slightly higher than that of Fire Scenario D of 811°C. For Fire Scenarios D, the building collapses after snap-through buckling. In all cases, the maximum outward eaves rotation by 890°C is 1.7°; the inwards rotation is 34.1°.

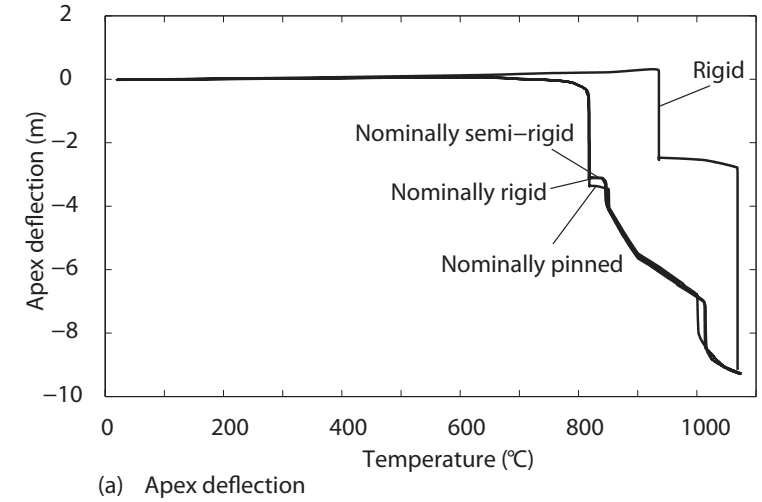

(a) Apex deflection

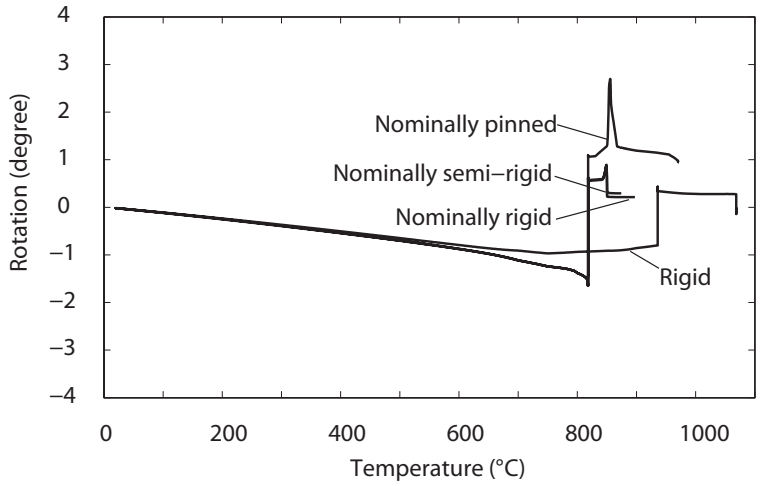

(b) Left eaves rotation

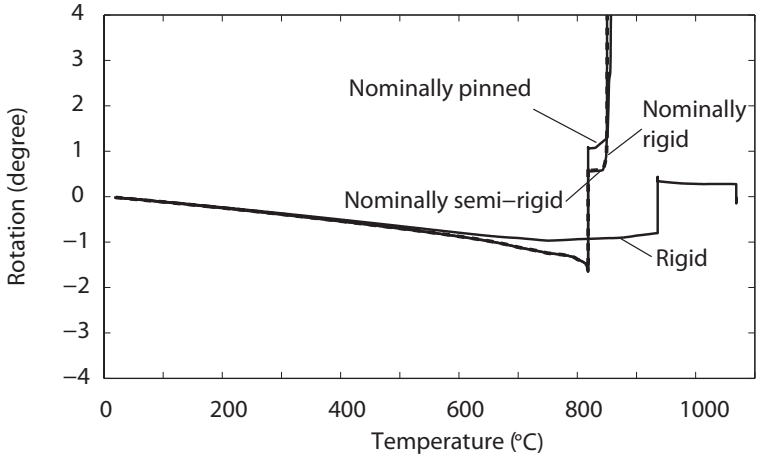

(c) Right eaves rotation

Figure 4.28: Variation of deflection and eaves rotation against temperature for Standard Building analyzed as a 2-D plane frame (Fire scenario D) with column base having a value of M_{OTM} of M_{SCI} (61.2kNm) with different base rigidity : (a) apex deflection, (b) left eaves rotation, (c) right eaves rotation

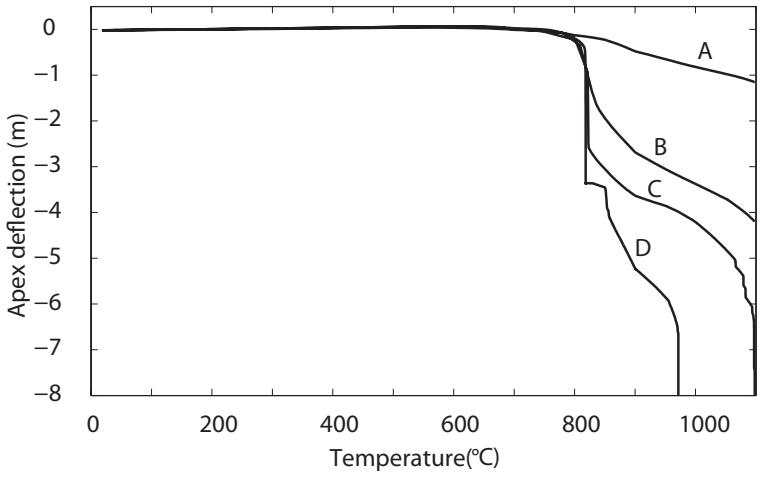

(a) Apex deflection

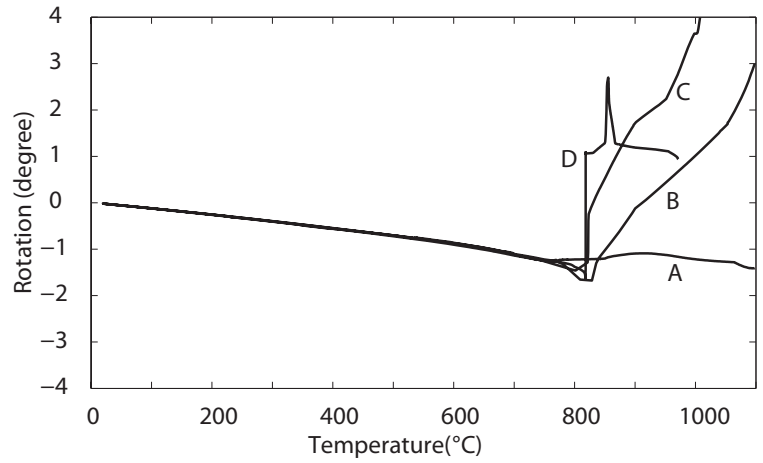

(b) Left eaves rotation

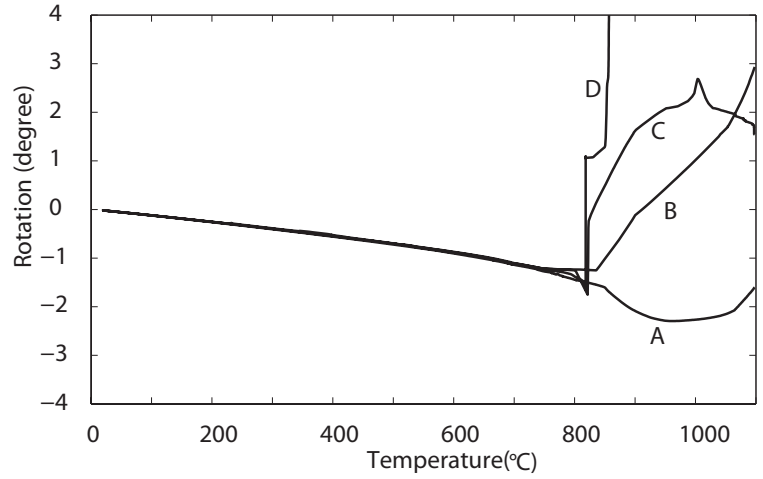

(c) Right eaves rotation

Figure 4.29: Variation of deflection and eaves rotation against temperature for Standard Building with nominally pinned partial strength column base having a value of M_{OTM} of $1.0M_{SCL}$(61.2kNm) for different fire scenarios: (a) apex deflection, (b) left eaves rotation, (c) right eaves rotation

Table 4.7: Summary of behaviour of Standard Building having nominally pinned column bases with a value of M_{OTM} of M_{SCI}

Fire scenario	Snap-through-buckling temperature °C	Collapse temperature °C	Maximum outward column rotation by 890 °C	Maximum inward column rotation by 890 °C
A	n/a	>1100	2.3°	0.40°
B	828	>1100	1.7°	2.49°
C	818	>1100	1.8°	3.23°
D	818	869	Collapsed	Collapsed

M_{OTM} of 2.0M_{SCI}

Figure 4.30, shows the variation of deflection against temperature for the Standard Building for the case of a nominally pinned column base with the overturning moment limited to M_{OTM} of $2.0M_{SCI}$ i.e. 122.4kNm. The results are summarized in Table 4.8.

Table 4.8: Summary of behaviour of Standard Building having nominally pinned column bases with a value of M_{OTM} of $2M_{SCI}$

Fire Scenario	Snap-through-buckling temperature °C	Maximum outward column rotation by 890 °C	Maximum inward column rotation by 890 °C
A	>1100	1.4°	n/a
B	831	1.4°	1.5°
C	826	1.5°	1.5°
D	822	1.4°	3.25°

As can be seen, the inward rotation for the frame of Fire Scenario D at 890°C is 3.25° as opposed to the columns collapsing. Figure 4.31, shows the effect of increasing the overturning moment on the variation of frame deflection against temperature.

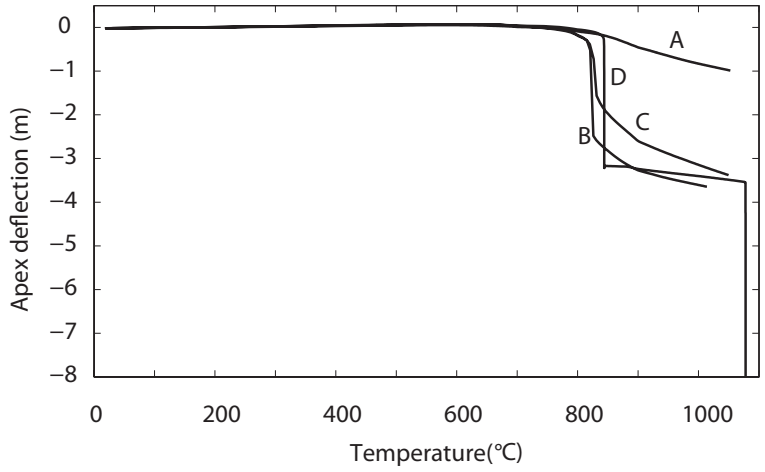

(a) Apex deflection

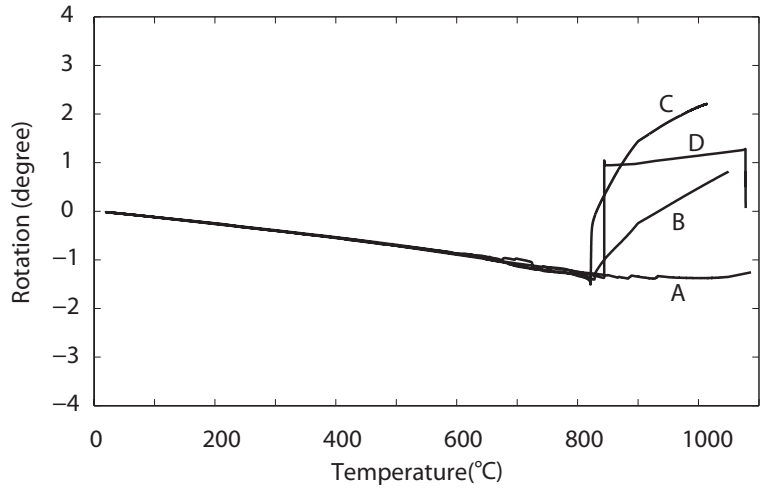

(b) Left eaves rotation

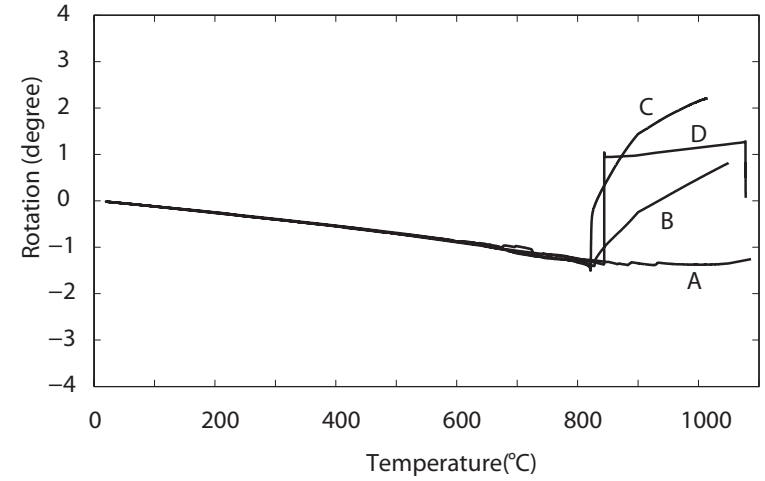

(c) Right eaves rotation

Figure 4.30: Variation of deflection and eaves rotation against temperature for Standard Building with nominally pinned partial strength column base having a value of M_{OTM} of $2.0M_{SCI}$ (122.4kNm) for different fire scenarios: (a) apex deflection, (b) left eaves rotation, (c) right eaves rotation

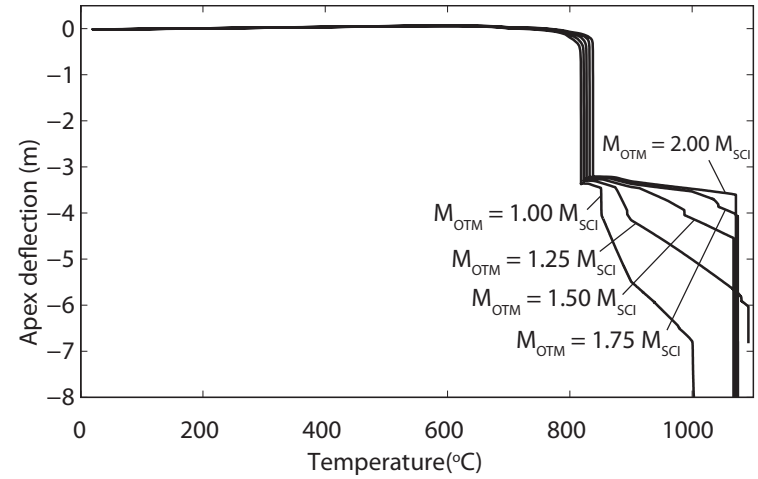

(a) Apex deflection

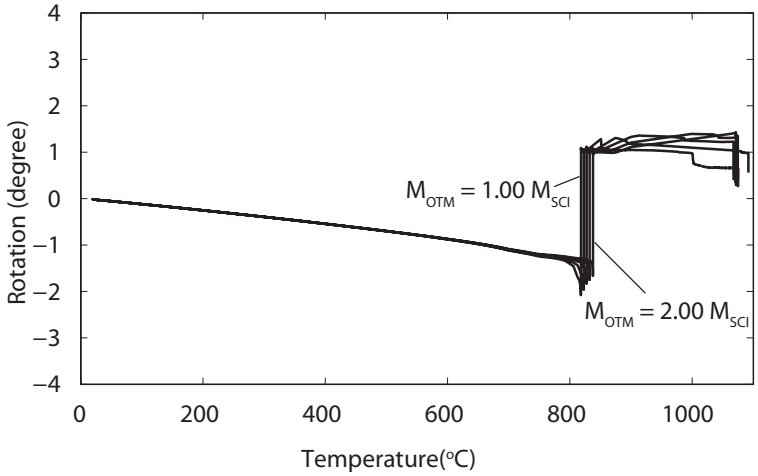

(b) Left eaves rotation

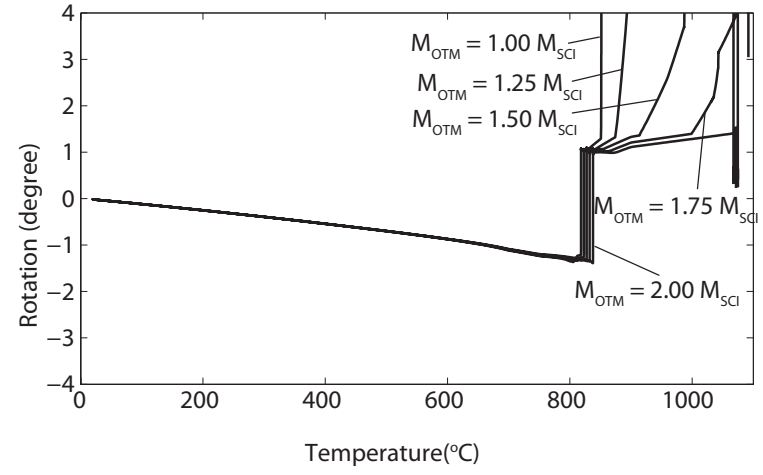

(c) Right eaves rotation

Figure 4.31: Variation of deflection and eaves rotation against temperature for Standard Building with nominally pinned partial strength column base having different M_{OTM}: (a) apex deflection, (b) left eaves rotation, (c) right eaves rotation

4.8 Parametric study

4.8.1 Introductory remarks

In the previous Sections, it was shown that that the finite element model can reproduce similar results to those reported in the literature for both a 2-D frame and a 3-D building. For the Standard Building, it was also shown that if the number of frames in fire can be taken into account, then the collapse temperature will increase and the column rotations will decrease.

In this Section, a parametric study will be undertaken using the lower bound 2-D plane frame. The results will be compared against the criterion assumed by the SCI design guidance, that at 890°C the columns will not have exceeded rotation of 1° from the vertical.

4.8.2 Scope of parametric study

A total of twenty-seven portal frames are used for the parametric study. The dimensions of these frames are shown in Table 4.9. As can be seen from Table 4.9, the section sizes, moment capacities of the sections, as well as M_{SCI} are provided. Also included in Table 4.9 are the ratios of M_{SCI} to the plastic moment capacity of the column, $M_{pl,c}$, which range from 0.14 to 0.3.

Frames S1, S2, and S3 are shown in Figure 4.32. These frames are taken from designs reported in a survey of portal frames by practicing engineers (Lim *et al.*, 2005). Frames P1 to P23 are designed by the Authors based on charts presented in Todd (1996).

For all the frames investigated in the parametric study, the column bases are nominally pinned. A uniformly distributed load of 0.2 kN/m^2 is applied on the roof; a nominal horizontal force of 0.5% of the vertical load is applied at the eaves. Values of M_{OTM} of both M_{SCI} and $2.0M_{SCI}$ are considered.

4.8.3 Results of parametric study

Table 4.10 shows the parametric study results for column rotation for three values of M_{OTM}: $1.0M_{SCI}$, $1.5M_{SCI}$ and $2.0M_{SCI}$. As expected, increasing M_{OTM} from M_{SCI} to $2M_{SCI}$ has very little effect on the outward rotation. For the column base having a value of M_{OTM} of M_{SCI}, the average maximum outward rotation is 1.8°, which is of a similar order of magnitude to the 1o specified by the SCI design method. Table 4.10 also shows the inward rotations. As expected, the rotations are much higher than the 1° specified by the SCI design method.

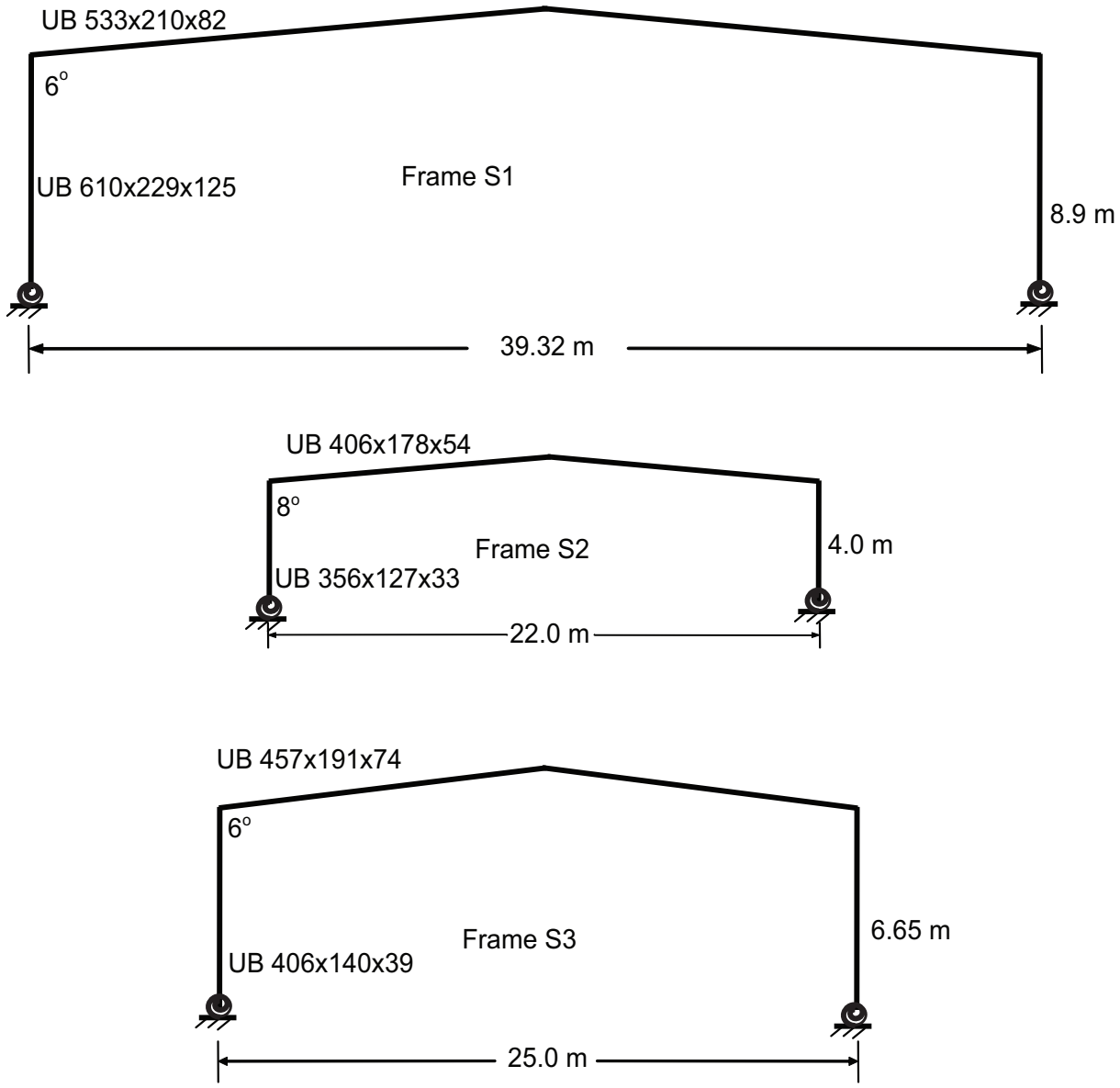

Figure 4.32: Frames designed from a survey of practicing engineers (Lim *et al.*, 2005).

Similarly, in terms of snap-through-buckling temperatures, there is very little difference in increasing M_{OTM} from M_{SCI} to $2.0M_{SCI}$. Both the snap-through -buckling temperatures and collapse temperatures are shown in Table 4.11. As can be seen, the increase in the snap-through buckling temperature, as a result of increasing M_{OTM} from M_{SCI} to $2.0M_{SCI}$ is only 10°C.

However, in terms of collapse temperatures, the majority of frames having a value of M_{OTM} of M_{SCI} have collapsed by 890°C. The effect of increasing M_{OTM} from M_{SCI} to $2.0M_{SCI}$ results in the average collapse temperature being increased from 845°C to 1034°C. The results for M_{OTM} having a value of 1.5MSCI are also shown in Table 4.11. As can be seen, the average collapse temperature for a value of M_{OTM} of $1.5M_{SCI}$ is 958°C, which is higher than the temperature assumed in the SCI design of 890°C.

4.8.4 Comparison against Wong's method

As discussed in Section 4.7.1, Wong (2001) described a method for determining the snap-through buckling temperature for pinned column base portal frames. Table 4.12 shows a comparison of the snap-through buckling temperature of Wong's method and the ABAQUS model using nominally pinned column bases and M_{OTM} of M_{SCI}. It can be seen that Wong's method is slightly under-conservative, even though it is based on pinned column bases. Wong's method is, however, useful for quickly assessing the snap-through-buckling temperature.

4.9 Conclusions

The following conclusions can be drawn:

- The 3-D model increases the collapse temperature and reduces the rotations, but the number of frames in fire is significant.
- SCI method does not take into account the partial strength of column base. If the partial strength of the column base is taken into account, the column base rotational stiffness has little effect on the collapse behaviour of the frame, with the column base behaving as a pin once the column base moment capacity has been exceeded.
- The 2-D frames considered in the parametric study all collapsed before 890°C when the rotational strength of the column base was $1.0M_{SCI}$. However, when the rotational strength of the column base was increased to $2.0M_{SCI}$ all the frames were stable at 890°C. Intermediate results for $1.5M_{SCI}$ were also provided. It is acknowledged by the Authors that this conclusion

should not be taken too generally as only a limited number of frames were considered.

- The average outward rotation of the columns where the rotational strength of the column base was M_{SCI} was 1.8°. This outward rotation was only slightly higher than the 1° assumed by the SCI design method.
- The inward rotation was significantly higher than 1°.
- It has been shown that the value of the overturning moment, calculated in accordance with the SCI design method, may not be sufficient to prevent collapse of the frame before 890°C. However, by taking into account both the number of bays in fire, as well as the strength of the column base, a frame may be able to be shown to satisfy the assumptions of the SCI design criteria of the columns remaining 1° from the vertical and stability up to a temperature of 890°C.

Table 4.9: Parameters of frames used in parametric study

Frame	L	h	θ	$\frac{L}{h}$	Column section	Rafter section	$M_{pl,r}$	$M_{pl,c}$	M_{SCI}	$\frac{M_{SCI}}{M_{pl,c}}$	r
	m	m	°		UB	UB	kNm	kNm	kNm		
Std	22	5.7	6	3.9	457x152x52	457x152x52	296	296	61	0.21	0.09
S1	39.3	8.9	6	4.4	610x229x125	533x210x82	642	1341	258	0.19	0.2
S2	22	4	8	5.5	406x178x54	356x127x33	110	253	75	0.3	0.22
S3	25	6.7	6	3.8	457x191x74	406x140x39	168	453	115	0.25	0.24
P1	40	6	6	6.7	686x254x140	533x210x92	649	1253	196	0.16	0.18
P2	35	6	6	5.8	686x254x125	533x210x82	566	1098	148	0.14	0.16
P3	30	6	6	5	610x229x101	457x191x67	405	792	120	0.15	0.12
P4	25	6	6	4.2	533x210x82	406x178x54	290	566	90	0.16	0.16
P5	20	6	6	3.3	457x191x67	406x140x39	181	405	57	0.14	0.15
P6	15	6	6	2.5	356x171x45	305x102x28	111	213	43	0.2	0.15
P7	40	8	6	5	762x267x147	533x210x92	649	1418	213	0.15	0.18
P8	35	8	6	4.4	686x254x125	533x210x82	566	1098	174	0.16	0.16
P9	30	8	6	3.8	610x229x101	457x191x67	405	792	143	0.18	0.17
P10	25	8	6	3.1	533x210x82	406x178x54	290	566	108	0.19	0.16
P11	20	8	6	2.5	457x191x67	406x140x39	181	405	67	0.17	0.15
P12	15	8	6	1.9	356x171x45	305x102x28	111	213	59	0.28	0.16
P13	40	10	6	4	762x267x147	610x229x101	792	1418	243	0.17	0.15
P14	35	10	6	3.5	686x254x125	533x210x82	566	1098	200	0.18	0.16
P15	30	10	6	3	610x229x113	457x191x67	405	902	138	0.15	0.17
P16	25	10	6	2.5	533x210x92	406x178x54	290	649	100	0.15	0.16
P17	20	10	6	2	457x191x67	406x140x39	181	405	89	0.22	0.16
P18	15	10	6	1.5	356x171x51	305x102x28	111	246	48	0.19	0.16
P19	40	12	6	3.3	762x267x147	610x229x101	792	1098	344	0.31	0.15
P20	35	12	6	2.9	686x254x125	533x210x82	566	1098	225	0.21	0.16
P21	30	12	6	2.5	610x229x113	457x191x67	405	902	154	0.17	0.17
P22	25	12	6	2.1	533x210x92	406x178x54	290	649	111	0.17	0.17
P23	20	12	6	1.7	457x191x67	406x140x39	181	405	100	0.25	0.16

Table 4.10: Parametric study results for column rotation

Frame	Maximum outward column rotation by 890 °C			Maximum inward column rotation by 890 °C		
	$M_{OTM} = M_{SCI}$	$M_{OTM} = 1.5M_{SCI}$	$M_{OTM} = 2.0M_{SCI}$	$M_{OTM} = M_{SCI}$	$M_{OTM} = 1.5M_{SCI}$	$M_{OTM} = 2.0M_{SCI}$
	°	°	°	°	°	°
Std	1.7	1.5	1.5	Collapsed	8.4	1.5
S1	3.7	1.6	1.6	Collapsed	Collapsed	22.0
S2	3.8	3.8	3.6	Collapsed	Collapsed	3.0
S3	1.3	1.4	1.4	Collapsed	Collapsed	4.9
P1	2.6	2.6	2.6	Collapsed	Collapsed	1.0
P2	2.9	2.4	2.3	Collapsed	Collapsed	2.6
P3	3.6	3.0	2.4	Collapsed	11.5	2.8
P4	2.7	1.9	1.4	Collapsed	13.7	3.5
P5	2.0	1.9	1.8	Collapsed	25.5	8.1
P6	1.1	1.1	1.1	Collapsed	14.2	3.6
P7	2.2	2.1	2.0	Collapsed	Collapsed	3.3
P8	2.9	2.3	2.0	Collapsed	13.9	3.3
P9	2.1	1.9	1.8	Collapsed	11.8	2.9
P10	1.3	1.3	1.3	Collapsed	12.3	3.4
P11	1.1	1.1	1.1	Collapsed	23.1	6.4
P12	0.8	0.8	0.8	52.1	4.3	2.8
P13	2.4	2.0	1.9	Collapsed	12.6	3.0
P14	1.7	1.6	1.4	Collapsed	12.7	3.2
P15	1.3	1.3	1.3	Collapsed	26.9	7.2
P16	1.1	1.1	1.1	Collapsed	36.2	8.9
P17	0.8	0.8	0.8	Collapsed	9.1	2.6
P18	0.7	0.7	0.7	67.3	8.5	6.0
P19	1.4	1.3	1.3	31.5	3.4	1.7
P20	1.3	1.2	1.2	Collapsed	11.3	2.8
P21	1.0	1.0	1.0	Collapsed	25.8	6.6
P22	0.9	0.9	0.9	Collapsed	12.7	8.0
P23	0.7	0.7	0.7	57.0	7.4	3.2
Average	1.8	1.6	1.5			

Table 4.11: Results of parametric study for snap-through-buckling and collapse temperature

Frame	Snap-through buckling Temperature			Collapse temperature		
	$M_{OTM} = M_{SCI}$	$M_{OTM} = 1.5M_{SCI}$	$M_{OTM} = 2.0M_{SCI}$	$M_{OTM} = M_{SCI}$	$M_{OTM} = 1.5M_{SCI}$	$M_{OTM} = 2.0M_{SCI}$
	°C	°C	°C	°C	°C	°C
Std	818	828	838	869	986	1071
S1	620	621	624	664	695	979
S2	672	682	694	762	783	936
S3	643	645	647	698	875	918
P1	711	721	736	793	850	1047
P2	737	741	751	808	880	1057
P3	781	786	793	885	1042	1054
P4	732	736	742	849	941	1008
P5	742	743	747	793	974	1031
P6	740	740	741	808	941	977
P7	701	702	710	792	881	1063
P8	731	735	741	847	1001	1053
P9	725	728	733	859	967	1043
P10	731	732	734	852	974	1048
P11	745	746	747	791	940	1027
P12	746	746	747	985	985	986
P13	743	746	751	863	987	1068
P14	729	732	736	859	983	1061
P15	723	724	726	795	967	1053
P16	730	728	731	776	1032	1060
P17	750	750	751	892	1002	1010
P18	748	749	749	1026	1040	1048
P19	740	741	743	1096	1097	1098
P20	728	728	729	882	979	1054
P21	724	725	726	790	994	1058
P22	727	729	729	782	1041	1063
P23	751	752	753	1007	1029	1045
Average	725	731	735	845	954	1034

Table 4.12: Comparison of snap-through buckling temperature against Wong's method

Frame	Snap-through buckling temperature	
	°C	°C
Std	809	709
S1	618	757
S2	653	661
S3	636	679
P1	702	761
P2	728	774
P3	773	769
P4	724	770
P5	730	765
P6	725	773
P7	701	755
P8	725	770
P9	718	765
P10	720	767
P11	729	762
P12	720	771
P13	737	777
P14	723	768
P15	716	763
P16	718	765
P17	726	761
P18	712	770
P19	738	776
P20	725	766
P21	714	761
P22	715	764
P23	722	760

Chapter 5

Effect of column base strength to other types of portal frame buildings in fire

5.1 Introductory remarks

The effect of column base strength of single-storey symmetric steel portal frames at elevated temperature has been investigated in Chapter 4. The characteristic failure mode up to snap-through-buckling collapse has been determined and further explored in parametric studies. The same FE model that has been developed in Chapter 3 and used in Chapter 4 can be readily applied to investigate the behaviour of other types of steel frames, such as, multiple span portal frames, portalised truss frames and asymmetric portal frames, in fire. In order to evaluate the adequacy of the SCI method applicable to these frames, it is necessary to know how these frames behave at elevated temperature with limited column base strength. In this Chapter, an FE study has been conducted to determine these behaviours.

5.2 Previous study

The European Commission (Vassart, 2007) has conducted an investigation of multi-span portal frames, where they have considered three and five span frames. These investigations have mainly been concerned with the catenary characteristics of rafter of portal frames with pinned and fixed column bases only. The SCI

method outlined an experimental studies on multi-span portal frames and found that out of eight frames only one internal column has been collapsed. The SCI laboratory has also conducted a comparative study between a single span portal frame and a portalised lattice rafters; and they concluded that the SCI method can be applicable to portalised lattice rafter frames with the only exception that the haunch should not be considered and calculation of plastic moment of rafter is not necessary as they are formed of truss members. They have developed mathematical model for calculation of maximum catenary force at the column tops.

However, it should be noted that no study has considered the effect of column base strength on frames at elevated temperature. It is also to be noted that no study has been performed for the asymmetric frames in fire so far. In this Chapter, the characteristics of different portalised frame in fire will be determined using the model developed in Chapter 3.

5.3 Different frames for study

Three different types of steel portal frames have been selected for investigating the effects of column base strength on the corresponding frames at elevated temperatures. The frames are:

- Multi-span portal frames;
- Portalised truss frames or lattice rafters; and
- Asymmetric portal frames.

5.4 Multi-span portal frames

This type of frame is essentially a lateral extension of single-span portal frame with more than one span, as can be seen in Figure 5.1.

5.4.1 Standard multi-span portal frames (SMSPF)

Two different frames, as can bee seen in Figure 5.1, have been selected for the present study. These are two-span and three-span frames. The section properties and geometric dimensions of such frames are given in Table 5.1 and Table 5.2 respectively. Hot-rolled steel section of grade S275 has been used in both cases. For convenience, these buildings will be referred to as the "Standard Multi-Span

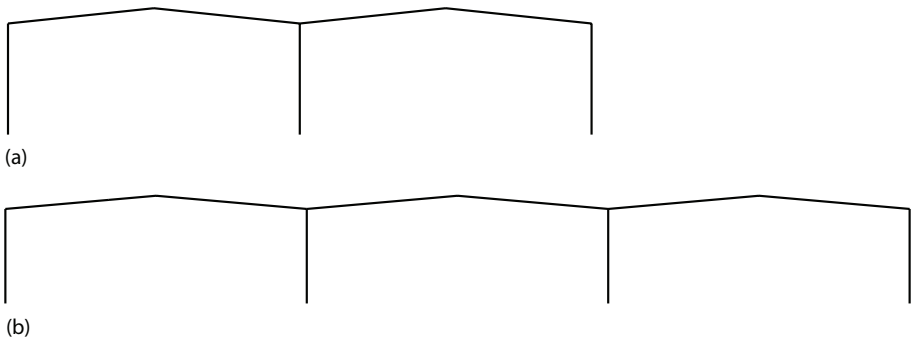

Figure 5.1: Multi-span portal frames (a) double-span frame; (b) triple-span frame

Table 5.1: Properties of equivalent steel sections (without fillets) used for the standard multi-span portal frame building

Type of frame	Members	Section	Area	I_{maj}	W_{pl}	$M_{pl,c}$
		UB	cm^2	cm^4	cm^3	kNm
Double-span	Columns	457x191x67	84	29000	1450	399
	Rafters	457x152x52	66	20969	1077	296
Triple-span	Columns	762x267x147	185	168000	5100	1403
	Rafters	457x191x74	94	33300	1640	451

Table 5.2: Geometry of standard multi-span portal frame buildings

Frame	Column section	Rafter section	Span	Eaves height	Apex height	Pitch	Frame c/c
	UB	UB	m	m	m	°	m
Double span	457x191x67	457x152x52	25.4	9.67	11	6	7.354
Triple span	762x267x147	457x191x74	37.0	11.6	13.22	5	8

Portal Frame" or SMSPF. Only 2-D finite element models of such buildings in fire will be considered as it has been established in Chapter 4 that a frame represented as 2-D model gives the lower bound solutions. The 3-D model represents the upper bound solution and is not considered for the present study.

In order to simplify the model, haunches are excluded from the model as it is found that inclusion of haunch has no other effect other than reducing the effective span of frames. Similar to the single-span symmetric steel portal frames, it should also be noted that the cross-section properties used for the members are slightly different than those given in standard section property tables, as can be seen in Table 5.1. This is because the finite element program ABAQUS used for the analysis is unable to provide default cross-sections with fillets and modelling such cross-sections with fillets using the Arbitrary Section Method provided in ABAQUS usually increases the computational time significantly.

A vertical load of $0.3kN/m^2$ has been applied on rafters as distributed load for both two-span and three-span frames. This vertical dead load is consistent with the SCI method in which the self-weight of the purlins is also included. As movement in the out-of-plane direction is restricted, the purlins are not physically modelled.

5.4.2 Overturning moments for SMSPF

Based on the method given in the SCI method for single-storey symmetric portal frames, it has been found that the value of M_{OTM} that needs to be resisted by the two-span and three-span frames are 216 kNm and 228 kNm that represents approximately 54% and 16% of the plastic moment capacity of column section, $M_{pl,c}$, of 398 kNm and 1403 kNm, respectively. The SCI method assumes that both the columns and the column bases are fully protected from fire. In reality, when column is protected from fire with concrete covering, the temperature usually does not rise above 350° C, and almost all of the strength of the material is retained. It should be noted that, the SCI method does not state the rotational stiffness of the column bases.

5.4.3 Material properties at elevated temperature and fire model

The same material properties and fire model that have been used for single-span steel portal frames are used here. For details, the readers are referred to Chapter 3.

5.4.4 Finite element modelling

The same finite element model that have been developed and validated in Chapter 3 has been used here for analyzing the two-span and three-span frames. However, there are some exceptions in terms of number of elements and relaxation of some tolerance parameters for achieving a solution by avoiding severe convergence difficulties which was not encountered while analyzing single-span portal frame models.

As the number of spans are increased, the number of elements are also increased. Based on a mesh sensitivity study, it has been found that a set of 176 and 256 elements is sufficient for the analysis with 16 elements for each column and 64 elements for each rafter for two-span and three-span frame, respectively. Similar to the single span-frame, all the columns and rafters are modelled using beam elements B21; and other possible second order elements are avoided due to the so-called 'volumetric locking' problem induced by the large elemental strain in the deformed configuration. Rotational spring elements 'SPRING2' are used to model the rotational stiffness of the column bases. As usual the non-dimensional rotational stiffness, K_b, is considered as 0.4 for nominally pinned column bases.

Unlike single span frames, where the model is solved comparatively faster, usually within one to five minutes by using the implicit dynamic solver, the solver time (CPU time) is increased monumentally for the same model when it is used to analyze multi-span portal frames. It has been found that inclusion of one additional frame takes almost 30 hours and inclusion of two additional frames 50 hours, both of which essentially are couple of hundred times more than when there is only a single-span frame involved. To achieve efficiency in cost of computation, some tight default tolerance parameters in terms of residual forces and displacements have been relaxed. In order to avoid premature convergence error, the number of cutback, i.e. a reduction in time increment, is increased. The command *CONTROLS with parameters FIELD and TIME INCREMENTATION has been used for this purpose.

The analysis steps follow the transient method where the loads on rafter and at eaves are applied in the first step, and temperature is applied and increased in the second step.

5.5 Study on SMSPF

5.5.1 Frames and fire scenarios

Since there is no restraint provided by purlins or other secondary members and out-of-plane deflections are not allowed, the 2-D plane frame model is considered

as being a lower bound solution. The frames considered for study are shown in Figure 5.2. For convenience, the numbering of different parts of frames are shown

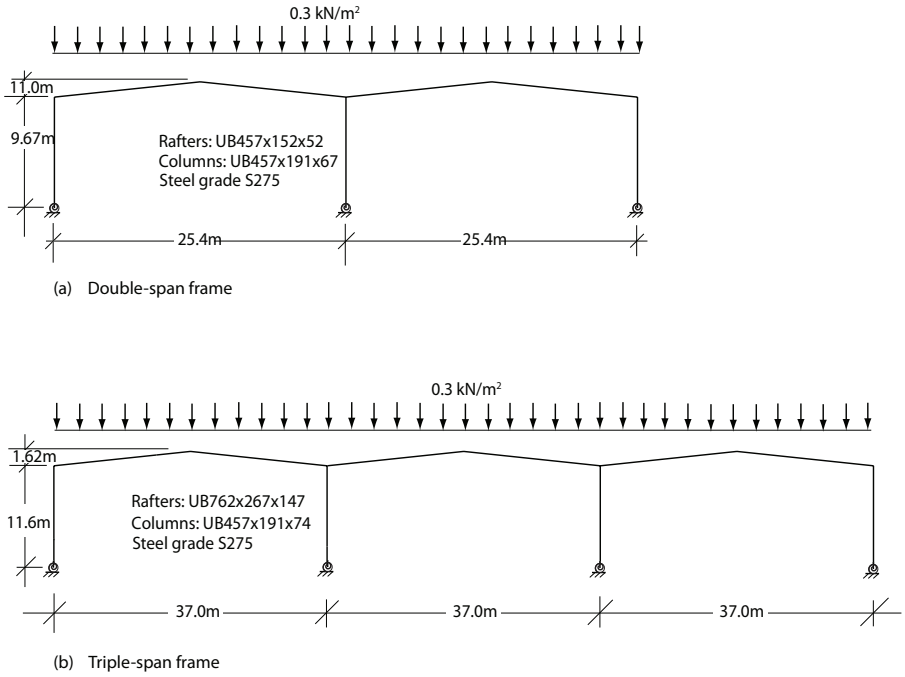

Figure 5.2: Standard multi-span portal frames (SMSPF) for study

in Figure 5.3.

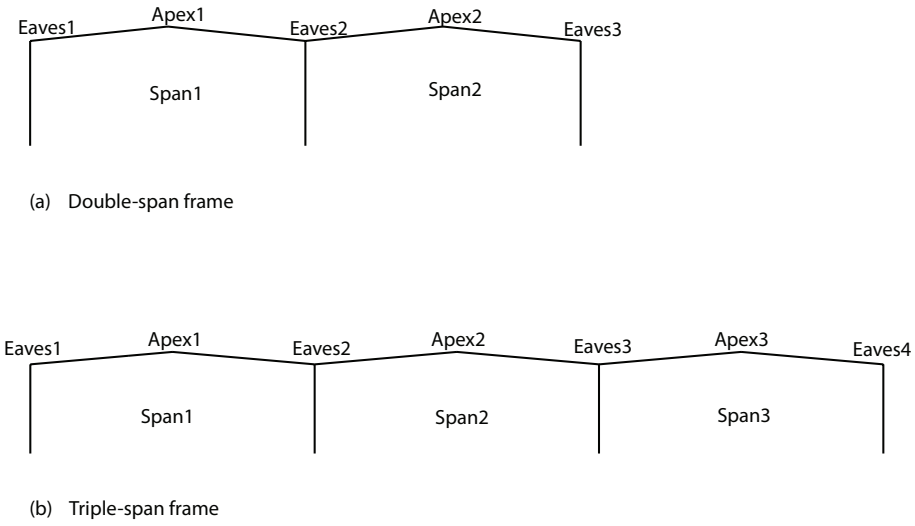

Figure 5.3: Numbering scheme of SMSPFs

A number of different fire scenarios is considered. Fire scenarios are denoted

by 'SX-Y', where S is for the standard frame, X is for the number of frames, which are 2 and 3 for two-span and three-span frames, respectively; and Y is for the fire scenario, which are 'A' for all rafter in fire, 'B' for two adjacent rafters in fire including the middle rafter and 'C' for only the middle rafter in fire, respectively. So, for a two-span frame the fire scenarios are denoted by S2-A and S2-B, representing all rafters and only one rafter in fire, respectively; and for a three-span frame, by S3-A, S3-B, and S3-C representing all rafters, two adjacent rafter including the middle rafter, and only middle rafter in fire, respectively. For clarity, the fire scenarios are shown in Figure 5.4 and Figure 5.5 for two-span and

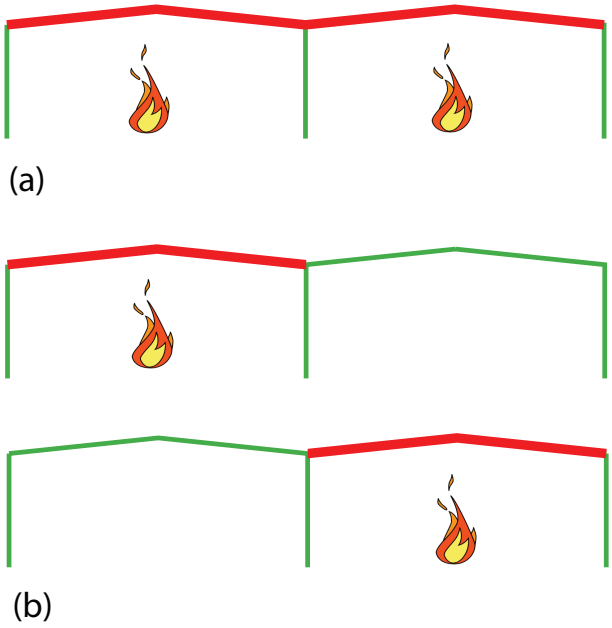

Figure 5.4: Fire scenarios for double-span portal frame: (a) S2-A: all rafters in fire, (b) S2-B: only one rafter in fire. Columns are protected from fire in all cases. Thick red indicates members in fire and thin green indicates member at ambient temperature.

three-span, respectively. In all cases, columns remain at ambient temperature as they are protected from fire. An unprotected columns are not usually used in construction as they require thick section which is not economical.

In this section, the effects of different partial strength of column bases are investigated for each of the fire scenarios described in Figures 5.4 and 5.5.

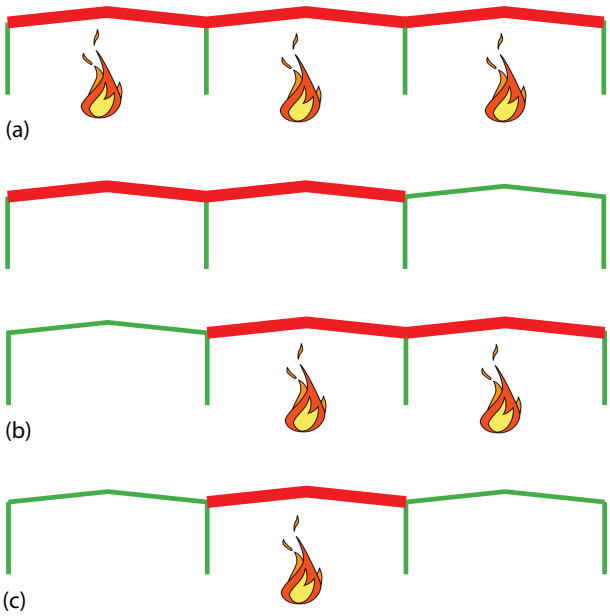

Figure 5.5: Fire scenarios for triple-span portal frame: (a) S3-A: all rafters in fire, (b) S3-B: two adjacent rafters in fire, and (c) S3-C: only mid rafter in fire. Columns are protected from fire in all cases. Thick red indicates members in fire and thin green indicates member at ambient temperature.

5.5.2 Behaviour of SMSPF with perfectly-pinned column bases

The results for perfectly pinned column bases are shown in Figure 5.6 to Figure 5.12. Figure 5.6 and Figure 5.7 show the deflected shapes for two-span and three-span frame respectively for different fire scenarios. Figure 5.8 to Figure 5.12 show the variation of apex deflection and column eaves rotation against temperatures of those frames. The results for perfectly pinned column bases are summarized in Table 5.3.

As can be seen, all the rafters kept at elevated temperatures have been collapsed by snap-through-buckling for fire scenarios S2-A and S3-A. However, when the frames encounter partial fire (i.e. fire scenarios S2-B, S3-B and S3-C), the rafters that are kept at elevated temperatures always collapse. The cold rafters of the frame i.e. those rafters of the frame that are kept at ambient temperature do not collapse for both double-span and triple-span frame. However, for the triple-span frame for fire scenario S3-C, the rafter at the right hand side collapses while the rafter at the left hand side retains its stability and does not collapse. It can be explained that, for fire scenarios S2-B and S3-B, the rafter at ambient temperature do not collapse as the catenary pulling force is weaker than the force

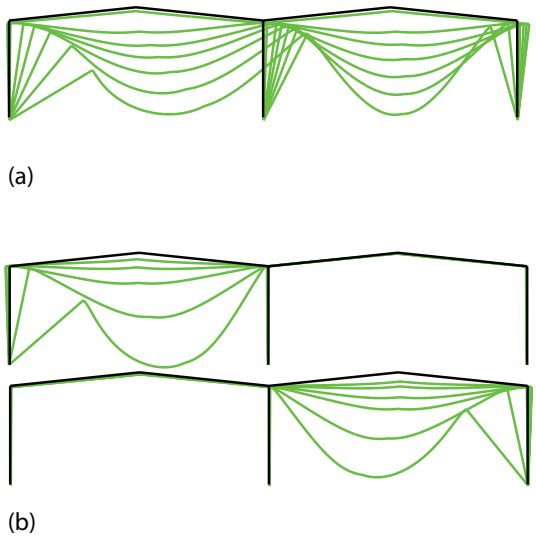

Figure 5.6: Deformed shape for SMSPF double-span frame with perfectly-pinned column bases for two fire scenarios (a) Fire Scenario S2-A; (b) Fire Scenario S2-B.

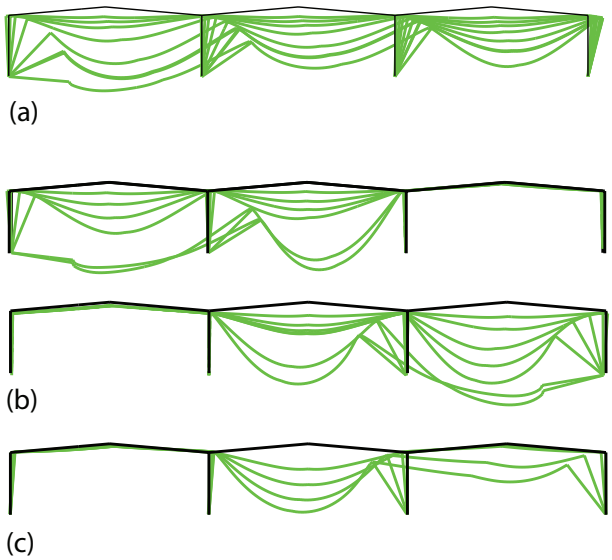

Figure 5.7: Deformed shape for SMSPF triple-span frame with perfectly-pinned column bases for three fire scenarios (a) Fire Scenario S3-A; (b) Fire Scenario S3-B; (c) Fire Scenario S3-C.

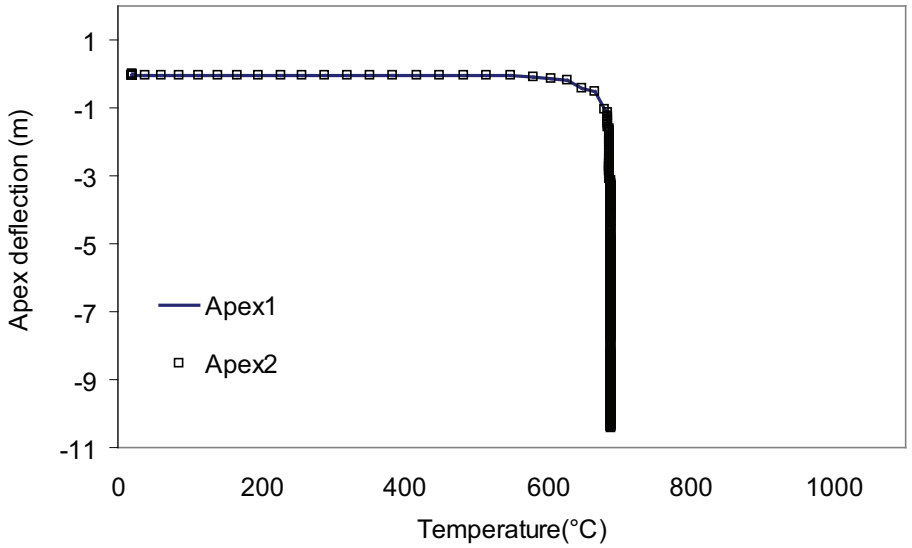

(a) apex deflection

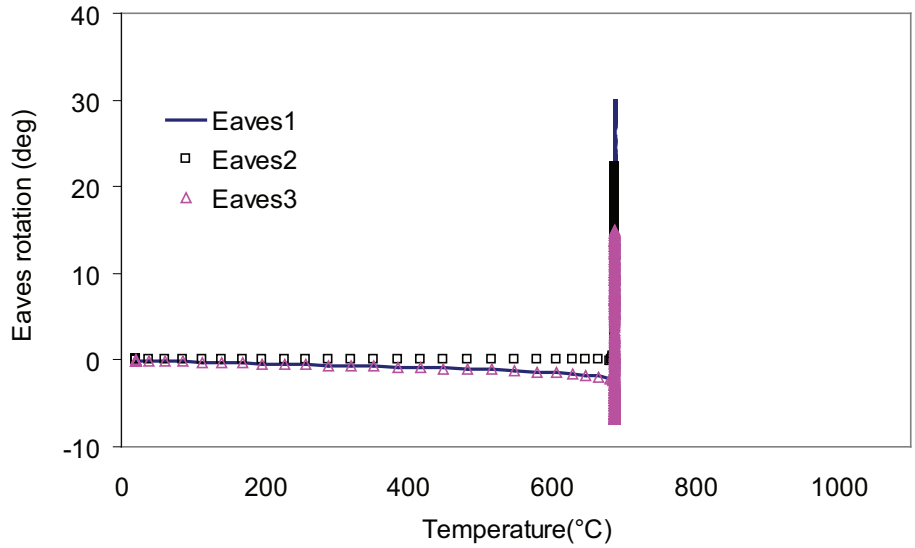

(b) Eaves rotation

Figure 5.8: Variation of apex deflections and eaves rotations against temperature for SMSPF double-span frame: perfectly-pinned column bases, S2-A.

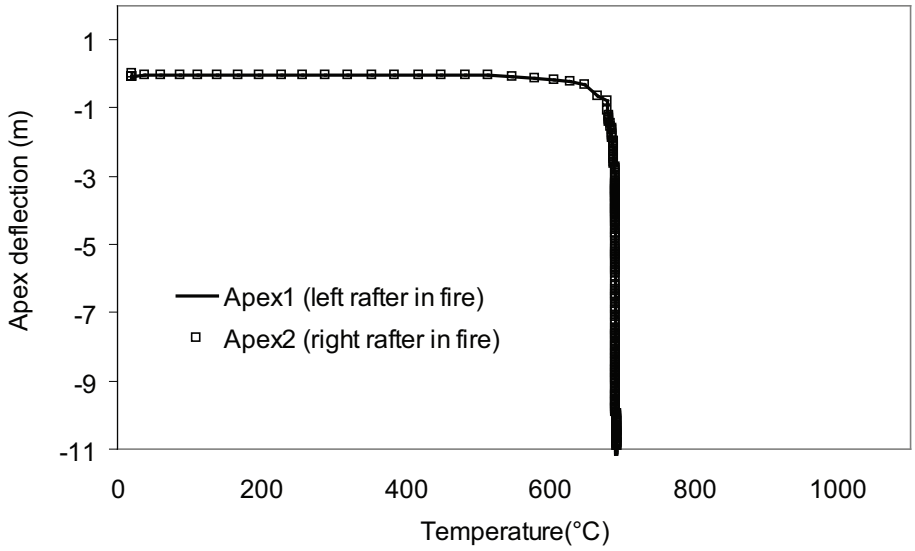

(a) apex deflection

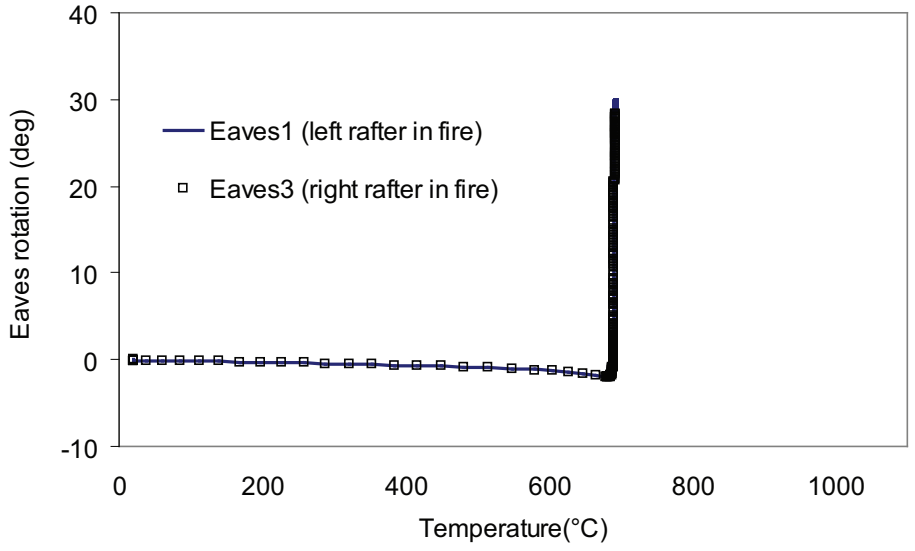

(b) Eaves rotation

Figure 5.9: Variation of apex deflections and eaves rotations against temperature for SMSPF double-span frame: perfectly-pinned column bases, S2-B.

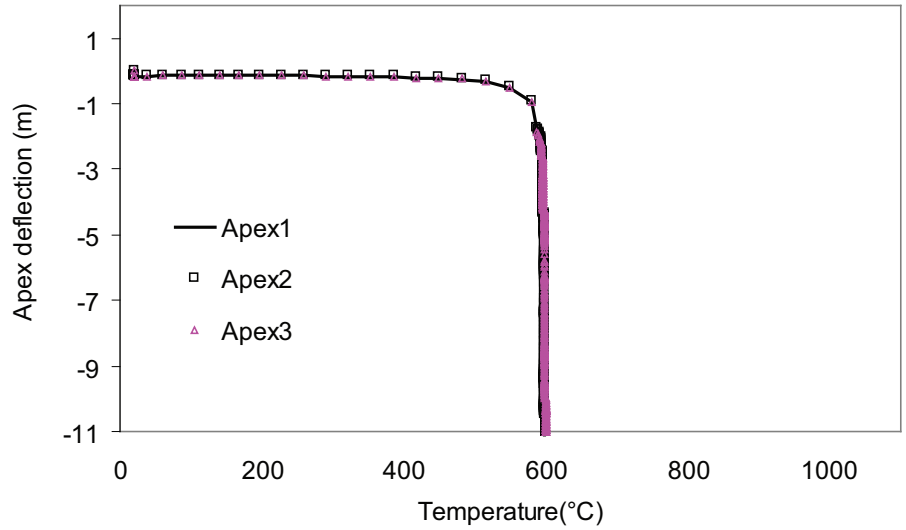

(a) apex deflection

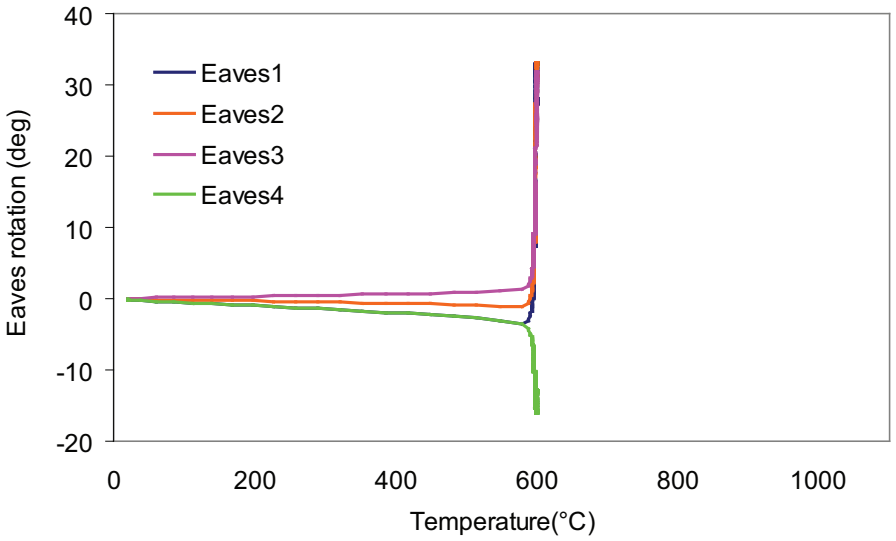

(b) Eaves rotation

Figure 5.10: Variation of apex deflections and eaves rotations against temperature for SMSPF double-span frame: perfectly-pinned column bases, S3-A.

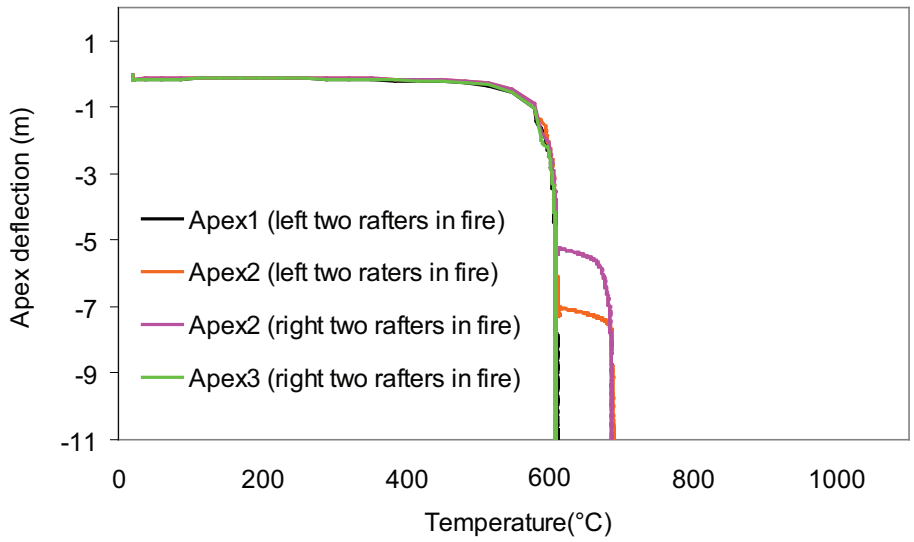

(a) apex deflection

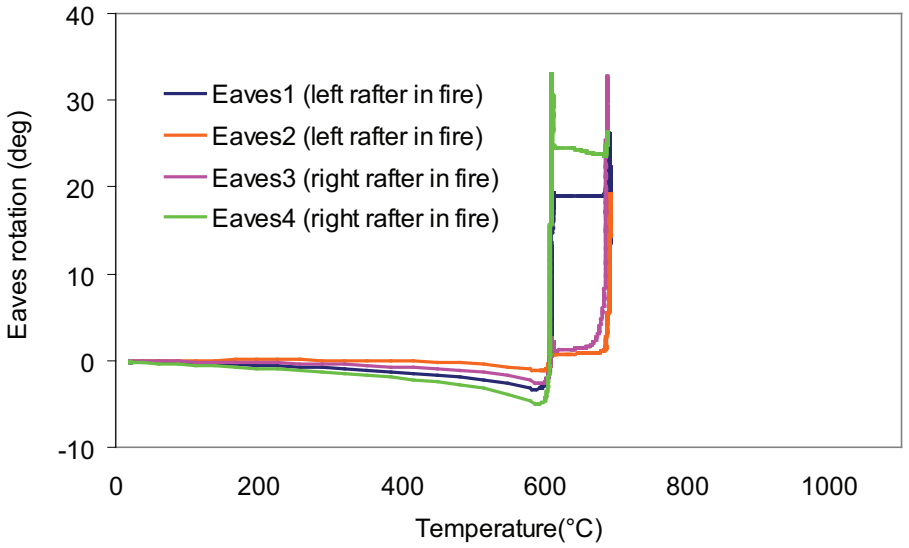

(b) Eaves rotation

Figure 5.11: Variation of apex deflections and eaves rotations against temperature for SMSPF double-span frame: perfectly-pinned column bases, S3-B.

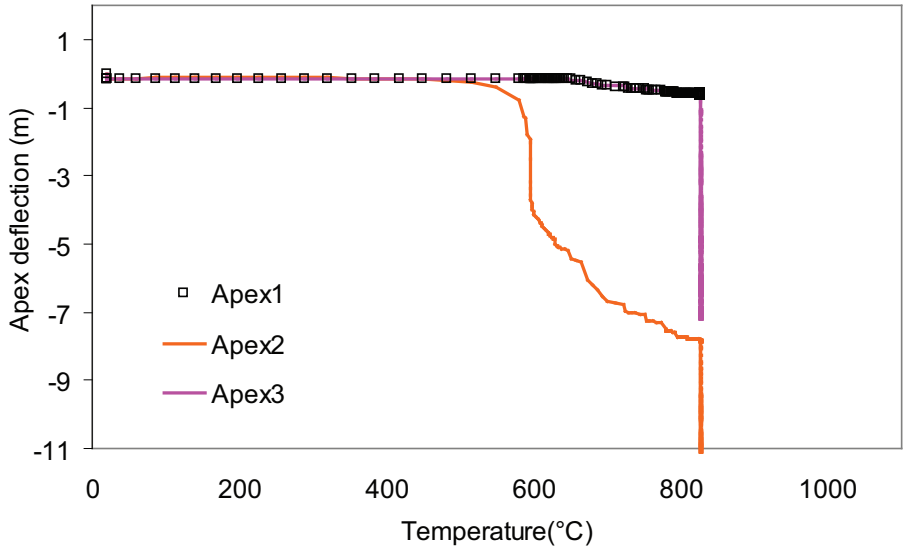

(a) apex deflection

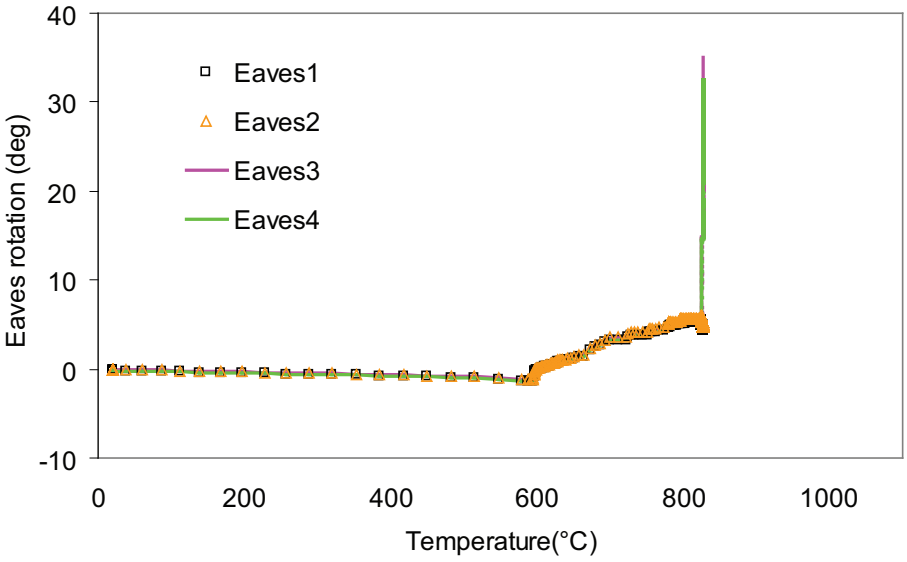

(b) Eaves rotation

Figure 5.12: Variation of apex deflections and eaves rotations against temperature for SMSPF double-span frame: perfectly-pinned column bases, S3-C.

Table 5.3: Summary of results of standard frames with perfectly pinned column base

Span	Fire Scenario	Snap-through-buckling temperature	Collapse temperature	Maximum inward column rotation by 890°C	Maximum outward column rotation by 890°C
		°C	°C	°	°
Double-span	S2-A	688	689	30	6.9
	S2-B	692	693	29	2.1
As single-span	Rafter in fire	687	688	-	-
Triple-span	S3-A	598	599	33	16
	S3-B	607	685	32	4.9
	S3-C	591	826	32	1.4
As single-span	Rafter in fire	596	597	-	-

generated by structural rigidity; however, for fire scenario S3-C, the cold rafter at the right hand side looses its stability due to the catenary pulling force from the hot rafter in the middle part of the frame. The catenary pulling force from the middle part of the frame is much stronger than the structural rigidity at ambient temperature for this case.

From Table 5.3 and Figure 5.8 to Figure 5.12, it can also be noted that the snap-through buckling temperature decreases slightly from 692°C for fire scenario S2-B to 688°C for fire scenario S2-A for a double-span frame. For a triple-span frame, in a similar fashion, the snap-through-buckling temperature decreases slightly from 607°C for fire scenario S3-B to 598°C for fire scenario S3-A. The collapse temperature for all the frames remains almost the same apart from the fire scenario S3-C. For fire scenario S3-C, the frames collapses at a higher temperature of 826°C because of higher restraints provided by the adjacent members at ambient temperature. In all other cases, the restraints provided by the adjacent members are much lower and cannot resist the collapse. All of the frames collapse much earlier than 890°C as the SCI method assumed. It should be noted that all of the frames exceed the limit of eaves rotation of 1° given by the SCI method and reaches as high as 16°.

It should also be noted from Table 5.3 that when all the rafters are subjected to fire, i.e. fire scenario S2-A or S3-A, the snap-through buckling temperature is

almost identical to the single-span frames.

5.5.3 Effect of partial strength of column bases on SMSPF

In order to determine the effect of partial strength of column bases on SMSPF, two different cases of overturning moment of column bases, M_{OTM}, have been considered. They are: M_{OTM}=1.0M_{SCI} and M_{OTM}=2.0M_{SCI}, where M_{SCI} is the column base moment calculated by using the SCI method for single span symmetric portal frames. In all cases, nominally pinned column bases with non-dimensional rotational stiffness i.e. the gradient of the moment-rotation curve, K_b, of 0.4 have been considered. Different bi-linear moment-rotation curves for establishing partial strength of column bases are shown Figure 5.13.

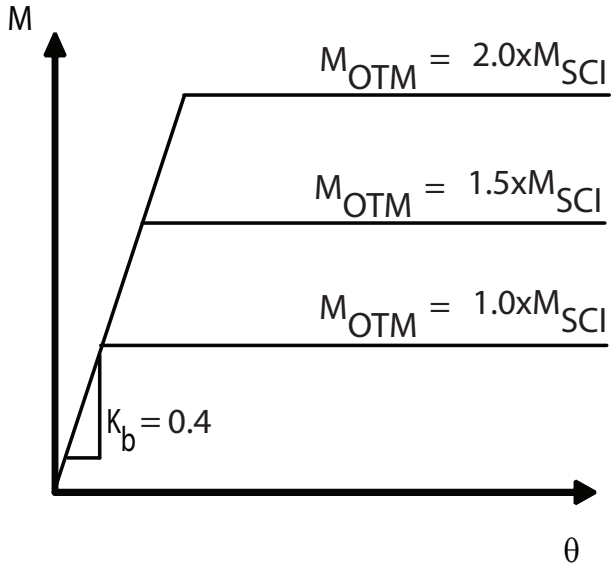

Figure 5.13: Moment-rotation curve for partial strength of column base.

M_{OTM} of 1.0M_{SCI}

In Section 5.4.2, it has been described that in accordance with the SCI method, the column base needs only to be designed to sustain an overturning moment, M_{OTM}, of 216 kNm and 228 kNm for double-span and triple-span frames, respectively. Such overturning moments represent approximately 54% and 16% of the plastic moment capacity of column section, $M_{pl,c}$, of 398 kNm and 1403 kNm, respectively.

Figure 5.14 to Figure 5.38 show the variation of deflection against temperature

for different fire scenarios for a partial strength M_{OTM} of M_{SCI} for two-span frames (Figure 5.14 to Figure 5.21) and three-span frames (Figure 5.22 to Figure 5.38). The results of Figure 5.14 to Figure 5.38 are summarized in Table 5.4 to Table 5.8.

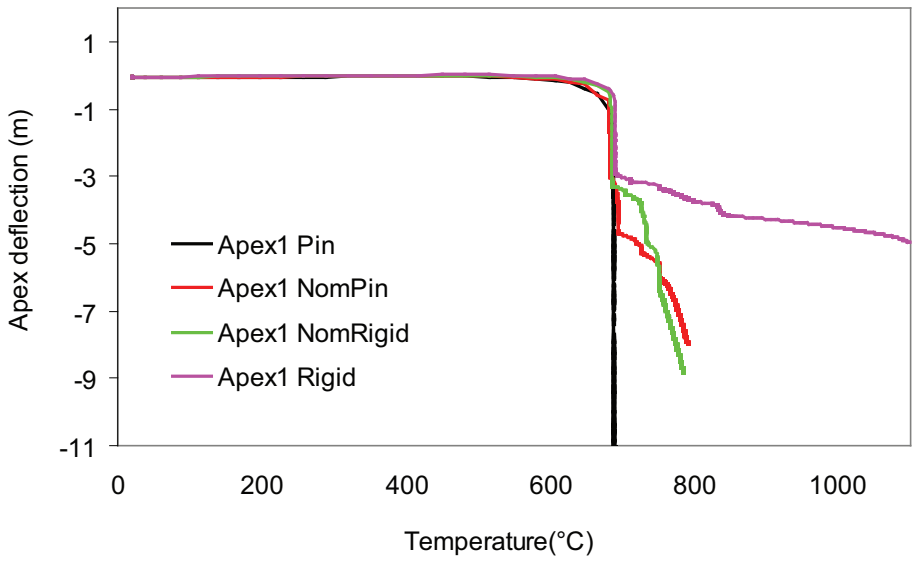

Figure 5.14: Variation of apex deflections against temperatures (SMSPF): Apex1 (S2-A, $M_{OTM} = M_{SCI}$)

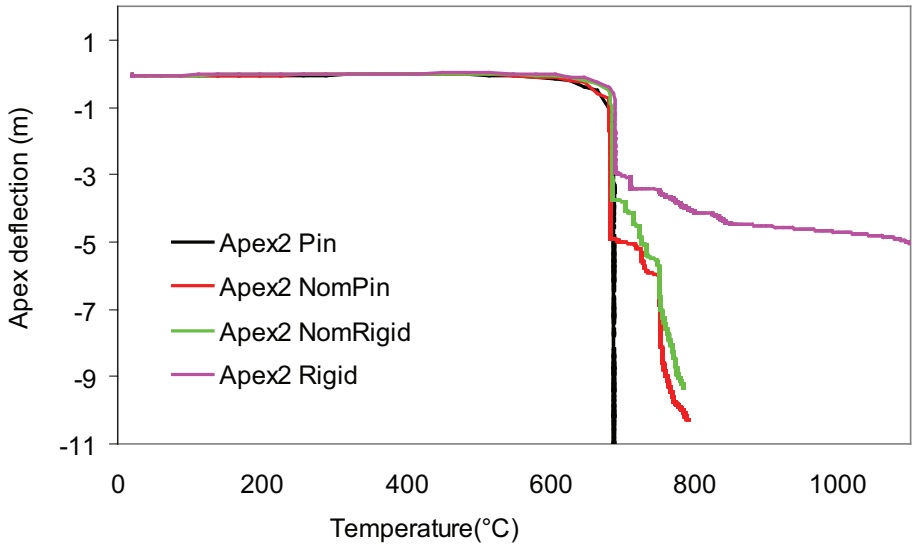

Figure 5.15: Variation of apex deflections against temperatures (SMSPF): Apex2 (S2-A, $M_{OTM} = M_{SCI}$)

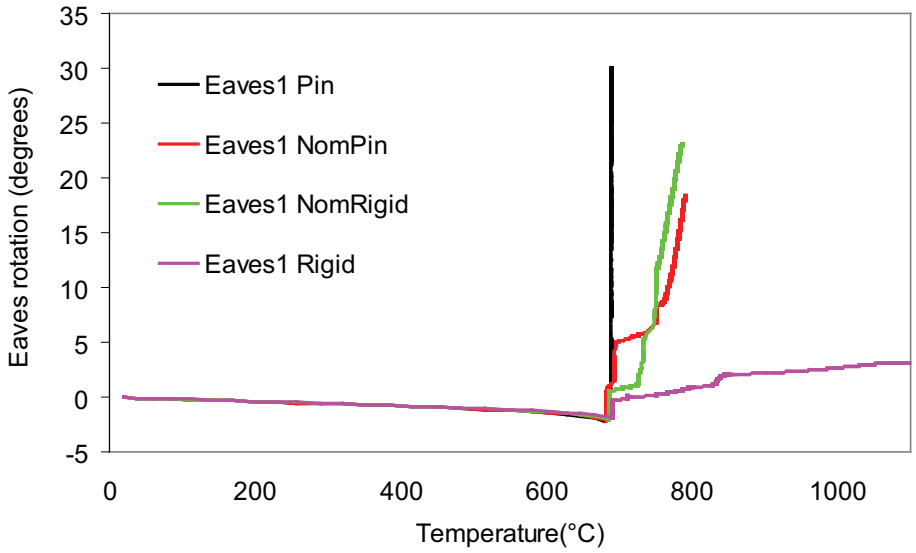

Figure 5.16: Variation of eaves rotations against temperatures (SMSPF): Eaves1 (S2-A, $M_{OTM} = M_{SCI}$)

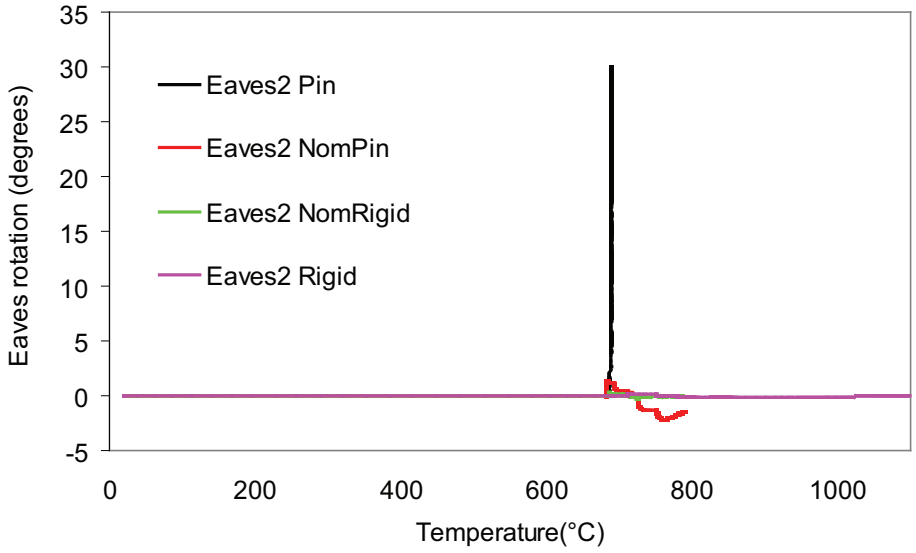

Figure 5.17: Variation of eaves rotations against temperatures (SMSPF): Eaves2 (S2-A, $M_{OTM} = M_{SCI}$)

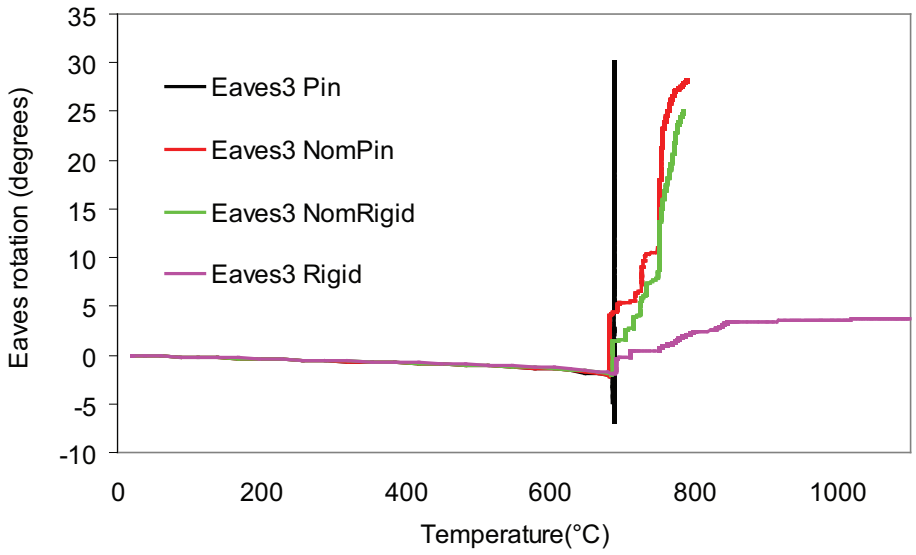

Figure 5.18: Variation of eaves rotations against temperatures (SMSPF): Eaves3 (S2-A, $M_{OTM} = M_{SCI}$)

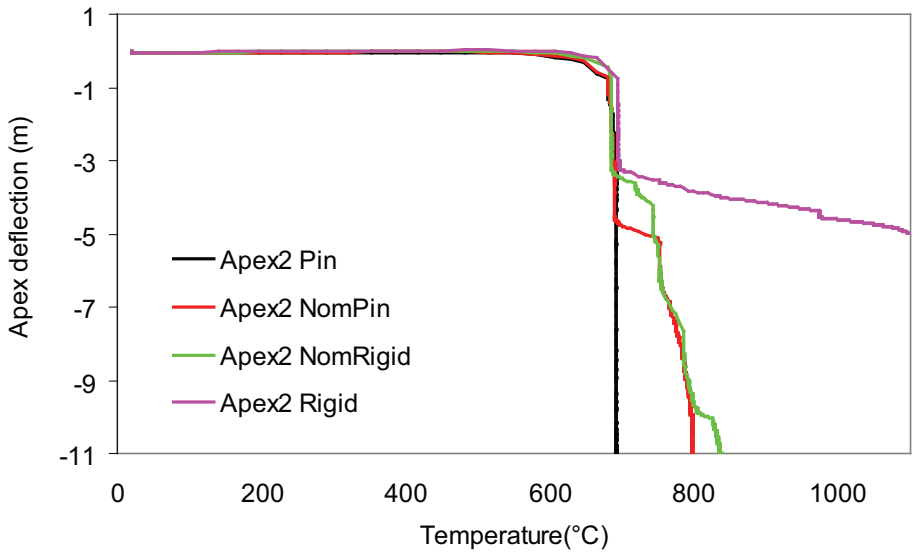

Figure 5.19: Variation of apex deflections against temperatures (SMSPF): Apex2 (S2-B, $M_{OTM} = M_{SCI}$)

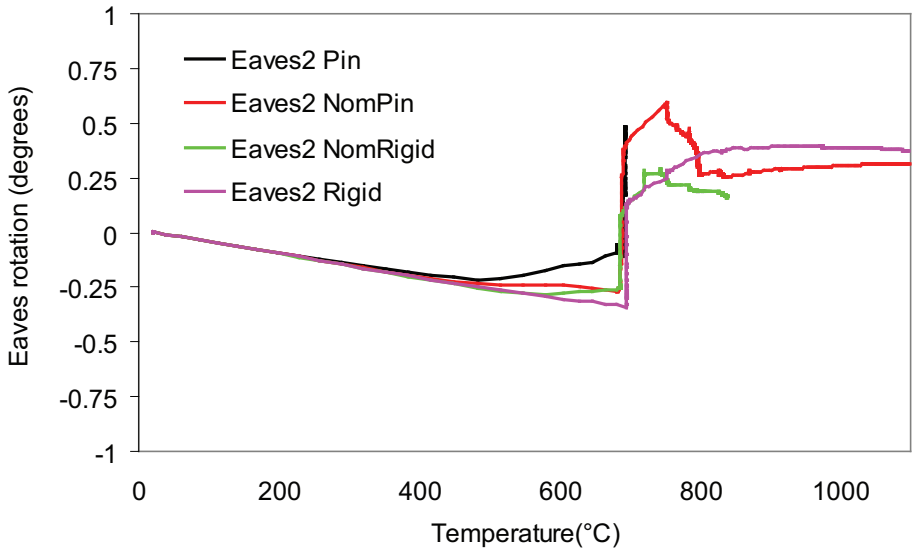

Figure 5.20: Variation of eaves rotations against temperatures (SMSPF): Eaves2 (S2-B, $M_{OTM} = M_{SCI}$)

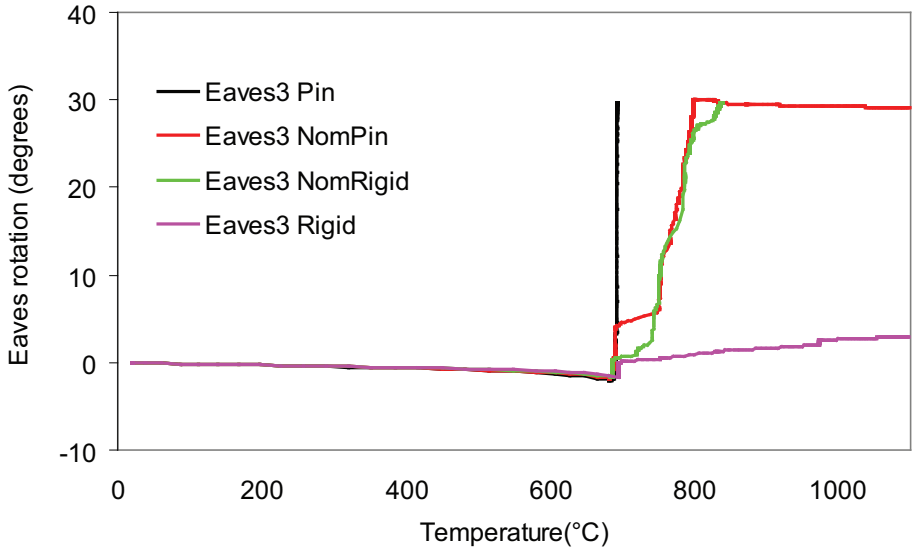

Figure 5.21: Variation of eaves rotations against temperatures (SMSPF): Eaves3 (S2-B, $M_{OTM} = M_{SCI}$)

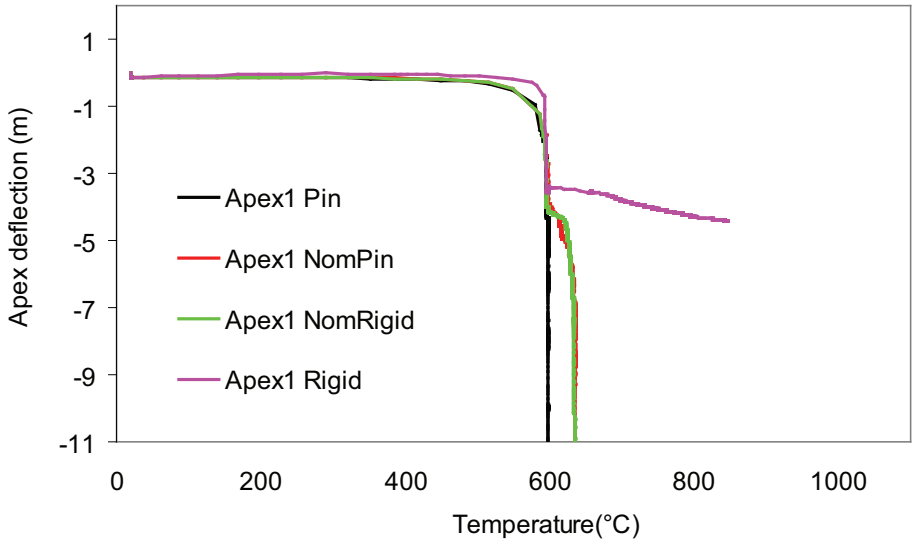

Figure 5.22: Variation of apex deflections against temperatures (SMSPF): Apex1 (S3-A, $M_{OTM} = M_{SCI}$)

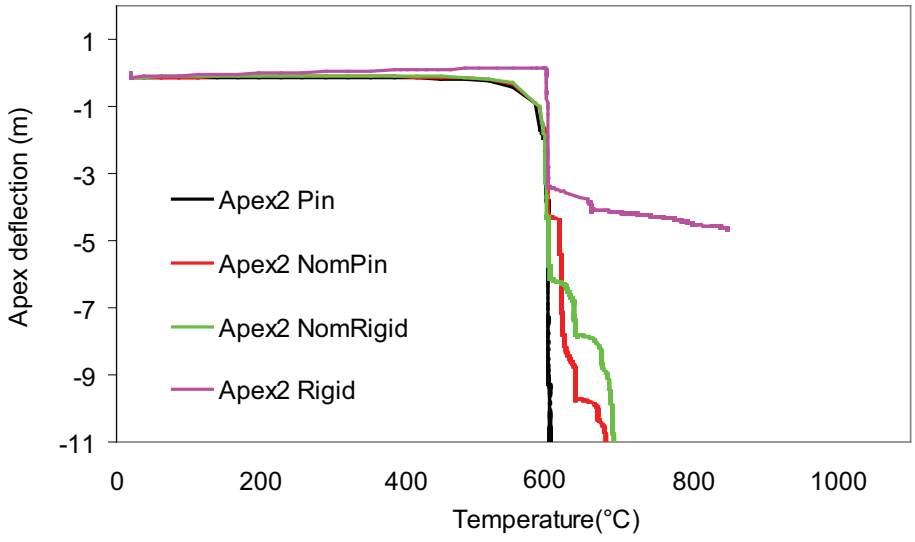

Figure 5.23: Variation of apex deflections against temperatures (SMSPF): Apex2 (S3-A, $M_{OTM} = M_{SCI}$)

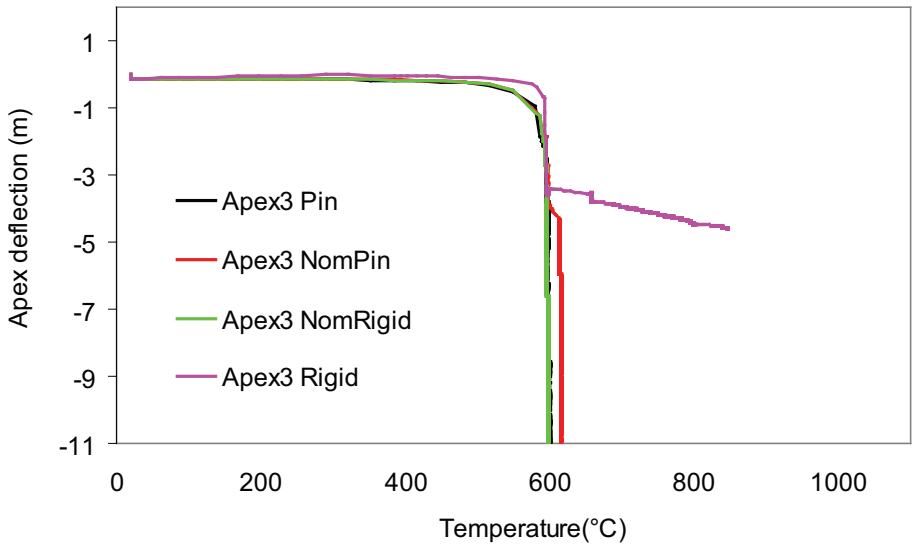

Figure 5.24: Variation of apex deflections against temperatures (SMSPF): Apex3 (S3-A, $M_{OTM} = M_{SCI}$)

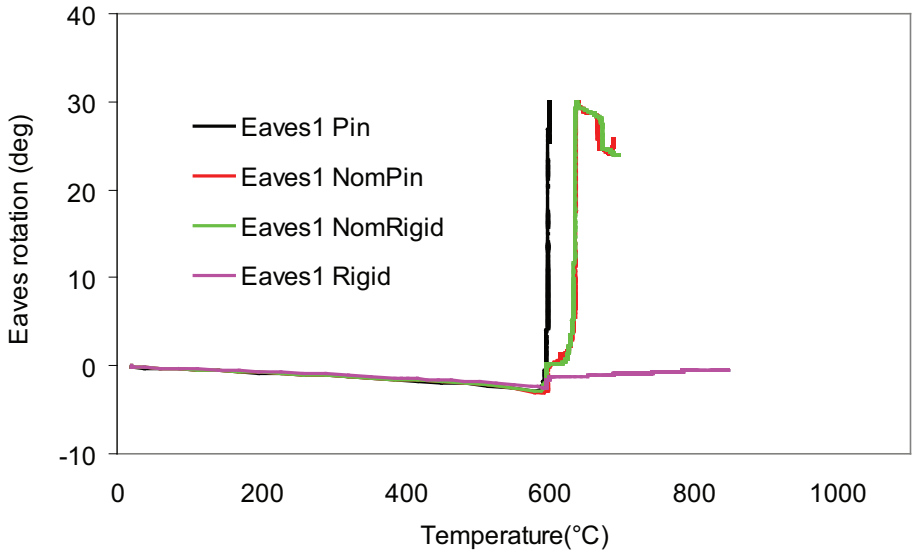

Figure 5.25: Variation of eaves rotations against temperatures (SMSPF): Eaves1 (S3-A, $M_{OTM} = M_{SCI}$)

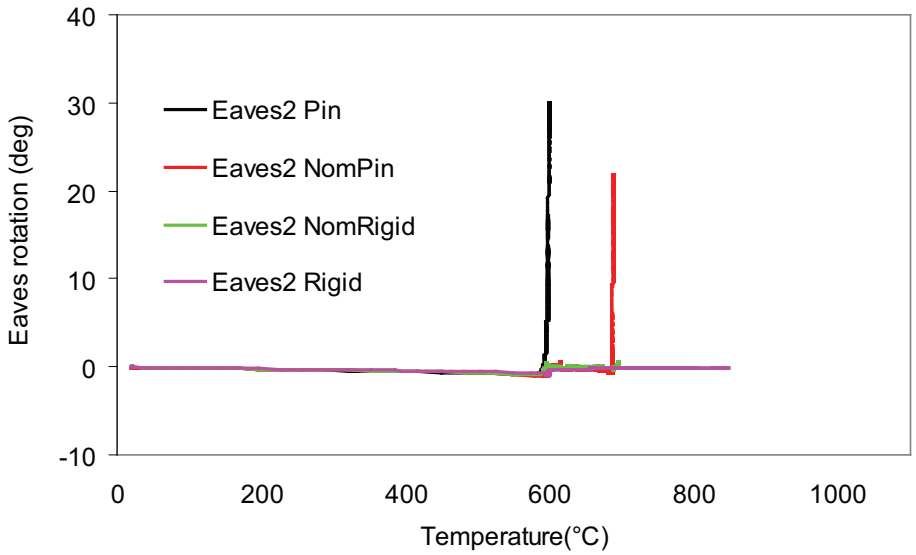

Figure 5.26: Variation of eaves rotations against temperatures (SMSPF): Eaves2 (S3-A, $M_{OTM} = M_{SCI}$)

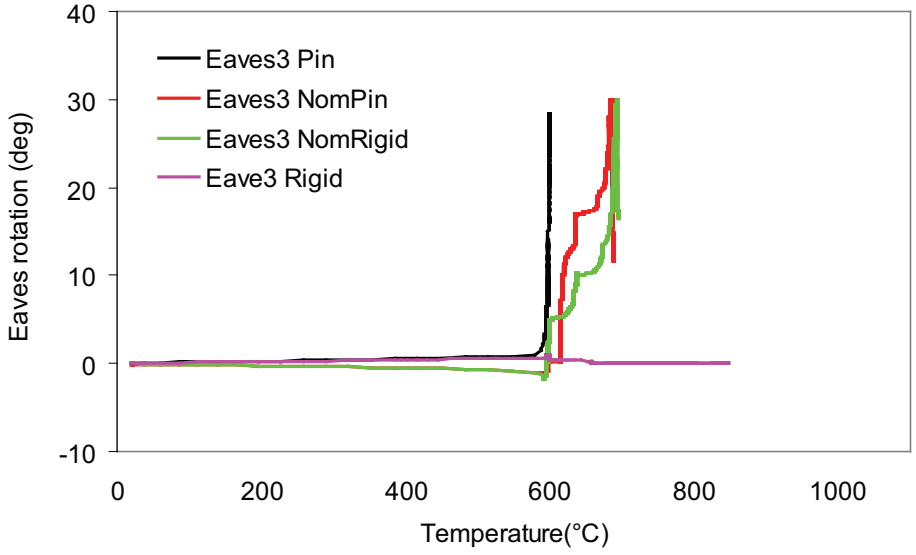

Figure 5.27: Variation of eaves rotations against temperatures (SMSPF): Eaves3 (S3-A, $M_{OTM} = M_{SCI}$)

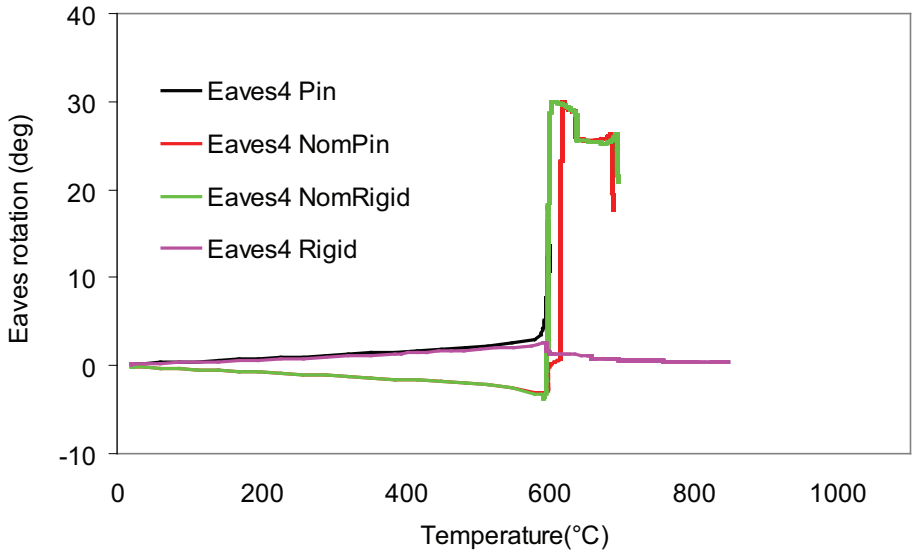

Figure 5.28: Variation of eaves rotations against temperatures (SMSPF): Eaves4 (S3-A, $M_{OTM} = M_{SCI}$)

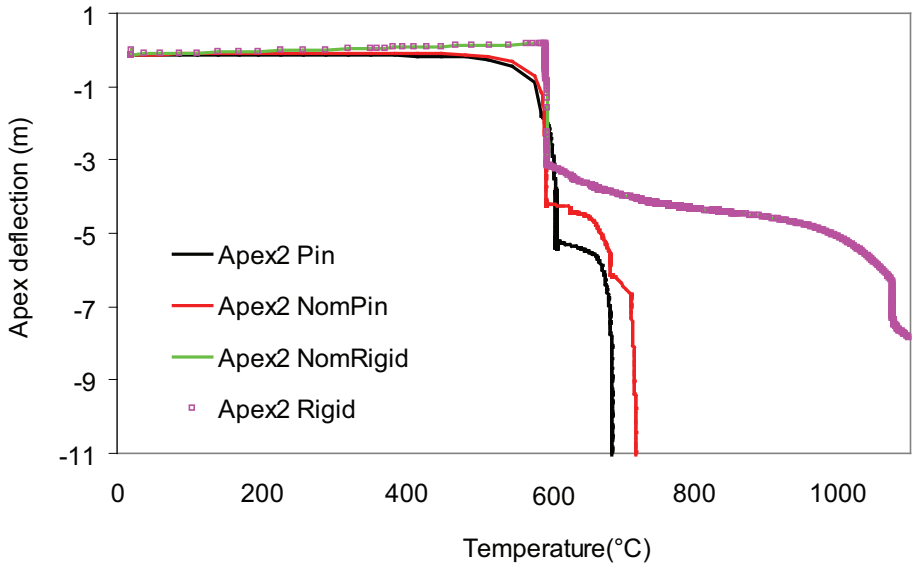

Figure 5.29: Variation of apex deflections against temperatures (SMSPF): Apex2 (S3-B, $M_{OTM} = M_{SCI}$)

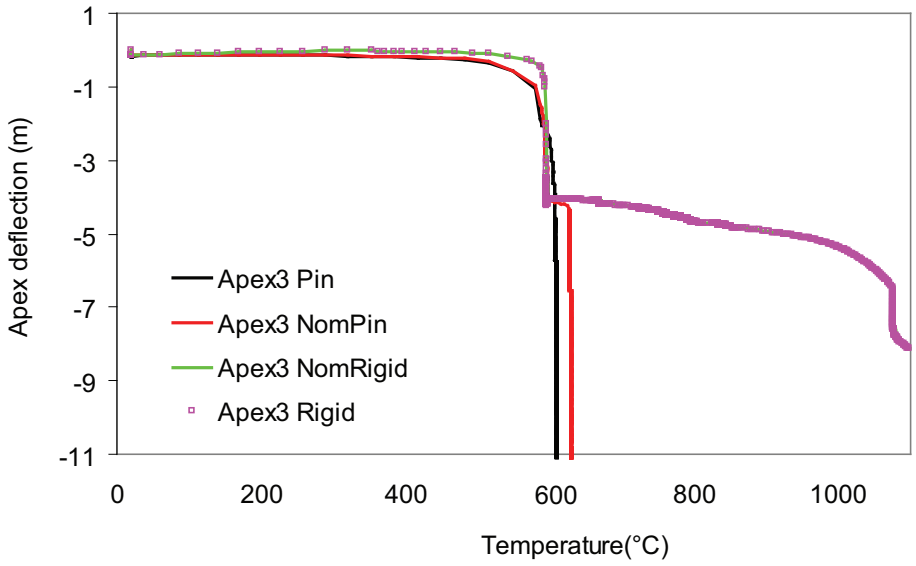

Figure 5.30: Variation of apex deflections against temperatures (SMSPF): Apex3 (S3-B, $M_{OTM} = M_{SCI}$)

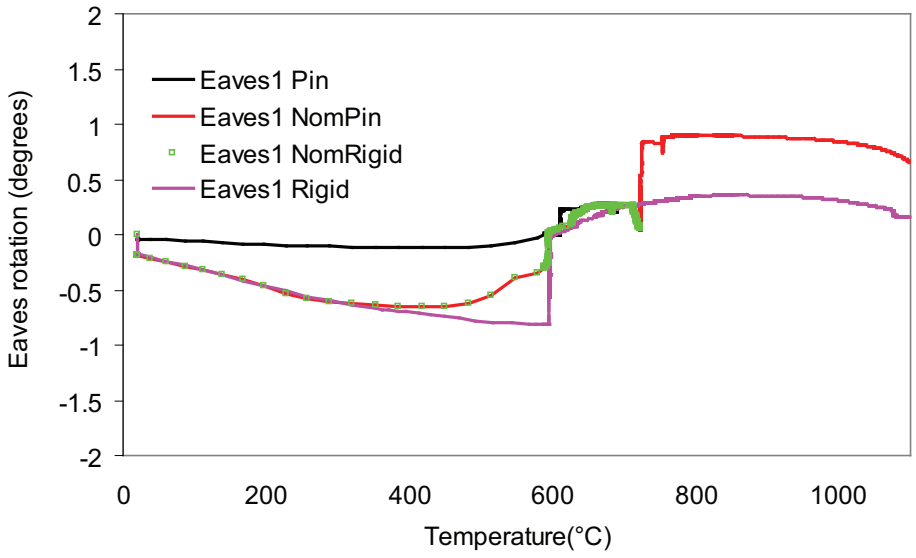

Figure 5.31: Variation of eaves rotations against temperatures (SMSPF): Eaves1 (S3-B, $M_{OTM} = M_{SCI}$)

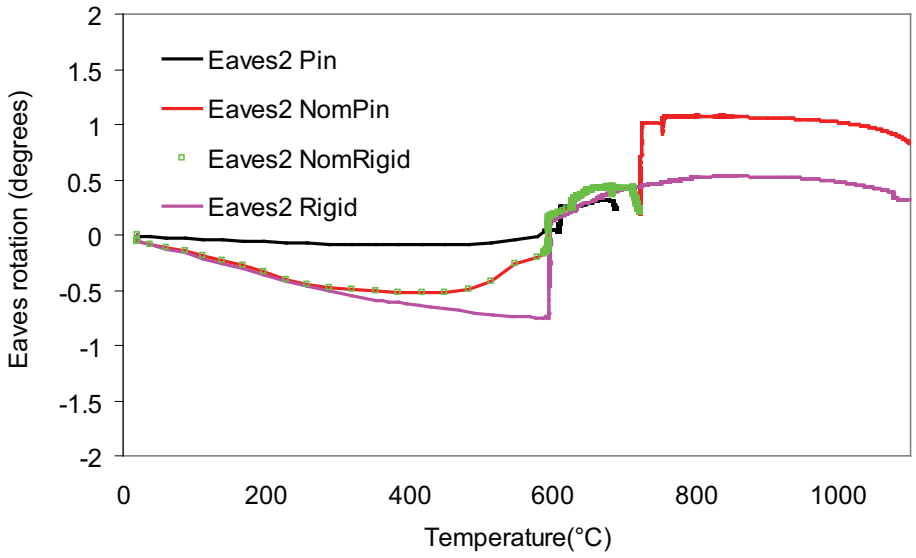

Figure 5.32: Variation of eaves rotations against temperatures (SMSPF): Eaves2 (S3-B, $M_{OTM} = M_{SCI}$)

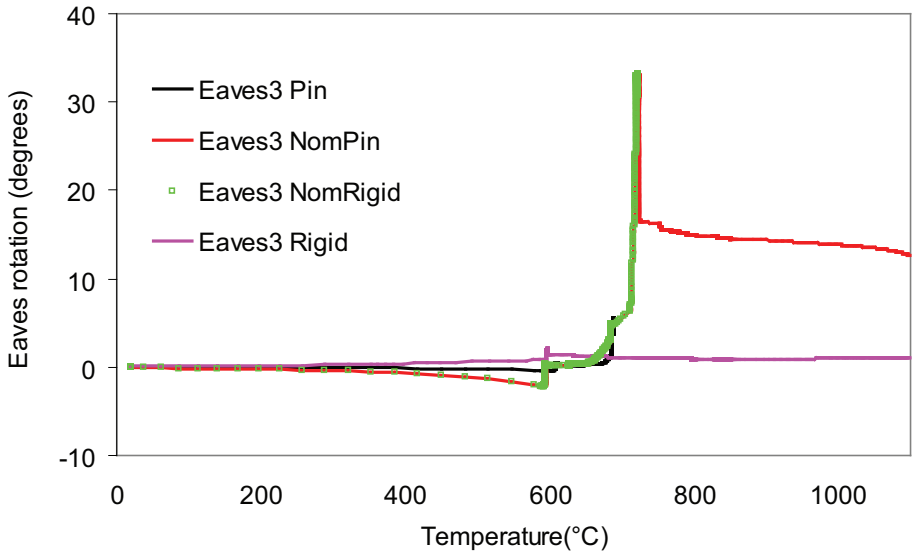

Figure 5.33: Variation of eaves rotations against temperatures (SMSPF): Eaves3 (S3-B, $M_{OTM} = M_{SCI}$)

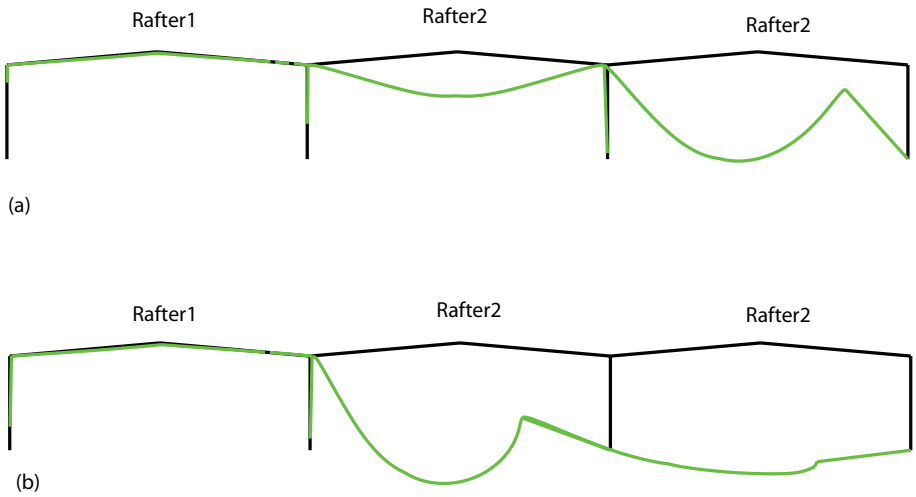

Figure 5.34: Deflected shape and sequence of collapse (a) Rafter3 collapses first; (b) Rafter2 follows afterwards. Rafter1 remains unaffected. (SMSPF): S3-B, $M_{OTM} = M_{SCI}$

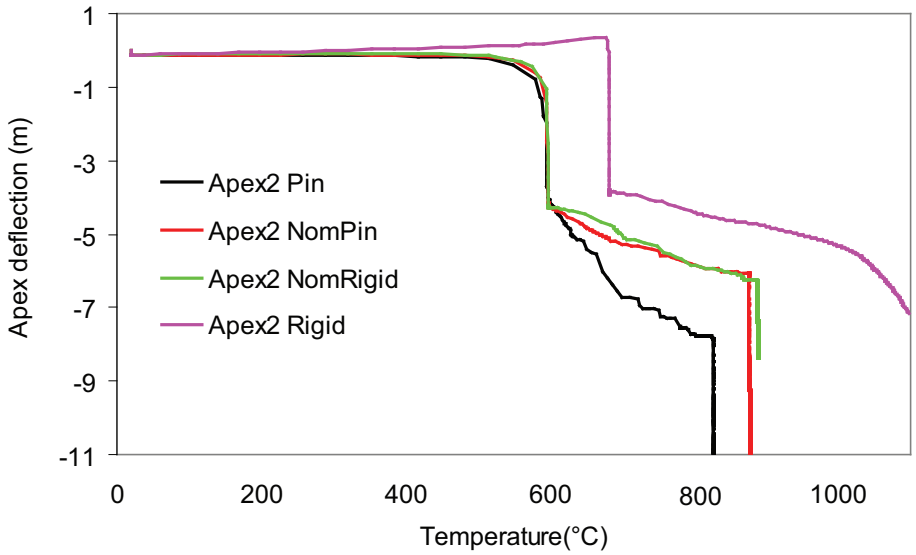

Figure 5.35: Variation of apex deflections against temperatures (SMSPF): Apex2 (S3-C, $M_{OTM} = M_{SCI}$)

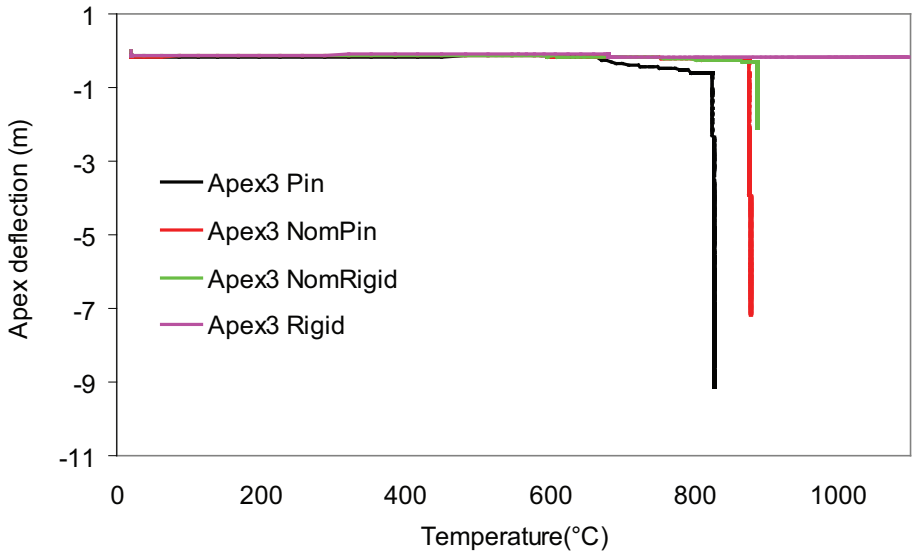

Figure 5.36: Variation of apex deflections against temperatures (SMSPF): Apex3 (S3-C, $M_{OTM} = M_{SCI}$)

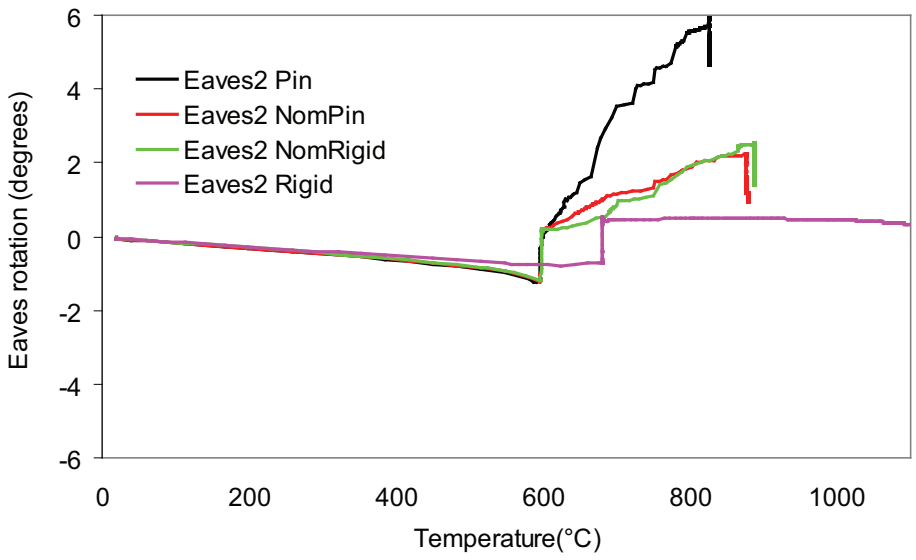

Figure 5.37: Variation of eaves rotations against temperatures (SMSPF): Eaves2 (S3-C, $M_{OTM} = M_{SCI}$)

Table 5.4: Summary of behaviour of SMSPF: S2-A, M_{OTM}=M_{SCI}

Column base	Snap-through-buckling temperature		Collapse temperature		Maximum inward column rotation by 890°C			Maximum outward column rotation by 890°C		
	Span1	Span2	Span1	Span2	Eaves1	Eaves2	Eaves3	Eaves1	Eaves2	Eaves3
	°C	°C	°C	°C	°	°	°	°	°	°
Pin	688	688	689	690	30	22.2	14.9	2.2	-[a]	6.9
Nom. Pin	686	683	825	821	30	2.2	30	2.1	-	2.2
Nom. Rigid	682	686	819	826	24.8	0.2	26.2	2	-	2
Rigid	690	690	>1100	>1100	3.2	0.2	3.7	2	-	2

[a]Outward eaves rotation is not available as the eaves is inside the frame

Table 5.5: Summary of behaviour of SMSPF: S3-A, M_{OTM}=M_{SCI}

Column base	Snap-through-buckling temperature			Collapse temperature			Maximum inward column rotation by 890°C				Maximum outward column rotation by 890°C			
	Span1	Span2	Span3	Span1	Span2	Span3	Eaves1	Eaves2	Eaves3	Eaves4	Eaves1	Eaves2	Eaves3	Eaves4
	°C	°C	°C	°C	°C	°C	°	°	°	°	°	°	°	°
Pin	587	589	587	598	599	599	30	30	28.4	13.5	3	-[a]	-	0
Nom. Pin	594	591	591	634	677	616	30	21.8	30	30	3.1	-	-	3.1
Nom. Rigid	597	593	590	636	687	598	30	0.6	30	30	2.9	-	-	3.7
Rigid	598	597	594	>1100	>1100	>1100	0	0	1	2.6	2.6	-	-	0

[a]Outward eaves rotation is not available as the eaves is inside the frame

Table 5.6: Summary of behaviour of SMSPF: S2-B, M_{OTM}=M_{SCI}

Column base	Snap-through-buckling temperature	Collapse temperature	Max inward column rotation by 890°C				Max outward column rotation by 890°C		
	Span1	Span2	Span1	Span2	Eaves1	Eaves2	Eaves3	Eaves1	Eaves2	Eaves3
	°C	°C	°C	°C	◦	◦	◦	◦	◦	◦
Pin	-[a]	680	-	692	<1	<1	44.7	<1	<1	2.1
Nom. Pin	-	680	-	799	<1	<1	45	<1	<1	2.2
Nom. Rigid	-	685	-	844	<1	<1	44	<1	<1	2.1
Rigid	-	695	-	1094	<1	<1	<1	<1	<1	2.1

[a]This part of the frame is ambient temperature and retains its rigidity and did not collapse

Table 5.7: Summary of behaviour of SMSPF: S3-B, M_{OTM}=M_{SCI}

Column base	Snap-through-buckling temperature			Collapse temperature			Maximum inward column rotation by 890°C				Maximum outward column rotation by 890°C			
	Span1	Span2	Span3	Span1	Span2	Span3	Eaves1	Eaves2	Eaves3	Eaves4	Eaves1	Eaves2	Eaves3	Eaves4
	°C	°C	°C	°C	°C	°C	◦	◦	◦	◦	◦	◦	◦	◦
Pin	-[a]	609	605	-	687	609	<1	<1	2.2[b], 40.4[c]	40.4	<1	-[d]	-	4.2
Nom. Pin	-	594	594	-	721	630	<1	<1	2.2, 40.5	41.4	<1	-	-	4
Nom. Rigid	-	594	594	-	715	628	<1	<1	2.2, 40.0		<1	-	-	
Rigid	-	594	594	-	1096	1096	<1	<1	<1	<1	<1	-	-	< 1

[a]This part of the frame is ambient temperature and retains its rigidity and did not collapse
[b]rotation of Eaves3 when Eaves4 ic collapsed
[c]rotation of Eaves4 when it is collapsed
[d]Outward eaves rotation is not available as the eaves is inside the frame

Table 5.8: Summary of behaviour of SMSPF: S3-C, M_{OTM}=M_{SCI}

Column base	Snap-through-buckling temperature			Collapse temperature			Maximum inward column rotation by 890°C				Maximum outward column rotation by 890°C			
	Span1	Span2	Span3	Span1	Span2	Span3	Eaves1	Eaves2	Eaves3	Eaves4	Eaves1	Eaves2	Eaves3	Eaves4
	°C	°C	°C	°C	°C	°C	◦	◦	◦	◦	◦	◦	◦	◦
Pin	-	595	826	-	826	826	4.2	4.2	38.8	34.3	-	-	-	-
Nom. Pin		597	-	-	877	-	<1	<1	38.4	34	-	-	-	-
Nom. Rigid	-	597	-	-	887	-	<1	<1	10.5	10	-	-	-	-
Rigid	-	681	-	-	1095	-	<1	<1	<1	<1	-	-	-	-

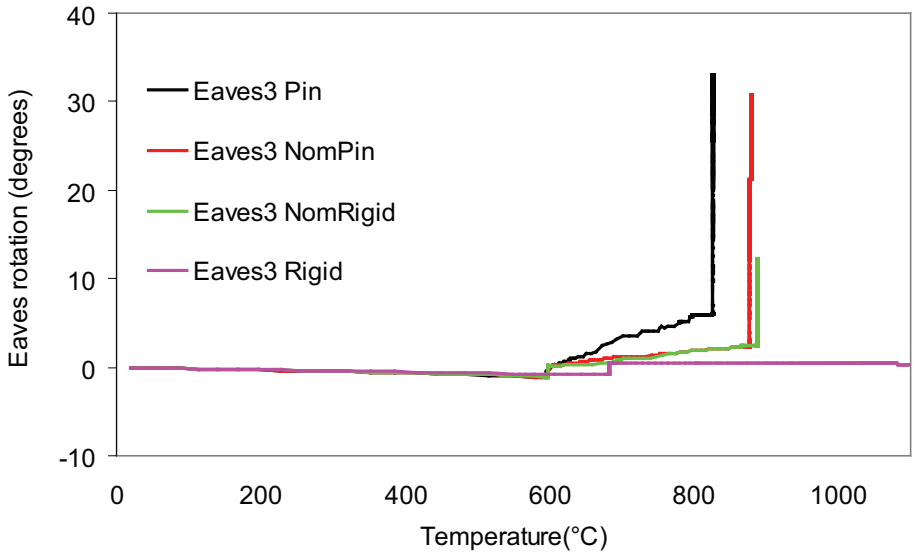

Figure 5.38: Variation of eaves rotations against temperatures (SMSPF): Eaves3 (S3-C, $M_{OTM} = M_{SCI}$)

- Fire Scenario A:

It can be seen from Table 5.4, for the two-span frame for nominally pinned and nominally rigid column bases, that the snap-through buckling temperature varies between 682°C and 686°C which is slightly lower than 688°C for pinned column bases. The maximum outward column rotation is 2.2°. Similarly, from Table 5.5, it can be seen, for three-span frame for nominally pinned and nominally rigid column bases that the snap-through buckling temperature varies between 591°C and 597°C which is slightly higher than 587°C for pinned column bases. The maximum outward column rotation is 3.7°. The effect of the partial strength column base in both two and three-span frames is that the behaviour of the frames are similar to that of frames with perfectly pinned column bases. Increasing the column base rotational stiffness from nominally pinned to nominally rigid has very little effect.

- Fire Scenario B:

It can be seen from Table 5.6, for two-span frame for nominally pinned and nominally rigid column bases, that the snap-through buckling temperature varies between 680°C and 685°C which is almost similar to 680°C for pinned column bases. The maximum outward column rotation is 2.1°. Similarly, from Table 5.7, it can be seen, for the three-span frame for nominally pinned and nominally rigid column bases, that the snap-through buckling temperature 594°C which is lower than 609°C for pinned column bases. The maximum outward column rotation is

4.2°. For three-span frame, it should be noted that the rightmost rafter collapses in the first place while at the same time the mid-rafter remains suspended (Figure 5.34). When temperature further increases the middle rafter collapses. The effect of the partial strength column base in both two-span and three-span frames is that the frames behave similarly to that of a frame with a perfectly pinned column base. Increasing the column base rotational stiffness from nominally pinned to nominally rigid has very little effect too.

- Fire Scenario C:

This fire scenario is applicable to only a three-span frame. As can be seen from Table 5.8, for nominally pinned and nominally rigid column bases, that the snap-through buckling temperature is 597°C which is almost similar to 595°C for pinned column bases. There is no outward column rotation. It should be noted that when the temperature in mid rafter is 826°C for pinned column bases, the rightmost rafter collapses even if it is in ambient temperature.

M_{OTM} of $2.0M_{SCI}$

Figure 5.39 to Figure 5.62 show the variation of deflection against temperature for different fire scenarios for a partial strength M_{OTM} of $2.0M_{SCI}$ for two-span frames(Figure 5.39 to Figure 5.45) and three-span frames(Figure 5.46 to 5.62). The results of Figure 5.39 to Figure 5.62 are summarized in Table 5.9 to Table 5.13.

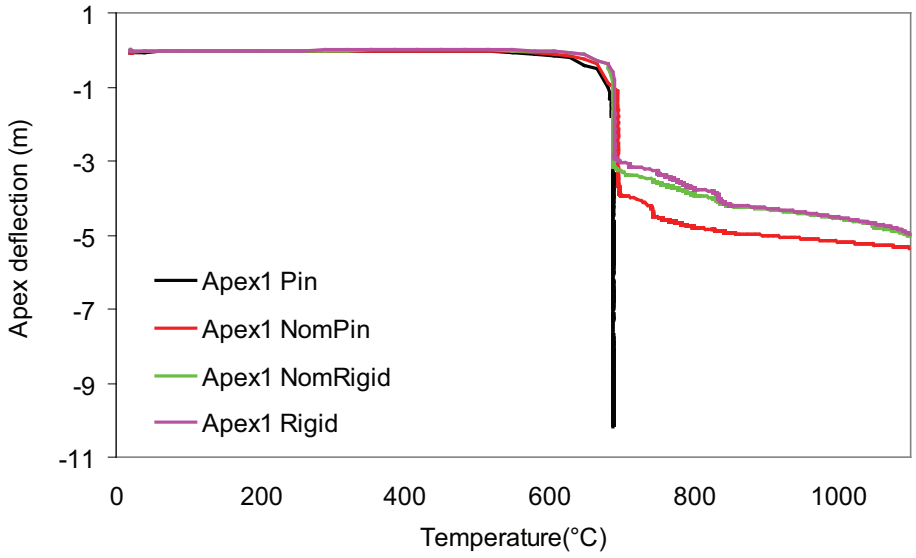

Figure 5.39: Variation of apex deflections against temperatures (SMSPF): Apex1 (S2-A, $M_{OTM} = 2.0M_{SCI}$)

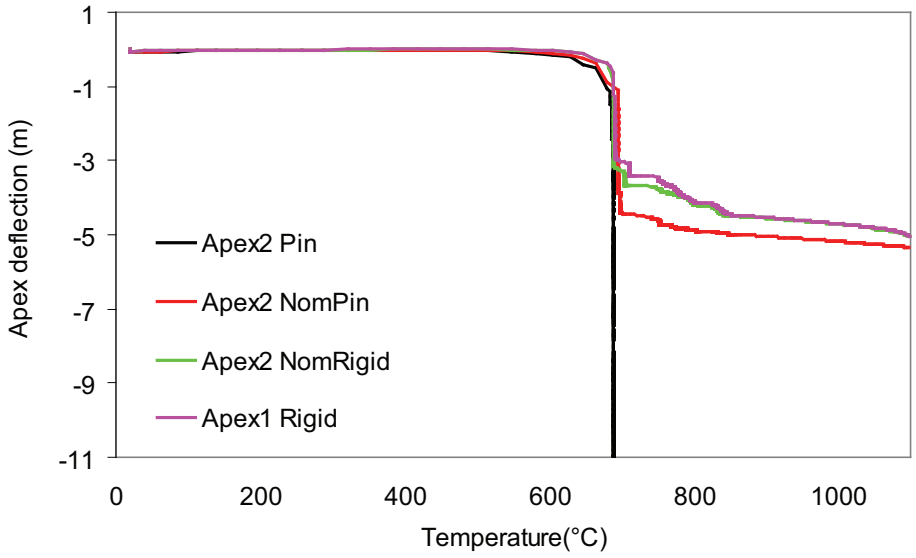

Figure 5.40: Variation of apex deflections against temperatures (SMSPF): Apex2 (S2-A, $M_{OTM} = 2.0M_{SCI}$)

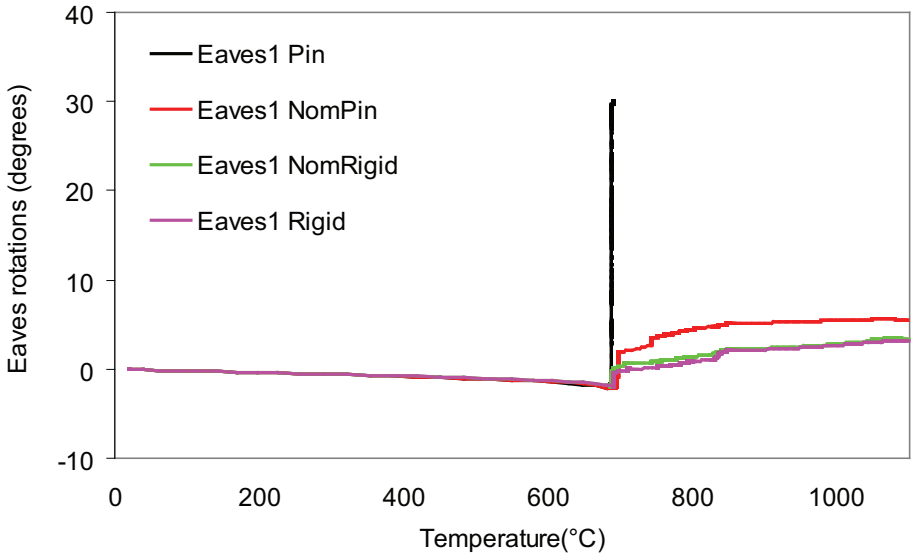

Figure 5.41: Variation of eaves rotaions against temperatures (SMSPF): Eaves1 (S2-A, $M_{OTM} = 2.0M_{SCI}$)

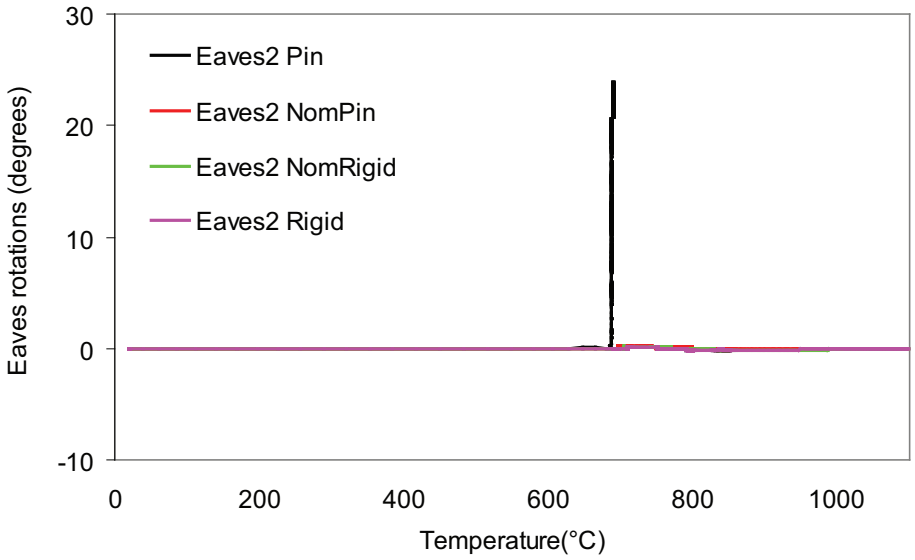

Figure 5.42: Variation of eaves rotaions against temperatures (SMSPF): Eaves2 (S2-A, $M_{OTM} = 2.0M_{SCI}$)

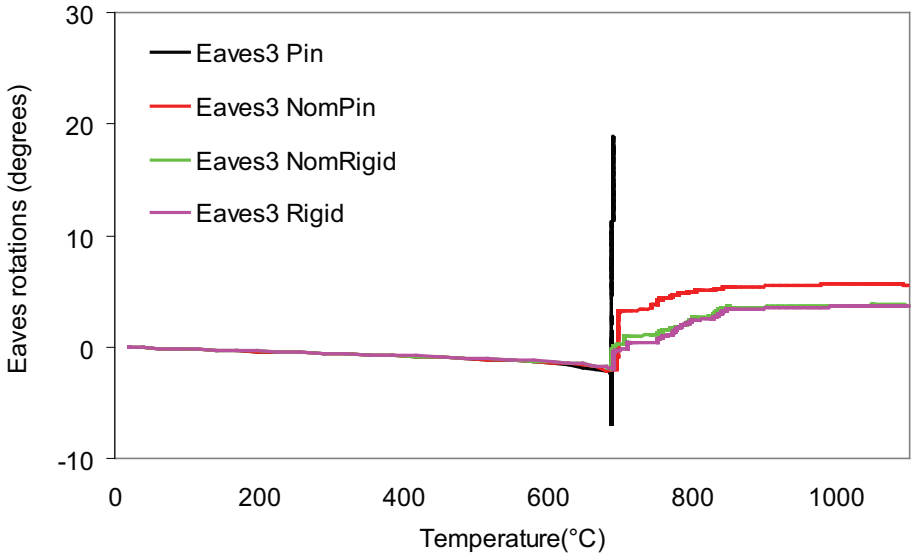

Figure 5.43: Variation of eaves rotaions against temperatures (SMSPF): Eaves3 (S2-A, $M_{OTM} = 2.0M_{SCI}$)

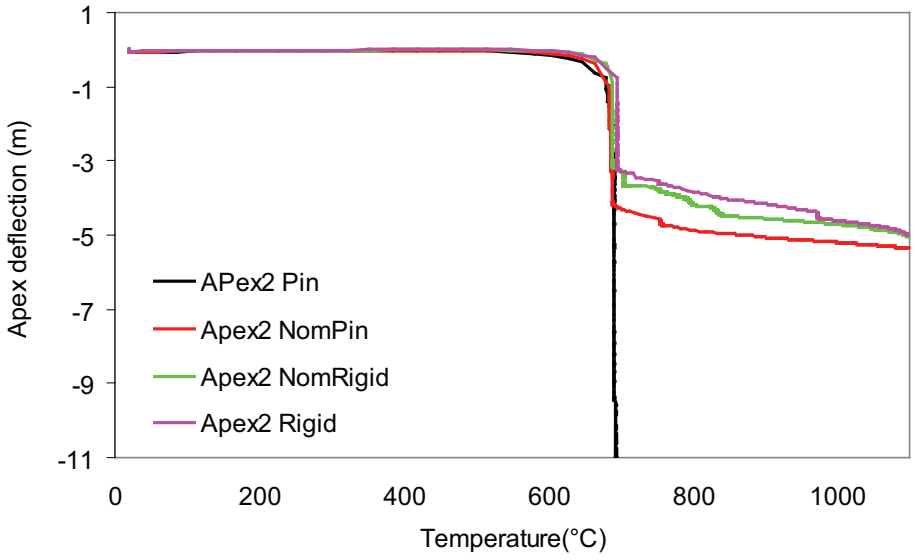

Figure 5.44: Variation of apex deflections against temperatures (SMSPF): Apex2 (S2-B, $M_{OTM} = 2.0M_{SCI}$)

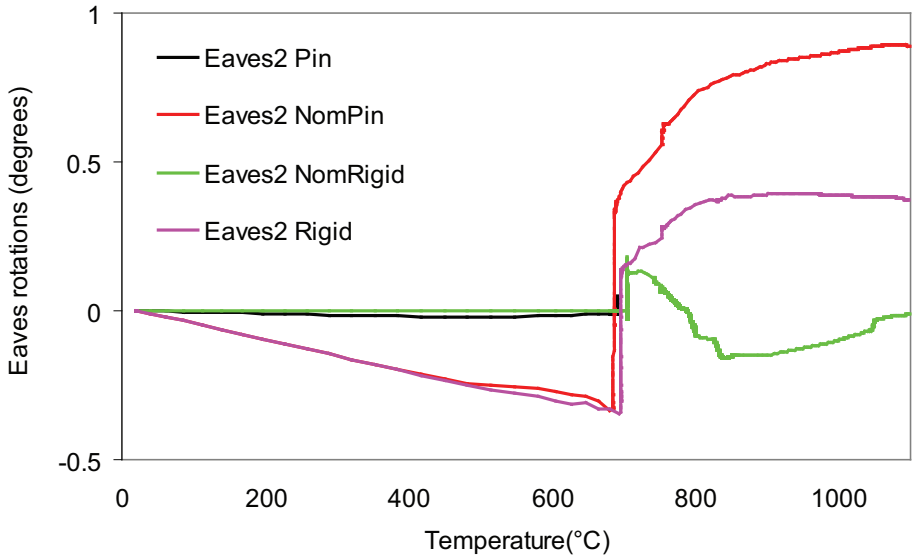

Figure 5.45: Variation of eaves rotations against temperatures (SMSPF): Eaves3 (S2-B, $M_{OTM} = 2.0M_{SCI}$)

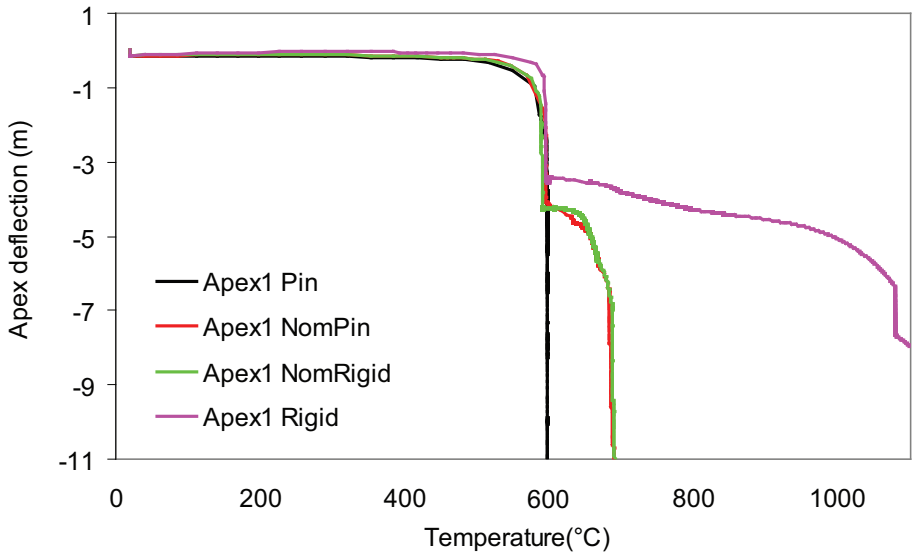

Figure 5.46: Variation of apex deflections against temperatures (SMSPF): Apex1 (S3-A, $M_{OTM} = 2.0M_{SCI}$)

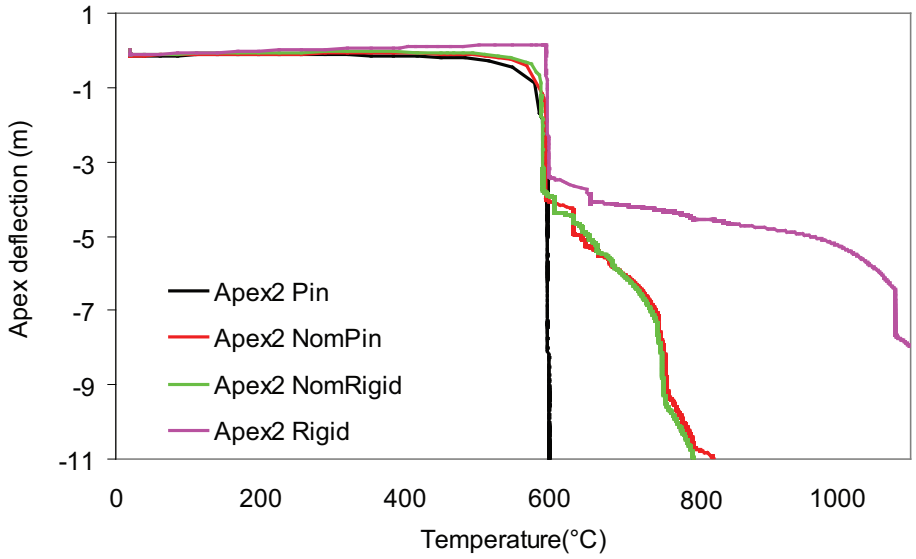

Figure 5.47: Variation of apex deflections against temperatures (SMSPF): Apex2 (S3-A, $M_{OTM} = 2.0M_{SCI}$)

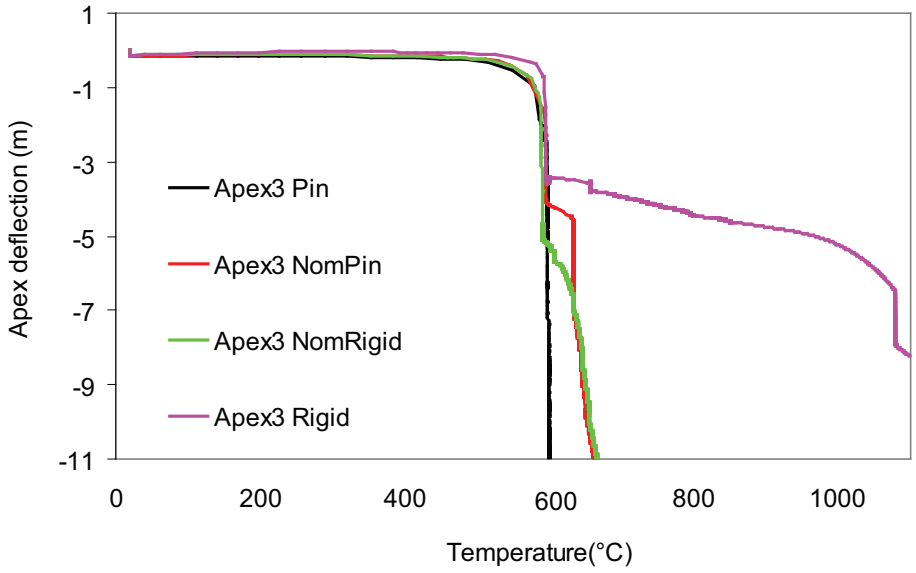

Figure 5.48: Variation of apex deflections against temperatures (SMSPF): Apex3 (S3-A, $M_{OTM} = 2.0M_{SCI}$)

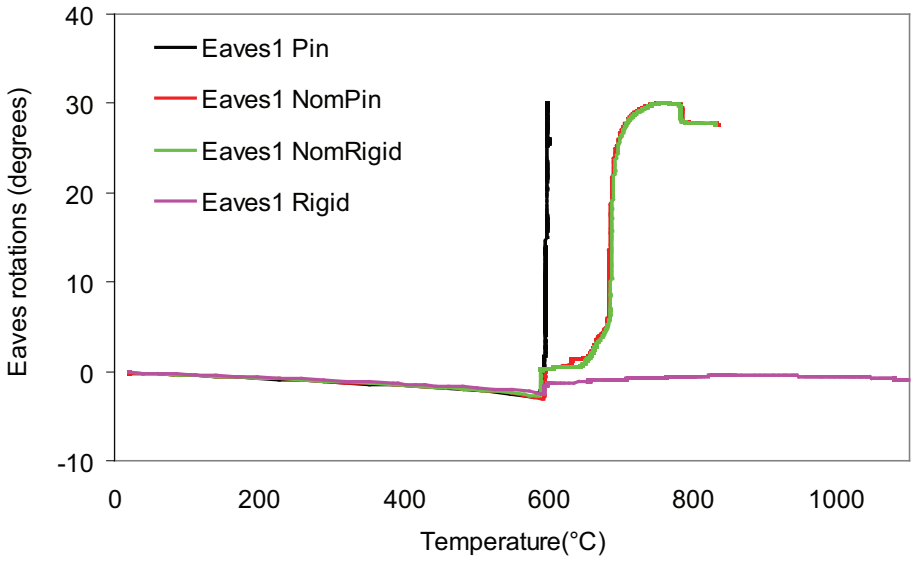

Figure 5.49: Variation of eaves rotations against temperatures (SMSPF): Eaves1 (S3-A, $M_{OTM} = 2.0M_{SCI}$)

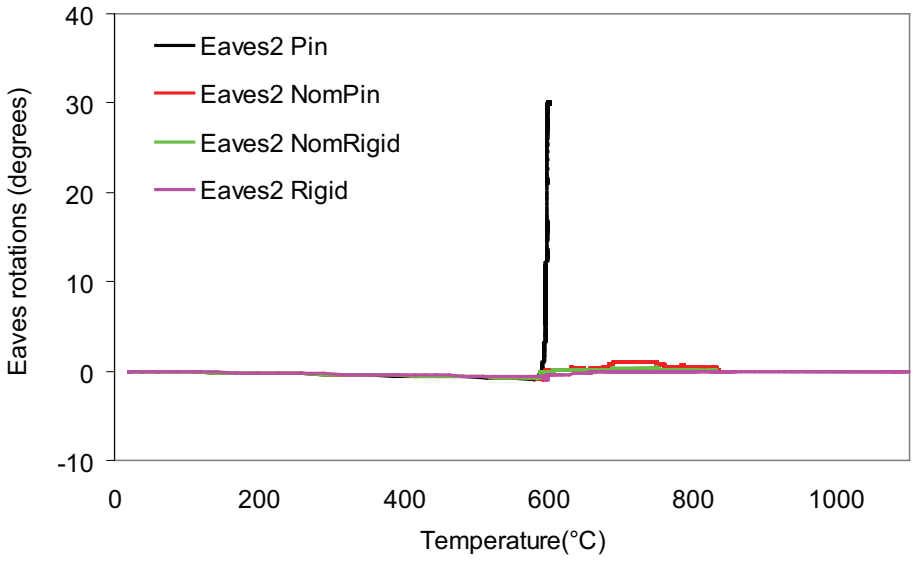

Figure 5.50: Variation of eaves rotations against temperatures (SMSPF): Eaves2 (S3-A, $M_{OTM} = 2.0M_{SCI}$)

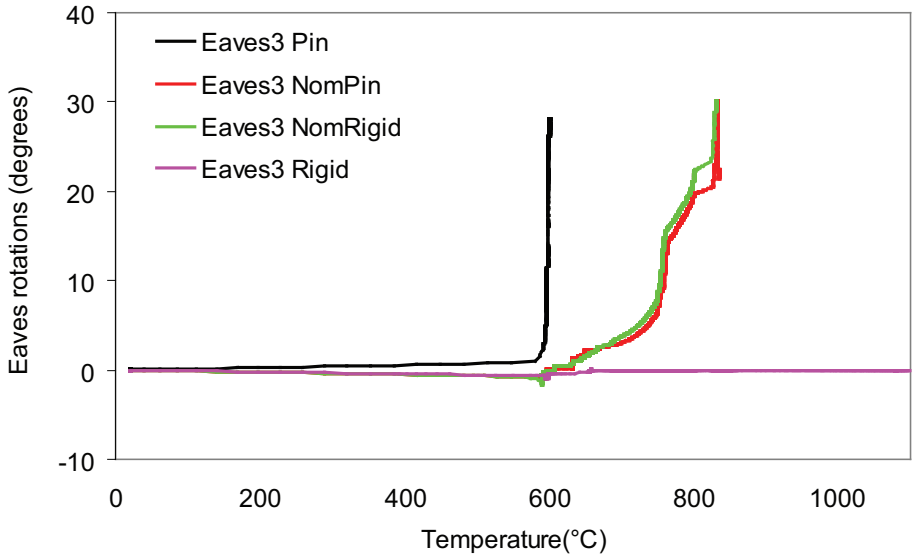

Figure 5.51: Variation of eaves rotations against temperatures (SMSPF): Eaves3 (S3-A, $M_{OTM} = 2.0M_{SCI}$)

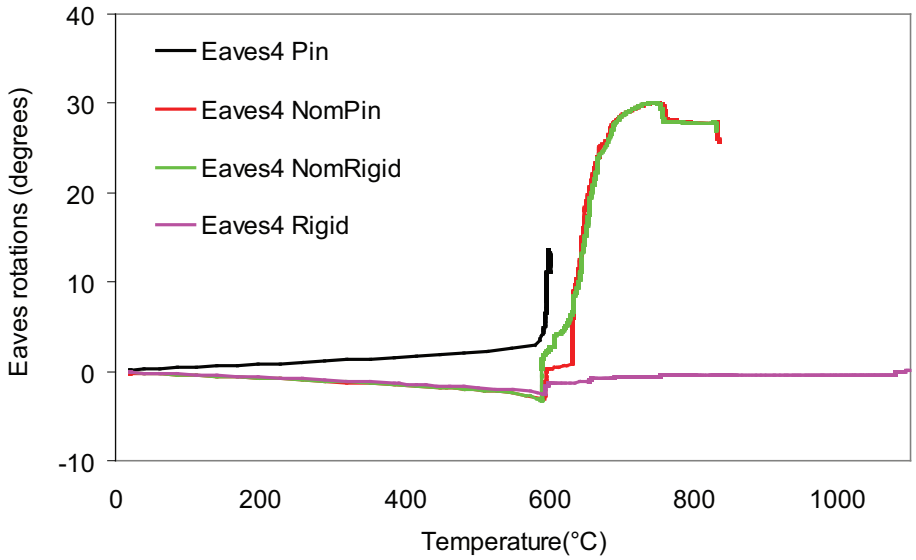

Figure 5.52: Variation of eaves rotations against temperatures (SMSPF): Eaves4 (S3-A, $M_{OTM} = 2.0M_{SCI}$)

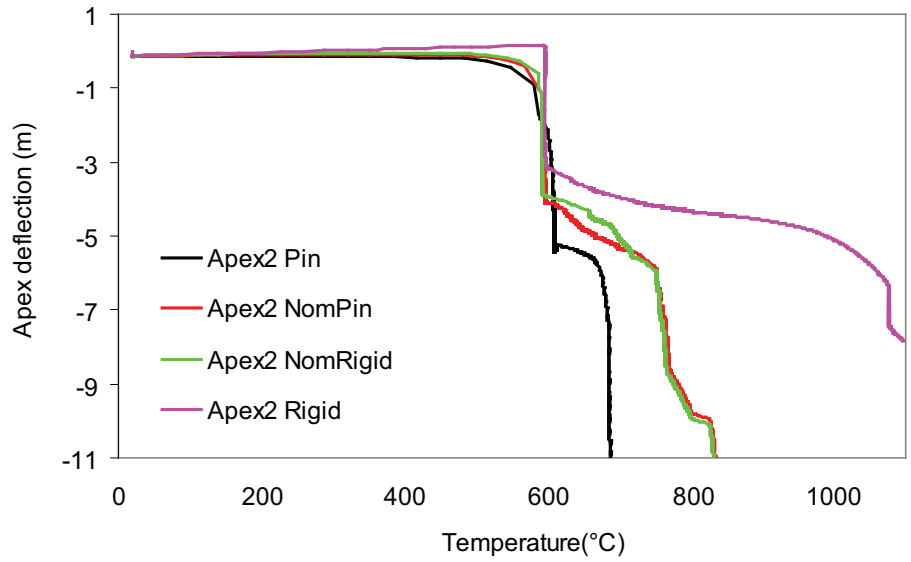

Figure 5.53: Variation of apex deflections against temperatures (SMSPF): Apex1 (S3-B, $M_{OTM} = 2.0M_{SCI}$)

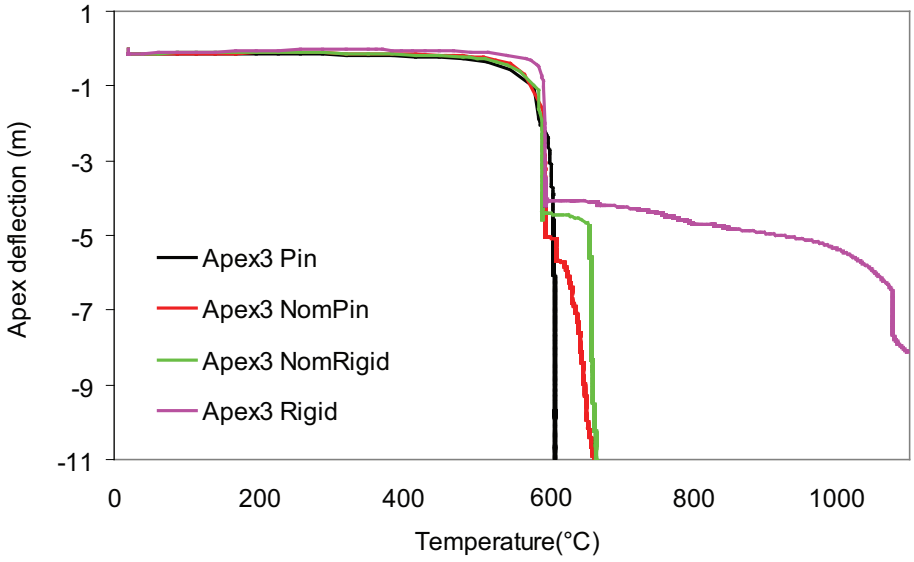

Figure 5.54: Variation of apex deflections against temperatures (SMSPF): Apex2 (S3-B, $M_{OTM} = 2.0M_{SCI}$)

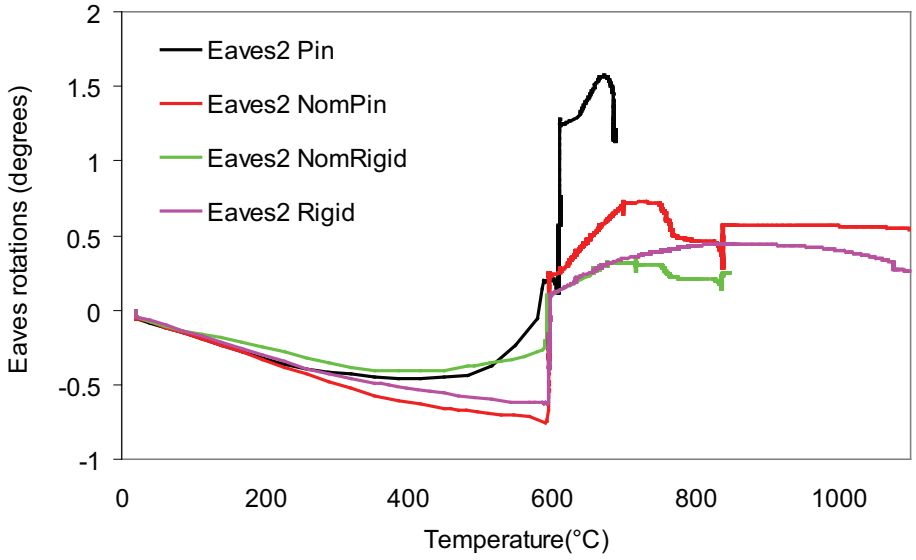

Figure 5.55: Variation of eaves rotations against temperatures (SMSPF): Eaves2 (S3-B, $M_{OTM} = 2.0M_{SCI}$)

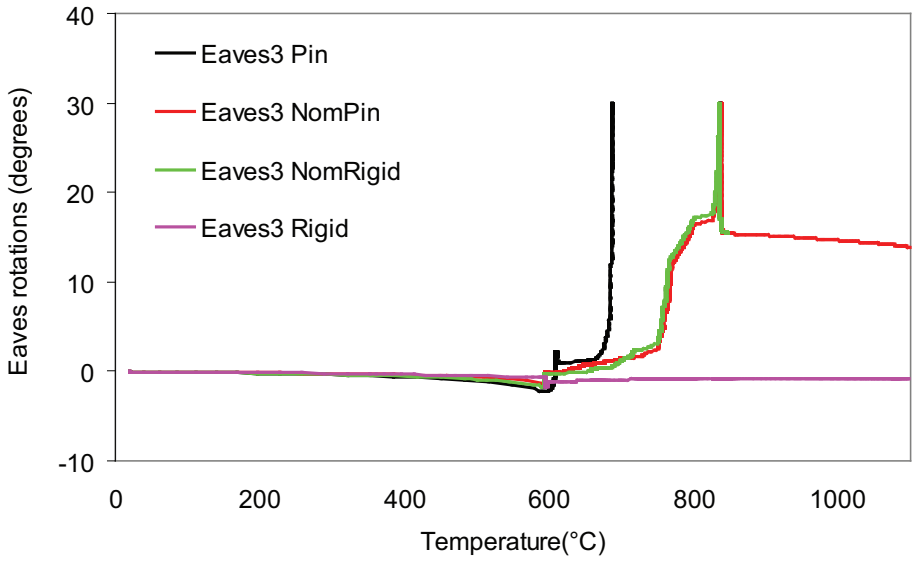

Figure 5.56: Variation of eaves rotations against temperatures (SMSPF): Eaves3 (S3-B, $M_{OTM} = 2.0M_{SCI}$)

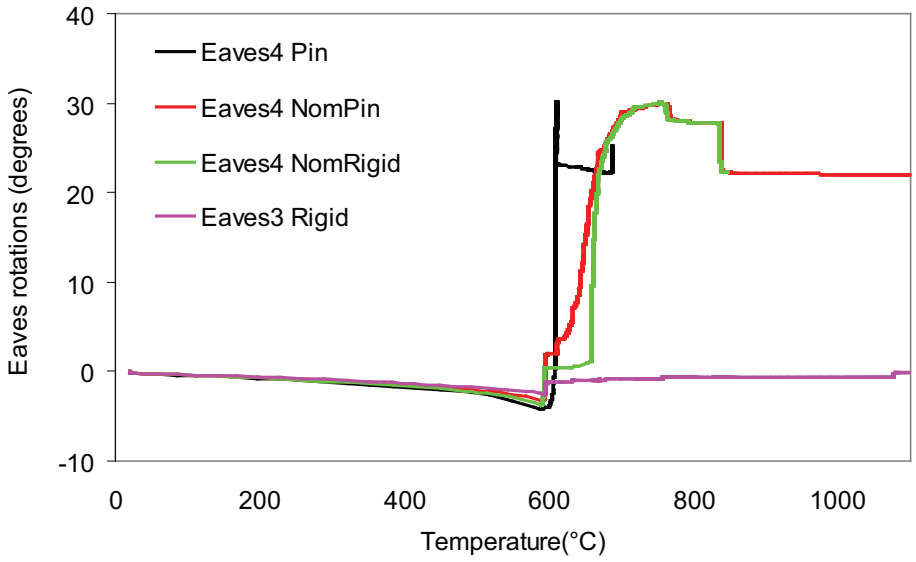

Figure 5.57: Variation of eaves rotations against temperatures (SMSPF): Eaves4 (S3-B, $M_{OTM} = 2.0M_{SCI}$)

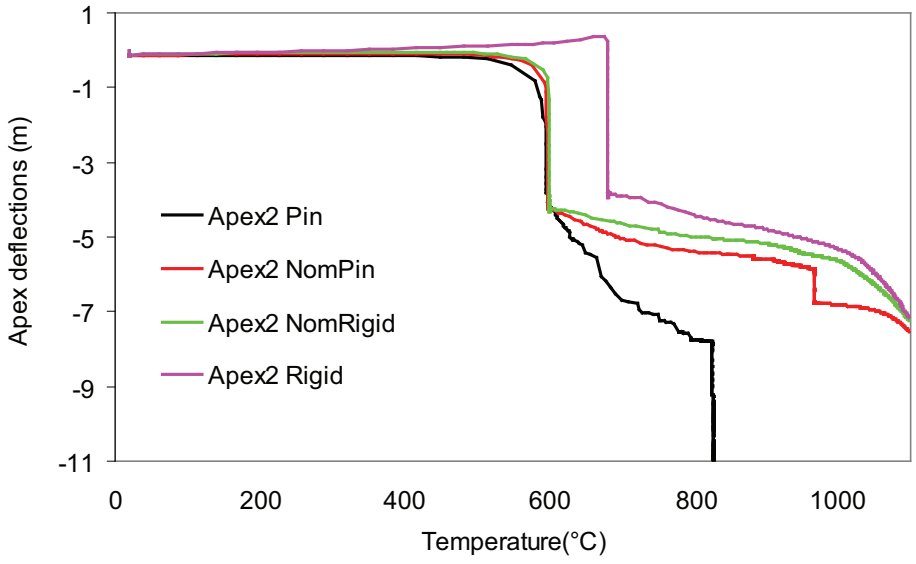

Figure 5.58: Variation of apex deflections against temperatures (SMSPF): Apex2 (S3-C, $M_{OTM} = 2.0M_{SCI}$)

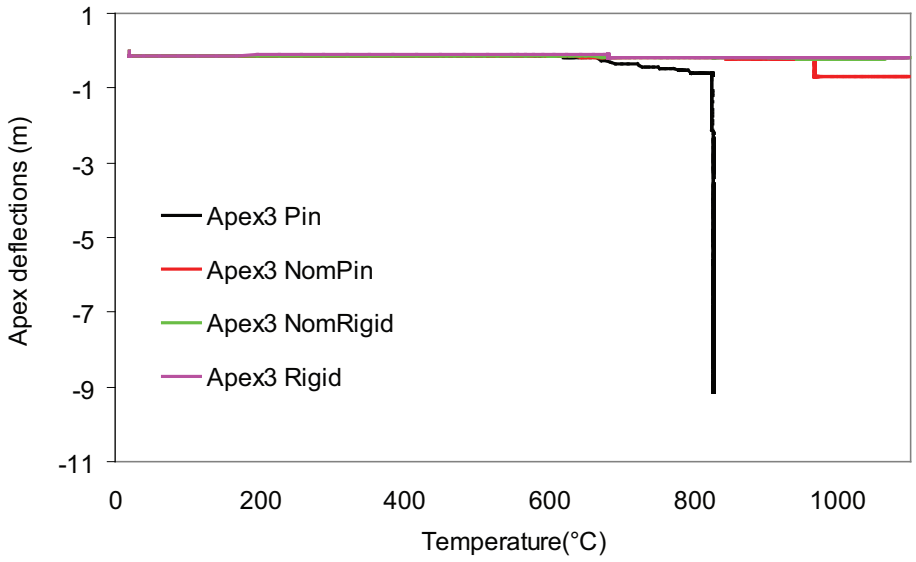

Figure 5.59: Variation of apex deflections against temperatures (SMSPF): Apex2 (S3-C, $M_{OTM} = 2.0M_{SCI}$)

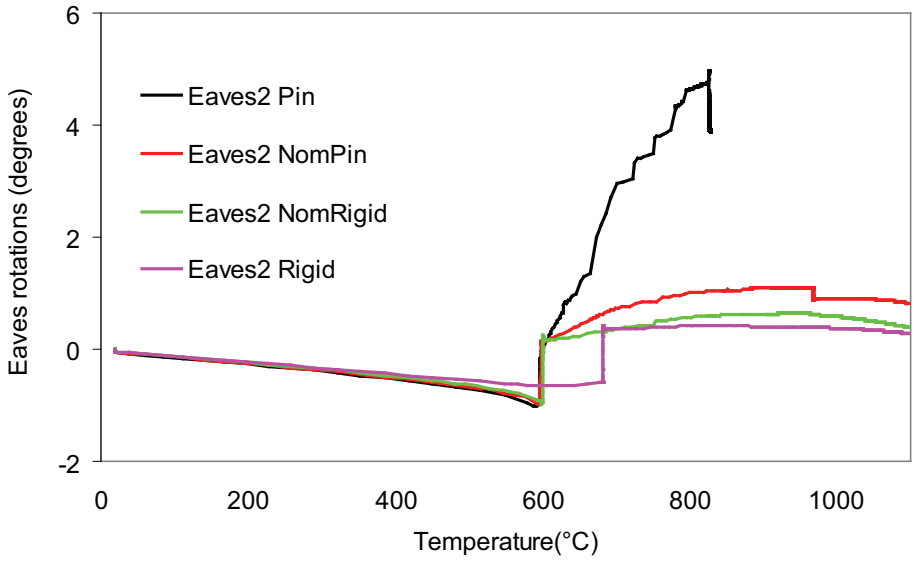

Figure 5.60: Variation of eaves rotations against temperatures (SMSPF): Eaves2 (S3-C, $M_{OTM} = 2.0M_{SCI}$)

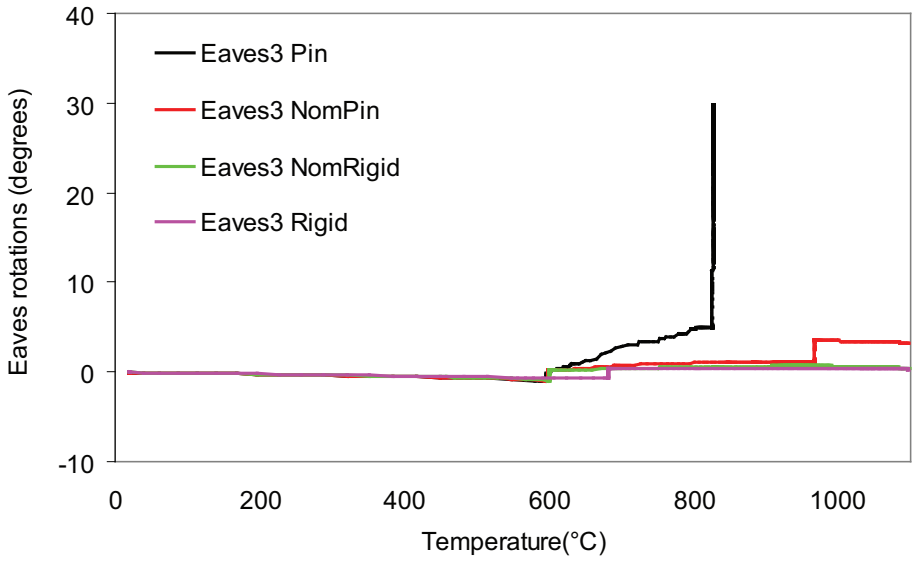

Figure 5.61: Variation of eaves rotations against temperatures (SMSPF): Eaves3 (S3-C, $M_{OTM} = 2.0M_{SCI}$)

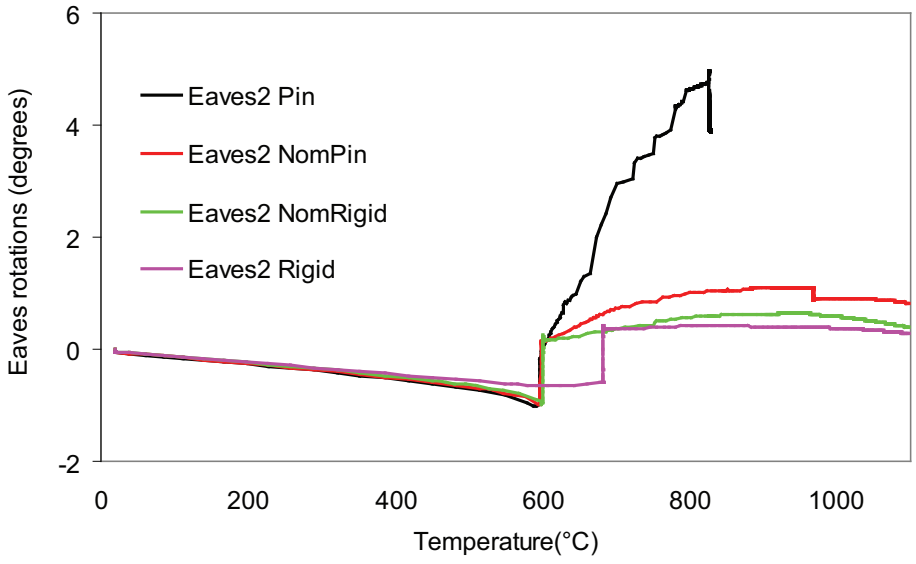

Figure 5.62: Variation of eaves rotations against temperatures (SMSPF): Eaves4 (S3-C, $M_{OTM} = 2.0M_{SCI}$)

Table 5.9: Summary of behaviour of SMSPF: S2-A, M_{OTM}=2.0M_{SCI}

Col. base	Snap-through-buckling temperature			Collapse temperature			Maximum inward column rotation by 890°C				Maximum outward column rotation by 890°C			
	Span1	Span2	Span3	Span1	Span2	Span3	Eaves1	Eaves2	Eaves3	Eaves4	Eaves1	Eaves2	Eaves3	Eaves4
	°C	°C	°C	°C	°C	°C	°	°	°	°	°	°	°	°
Pin	-	595	826	-	826	826	4.2	4.2	38.8	34.3	-	-	-	-
Nom. Pin		597	-	-	877	-	<1	<1	38.4	34	-	-	-	-
Nom. Rigid	-	597	-	-	887	-	<1	<1	10.5	10	-	-	-	-
Rigid	-	681	-	-	1095	-	<1	<1	<1	<1	-	-	-	-

Table 5.10: Summary of behaviour of SMSPF: S3-A, M_{OTM}=2.0M_{SCI}

Col. base	Snap-through-buckling temperature			Collapse temperature			Maximum inward column rotation by 890°C				Maximum outward column rotation by 890°C			
	Span1	Span2	Span3	Span1	Span2	Span3	Eaves1	Eaves2	Eaves3	Eaves4	Eaves1	Eaves2	Eaves3	Eaves4
	°C	°C	°C	°C	°C	°C	°	°	°	°	°	°	°	°
Pin	587	589	587	598	599	599	30.0	30.0	28.4	13.5	3.0	-	-	0.0
Nom. Pin	595	595	595	659	733	612	30.0	<1	30.0	31.0	3.0	-	-	3.0
Nom. rigid	590	590	590	659	716	597	31.0	<1	30.0	31.0	3.0	-	-	2.0
Rigid	598	597	594	>1100	>1100	>1100	0.0	0.0	1.0	2.6	2.6	-	-	0.0

Table 5.11: Summary of behaviour of SMSPF: S2-B, M_{OTM}=2.0M_{SCI}

Col. base	Snap-through-buckling temperature		Collapse temperature		Maximum column rotation by 890°C			inward rotation by 890°C		Maximum column rotation by 890°C		outward rotation by
	Span1	Span2	Span1	Span2	Eaves1	Eaves2	Eaves3	Eaves1	Eaves2	Eaves1	Eaves2	Eaves3
	°C	°C	°C	°C	°	°	°	°	°	°	°	°
Pin	-	680	-	692	<1	<1	44.7	-		<1	2.1	
Nom. Pin	-	685	-	1093	<1	<1	9.7	-		-	2	
Nom. Rigid	-	687	-	1094	<1	<1	10	-		-	1.9	
Rigid	-	695	-	1094	<1	<1	<1	<1		-	2.1	

Table 5.12: Summary of behaviour of SMSPF: S3-B, M_{OTM}=2.0M_{SCI}

Col. base	Snap-through-buckling temperature			Collapse temperature			Maximum inward column rotation by 890°C				Maximum outward column rotation by 890°C			
	Span1	Span2	Span3	Span1	Span2	Span3	Eaves1	Eaves2	Eaves3	Eaves4	Eaves1	Eaves2	Eaves3	Eaves4
	°C	°C	°C	°C	°C	°C	°	°	°	°	°	°	°	°
Pin	-	609	605	-	687	609	<1	<1	2.2[a], 40.4[b]	40.4	<1	-	-	4.2
Nom. Pin	-	589	590	-	754	621	<1	<1	2.0, 38.0	38	<1	-	-	3.9
Nom. Rigid	-	588	588	-	>1100	>1100	<1	<1	<1	<1	<1	-	-	<1
Rigid	-	594	594	-	1096	1096	<1	<1	<1	<1	<1	-	-	<1

[a]rotation of Eaves3 when Eaves4 is collapsed
[b]rotation of Eaves4 when it is collapsed

Table 5.13: Summary of behaviour of SMSPF: S3-C, M_{OTM}=2.0M_{SCI}

Col. base	Snap-through-buckling temperature			Collapse temperature			Maximum inward column rotation by 890°C				Maximum outward column rotation by 890°C			
	Span1	Span2	Span3	Span1	Span2	Span3	Eaves1	Eaves2	Eaves3	Eaves4	Eaves1	Eaves2	Eaves3	Eaves4
	°C	°C	°C	°C	°C	°C	◦	◦	◦	◦	◦	◦	◦	◦
Pin	-	595	826	-	826	826	4.2	4.2	38.8	34.3	-	-	-	-
Nom. Pinned	-	597	-	-	1087	-	<1	<1	5.9	5.8	-	-	-	-
Nom. Rigid	-	596	-	-	1090	-	<1	<1	5.5	5.6	-	-	-	-
Rigid	-	681	-	-	1095	-	<1	<1	<1	<1	-	-	-	-

- Fire Scenario A:

It can be seen from Table 5.9, for two-span frame for nominally pinned and nominally rigid column bases that the snap-through buckling temperature varies between 686°C and 695°C which is slightly higher than 688°C for pinned column bases. The maximum outward column rotation is 1.6°. Similarly, from Table 5.10, it can be seen, for a three-span frame for nominally pinned and nominally rigid column bases, that the snap-through buckling temperature varies between 590°C and 595°C which is slightly higher than 587°C for pinned column bases. The maximum outward column rotation is 3.0°.

- Fire Scenario B:

It can be seen from Table 5.11, for a two-span frame for nominally pinned and nominally rigid column bases, that the snap-through buckling temperature varies between 685°C and 687°C which is almost similar to 680°C for pinned column bases. The maximum outward column rotation is 2.0°. Similarly, from Table 5.12, it can be seen, for a three-span frame for nominally pinned and nominally rigid column bases, that the snap-through-buckling temperature 588°C which is lower than 609°C for pinned column bases. The maximum outward column rotation is 3.9°. For three-span frame, it should be noted that the rightmost rafter collapses in the first place while at the same time the mid-rafter remains suspended.

- Fire Scenario C:

This is applicable to only three-span frame. As can be seen from Table 5.13, for nominally pinned and nominally rigid column bases, that the snap-through buckling temperature is 597°C which is almost similar to 595°C for pinned column bases. There is no outward column rotation.

5.6 Portalised Truss Frames

Roof rafters spanning more than 20.0m can often be designed, quite economically, in the form of trusses instead of typical portal frames. This is due to the fact that trusses are usually lighter if compared with portal frames. The most common form of trusses, the Warren and Pratt types, can easily span up to 40.0 m without imposing any construction difficulty (Gorenc *et al.*, 2005). As trusses are usually constructed with relatively slender members, they may particularly be sensitive and vulnerable to fire due to the rapid rise of temperature within the section of these members. However, their behaviour at elevated temperature is still quite unknown. Figure 5.63 shows a typical portalised truss frame.

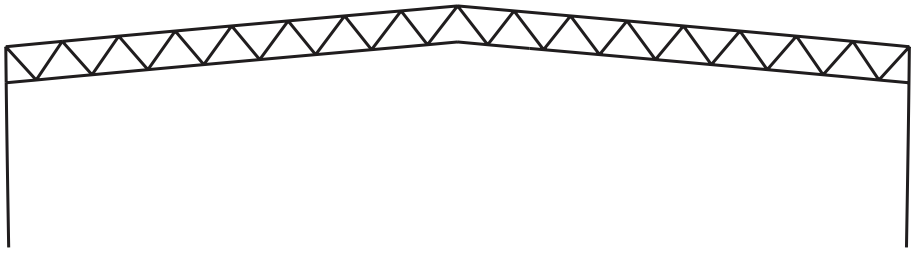

Figure 5.63: A typical portalised truss frame

The SCI method has outlined a very brief description of a comparison of portal frames and portalised truss frames. This guideline is aimed for prescriptive-based design and most of the assumptions in this guidelines are arbitrary.

In this section, behaviour of portalised steel truss frames, typically used in industrial frames where large span is necessary, at elevated temperatures has been investigated.

5.6.1 Standard portalised truss frames (SPTF)

The standard portalised truss frame (SPTF) that is considered for analysis is taken from exemplar benchmark model given by the SCI method as can be seen in Figure 5.64. The tables 5.14, 5.15 and 5.16 give the details of the frame

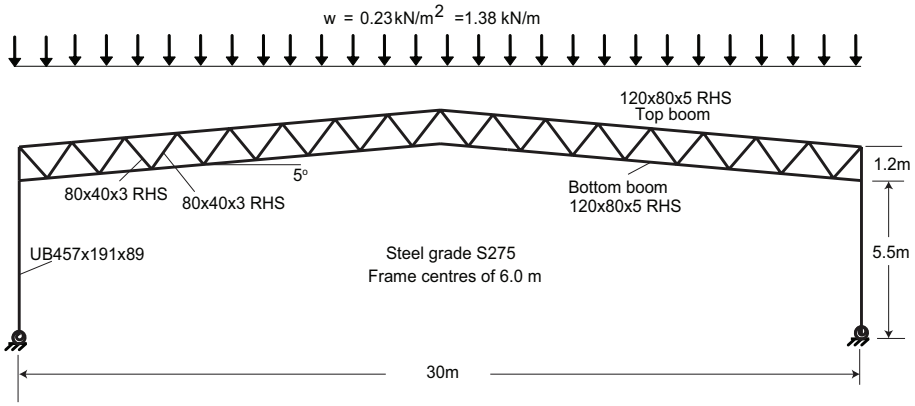

Figure 5.64: Standard portalised truss frame for study

geometry and section dimensions. As can be seen, for the columns, universal beam sections (UB) have been used while Rectangular Hollow Sections (RHS) (Figure 5.65) have been used for the top and bottom chords, and diagonals of the truss. The frame is built up of hot-rolled steel and has the dimensions of 30.0 m span with a spacing of 6.0 m and a roof pitch of 5°. The roof truss is

Table 5.14: Frame dimension

Span	Height up to eaves level	Depth of truss	Roof pitch	Frame spacing
m	m	m	^{o}	m
30	6.7	1.2	5	6

Table 5.15: Truss member section dimensions and properties (see Figure 5.65)

Member	Size	W	D	t	r_E	r_I	A	I_x	I_y
	RHS	mm	mm	mm	mm	mm	cm^2	cm^4	cm^4
Top boom	120x80x5	120	80	5	7.5	5	18.7	365	193
Bottom boom	120x60x5	120	60	5	7.5	5	16.7	299	98.8
Diagonal1	80x40x5	80	40	5	7.5	5	10.7	80.3	25.7
Diagonal2	60x40x3	60	40	5	4.5	5	5.54	26.5	13.9

Table 5.16: Column member section dimensions and properties

Section	D	W	t_w	t_f	r_r	A	I_x	I_y	Elastic mod.	Plastic mod.
UB	mm	mm	mm	mm	mm	cm^2	cm^4	cm^4	cm^3	cm^3
457x191x89	463.4	191.9	10.5	17.7	10.2	114	41000	2090	1770	2010

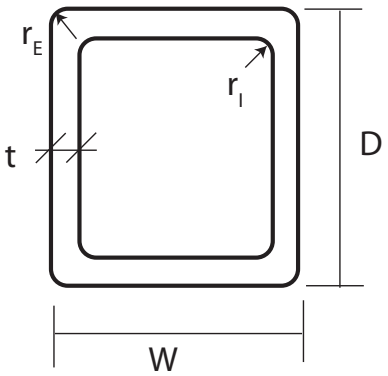

Figure 5.65: Typical Rectangular Hollow Section (RHS)

rigidly connected to the column. As there is possibility that sway in the truss would be occurred, the whole frame has been studied without taking advantage of symmetry of the structure.

An unfactored load of 0.3 $\frac{kN}{m^2}$ (purlins 0.07 $\frac{kN}{m^2}$, lattice rafter 0.10 $\frac{kN}{m^2}$ and cladding 0.13 $\frac{kN}{m^2}$) calculated according to the British Standard and the SCI method has been used throughout the study. The load is assumed to be applied vertically downward as uniformly distributed load on the top chord of the rafter. The depth of the rafter is assumed as 1.2m (span/25). Usually a deflection limit of span/20 is commonly applied to structural fire design (BS5950, 1990), however, as the material properties and geometry of the structure are significantly changed as temperature rises, it is difficult to calculate deflection of such systems at elevated temperatures. Since, it a 2-D model, the purlins are not physically modelled.

The frame is inherently overdesigned (possessing a load ratio of 0.80 at the ultimate limit state) to optimize the performance in fire in relation to loading and boundary conditions.

5.6.2 Overturning moments of SPTF

Based on the method given in the SCI method for single-storey symmetric portal frames, it has been found that the value of M_{OTM} that needs to be resisted by portalised truss frame is 264 kNm that represents approximately 48% of the plastic moment capacity of column section, $M_{pl,c}$, of 553 kNm. Since rafter is composed of different truss members, the residual moments in the trussed rafter are assumed to be zero and the haunch length is also assumed to be zero. So, in determining the M_{OTM}, calculation of plastic moment capacity of rafter is not necessary.

The SCI method assumes that both the columns and the column bases are fully protected from fire. In reality, similar to portal frames, when column is protected from fire with concrete covering, the temperature usually does not rise more than 350°C, and almost all of the strength of the material is retained. It should be noted that, the SCI method does not state the rotational stiffness of the column base.

5.6.3 Material properties at elevated temperature and fire model

The same material properties and fire model that have been used for single-span steel portal frames are used here. For details, the readers are referred to Chapter

3.

5.6.4 Finite element modelling

The same finite element model that have been developed and validated in Chapter 3 has been used here for analyzing portalised truss frames. However, similar to SMSPF, there are some exceptions in terms of number of elements and relaxation of some tolerance parameters for achieving a solution avoiding severe convergence difficulties that was not encountered in single-span portal frame models.

The numbers of elements are more than a typical portal frame or an SMSPF due to the top chord, bottom chord and web diagonals in the lattice rafter in addition to column member. It has been found that 224 elements are sufficient for the analysis with 16 elements for each column and 96 elements for each half of rafter. Similar to the single span-frame and SMSPF, all the columns and rafters are modelled using beam elements B21; and other possible second order elements are avoided due to so-called volumetric locking' problem induced by the large elemental strain in the deformed configuration. Rotational spring elements SPRING2 are used to model the rotational stiffness of the column bases. As usual the non-dimensional rotational stiffness, K_b, is considered as 0.4 for nominally pinned column bases.

The analysis steps follows the transient method where the loads on rafter and at eaves are applied in the first step, and temperature is applied and increased in the second step, as before.

5.7 Study on SPTF

5.7.1 Frames and fire scenarios

Since there is no restraint provided by purlins or by other secondary members and since out-of-plane deflections are not allowed, the 2-D plane frame model is considered as being a lower bound solution. The frames considered for study are shown in Figure 5.64. It is considered that the columns are fire protected while the roof truss is always unprotected from fire as can be seen in Figure 5.66.

For convenience, the numbering of different parts of frames are shown in Figure 5.67.

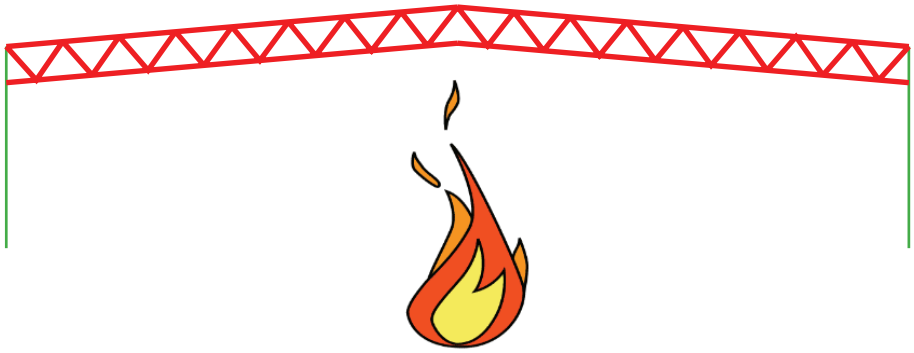

Figure 5.66: Fire scenarios for standard portalised truss frame. Thick red indicates members in fire and thin green indicates member at ambient temperature.

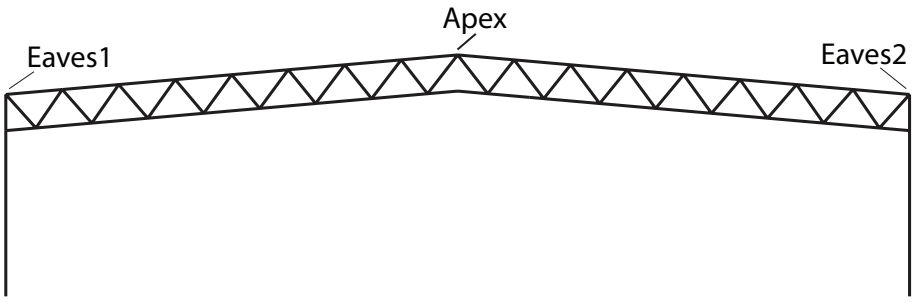

Figure 5.67: Numbering scheme of portalised truss frame.

5.7.2 Behaviour of SPTF with perfectly-pinned column bases

The deflected shape of the frames are shown in Figure 5.68 and the results for perfectly pinned column bases in Figure 5.69 to Figure 5.71 respectively. The

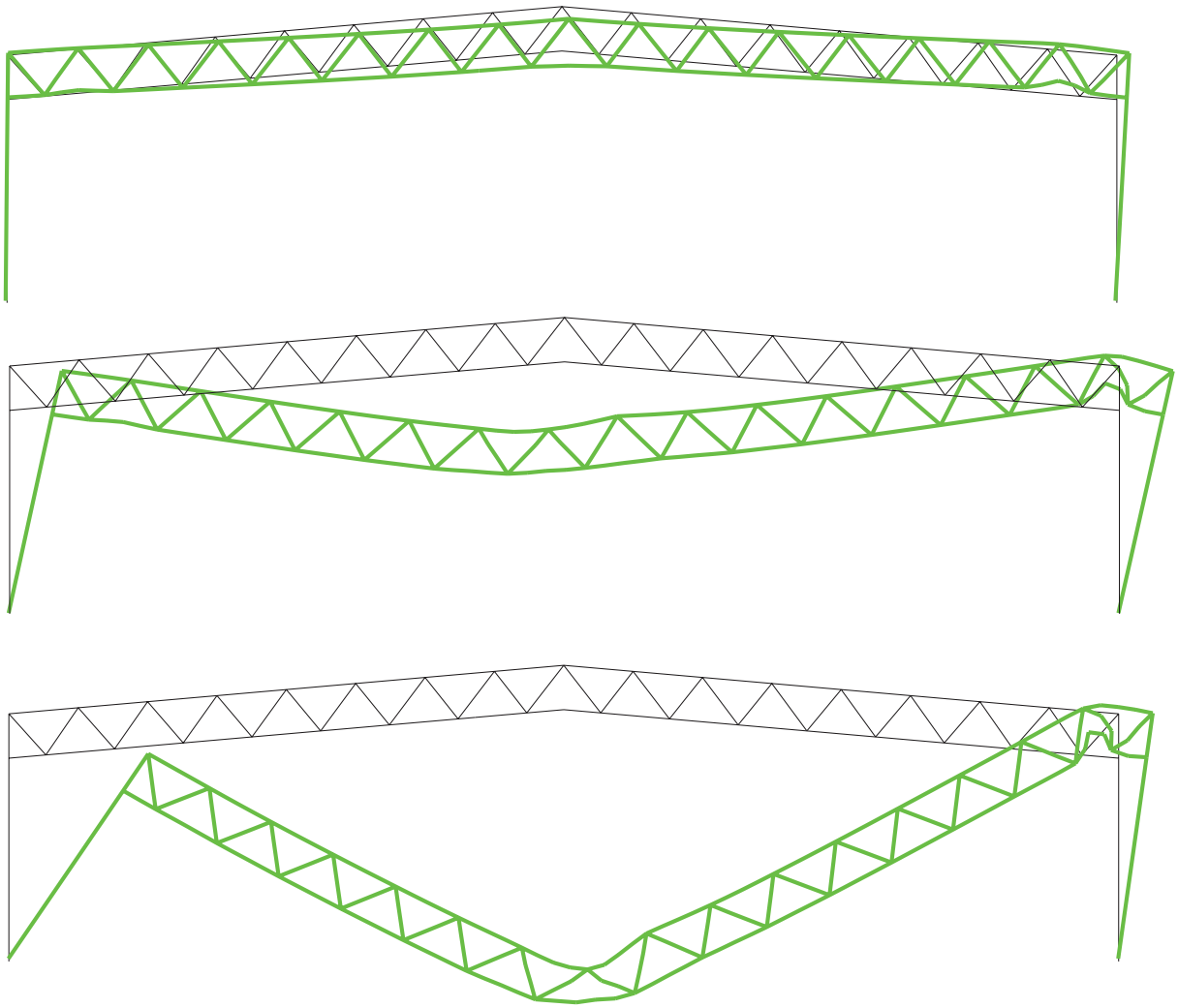

Figure 5.68: Deformed shape of SPTF: perfectly-pinned column bases. Green indicates deflected shape and black indicates undeflected shape.

results are summarized in Table 5.17.

As can be seen, the rafter that are kept at elevated temperatures have been collapsed by snap-through buckling at 639°C and complete collapses at 642°C. The maximum outward rotation is 12° and the maximum inward rotation is 27°, both of which are much higher than 1°, the limit of eaves rotation given by the SCI method.

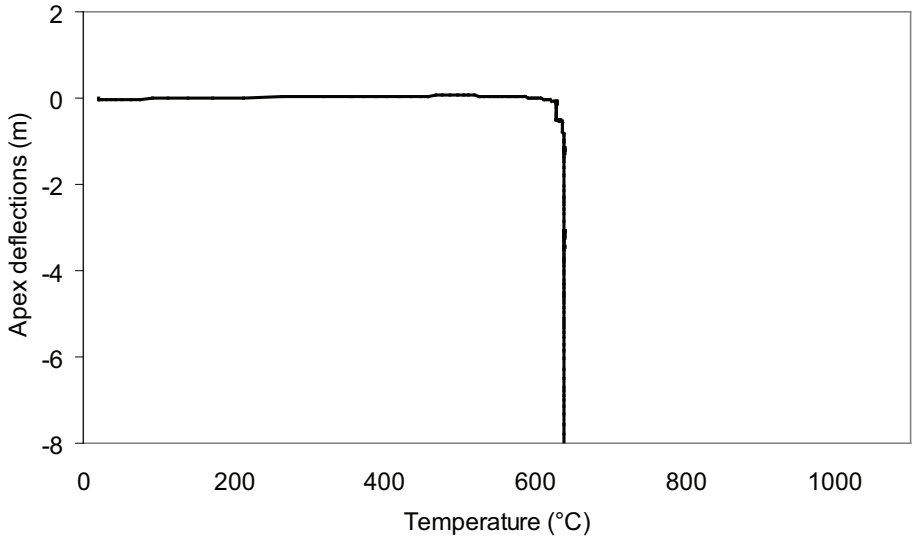

Figure 5.69: Variations of apex deflections against temperature (SPTF): Apex (perfectly pinned column bases)

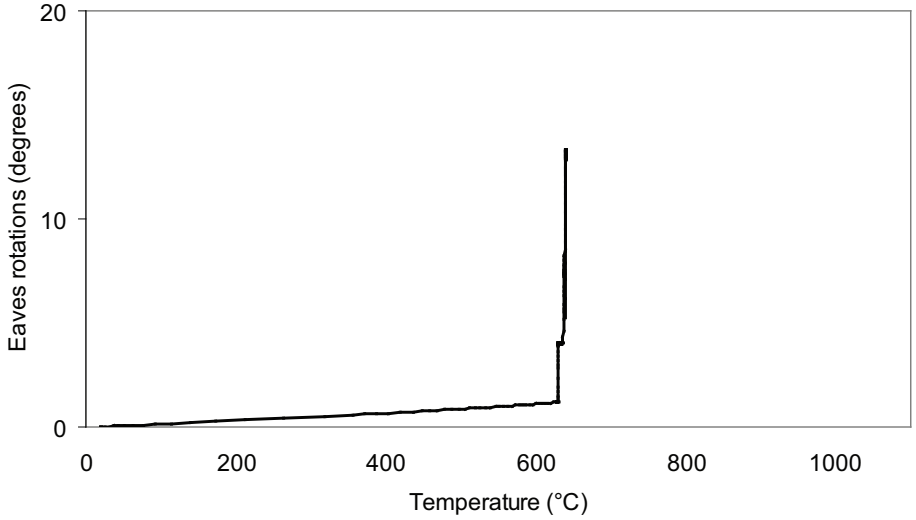

Figure 5.70: Variations of eaves rotations against temperature (SPTF): Eaves1 (perfectly pinned column bases)

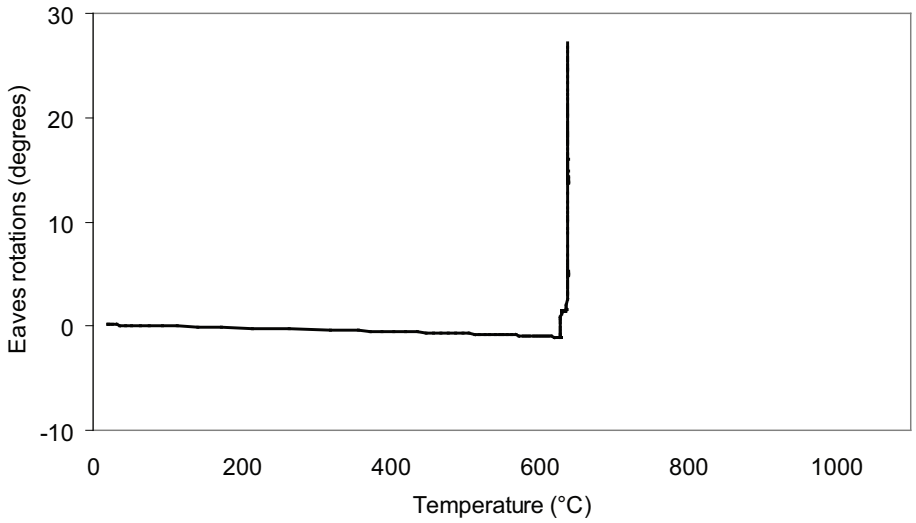

Figure 5.71: Variations of eaves rotations against temperature (SPTF): Eaves2 (perfectly pinned column bases)

Table 5.17: Summary of behavior of SPTF for pinned column bases

Fire Scenario	Snap-through-buckling temperature	Collapse temperature	Maximum inward column rotation by 890 °C	Maximum outward column rotation by 890 °C
	°C	°C	°	°
Rafter in fire	639	641	27	12

5.7.3 Effect on SPTF of partial strength column bases

M_{OTM} of $1.0M_{SCI}$

In Section 5.6.3 it was stated that in accordance with the SCI method, the column base needs to be designed to sustain an overturning moment, M_{OTM}, of 264 kNm. Such an overturning moment represents approximately 48% of the plastic moment capacity of the section.

Figures 5.72 to 5.74 show the variation of apex deflections and eaves rotations

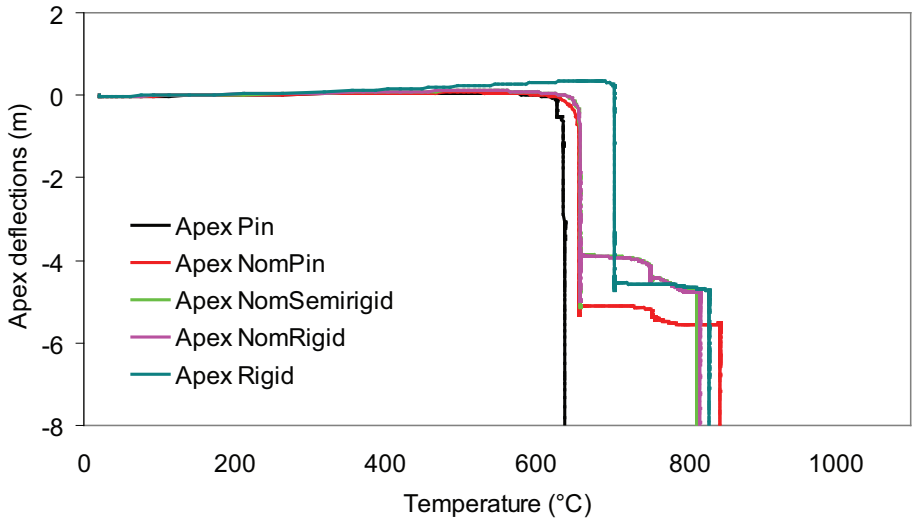

Figure 5.72: Variations of apex deflections against temperature (SPTF): Apex1 M_{OTM} of M_{SCI})

against temperature for three different column bases, i.e. nominally pinned, nominally semirigid and nominally rigid, having partial strength M_{OTM} of $1.0M_{SCI}$. The results are summarized in Table 5.18. As can be seen, for all three different column base rotational stiffness, the snap-through buckling temperature is 660°C, only slightly higher than 639°C for the pinned column bases. The maximum outward column rotation is 1.3° and maximum inward rotation is 7° for nominally pinned column base. The snap-through-buckling of 705°C and collapse temperature of 831°C are higher for rigid column bases.

M_{OTM} of $1.5M_{SCI}$ and M_{OTM} of $2.0M_{SCI}$

Figure 5.75 to Figure 5.80 shows the variation of deflection against temperature for the SPTF for three different column bases i.e. nominally pinned, nominally semirigid and nominally rigid, having partial strength M_{OTM} of $1.5M_{SCI}$ and

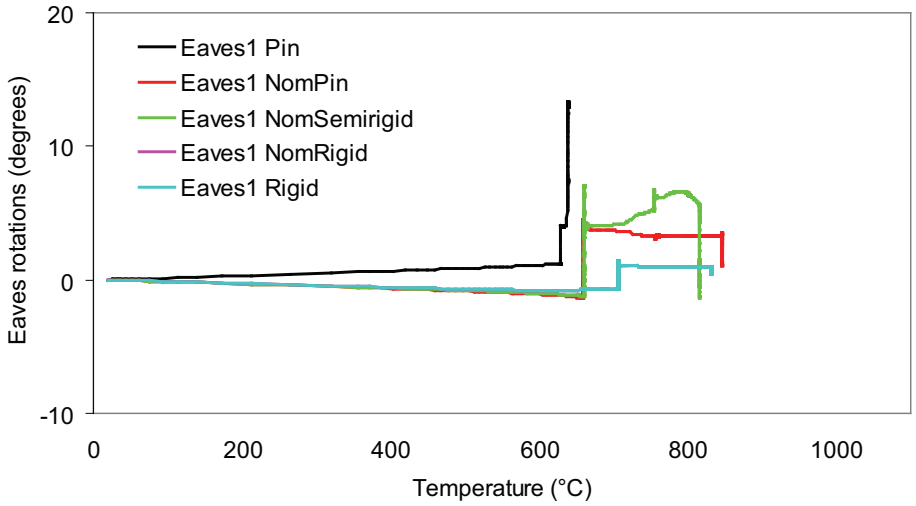

Figure 5.73: Variations of eaves rotations against temperature (SPTF): Eaves2 M_{OTM} of M_{SCI})

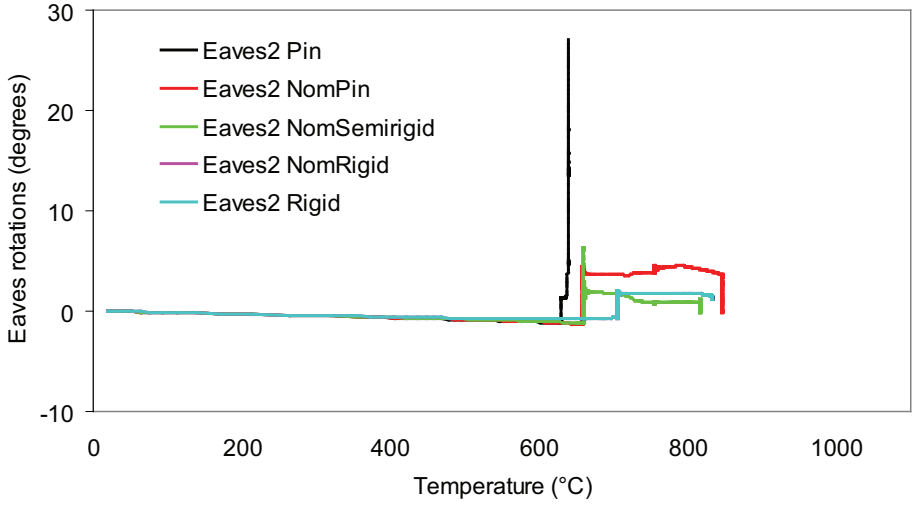

Figure 5.74: Variations of eaves rotations against temperature (SPTF): Eaves3 M_{OTM} of M_{SCI})

Table 5.18: Summary of behaviour of SPTF: M_{OTM} of M_{SCI}

Column base stiffness	Snap-through-buckling temperature	Collapse temperature	Maximum inward column rotation by 890°C	Maximum outward column rotation by 890°C
	°C	°C	°	°
Pin	639	641	27	12
Nom. Pin	660	845	7	1.3
Nom. Semirigid	660	820	4.5	1.3
Nom. Rigid	660	815	2.1	<1
Rigid	705	831	2.1	<1

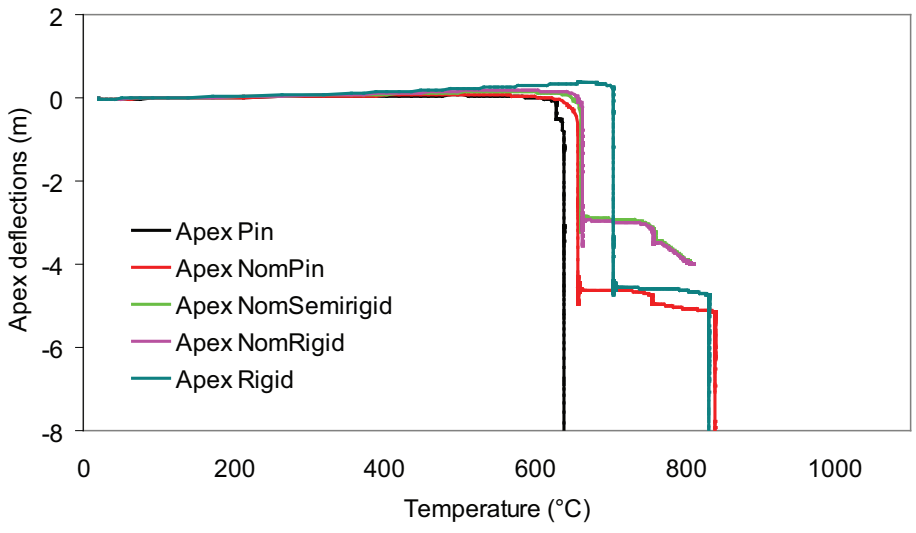

Figure 5.75: Variations of apex deflections against temperature (SPTF): Apex M_{OTM} of $1.5M_{SCI}$)

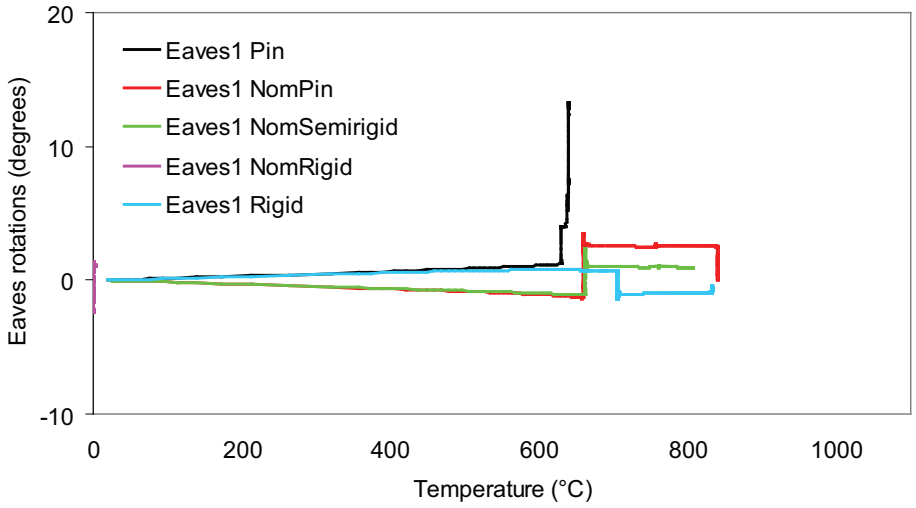

Figure 5.76: Variations of eaves rotations against temperature (SPTF): Eaves1 M_{OTM} of $1.5M_{SCI}$)

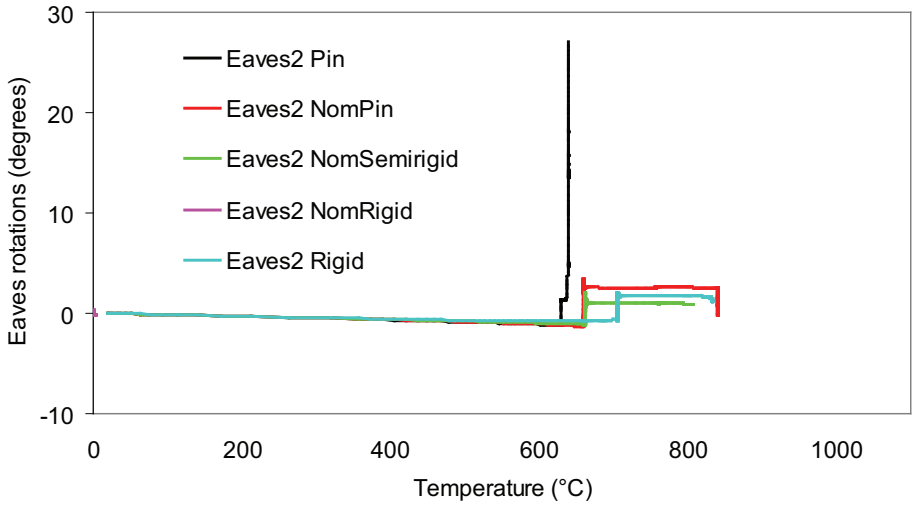

Figure 5.77: Variations of eaves rotations against temperature (SPTF): Eaves2 M_{OTM} of $1.5M_{SCI}$)

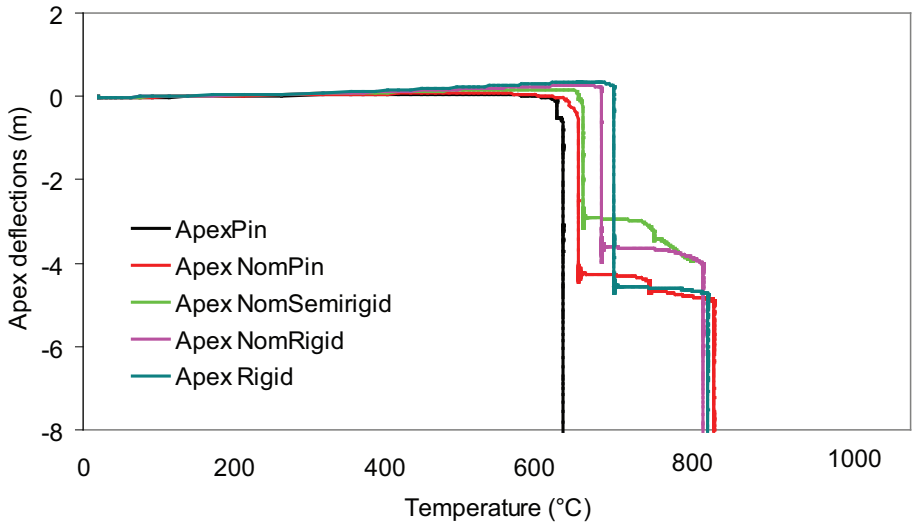

Figure 5.78: Variations of apex deflections against temperature (SPTF): Apex M_{OTM} of $2.0M_{SCI}$)

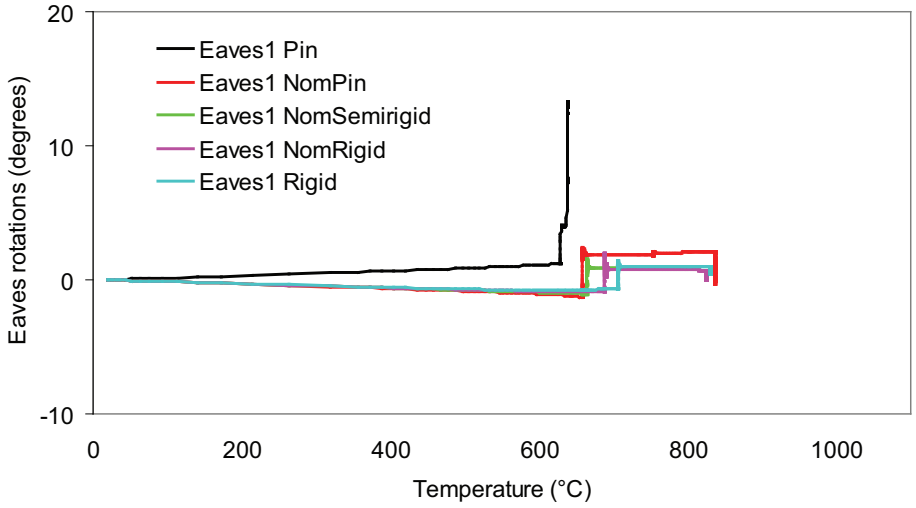

Figure 5.79: Variations of eaves rotations against temperature (SPTF): Eaves1 M_{OTM} of $2.0M_{SCI}$)

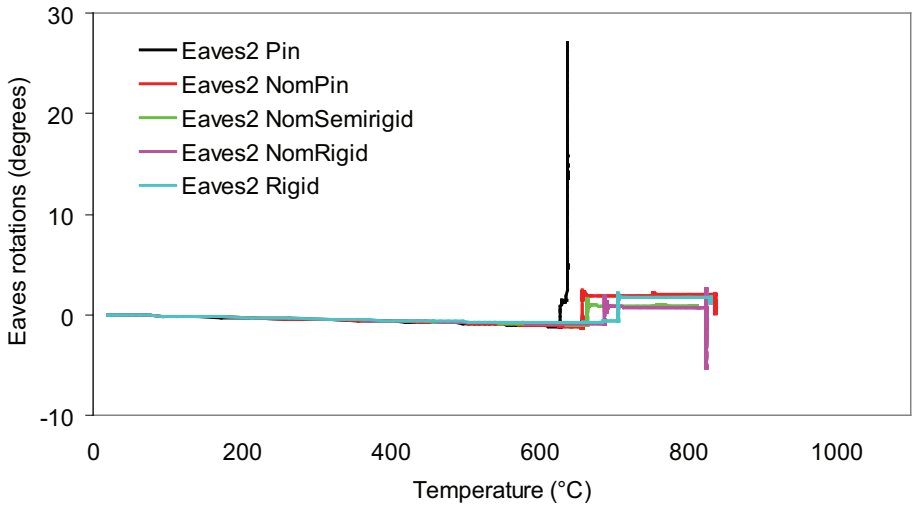

Figure 5.80: Variations of eaves rotations against temperature (SPTF): Eaves2 M_{OTM} of $2.0M_{SCI}$)

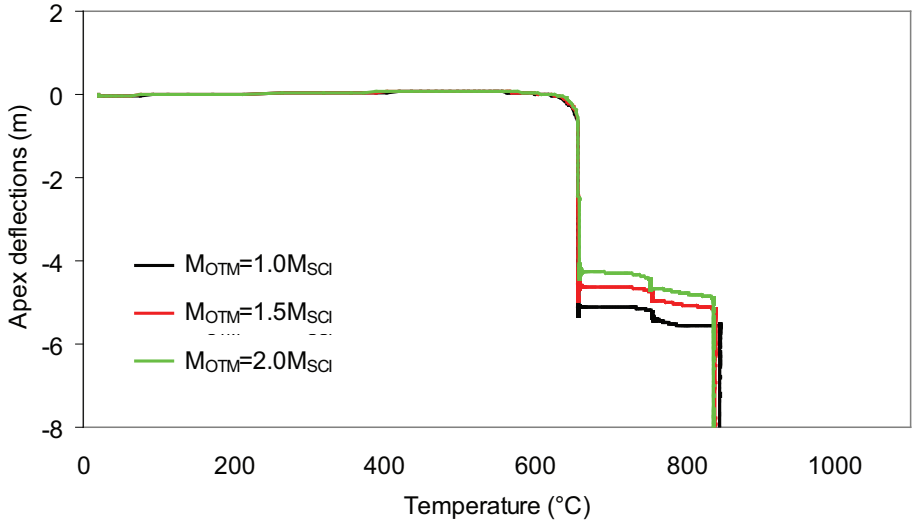

Figure 5.81: Variations of apex deflections against temperature (SPTF): Apex (different M_{OTM})

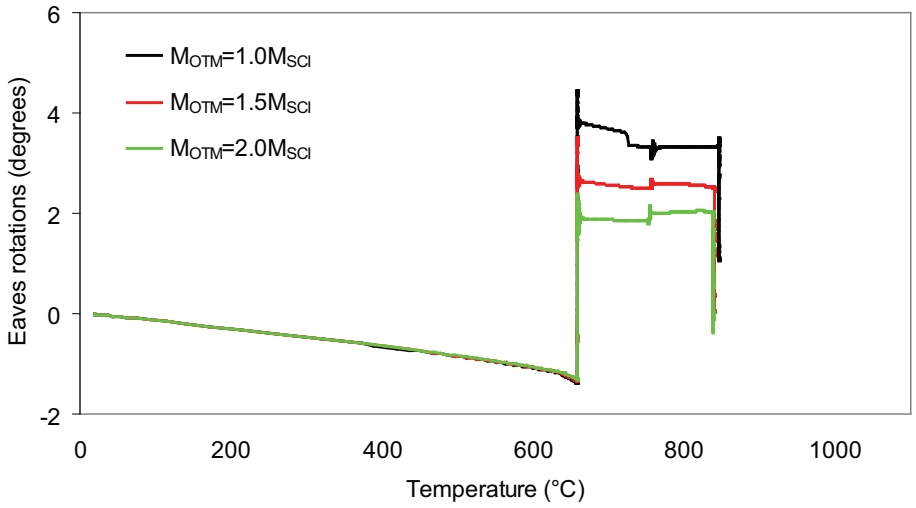

Figure 5.82: Variations of eaves rotations against temperature (SPTF): Eaves1 (different M_{OTM})

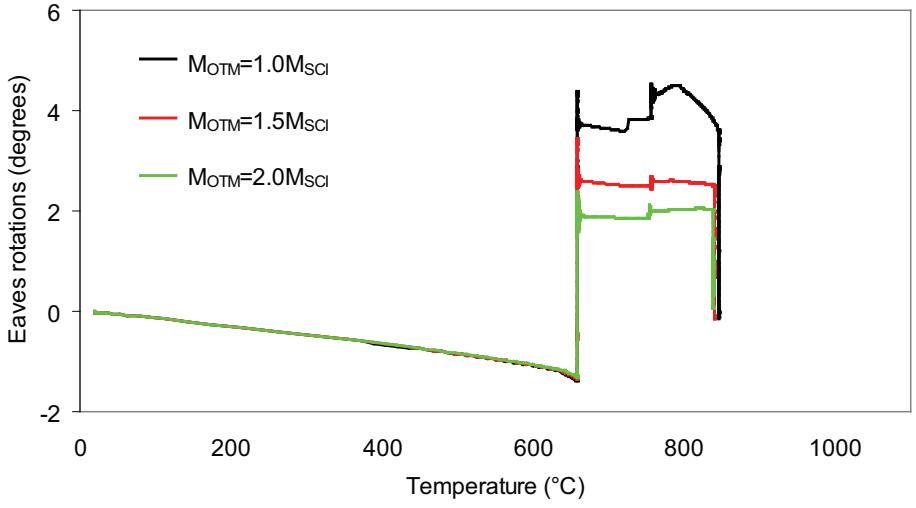

Figure 5.83: Variations of eaves rotations against temperature (SPTF): Eaves2 (different M_{OTM})

$2.0M_{SCI}$, respectively. The results are summarized in Figure 5.81 to 5.83 and in Table 5.19 and Table 5.20.

Table 5.19: Summary of behaviour of SPTF: M_{OTM} of $1.5M_{SCI}$

Column base stiffness	Snap-through-buckling temperature	Collapse temperature	Maximum inward column rotation by 890°C	Maximum outward column rotation by 890°C
	°C	°C	°	°
Pin	639	641	27	12
Nom. Pin	661	839	3.5	<1
Nom. Semirigid	662	816	2.2	<1
Nom. Rigid	663	811	2.1	<1
Rigid	705	831	2.1	<1

Table 5.20: Summary of behaviour of SPTF: M_{OTM} of $2.0M_{SCI}$

Column base stiffness	Snap-through-buckling temperature	Collapse temperature	Maximum inward column rotation by 890°C	Maximum outward column rotation by 890°C
	°C	°C	°	°
Pin	639	641	27	12
Nom. Pin	662	845	2.2	<1
Nom. Semirigid	669	821	2.1	<1
Nom. Rigid	687	815	2.1	<1
Rigid	705	831	2.1	<1

As can be seen, for all three different column base rotational stiffness, the snap-through-buckling temperature is between 661°C and 663°C for M_{OTM} of

$1.5M_{SCI}$ and between 662°C and 687°C for M_{OTM} of $2.0M_{SCI}$, respectively. This snap-through-buckling temperature is slightly higher than 660°C for the case of M_{OTM} of $1.5M_{SCI}$ from the previous M_{OTM} of M_{SCI} case, but much higher for the case of M_{OTM} of $2.0M_{SCI}$. This indicates that lower M_{OTM} has very little effect; however, Increasing M_{OTM} to a higher value has significant effect on eaves rotation as it can be seen from tables 5.18, 5.19 an 5.20 that the inward eaves rotation is reduced from 7° for M_{OTM} of M_{SCI} to 2.1° for M_{OTM} of $2.0M_{SCI}$. and outward rotation all reduced to less than 1°.

5.8 Asymmetrical portal frames

Usually an asymmetric frame have an off-centre apex or columns of different heights that is very common form of industrial building construction.

5.8.1 Standard asymmetrical portal frames (SAPF)

The asymmetrical portal frame that is considered for analysis is taken from practicing engineer designed by Chartered Structural Engineers, Belfast by personal communication. A typical asymmetrical portal frame can be seen in Figure 5.84. The Table 5.21 and Table 5.22 give the details of the frame geometry and section

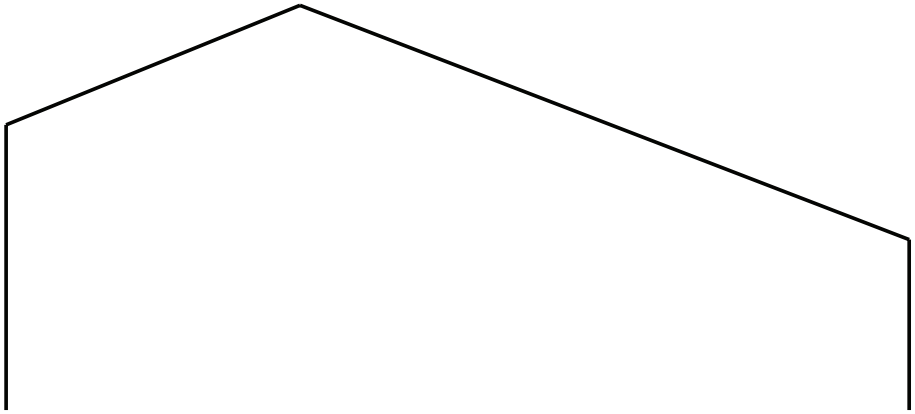

Figure 5.84: A typical asymmetrical portal frame

dimensions. As can be seen, for the columns, universal beam section (UB) has been used for both column and rafter members. The frame is built up of hot-rolled steel with a span of 14.32 m span, spacing of 5.0 m, apex height of 6.42m, left column height of 4.524m and right column height of 2.704m. The apex is located at 4.66m from left column and 9.66m from right column. The rafter is

Table 5.21: Frame geometry

Span	Height up to eaves level		Height from base up to apex level	Frame spacing	Apex distance	
	Left column	Right column			From left Col.	From right Col.
m	m	m	m	m	m	m
14.32	4.52	2.7	6.42	6	4.66	9.66

Table 5.22: Asymmetric portal frame member section sizes

Member	Size	W	D	t_w	t_f	A	I_x	I_y
	UB	mm	mm	mm	mm	cm^2	cm^4	cm^4
Column	305x165x40	165	303.4	6	10.2	51.3	8500	764
Rafter	406x140x39	141.8	398	6.4	8.6	49.7	12500	410

rigidly connected to the column. There is no haunch considered while analyzing the frame.

An unfactored load of 0.41 $\frac{kN}{m^2}$ calculated according to the British Standard and SCI method has been used throughout the study. The load is assumed to be applied vertically downward as uniformly distributed load on the top chord of the rafter. Since, it is a 2-D model, the purlins are not physically modelled.

5.8.2 Overturning moments of SAPF

Calculation of overturning moment, M_{OTM}, for asymmetrical portal frame is different from symmetrical pitched portal frame. For such frames, overturning moments are calculated based on an equivalent symmetrical portal frame. The length of rafters are kept unchanged while developing an equivalent symmetrical portal frame. To, make it possible, the rise between eaves and apex would not be the same as the original frame. Two different equivalent frames are constructed in this way by considering each column as the column height for each frame. The overturning moment are then calculated by usual way for each of the symmetrical pitched portal frame. The resulting overturning moment, M_{OTM}, is the average value of overturning moment of these two equivalent frames. Based on this method given in the SCI method, it has been found that the value of M_{OTM} that needs to be resisted by portalised truss frame is 101.9 kNm that represents

approximately 59% of the plastic moment capacity of column section, $M_{pl,c}$, of 171 kNm.

The SCI method assumes that both the columns and the column bases are fully protected from fire. In reality, similar to portal frames, when column is protected from fire with concrete covering, the temperature usually does not rise more than 350°C, and almost all of the strength of the material is retained. It should be noted that, the SCI method does not state the rotational stiffness of the column base.

5.8.3 Material properties at elevated temperature and fire model

The same material properties and fire model that have been used for single-span steel portal frames are used here.

5.8.4 Finite element modelling

The same finite element model that have been developed and validated in Chapter 3 has been used here for analyzing asymmetrical portal frames.

It has been found that 72 elements are sufficient for the analysis with 16 elements for left column, 8 elements for right column, 16 element for left rafter member and 32 elements for right rafter member. Similar to the single-span symmetrical portal frame, all the columns and rafters are modelled using beam elements B21; and other possible second order elements are avoided due to so-called 'volumetric locking' problem induced by the large elemental strain in the deformed configuration. Rotational spring elements SPRING2 are used to model the rotational stiffness of the column bases. As usual the non-dimensional rotational stiffness, K_b is considered as 0.4 for nominally pinned column bases.

The analysis steps follows the transient method where the loads on rafter and at eaves are applied in the first step, and temperature is applied and increased in the second step, as before.

5.9 Study on SAPF

5.9.1 Frames and fire scenarios of SAPF

Since there is no restraint provided by purlins or other secondary members and since out-of-plane deflections are not allowed, the 2-D plane frame model is considered as being a lower bound solution. The frame considered for study is shown in Figure 5.85.

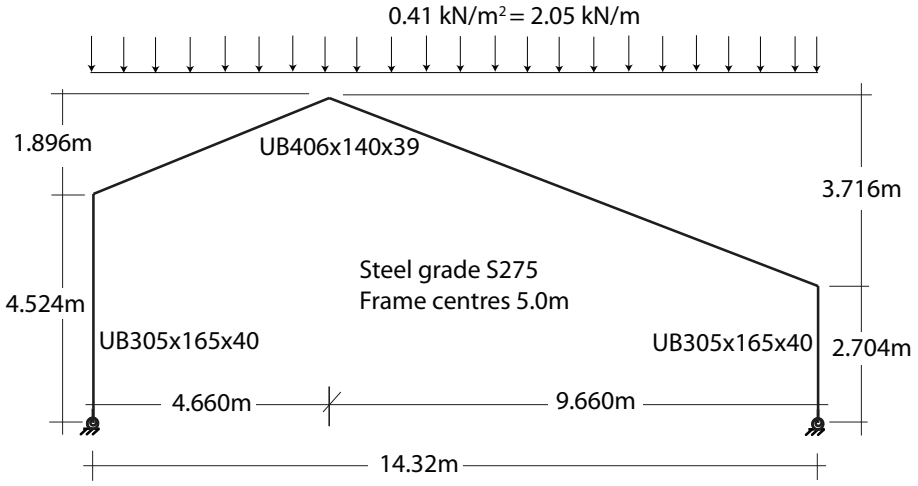

Figure 5.85: Standard asymmetrical portal frame for study

It is considered that the columns are fire protected while the roof truss is always unprotected from fire as can be seen in Figure 5.86. For convenience, the numbering of different parts of frames is shown in Figure 5.86.

5.9.2 Behaviour of SAPF with perfectly-pinned column bases

The deflected shape of the frame is shown in Figure 5.88 and results for perfectly pinned column bases are given in Figure 5.89 to 5.91 respectively. The results of Figure 5.89 to 5.91 are summarized in Table 5.23.

As can be seen, the rafter that are kept at elevated temperatures have been collapsed by snap-through buckling at 739°C and complete collapses at 740°C. The maximum outward rotation is 19.9° and the maximum inward rotation is 20.6°, both of which are much higher than 1°, the limit of eaves rotation given by the SCI method.

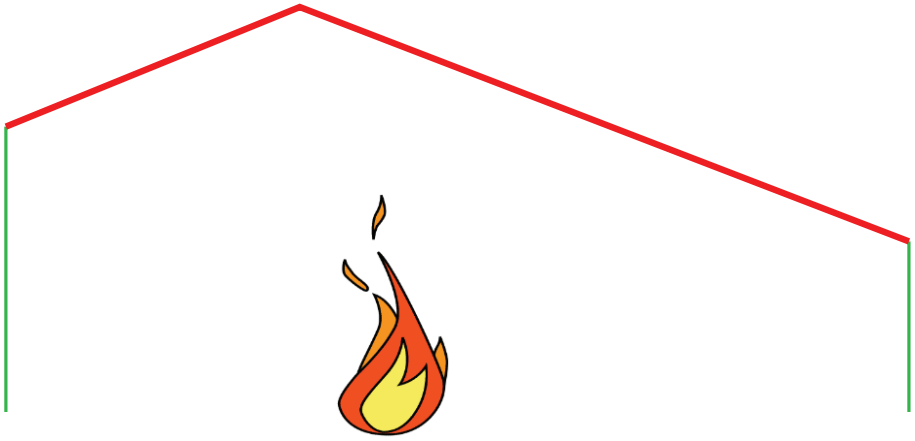

Figure 5.86: Fire scenarios for standard asymmetrical portal frame. Red indicates members in fire and green indicates member at ambient temperature.

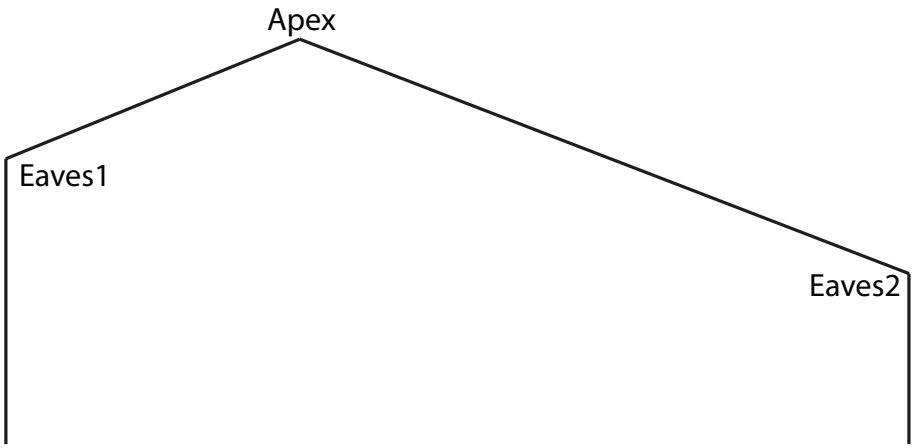

Figure 5.87: Numbering scheme of asymmetrical portal frame

Table 5.23: Summary of behaviour of SAPF: perfectly pinned column base

Fire Scenario	Snap-through-buckling temperature	Collapse temperature	Maximum inward column rotation by 890°C	Maximum outward column rotation by 890°C
	°C	°C	°	°
Rafter in fire	739	740	20.6	19.9

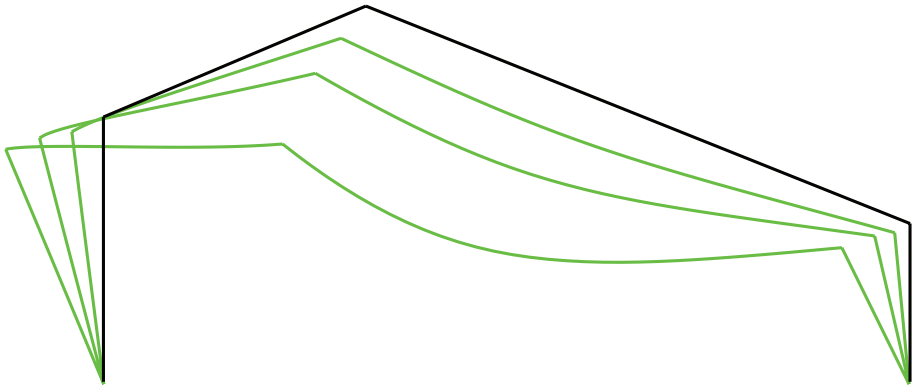

Figure 5.88: Deformed shape of SAPF: perfectly-pinned column bases. Green indicates deflected shape and black indicates undeflected shape.

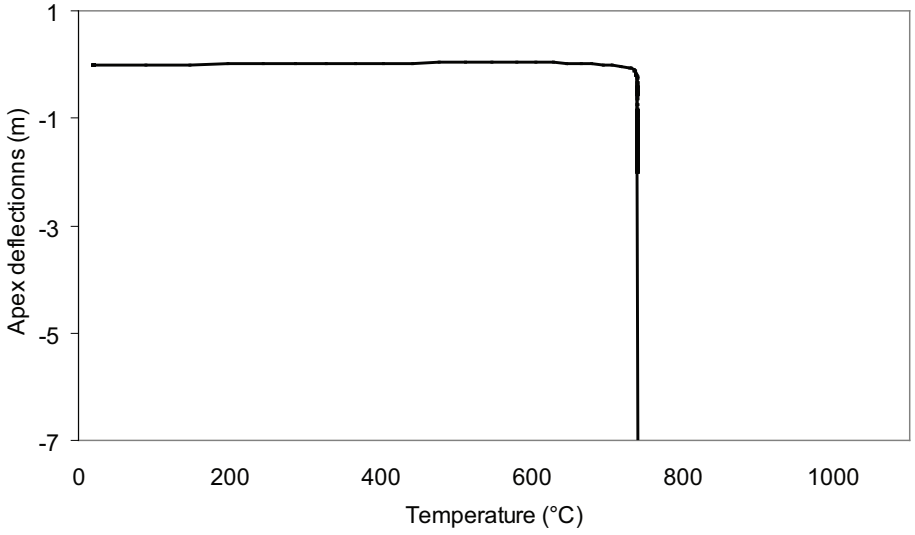

Figure 5.89: Variation of apex deflections against temperatures of SPAF: Apex, perfectly pinned column base

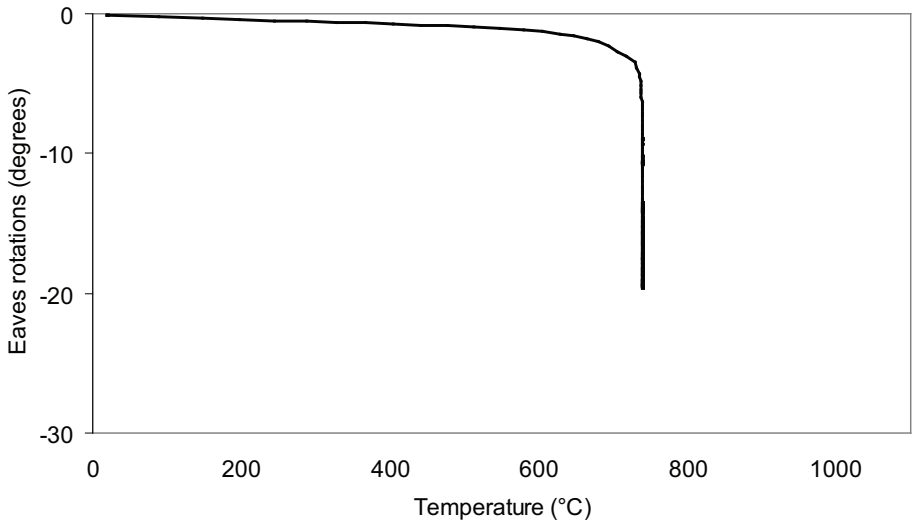

Figure 5.90: Variation of eaves rotations against temperatures of SPAF: Eaves1, perfectly pinned column base

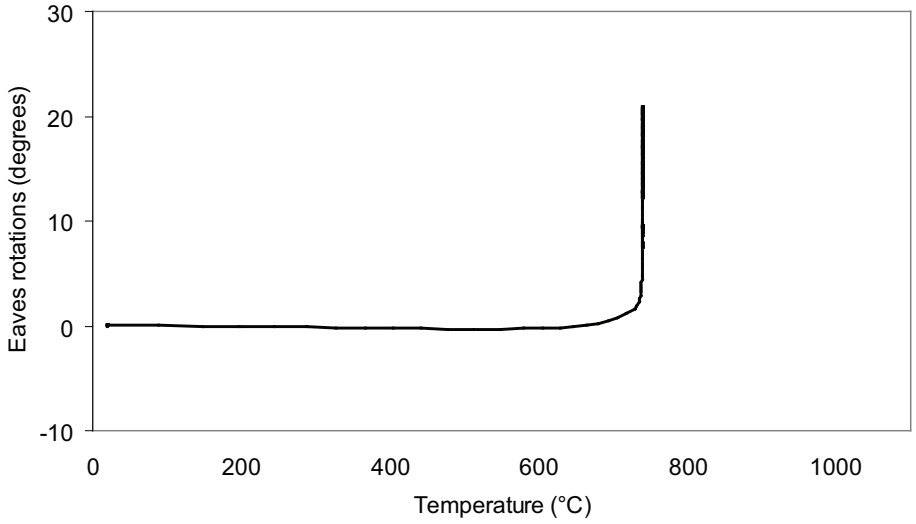

Figure 5.91: Variation of eaves rotations against temperatures of SPAF: Eaves2, perfectly pinned column base

5.9.3 Effect on asymmetrical portal frames of partial strength column

M_{OTM} of M_{SCI}

In Section 5.9.1 it was stated that in accordance with the SCI method, the column base needs to be designed to sustain an overturning moment, M_{OTM}, of 101.78 kNm. Such an overturning moment represents approximately 59% of the plastic moment capacity of the section.

Figure 5.92 to Figure 5.94 show the variation of apex deflections and eaves

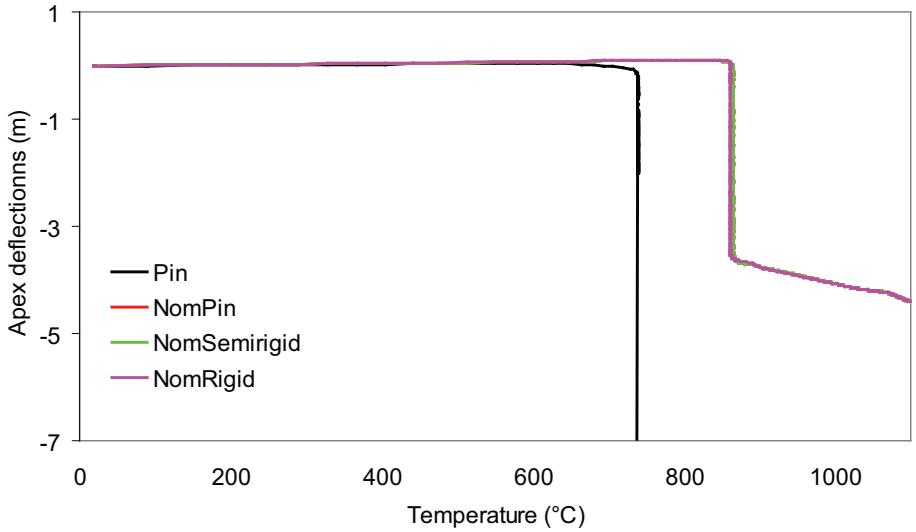

Figure 5.92: Variation of apex deflections against temperatures of SPAF: Apex (M_{OTM} of M_{SCI})

rotations against temperature for three different column base rotational stiffness having partial strength M_{OTM} of $1.0M_{SCI}$. The results are summarized in Table 5.24.

As can be seen, for three different column bases, i.e. nominally pinned, nominally semirigid and nominally rigid, the snap-through buckling temperature is between 861°C and 865°C, considerably higher than 739°C for the pinned column bases. The maximum outward column rotation is 1.3° and maximum inward rotation is 10.1° for nominally pinned column base.

M_{OTM} of $1.5M_{SCI}$ and M_{OTM} of $2.0M_{SCI}$

Figure 5.95 to Figure 5.100 show the variation of deflection against temperature

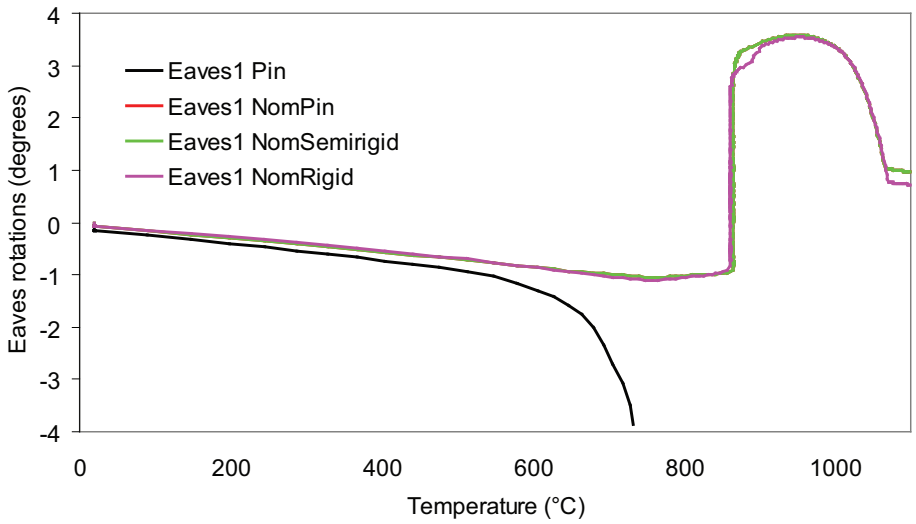

Figure 5.93: Variation of eaves rotations against temperatures of SPAF: Eaves1 (M_{OTM} of M_{SCI})

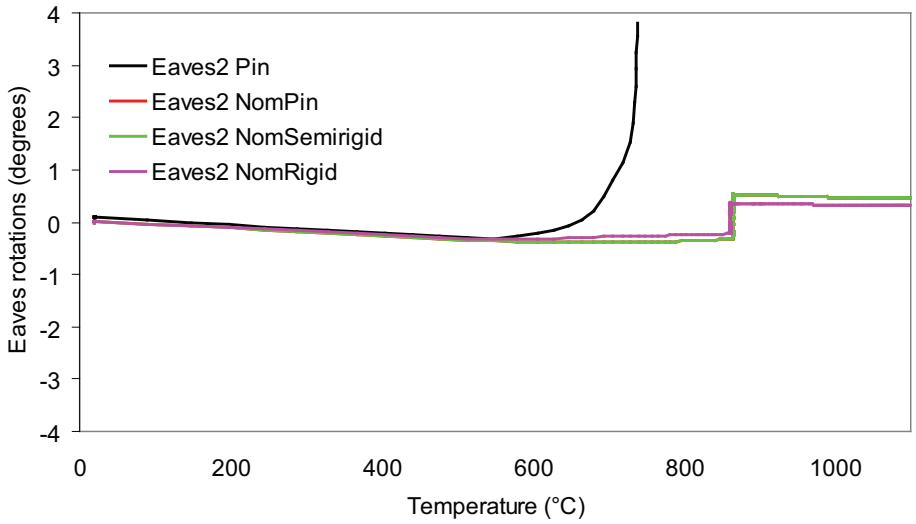

Figure 5.94: Variation of eaves rotations against temperatures of SPAF: Eaves2 (M_{OTM} of M_{SCI})

Table 5.24: Summary of behaviour of SAPF: M_{OTM} of M_{SCI}

Col. base	Snap-through-buckling temperature	Collapse temperature	Maximum inward column rotation by 890°C	Maximum outward column rotation by 890°C
	°C	°C	°	°
Pin	739	739	20.6	19.9
Nom. pin	861	>1100	10.1	1.3
Nom. semirigid	863	>1100	9.6	1.2
Nom. rigid	865	>1100	9.5	1.2

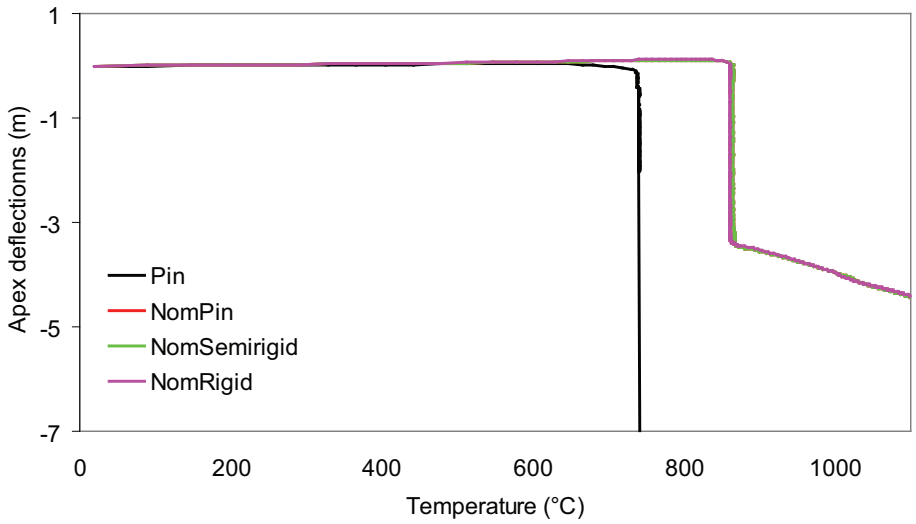

Figure 5.95: Variation of apex deflections against temperatures of SPAF: Apex (M_{OTM} of $1.5M_{SCI}$)

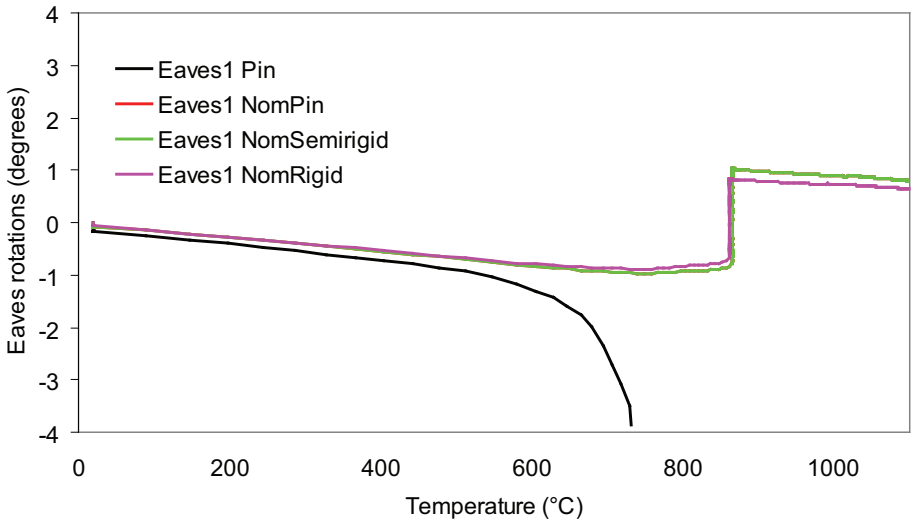

Figure 5.96: Variation of eaves rotations against temperatures of SPAF: Eaves1 (M_{OTM} of $1.5M_{SCI}$)

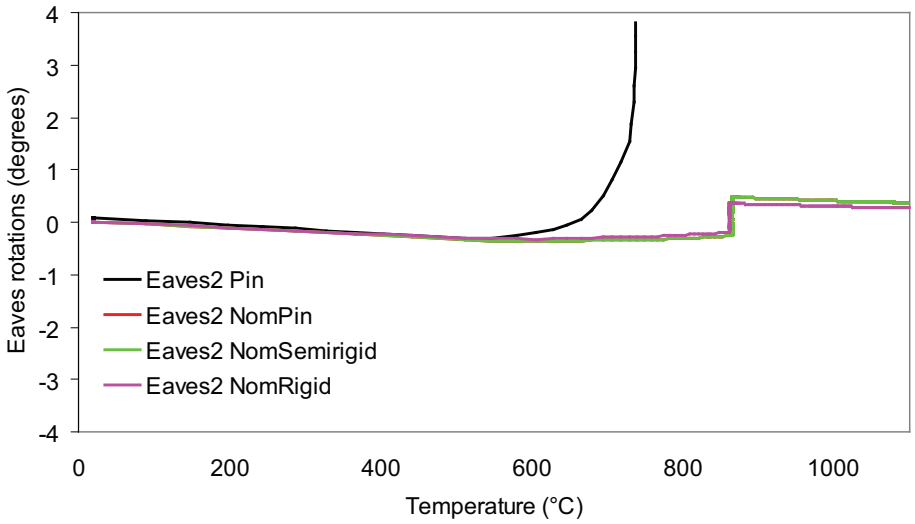

Figure 5.97: Variation of eaves rotations against temperatures of SPAF: Eaves2 (M_{OTM} of $1.5M_{SCI}$)

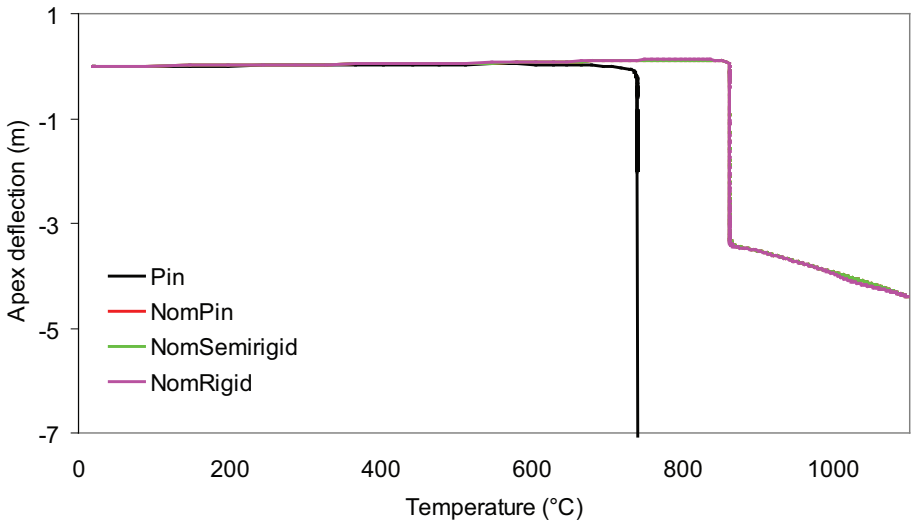

Figure 5.98: Variation of apex deflections against temperatures of SPAF: Apex (M_{OTM} of $2.0M_{SCI}$)

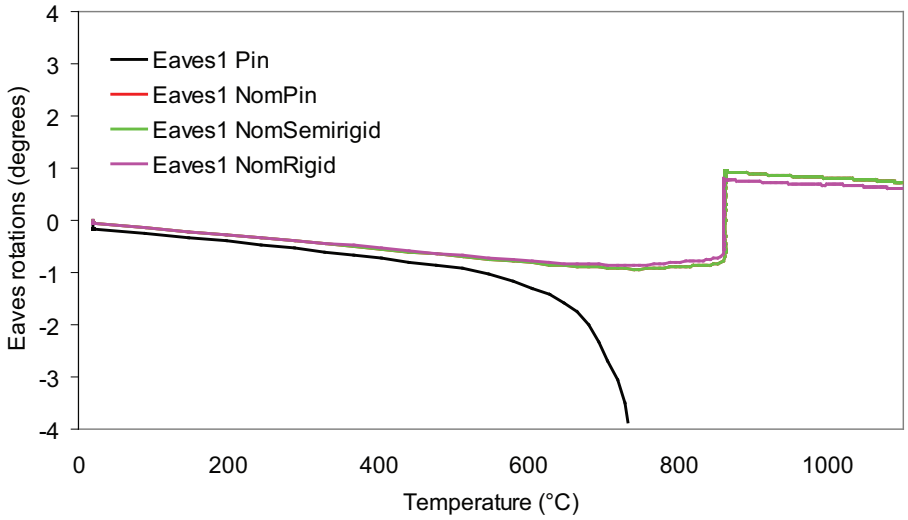

Figure 5.99: Variation of eaves rotations against temperatures of SPAF: Eaves1 (M_{OTM} of $2.0M_{SCI}$)

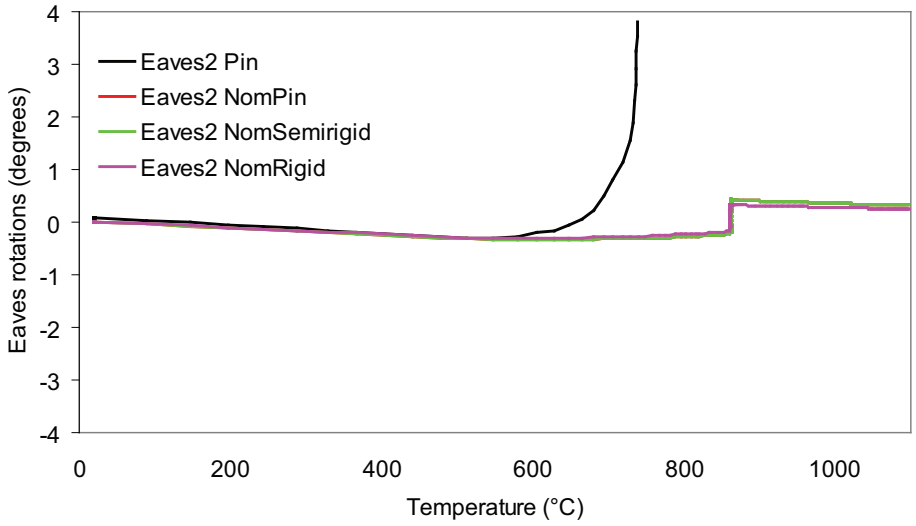

Figure 5.100: Variation of eaves rotations against temperatures of SPAF: Eaves2 (M_{OTM} of $2.0M_{SCI}$)

for the asymmetrical portal frame for three different column base rotational stiffness having partial strength M_{OTM} of $1.5M_{SCI}$ and $2.0M_{SCI}$, respectively. The results are summarized in Table 5.25 and Table 5.26.

Table 5.25: Summary of behaviour of SAPF: M_{OTM} of $1.5M_{SCI}$

Col. base	Snap-through-buckling temperature	Collapse temperature	Maximum inward column rotation by 890°C	Maximum outward column rotation by 890°C
	°C	°C	°	°
Pin	739	739	20.6	19.9
Nom. pin	863	>1100	1.1	<1
Nom. semirigid	867	>1100	<1	<1
Nom. rigid	870	>1100	<1	<1

As can be seen, for all three different column base rotational stiffness, the snap-through-buckling temperature is between 863°C and 870°C for M_{OTM} of $1.5M_{SCI}$ and 865°C to 871°C for M_{OTM} of $2.0M_{SCI}$, respectively. Though this snap-through-buckling temperature is considerably higher than 739°C for pinned column bases, it can be seen that variation of M_{OTM} has little affect on snap-through buckling temperature for asymmetrical frame. However, a higher M_{OTM}

Table 5.26: Summary of behaviour of SAPF: M_{OTM} of $2.0M_{SCI}$

Column base stiffness	Snap-through-buckling temperature	Collapse temperature	Maximum inward column rotation by 890°C	Maximum outward column rotation by 890°C
	°C	°C	°	°
Pinned	739	739	20.6	19.9
Nom. pin	865	>1100	<1	<1
Nom. semirigid	868	>1100	<1	<1
Nom. rigid	871	>1100	<1	<1

has significant effect on eaves rotation as can be seen in Table 5.24, Table 5.25 and Table 5.26. It can be observed that the inward eaves rotation is reduced from 10.17° for M_{OTM} of M_{SCI} to less than 1° for M_{OTM} of $2.0M_{SCI}$ and outward rotation all reduced to less than 1°.

Figure 5.101 to Figure 5.103 show the effect of increasing the overturning

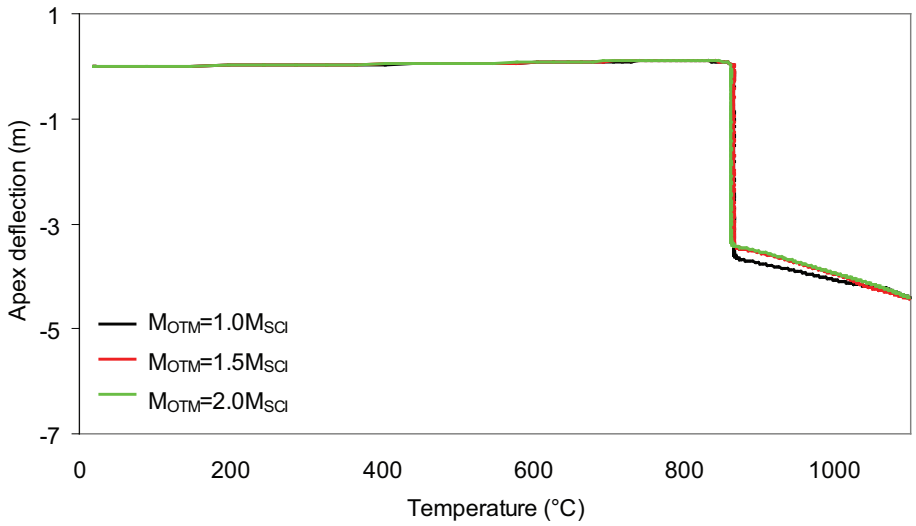

Figure 5.101: Variation of apex deflections against temperatures of SPAF: Apex (different M_{OTM})

moment on the variation of frame deflection against temperature. As can be seen, the eaves rotation is almost 4° when M_{OTM} of M_{SCI}; however, when M_{OTM} is increased to $1.5M_{SCI}$ the eaves rotation is reduced to below 1° (Figure 5.102. This phenomenon establishes the fact that the overturning moment provided by

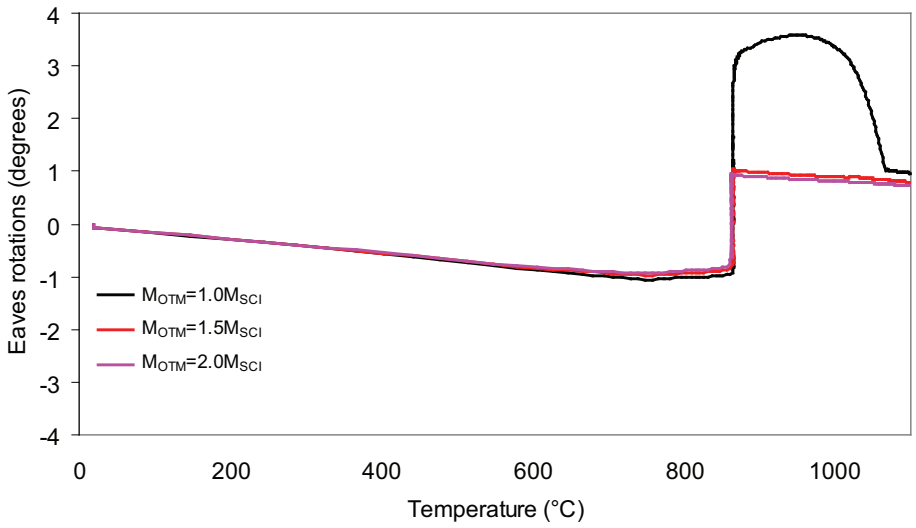

Figure 5.102: Variation of eaves rotations against temperatures of SPAF: Eaves1 (different M_{OTM})

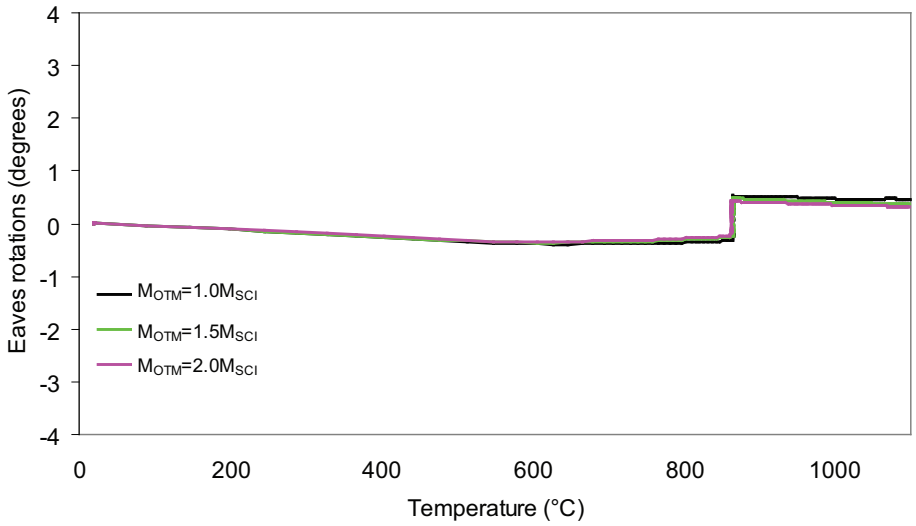

Figure 5.103: Variation of eaves rotations against temperatures of SPAF: Eaves2 (different M_{OTM})

the SCI method should be increased to at least 1.5 times for safe design.

5.10 Concluding remarks

In this chapter, the finite element method that has been developed in chapter 3 has been used for three different types of portalised frames, such as, multi-span portal frames, portalised truss frame and asymmetric portal frames. It is found that, apart from the multi-span frame, the model can be readily applied to the portalised truss frames and asymmetric portal frames without any computational overhead and loss of accuracy. However, for the multi-span frame, the cost of computation is increased significantly. The computational cost is reduced by relaxing some tight tolerance parameters without losing any accuracy.

For all of the frames, it has been observed that all the frames of collapses when the column bases are perfectly pinned. However, when a partial strength is introduced at the column bases, the behaviour of the frames changed considerably. It is found that though the snap-through-buckling temperatures remain almost same, however, the collapse temperatures vary and the eaves rotations differ significantly. It has been found that when M_{OTM} is increased to $1.5M_{SCI}$ or $2.0M_{SCI}$, the eaves rotations are reduced significantly below 1°, the limit specified by the SCI method.

It is suggested that based on the study on different frames, the M_{OTM} given by the SCI method should be increased within the region of $1.5M_{SCI}$ to $2.0M_{SCI}$.

Chapter 6

Conclusions

6.1 Major findings

The aim of this study is to provide computational techniques and solutions for studying the possible behaviour of hot-rolled steel portal frame at elevated temperatures and in particular the snap-through-buckling details. We have mainly studied an exemplar hot-rolled steel portal frame given by the Steel Construction Institute (Simms and Newman, 2002) with the particular material properties given in Figures 4.6, 4.7 and 4.6, section properties given in Table 4.1, and frame geometries in Section 4.2. The main achievements and findings are summarized below.

A set of viable numerical models has been developed and validated. A comparative study has been conducted for determining whether an implicit dynamic or an explicit dynamic method would be selected for the study. It has been established that the implicit dynamic method is more efficient than the explicit dynamic method both in terms of cost of computation and the number of processors involved in the computation. Throughout the study, the rafter was kept unprotected from fire and was allowed to collapse to the ground while the columns were always kept protected from fire. A series of numerical parametric studies has been performed extensively on the benchmark exemplar portal frame given by the SCI method by using the developed numerical model for observing the effect of column base strength with the particular geometries and material properties. Based on the results it has been established that the portal frame designed on the basis of SCI method is found to be unsafe and the structure may collapse at a lower temperature than forecasted by the SCI method. The developed model has later been used to analyze three different types of portalised frames. These are: multi-span portal frames, portalised truss frames and asymmetric portal frames. It has been suggested that to avoid premature collapse of different portal frames

at elevated temperature the overturning moment calculated by the SCI method should be increased by 1.5 to 2.0 times.

6.2 Key results and conclusions

Before simulating the behaviour of portal frame at elevated temperature, a comparison of performance between the implicit and the explicit dynamic solvers has been conducted in Chapter 3 in order to determine which solver would be the best candidate for our analysis. It has been shown that both methods of analysis produce similar results when the solution options within ABAQUS are selected to achieve the most accurate results, with the implicit dynamic method solving in 40 minutes compared with 15 hours for the explicit dynamic method. However, the the cost of computation for the implicit dynamic method can be reduced to 19 seconds with only 1% loss in accuracy of the snap-through-buckling temperature by setting haftol of 100 and numerical damping of -0.15. On the other hand, reducing the cost of computation for the explicit method to under 4 hours was achieved within 10% loss in accuracy by setting a mass scaling factor of 4.0. In most cases, a desktop computer usually made of a single faster processor is suitable for the implicit dynamic method. The implicit dynamic method is therefore seen to be both more accurate and significantly more computationally efficient and viable than the explicit dynamic method for simulating the collapse of steel portal frames in fire. Once the proper solver i.e. the implicit dynamic method has been selected, all of the analysis of portal frame at elevated temperature have been conducted by using this particular solver.

In Chapter 4, the main focus of the study is the behaviour of portal frames at elevated temperature. The standard building outlined in Section 4.2 has been used for the study which followed a series of parametric study. It has been found that the 3-D model increases the collapse temperature and reduces the rotations, but the number of frames in fire is significant. The SCI method does not take into account the partial strength of column base. If the partial strength of the column base is taken into account, the column base rotational stiffness has little effect on the collapse behaviour of the frame, with the column base behaving as a pin once the column base moment capacity has been exceeded. All the 2-D frames considered in the parametric study have been collapsed before 890°C when the rotational strength of the column base was $1.0M_{SCI}$. However, when the rotational strength of the column base was increased to $2.0M_{SCI}$ all the frames were stable at 890°C. Intermediate results for $1.5M_{SCI}$ were also provided. The average outward rotation of the columns where the rotational strength of the column base was M_{SCI} was 1.8°. This outward rotation was only slightly higher than the 1° assumed by the SCI design method. The inward rotation was significantly higher than 1°. It has been shown that the value of the overturning moment, calculated in accordance with the SCI design method, may not be sufficient to

prevent collapse of the frame before 890°C. However, by taking into account both the number of bays in fire, as well as the strength of the column base, a frame may be able to be shown to satisfy the assumptions of the SCI design criteria of the columns remaining 1° from the vertical and stability up to a temperature of 890°C.

In Chapter 5, the finite element method that has been developed in chapter 3 has been used for three different types of portalised frames, such as, multi-span portal frames, portalised truss frames and asymmetric portal frames. It is found that, apart from the multi-span frame, the model can be readily applied to the portalised truss frames and asymmetric portal frames without any computational overhead and loss of accuracy. However, for the multi-span frame, the cost of computation is increased significantly. The computational cost is reduced by relaxing some tight tolerance parameters without losing any accuracy.

It has been observed that all the frames collapses when the column bases are perfectly pinned. However, when a partial strength is introduced at the column bases, the behaviour of the frames changed considerably. It is found that though the snap-through-buckling temperatures remain almost same, however, the collapse temperatures vary and the eaves rotations differ significantly. It has been found that when M_{OTM} is increased to $1.5M_{SCI}$ or $2.0M_{SCI}$, the eaves rotations are reduced significantly and reached close to 1°, the limit specified by the SCI method.

It is suggested that based on the study on different frames, the M_{OTM} given by the SCI method should be increased within the region of $1.5M_{SCI}$ to $2.0M_{SCI}$.

6.3 Future Work

The work presented in this research can be improved and extended in a number of areas:

Performance-based design is getting the global attention where natural fire and structural behaviour subjected to such fire incorporate a certain degree of risk assessment for determination of partial safety factors. A natural fire analysis may be able to establish the fact that complete fire within an entire compartment is unlikely; and therefore some frames will not attain elevated temperatures and retains the stiffness; and consequently those frames can provide extra restraint to support other part of the structure that are in the immediate vicinity of fire. With proper study, it can be established that such an approach can improve the design of steel frame subjected to fire.

As one of the major objectives of this study was to justify the validity of the SCI method, the frame considered in this analysis has been limited to single-

storey single-span portal frame (with multiple-bay while 3-D analysis have been performed). However, in reality a portal frame can be multi-storeyed multi-span building. It is also unlikely that a complete natural fire throughout the compartment will be occurred. Further investigations are required to gain a better understanding in this aspect.

The material considered in this study has been limited to isotropic hot-rolled steel. Cold-formed steel and composite materials with concrete or orthotropic FRP bonded with steel is gaining popularity nowadays. Further investigations can be undertaken.

Bibliography

Ali, H. M., Senseny, P. E., and Alpert, R. L. (2004). Lateral displacement and collapse of single-story steel frames in uncontrolled fires. Engineering Structures, 26(5), 593-607. doi: 10.1016/j.engstruct.2003.12.007

Allison, H. (1991). Low- and medium-rise steel buildings : design guide for low- and medium-rise steel buildings. Chicago, IL: American Institute of Steel Construction.

Baker, J. B., and Heyman, J. (1980). Plastic design of frames. 1, Fundamentals. Cambridge: Cambridge University Press.

Bong, M. W. (2005). Structural fire performance of steel portal frame buildings. M.Eng. Thesis, University of Canterbury, Christchurch, New Zealand.

BS5950. (1990). Structural use of steelwork in building. Part 1, Code of practice for design in simple and continuous construction : hot rolled sections. London: British Standards Institution.

Buchanan, A. H. (2001). Structural design for fire safety. Chichester; New York: Wiley.

CEN. (2005). Committee European de Normalisation, BS EN 1993-1-2 Eurocode 3: Design of steel structures. Part 1-2: General rules - Structural fire design (Vol. Eurocode 3). Brussels, Belgium: British Standards Institute.

Clough, R. W., and Penzien, J. (1975). Dynamics of structures: McGraw-Hill.

Davies, J. M., Brown, B. A., and Steel Construction, I. (1996). Plastic design to BS 5950. London; Cambridge, Mass.: Blackwell Science.

FPA. (2008). Building regulations 2000. Approved document B, Fire safety. London: RIBA.

Franssen, J. M., and Gens, F. (2004, 10-11 May). Dynamic analysis used to cope with partial and temporary failure. Paper presented at the Third international workshop - Structures in fire, Ottawa, Canada.

Franssen, J. M., Kodur, V. K., and Mason, M. (2002). User's manual for SAFIR 2001: A computer program for analysis of structures submitted to fire (Version 2001). Belgium: University of Liege.

Gorenc, B., Gorenc, B. E., Tinyou, R., and Syam, A. (2005). Steel designers' handbook: UNSW Press.

Harewood, F. J., and McHugh, P. E. (2007). Comparison of the implicit and explicit finite element methods using crystal plasticity. Computational Materials Science, 39(2), 481-494. doi: 10.1016/j.commatsci.2006.08.002

Hilber, H. M., and Hughes, T. J. R. (1978). Collocation, dissipation and [overshoot] for time integration schemes in structural dynamics. Earthquake engineering and structural dynamics, 6(1), 99-117. doi: 10.1002/eqe.4290060111

Horne, M. R., and Morris, L. J. (1982). Plastic design of low-rise frames. Cambridge, Mass.: MIT Press.

ISO. (1975). International Organisation for Standardisation Fire resistance tests - Elements of building construction (ISO834). Geneva, Switzerland.

Kaitila, O. (2002). Finite element modeling of cold-formed steel members at high temperatures. Licentiate Thesis, Helsinki University, Helsinki.

King, C. M. (1995). Plastic design of single-storey pitched-roof portal frames to Eurocode 3. Ascot, England: The Steel Construction Institute.

Lamont, S. (2001). The behaviour of multi-storey composite steel framed structures in response to compartment fires. Ph.D. Thesis, University of Edinburgh.

Lim, J. B. P., King, C., Rathbone, A., Davies, J. M., and Edmondson, V. (2005). Eurocode 3 and the in-plane stability of portal frames. The Structural Engineer, 83(21), 43-49.

Moss, P. J., Dhakal, R. P., Bong, M. W., and Buchanan, A. H. (2009). Design of steel portal frame buildings for fire safety. Journal of Constructional Steel Research, 65(5), 1216-1224. doi: 10.1016/j.jcsr.2008.09.003

NZS3404. (1997). Steel Structures Standard. New Zealand: Standards New Zealand

NZS4203. (1992). Code of practice for general structural design, and design loadings for buildings (known as Loadings Code). New Zealand: Standards New Zealand

O'Meagher, A. J., Bennetts, I. D., Dayawansa, P. H., and Thomas, I. R. (1992). Design for single storey industrial buildings for fire resistance. [Journal]. Journal of the Australian Steel Institute, 26(2), 17.

Purkiss, J. A. (1996). Fire safety engineering design of structures. Oxford; Boston: Butterworth-Heinemann.

Rahman, M., Lim, J., Xu, Y., Hamilton, R., Comlekci, T., and Pritchard, D. (2011). Effect of column base strength on portal frame in fire. [Journal]. Journal of Structures and Buildings, Article-in-press.

Salter, P. R., Malik, A. S., and King, C. M. (2004). Design of single-span steel portal frames to BS 5950-1:2000. Ascot: The Steel Construction Institute.

Simms, W. I., and Newman, G. M. (2002). Single storey steel framed buildings in fire boundary conditions. Ascot, Berkshire: The Steel Construction Institute, (P313).

Simulia. (2010). Abaqus analysis user's manual (ver. 6.10-1) (Version 6.10-1). France: Dassault Systemes.

Soltani, B., Mattiasson, K., and Samuelsson, A. (1994). Implicit and dynamic explicit solutions of blade forging using the finite element method. Journal of Materials Processing Technology, 45(1-4), 69-74. doi: 10.1016/0924-0136(94)90320-4

Song, Y. (2008). Analysis of industrial steel portal frames under fire conditions. Ph.D. Thesis, University of Sheffield, Sheffield, UK.

Song, Y., Huang, Z., Burgess, I. W., and Plank, R. J. (2009). The behaviour of single-storey industrial steel frames in fire. Advanced Steel Construction, 5(3), 289-302.

Steadmans, A. (2010). Purlins, rails and eaves beams - Load tables. Cumbria: Steadman and Sons.

Sun, J. S., Lee, K. H., and Lee, H. P. (2000). Comparison of implicit and explicit finite element methods for dynamic problems. Journal of Materials Processing Technology, 105(1-2), 110-118. doi: 10.1016/s0924-0136(00)00580-x

Todd, A. J. (1996). Portal frames. London: Structural Advisory Service, British Steel.

Trahair, N. S. (2008). The behaviour and design of steel structures to EC3. London; New York: Taylor and Francis.

Vassart, O. (2007). Fire Safety of Industrial Halls and Low-rise Buildings: Realistic Fire Design, Active Safety Measures, Post-local Failure Simulation and Performance Based Requirements: Renouf Pub Co Ltd.

Wang, Y. C. (2002). Steel and composite structures : behaviour and design for fire safety. London; New York: Spon Press.

Wong, S. Y. (2001). The structural response of industrial portal frame structures in fire. Ph.D. Thesis, University of Sheffield, Sheffield, UK.

Woolcock, S. T., Kitipornchai, S., and Bradford, M. A. (1993). Limit state design of portal frame buildings. North Sydney, N.S.W.: Australian Institute of Steel Construction.

Zha, X. (2003). FE analysis of fire resistance of concrete filled CHS columns. Journal of Constructional Steel Research, 59(6), 769-779. doi: 10.1016/s0143-974x(02)00059-7

Appendix A

Sample ABAQUS Script

SCRIPT FOR IMPLICIT DYNAMIC ANALYSIS.

```
**————————— MODEL STEP———————————-
*HEADING
ANALYSIS OF A SINGLE-SPAN STEEL PORTAL FRAME IN FIRE
*PREPRINT, ECHO=YES, MODEL=YES, HISTORY=YES, CONTACT=NO
*RESTART, WRITE, OVERLAY, FREQUENCY=50
******************** MESH GENERATION **********************
*NODE
** FRAME NODES
1, 0, 0, 0
17, 0, 6.0, 0
49, 20, 8.102, 0
81, 40, 6.0, 0
97, 40, 0, 0
** GROUND NODES FOR SPRING CONNECTION
101, 0, 0, 0
197, 40, 0, 0
*NGEN
1, 17, 1
17, 49, 1
49, 81, 1
81, 97, 1
*NSET, NSET=ALL, GENERATE
1, 97, 1
*ELEMENT, TYPE=B21
1, 1, 2
*ELGEN
1, 96, 1, 1
```

```
*ELSET, ELSET=ALL,GENERATE
1, 96, 1
*ELSET, ELSET=APEX
48,
*NSET, NSET=COLUMNBASES
1, 97
*NSET, NSET=SUPPORT
101, 197
*NSET, NSET=LEFTEAVES
17,
*NSET, NSET=RIGHTEAVES
81,
*NSET, NSET=APEX
49,
*NSET, NSET=COLUMN, GENERATE
1, 17, 1
81, 97, 1
*ELSET, ELSET=COLUMN, GENERATE
1, 16, 1
81, 96, 1
*NSET, NSET=RAFTER,GENERATE
17, 81, 1
*ELSET, ELSET=RAFTER, GENERATE
17, 80, 1
********************* END OF MESH GENERATION **************
********************* SECTION DEFINITION ******************
**RAFTER SECTION: UB533X210X92
*BEAM SECTION, ELSET = RAFTER, MATERIAL = STEELMAT, TEM-
PERATURE = GRADIENTS, SECTION = I
0.26655, 0.5331, 0.2093, 0.2093, 0.0156, 0.0156, 0.0101
0., 0., -1.
**COLUMN SECTION: UB686X254X140
*BEAM SECTION, ELSET = RAFTER, MATERIAL = STEELMAT, TEM-
PERATURE = GRADIENTS, SECTION = I
0.342, 0.684, 0.254, 0.254, 0.019, 0.019, 0.0124
0., 0., -1.
********************* END OF SECTION DEFINITION ***********
********************* STANDARD TIME TEMPERATURE RELATIONSHIP*
*AMPLITUDE, NAME=ISO834
0., 20., 50., 325., 100., 419., 150., 476.
200., 517., 250., 550., 300., 576., 350., 599.
...
9800., 1095., 9850., 1096., 9900., 1097., 9950., 1097.
10000., 1098., 10050., 1099., 10100., 1100.
********** END OF STANDARD TIME TEMPERATURE RELATIONSHIP*****
```

```
****** DEVELOPED TIME TEMPERATURE RELATIONSHIP (EC3) *********
*AMPLITUDE, NAME = EC3RAFTER
...
*AMPLITUDE, NAME = EC3COLUMN
...
**** END OF DEVELOPED TIME TEMPERATURE RELATIONSHIP (EC3)
**********
******* STEEL MATERIAL DEFINITION ********************************
*MATERIAL, NAME = STEEL
*DAMPING, ALPHA=5.
*DENSITY
7850.,
*ELASTIC
2.1E+11, 0.3, 20.
2.1E+11, 0.3, 100.
1.89E+11, 0.3, 200.
...
9.45E+09, 0.3, 1000.
4.725E+09, 0.3, 1100.
*EXPANSION, ZERO=20.
1.23E-05, 20.
1.23E-05, 50..
...
1.46E-05,1100.
*PLASTIC
2.7536E+08, 0., 20.
2.76003E+08, 0.0023249, 20.
...
2.596E+06, 0.164965, 1100.
1.309E+06, 0.173676, 1100.
********************* NONLINEAR BOUNDARY CONDITIONS *******
** ROTATIONAL SPRING CONNECTIVITY
*ELEMENT, TYPE=SPRING2, ELSET=SPRINGELEMENT
101, 101, 1
197, 197, 97
*SPRING, ELSET=SPRINGELEMENT, NONLINEAR
** ROTATION IS 0.0102530562 RAD AND MOMENT IS 196.00 KNM
6,6
-196000, -0.0102530562
0,0
196000, +0.0102530562
*BOUNDARY
SUPPORT, ENCASTRE
COLUMNBASES, PINNED
********* END OF BOUNDARY CONDITIONS **********************
```

```
********* AMBIENT TEMPERATURE BEFORE FIRE ***************
*INITIAL CONDITIONS, TYPE=TEMPERATURE
ALL, 20.0
******** END OF AMBIENT TEMPERATURE **********************
** ——————ANALYSIS STEP——————-
****** STEP 1: APPLY STRUCTURAL LOAD *********************
*STEP, NAME="STRUCTURAL LOAD", NLGEOM=YES, INC=100
*STATIC
1., 1., 1E-5, 1.
*DLOAD
**** SELF WEIGHT ***
**ALL, GRAV,9.81, 0,-1,0
**** UDL ON RAFTER**
RAFTER, PY, -1300
*** CONC. LOAD******
*CLOAD
LEFTEAVES, 1, 6.5
RIGHTEAVES, 1, 6.5
****************** OUTPUT REQUESTS **********************
*OUTPUT, FIELD, FREQUENCY=1
*NODE OUTPUT, NSET=ALL
NT, RF, U
*ELEMENT OUTPUT, ELSET=ALL, DIRECTIONS=YES
SF, S
*OUTPUT, HISTORY, FREQUENCY=1
*NODE OUTPUT, NSET=ALL
NT, RF, U
*ELEMENT OUTPUT, ELSET=ALL, DIRECTIONS=YES
SF, S
*END STEP
***************** STEP 2: APPLY TEMPERATURE *************
*STEP, NAME="TEMPERATURE LOAD", NLGEOM=YES, INC=10000, EX-
TRAPOLATION=NO
*DYNAMIC, ALPHA=-0.10, HAFTOL=1E+02
1., 10000., 1E-15, 60.
**RELAX SOME TIGHT TOLERANCE FOR EASIER CONVERGENCE
*CONTROLS, PARAMETERS=FIELD, FIELD=GLOBAL
0.02, 1.0, 10.0
****** SELECT FIRE ***************************************
*TEMPERATURE, AMPLITUDE=ISO834
**TEMPERATURE, AMPLITUDE=EC3RAFTER
**TEMPERATURE, AMPLITUDE=EC3COLUMN
** APPLY FIRE ON RAFTER AND KEEP COLUMN COOL
RAFTER,1.0
*END STEP
```

SCRIPT FOR EXPLICIT DYNAMIC ANALYSIS

```
**————————- MODEL STEP ——————————
THE MODEL STEP IS SIMILAR TO IMPLICIT DYNAMIC ANALYSIS
** ———————— ANALYSIS STEP————————————
***** STEP 1: APPLY STRUCTURAL LOAD **********************
*STEP, NAME="STRUCTURAL LOAD", NLGEOM=YES
*DYNAMIC, EXPLICIT
, 1.
*FIXED MASS SCALING, FACTOR = 2, ELSET=ALL
*BULK VISCOSITY
0.06, 1.2
*DLOAD
**** SELF WEIGHT ***
**ALL, GRAV, 9.81, 0, -1,0
**** UDL ON RAFTER**
RAFTER, PY, -1300
*** CONC. LOAD******
*CLOAD
LEFTEAVES, 1, 6.5
RIGHTEAVES, 1, 6.5
******************** OUTPUT REQUESTS ********************
*FILE OUTPUT, NUMBER INTERVAL=50
*NODE FILE, NSET=ALL
U, NT
*EL FILE, ELSET=ALL
S, E, PE
**OUTPUT, FIELD, VARIABLE=PRESELECT
*OUTPUT, FIELD, TIME INTERVAL=50
*ELEMENT OUTPUT, ELSET=ALL
S, E, PEEQ, TEMP
*NODE OUTPUT, NSET=ALL
U
**OUTPUT, HISTORY, VARIABLE=PRESELECT
*END STEP
******************** STEP 2: APPLY TEMPERATURE ***********
*STEP, NAME="TEMPERATURE LOAD", NLGEOM=YES
*DYNAMIC, EXPLICIT
, 1200.
*FIXED MASS SCALING, FACTOR = 2, ELSET = ALL
*BULK VISCOSITY
0.06, 1.2
******************** OUTPUT REQUESTS ********************
```

```
**OUTPUT, FIELD, VARIABLE=PRESELECT
*OUTPUT, FIELD, TIME INTERVAL=1
*ELEMENT OUTPUT, ELSET=ALL
S, E, PEEQ, TEMP
*NODE OUTPUT, NSET=ALL
U, NT, RF
********************* SELECT FIRE ************************
*TEMPERATURE, AMPLITUDE=ISO834
**TEMPERATURE, AMPLITUDE=EC3RAFTER
**TEMPERATURE, AMPLITUDE=EC3COLUMN
** APPLY FIRE ON RAFTER AND KEEP COLUMN COOL
RAFTER, 1.0
*END STEP
```